EVALUATING ASR PHYSICOCHEMICAL PROCESS UNDER DISTINCT RESTRAINT CONDITIONS FOR A BETTER ASSESSMENT OF AFFECTED CONCRETE INFRASTRUCTURE

By

ANDISHEH ZAHEDI REZAIEH

Under Supervision of

Dr. Leandro F. M. Sanchez and Dr. Martin Noël

Thesis submitted to the University of Ottawa in partial fulfillment of the

requirements for the degree of

Doctor of Philosophy in Civil Engineering

Department of Civil Engineering

University of Ottawa

Ottawa

September 2021

I would like to dedicate this work to all victims of flight PS752, their families and friends who lost their loved ones on January 8th, 2020; a special dedication to my beloved friend and brother **"*Saeed Kadkhodazadeh Kashani*"** who was among that were killed in the Ukraine International Airlines crash. Looking forward to a day that justice would be brought for those who planned it, and those who were otherwise responsible for all 176 innocent victims.

You'll always be remembered!

ABSTRACT

Over the last decades, researchers have proposed a number of tools for the condition assessment of concrete infrastructure affected by alkali-silica reaction (ASR). Amongst those, increasing attention has been given to the Stiffness Damage Test (SDT), Damage Rating Index (DRI), and Residual Expansion (RE) laboratory test procedures that aim to determine the cause and extent (i.e., diagnosis) of damage along with the potential of further deterioration (i.e., prognosis) of affected concrete. Yet, most of the data gathered so far while using the aforementioned tools has been obtained on laboratory test specimens presenting distinct conditions from affected structural members in the field, especially regarding restraint effects. This work aims to understand the impact of restraint on ASR-induced expansion and damage. Thirty-two 450 mm by 450 mm by 675 mm concrete blocks with various reinforcement configurations (i.e., unreinforced, 1D and 2D reinforcement) and incorporating highly reactive coarse and fine aggregates (i.e., Springhill coarse and Texas sand) were manufactured and stored in conditions enabling ASR-induced development (i.e., 38°C and 100 R.H). Two expansion levels were selected for analysis (i.e., 0.08% and 0.15%); once reached, cores were extracted from three different directions (i.e., longitudinal, transversal and vertical) of all blocks and mechanical (i.e., SDT and compressive strength), microscopic (i.e., DRI, scanning electron microscope, etc.) and expansion (i.e., RE) test procedures were conducted on the concrete cores. Results suggest that the presence of restraint influences the induced expansion, resulting in an anisotropic response of the specimens. Furthermore, similar to the expansion behavior, an anisotropic distribution of induced damage and mechanical properties reduction are observed for the restrained concrete blocks in which the restraint configuration seems to significantly affect ASR-induced damage development and features. This led to the observation of a higher number of damage features, ASR development and mechanical properties reduction in cores obtained from unrestrained directions. Yet, some anticipated results from the current research will be studied in detail in the near future where the reliability of the existing techniques (i.e., residual expansion and soluble alkalis) for appraising ASR potential for further induced development and distress (i.e., prognosis) in affected concrete presenting distinct restraint scenarios will be evaluated.

Keywords: alkali- Silica reaction (ASR), damage rating index, stiffness damage test, residual expansion, restraint effects.

ACKNOWLEDGMENTS

Foremost, I would like to express my sincere gratitude to my supervisor and co-supervisor Prof. Leandro Sanchez and Prof. Martin Noël for the continuous support of my Ph.D study and related research, for their patience, motivation, and immense knowledge. Their guidance from initial to the final level helped me throughout my research and writing of this thesis. I could not have imagined having better advisors and mentors for my Ph.D study.

I would like to express my heartfelt appreciation to my wife “Saba”, for her love and constant support, for all the late nights and early mornings, and for keeping me sane over the past few months. Thank you for being my muse, editor, proofreader, and sounding board.

I must express my very profound gratitude to my mom “Sima”; for being a base even far from home, who provided me through moral and emotional support, for her continuous encouragement throughout my years of study and through the process of research and writing this thesis, and for all the sacrifices she made to give the opportunity to grow in my desired field. I would also thank to my dearest sister “Shadi” for providing me with unfailing support and continuous encouragement throughout my years of study.

I would also extent my thanks for my best friends “Saeed R” and “Saeed K” for their endless support in this very intense academic year.

Moreover, I would like to thank each one of my colleagues in the uOttawa concrete microstructure team, specially Nusrat Zubaida who have helped me with lab works, advice, and knowledge.

I also need to acknowledge all of the much-appreciated help, advice and companionships provided by our laboratory technical officers, Dr. Gamal Elnabelsya and Dr. Muslim Majeed, without their support this work could not have been successfully completed.

TABLE OF CONTENTS

ABSTRACT ..... **iii**
ACKNOWLEDGMENTS ..... **iv**
LIST OF TABLES ..... **xi**
LIST OF FIGURES ..... **xii**
FOREWORD ..... **xv**
1. INTRODUCTION **1**
2. LITERATURE REVIEW **3**
2.1 ASR distress mechanism in concrete under free expansion 3
2.1.1 ASR gel production 4
2.2 ASR effects on the mechanical properties of affected concrete under free expansion 8
2.3 Effects of confinement on ASR-induced expansion 10
2.3.1 Effects of confinement on ASR-induced crack orientation and mechanical properties 12
2.4 Assessment of cause and extent of damage 14
2.4.1 Stiffness Damage Test (SDT) 14
2.4.2 Damage Rating Index (DRI) 15
2.5 Potential for Further expansion of ASR affected concrete 18
2.5.1 In-situ investigations 18
2.5.2 Detailed laboratory investigations 18
2.5.2.1 Residual Expansion (RE) Tests 19
2.5.2.2 Hot-Water Extraction (soluble alkali -SA) 19
2.6 Tools for assessment of future damage caused by ASR 20
2.6.1 Residual Expansion Test (RE) 20
2.6.2 Hot-Water Extraction (soluble alkali -SA) 20
2.7 Predicting ASR expansion and damage through modeling 21
3. OBJECTIVE **30**
4. RESEARCH PROGRAM **32**
4.1 Experimental procedures 32
4.1.1 Visual inspection 34
4.1.2 Stiffness Damage Test (SDT) 35
4.1.3 Compressive strength 35
4.1.4 Damage Rating Index (DRI) 36

4.1.5 SEM/EDS and micro-indentation ... 36
5. CORE OF THE THESIS – SCIENTIFIC PAPERS ... **40**
5.1 General overview ... 40
5.2 Scope and objectives of the scientific papers ... 41
6. MICROSCOPIC ASSESSMENT OF ASR-AFFECTED CONCRETE UNDER RESTRAINT CONDITIONS ... **44**
Abstract ... 44
6.1 Introduction ... 44
6.2 Background ... 45
6.2.1 ASR-induced development under free expansion ... 45
6.2.2 Effect of confinement on ASR-induced development ... 46
6.2.3 Damage Rating Index (DRI) ... 48
6.3 Scope of the work ... 50
6.4 Materials and methods ... 50
6.4.1 Materials and mixture proportions ... 50
6.4.2 Manufacture of concrete blocks and cylinders ... 51
6.4.3 Experimental procedures ... 54
6.5 Results ... 55
6.5.1 ASR kinetics and development ... 55
6.5.2 Microscopic distress features and crack density ... 57
6.5.3 Crack widths/lengths versus degree of expansion/damage ... 60
6.5.4 Quantitative assessment of damage through DRI ... 61
6.6 Discussion ... 62
6.6.1 Effect of restraint on the "overall" ASR-induced expansion and damage development ... 62
6.6.3 Understanding ASR-induced damage development of unrestrained and restrained concrete ... 67
6.6.4 Evaluating ASR-induced damage development as a function of the depth of restrained and unrestrained concrete ... 71
6.6.5 Evaluating cracks orientation in unrestrained and restrained concrete ... 73
6.7 Conclusions ... 75
Acknowledgments ... 76
References ... 77
SUPPLEMENTARY MATERIALS ... 79

7. Evaluation of The Induced Mechanical Deterioration Of Alkali-Silica Reaction Affected Concrete Under Distinct Restraint Conditions Through The Stiffness Damage Test 81

Abstract 81

7.1 Introduction 81

7.2 Background 82

7.2.1 Influence of ASR-induced development on mechanical properties of concrete under free expansion 82

7.2.2 Influence of restraint on ASR-induced development and mechanical properties 83

7.2.3 Mechanical tools to assess damage of ASR-affected concrete 85

7.2.3.1. Tensile, compressive and shear strength tests 85

7.2.3.2. Stiffness Damage Test (SDT) 86

7.3 Research significance 87

7.4 Experimental investigation 88

7.4.1 Concrete ingredients and mix design 88

7.4.2 Concrete specimens manufacturing 88

7.4.3 Experimental procedures 91

7.4.3.1. Stiffness Damage Test (SDT) 91

7.4.3.2. Compressive Strength 92

7.5.1 ASR kinetics and development 92

7.5.2 Stiffness Damage Test (SDT) 94

7.6 Discussion 98

7.6.1 Effect of restraint on the kinetics and magnitude of ASR-induced expansions 98

7.6.2 Understanding the influence of ASR deterioration on the "overall" mechanical properties of unrestrained/restrained concretes 99

7.6.3 Understanding the effect of restraint orientation on the mechanical properties of ASR-affected concrete 102

7.6.4 Effect of restraint on the cracks' orientation of ASR-affected concrete 107

7.6.5 Validation of the SDT for assessing damage in concrete 108

7.7 Conclusion 110

Acknowledgments 111

References 112

SUPPLEMENTARY MATERIALS 116

8. CONDITION ASSESSMENT OF ALKALI-SILICA REACTION AFFECTED CONCRETE UNDER RESTRAINT CONDITIONS INCORPORATING DISTINCT REACTIVE AGGREGATE TYPES 118

Abstract 118
8.1. Introduction 118
8.2. Effects of confinement on physicochemical development of ASR 119
8.2.1 Tools for appraising concrete damaged by ASR 120
8.2.1.1. Stiffness Damage Test (SDT) 120
8.2.1.2. Damage Rating Index (DRI) 121
8.3. Scope of work 122
8.4. Materials and methods 122
8.4.1 Materials and mix proportions 122
8.4.2 Production of concrete specimens 123
8.4.3. Experimental procedures 126
8.4.3.1. Stiffness Damage Test (SDT) 127
8.4.3.2. Compressive Strength (CS) 127
8.4.3.3. Damage Rating Index (DRI) 127
8.5. Results 128
8.5.1 ASR kinetics and development 128
8.5.2 Stiffness Damage Test (SDT) 129
8.5.3 Compressive strength 132
8.5.4 Damage Rating Index (DRI) 133
8.6. Discussion 134
8.6.1 Understanding the impact of reinforcement on ASR-induced development 134
8.6.1.1. Induced expansion 134
8.6.1.2. Induced deterioration 135
8.6.2 Effect of reactive fine versus coarse aggregates on ASR-induced damage development under restraint 141
8.6.3 Impact of reinforcement on the cracks orientation of ASR affected concrete members 148
8.7. Conclusions 150
Acknowledgments 151
References 151
SUPPLEMENTARY MATERIAL 154
9. IMPROVING THE KNOWLEDGE OF VISUAL INSPECTION ON ASR AFFECTED CONCRETE UNDER VARIOUS RESTRAINT CONDITIONS **155**
Abstract 155

9.1. Introduction 155
9.2. Background 157
9.2.1. Alkali-silica reaction (ASR) 157
9.2.2. Diagnostic assessment tools 158
9.2.2.1. Surface assessment: cracking index (CI) 158
9.2.2.2. Internal deterioration appraisals: damage rating index (DRI) 159
9.3. Scope of work 160
9.4. Methodology 160
9.4.1 Materials and mixture proportions 161
9.4.2 Fabrication of concrete blocks 161
9.4.3 Experimental program 165
9.4.3.1. Visual Inspection and Imaging-based detection 165
9.4.3.2. Damage Rating Index 165
9.5. Results 166
9.5.1 ASR kinetics and development 166
9.5.2 Reinforcing steel expansion 167
9.5.3 Visual Inspection 168
9.5.3.1. Cracking Index (CI) 170
9.5.4 Quantitative assessment of damage through DRI 171
9.5.4.1 Internal damage (cored specimens) 171
9.5.4.2. External damage (surface of ASR affected blocks) 172
9.6. Discussion 173
9.6.1 Effects of restraint configuration on ASR-induced expansion 173
9.6.2 DRI measurements (block surface and cored specimens) vs cracking index 176
9.6.3 Empirical model to estimate induced expansion in ASR-affected concrete 178
9.6.4 Models of surface damage generation due to AAR 180
9.7. Conclusion 185
Acknowledgments 187
References 187
10. INFLUENCE OF THE RESTRAINT CONFIGURATION ON ALKALI-SILICA REACTION (ASR) REACTION PRODUCT'S FEATURES **190**
Abstract 190
10.1 Introduction 190

10.2 Background 191
10.2.1 Mechanism of ASR 191
10.2.2 Characteristics of ASR gel 192
10.3 Scope of Work 194
10.4 Materials and methods 194
10.4.1 Materials and mixture proportions 194
10.4.2 Manufacture of concrete blocks and cylinders 195
10.4.3 Experimental procedures 197
10.4.3.1 SEM/ EDS analysis 198
10.4.3.2 Micro indentation 198
10.5 Results 200
10.5.1 Morphology and chemical composition 200
10.5.2 Micro-indentation 203
10.6 Discussion 204
10.6.1 Effect of restraint on the chemical composition of ASR gel 204
10.6.1.1 Effect of restraint on the correlation of distinct chemical elements of ASR gel 210
10.6.2 Effect of restraint on the mechanical properties of ASR gel 213
10.6.2.1 Compressive strength of ASR gel 213
10.6.2.2 Hardness of ASR gel 214
10.7 Conclusions 217
Acknowledgments 218
References 218
SUPPLEMENTARY MATERIALS 221
11. FUTURE WORKS **227**
11.1 Experimental procedures 227
11.2 Anticipated results and outcomes impact 230
11.3 References 230
12. SCIENTIFIC AND ENGINEERING CONTRIBUTIONS OF THE PHD THESIS **231**
13. CONCLUSIONS AND RECOMMENDATIONS **233**
13.1 Conclusions 233
13.2 Recommendations for future works 236

LIST OF TABLES

Table 1: Testing matrix for cores obtained from each set of distinct restrained concrete blocks. 34
Table 2: Testing matrix for each family of concrete cylinders. 34
Table 3: Polishing procedure used in this study [11-12]..... 37
Table 4: Number of concrete blocks per expansion and restraint configuration for the future work. 228
Table 5: Number of concrete blocks per restraint condition kept in the environmental chamber for the future work..... 228
Table 6: Testing matrix for cores extracted from each set of distinct restrained concrete blocks for future work. 229

LIST OF FIGURES

Figure 1: Signatures of concrete damage due to alkali–silica reaction (ASR): A) a model and B) 2 mm size aggregate under thin section microscopy [6] (Reproduced with permission of Elsevier). 3
Figure 2: Qualitative model of crack propagation in ASR-affected concrete [12] (Reproduced with permission of Elsevier). 4
Figure 3: schematic diagram of silica structure that has undergone surface hydrolysis [21]. 5
Figure 4: Schematic molecular model of a typical alkali-silica reaction gel [46] (Reproduced with permission of Elsevier). 7
Figure 5: ASR product morphology: a rosette-like (or plate-like) micro-texture in the center of reactive aggregate particles and amorphous structure at the edge of the aggregate particle [30] (Reproduced with permission of Elsevier). 8
Figure 6: Mechanical properties reduction of ASR affected concrete. A) Tensile Strength reduction B) Modulus of Elasticity reduction [10] (Reproduced with permission of Elsevier). 10
Figure 7: Scheme of Multon's [68] tests [67] (Reproduced with permission of Elsevier). 12
Figure 8: Distinct cracking orientation on A) vertically extracted core and B) horizontally extracted core having ASR induced cracks before loading (black arrows) and after loading (dashed red arrows) [83] (Reproduced with permission of Elsevier)..... 13
Figure 9: Calculation of the stiffness damage index (SDI) and Plastic Deformation (PDI) [104] (Reproduced with permission of Elsevier). 15
Figure 10: Example of DRI chart for damaged concretes with different levels of distress incorporating reactive coarse aggregate. 16
Figure 11: Damage Rating Index: A) Current weighing factors as per [107] and B) Micrograph illustrating a 1cm2 section where some of the petrographic features listed in A can be observed and identified (Reproduced with permission of Elsevier)..... 16
Figure 12: Petrographic features of ASR in concrete incorporating reactive coarse aggregates. The distance between the vertical lines is 1 cm as [107]. A. closed cracks in the coarse aggregate particle; B. opened crack with Gel in the coarse aggregate particle; C. open crack in the coarse aggregate particle propagates to cement paste, and D. cracks with reaction products in the coarse aggregate particles and the cement paste. 17
Figure 13: ASR-induced expansion curve obtained from Larive's model [130] (Reproduced with permission of Elsevier). 22
Figure 14: Structure of the PhD project. 32
Figure 15: A) Schematic of Vickers hardness [13], B) Vickers hardness calculation [13] and C) typical load-indentation depth (P-h) curve. 38
Figure 16: Indentation distance profile across a crack in aggregate particles and cement paste. 38
Figure 17: Core of the PhD Thesis – links between the scientific papers..... 40
Figure 18: Structure of the future works of this PhD project..... 227
Figure 19 :Different storage conditions for ASR RE testing: (a) 38ºC and 100% R.H; (b) 0.7M NaOH solution at 38ºC and; (c) concrete mold containing a 0.4M NaOH solution and 38ºC. 230

LIST OF ACRONYMS

Acronyms	Description
AAR	Alkali-aggregate reaction
ASR	Alkali-Silica Reaction
ACR	Alkali-Carbonate Reaction
ASTM	American Society for Testing and Materials
BEC	Backscattered electrons
CAD	Coarse aggregate de-bonded
CCA	Closed Crack in the Aggregate
CCP	Crack in the Cement Paste
CCPG	Crack in the Cement Paste with Gel
CI	Cracking Index
CPT	Concrete Prism Test
CS	Compressive strength
CSA	Canadian Standard Association
Cyl.	Cylinders
DAP	Disaggregate/corroded aggregate particle
DRI	Damage Rating Index
GU	General Use
ITZ	Interfacial Transition Zone
L	Longitudinal cores
L_{max}	Maximum length of the cracks
LS	Limestone
LVDT	Linear Variable Differential Transformer
ME	Modulus of elasticity
NLI	Non-Linearity Index
OCA	Open Crack in the Aggregate
OCAG	Open Crack in the Aggregate with Gel
OT	Non-reactive Ottawa Sand
PDI	Plastic Deformation Index
RE	Residual expansion
RH	Relative humidity
SA	Soluble alkali
SDI	Stiffness Deformation Index
SDT	Stiffness Damage Test
SPR	Springhill
T	Transverse cores
TX	Texas
U.B.	Unrestrained concrete blocks
V	Vertical cores
W_{max}	Maximum width of the cracks

"*Ever tried. Ever failed. No matter. Try Again. Fail again. Fail better.*"

Samuel Beckett

FOREWORD

This PhD thesis presents and evaluates the results of a comprehensive investigation performed by the author on laboratory-made concrete specimens displaying various restraint configurations. The main goal of this study is to perform an in-depth assessment of the multi-level assessment, combining microscopic (i.e., Damage Rating Index) and mechanical (i.e., Stiffness Damage Test) techniques for improving the current understanding of the impact of reinforcement (e.g., restraint) on ASR physicochemical development and ultimately on the multi-level assessment outcomes.

This work is divided into a number of sections, with the core of the document corresponding to five scientific papers covering specific but complementary themes of the research. In order to make the content of this paper-based PhD thesis clearer to readers, initially section 1 introduces the global context and the structure of this document. A brief literature review of the current state-of art on the diagnosis and prognosis of ASR affected unrestrained and reinforced concrete elements is presented in section 2. Next section (section 3) displays a problem statement and the objectives of the study. The following section (section 4) gives a summary of the global experimental program proposed to achieve the above objectives, which is followed by a summary of the scope and technical content of the five scientific papers (section 5). Later, after conducting all required testing procedures and analyzing their results, the draft of five scientific papers are presented in sections 6 to 10. It is worth noting that the following papers have currently been submitted/published: a) first paper (Microscopic Assessment of ASR-Affected Concrete Under Restraint Conditions) has been peer-reviewed and published (April 2021) in Cement and Concrete Research Journal (Volume 145, pp.106456); b) second paper (Evaluation of the induced mechanical deterioration of alkali-silica reaction affected concrete under distinct restraint conditions through the Stiffness Damage Test) has been peer-reviewed and published (November 2021) in Cement and Concrete Composites Journal (Volume 126, pp.104343); c) third paper (Overall Assessment of Alkali-Silica Reaction Affected Concrete Under Restraint Conditions: Reactive Sand Versus Reactive Coarse Aggregate) has been submitted to the journal of Cement and Concrete Research and it is currently under evaluation; d) fourth paper (Improving the Knowledge of Visual Inspection on ASR Affected Concrete Under Various Restraint Conditions) has been submitted to the journal of Construction and Building Materials. The fifth and last paper is anticipated to be submitted over the fall 2021 to the journal Cement and Concrete Research.

Finally, based on the results gathered in this work, a series of future works, scientific contributions as along with conclusions and recommendations were prepared and are presented in sections 11, 12 and 13 of this document, respectively.

1. INTRODUCTION

Alkali-aggregate reaction (AAR), a chemical reaction between certain mineral phases from the aggregates and the alkali hydroxides from the pore solution of concrete, is one of the most important distress mechanisms affecting concrete infrastructure around the world [1]. AAR is generally divided into two main reaction types: Alkali-Silica Reaction (ASR) and Alkali-Carbonate Reaction (ACR). ASR is undoubtedly the most common reaction type identified worldwide and is the deterioration mechanism selected for this research. Over the past decades, a number of test protocols and recommendations have been developed, including a variety of laboratory test procedures to appraise the potential alkali reactivity of aggregates and the validity of preventive measures such as controlling the concrete alkali content, using supplementary cementitious materials (SCMs), etc., before their use in concrete. Currently, most researchers agree that, in general, building concrete infrastructure with low risk of ASR is possible. However, there is still no general agreement on the implementation of effective methods to mitigate ASR-affected structures in the field.

Several test protocols have been developed/optimized to assess the condition of critical infrastructure to determine the cause and extent of damage (i.e., diagnosis) and the potential of further distress (i.e., prognosis) of ASR-affected concrete. Those are critical steps in optimizing the rehabilitation methods and efficient application periods for ASR-affected concrete infrastructure. Amongst the proposed techniques, the multi-level assessment conducted through the use of the Stiffness Damage Test (SDT) and the Damage Rating Index (DRI) (respectively mechanical and microscopic procedures) showed to be quite suitable to appraise ASR-induced expansion and deterioration in concrete under unrestrained (i.e., free expansion) conditions [2,3] which does not reflect the real scenario of reinforced concrete members in the field [4,5]. Moreover, the use of Residual Expansion (RE) test methods has been widely used to investigate the potential of further deterioration of ASR-affected structures with more or less efficiency, depending on the structure type and condition [6]. Although few recent works have suggested the efficiency of the multi-level assessment and RE methods to appraise the condition of affected aging infrastructure [7–10], there is currently a lack of "quantitative" information on the effects of confinement (e.g., reinforcement) on ASR-induced physicomechanical development (i.e., kinetics and induced expansion, damage generation and propagation, crack pattern and orientation) and ultimately on the multi-level and RE outcomes. Therefore, this study aims to focus on a detailed laboratory investigation to assess the current and future condition of ASR-affected concrete blocks incorporating different reactive aggregate types (i.e., fine and coarse), displaying distinct reinforcement configurations (i.e., none, 1D and 2D) and expansion levels (i.e., 0.08% and 0.15%) through the use of the multi-level and RE test protocols. It is worth noting that the word "confinement" is defined in this work as any restraint provided by the reinforcement bars to ASR-induced development in a given direction.

1.1 References

[1] B. Fournier, M. Bérubé, Alkali–Aggregate Reaction in Concrete: a Review of Basic Concepts and Engineering Implications, Can. J. Civ. Eng. 27 (2000) 167–191. https://doi.org/10.1139/l99-072.
[2] L.F.M. Sanchez, B. Fournier, M. Jolin, D. Mitchell, J. Bastien, Overall assessment of Alkali-Aggregate Reaction (AAR) in concretes presenting different strengths and incorporating a wide range of reactive aggregate types and natures, Cem. Concr. Res. 93 (2017) 17–31. https://doi.org/http://dx.doi.org/10.1016/j.cemconres.2016.12.001.
[3] L.F.M. Sanchez, T. Drimalas, B. Fournier, D. Mitchell, J. Bastien, Comprehensive damage assessment in concrete affected by different internal swelling reaction (ISR) mechanisms, Cem. Concr. Res. 107 (2018) 284–303. https://doi.org/10.1016/j.cemconres.2018.02.017.
[4] L.F.M. Sanchez, B. Fournier, M. Jolin, J. Duchesne, Reliable quantification of AAR damage through assessment of the Damage Rating Index (DRI), Cem. Concr. Res. 67 (2015) 74–92. https://doi.org/10.1016/j.cemconres.2014.08.002.
[5] L.F.M. Sanchez, B. Fournier, M. Jolin, M.A.B. Bedoya, J. Bastien, J. Duchesne, Use of Damage Rating Index to quantify alkali-silica reaction damage in concrete: Fine versus coarse aggregate, ACI Mater. J. 113 (2016) 395–407. https://doi.org/10.14359/51688983.
[6] V.E. Saouma, Diagnosis & Prognosis of AAR Affected Structures, State-of-the-Art Report of the RILEM Technical Committee 259-ISR, 2020.
[7] L.F.M. Sanchez, B. Fournier, D. Mitchell, J. Bastien, Condition assessment of an ASR-affected overpass after nearly 50 years in service, Constr. Build. Mater. 236 (2020) 117554. https://doi.org/10.1016/j.conbuildmat.2019.117554.
[8] R. Rivard, Quantitative Petrographic Technique for Concrete Damage Due to ASR : Experimental and Application, (2000) 63–72.
[9] M. Thomas, K. Folliard, B. Fournier, P. Rivard, T. Drimalas, Methods for Evaluating and Treating ASR-Affected Structures: Results of Field Application and Demonstration Projects I, Report No. FHWA-HIF-14-0002, Federal Highway Administration, U. S. Department of Transportation, Washington, DC, 2013.
[10] B. Fournier, A. Bérubé, J. Folliard, M. Thomas, Report on the Diagnosis, Prognosis, and Mitigation of Alkali-Silica Reaction (ASR) in Transportation Structures, Report No. FHWA-HIF-09-004, Federal Highway Administration, U. S. Department of Transportation, Washington, DC, 2010.

2. LITERATURE REVIEW

2.1 ASR distress mechanism in concrete under free expansion

ASR is a complex physicochemical reaction between the alkali hydroxides (i.e., Na^+, K^+, OH^-) from the concrete pore solution and certain unstable mineral phases found in the aggregates used to make concrete; ASR produces a secondary reaction product (ASR gel) that swells upon moisture uptake, leading to expansion and cracking of the affected material [1–3]. ASR-induced expansion generates tensile stresses within the reactive aggregate particles along with compressive stresses at the particles' edges [4,5]. Hence, ASR cracks are initially generated within the aggregate particles and propagate to the cement paste with the increase in induced expansion [6,7]. Moreover, the ITZ often remains intact during ASR development, except in locations close to the radial cracks formed within the particles (Figure 1) [8,9]. The degree of deterioration of ASR-affected concrete is normally expressed by its level of expansion; although the relationship between expansion and deterioration is not necessarily linear, it is anticipated that the higher the expansion level, the higher the overall deterioration (i.e., loss of mechanical properties, physical integrity and stiffness) of affected concrete [10,11].

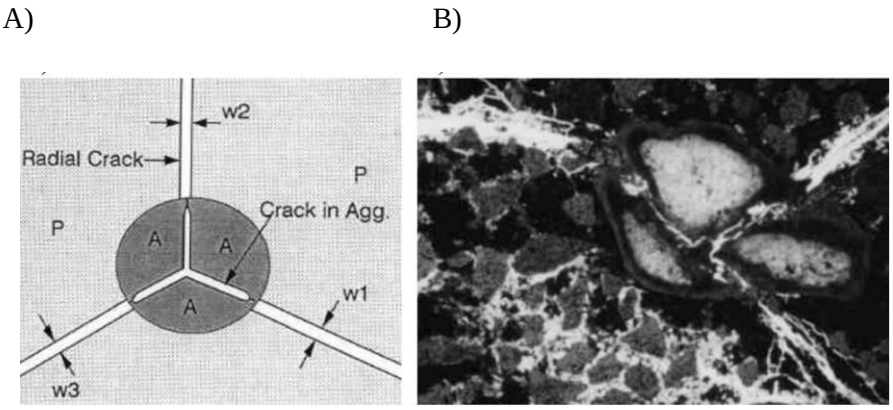

Figure 1: Signatures of concrete damage due to alkali–silica reaction (ASR): A) a model and B) 2 mm size aggregate under thin section microscopy [6] *(Reproduced with permission of Elsevier)*.

Regardless of the aggregate type, Sanchez et. al. [12] developed a qualitative and descriptive model to describe ASR-induced damage generation and propagation under unrestrained conditions (Figure 2) [12]. At low expansion levels (e.g., 0.05%), sharp and onion skin type cracks (represented by A and B in Figure 2, respectively) are generated within the reactive aggregate particles. As the reaction progresses, not only are new cracks formed in the aggregate particles but, more importantly, the previously developed cracks increase in length and width and may even begin to slightly extend into the cement paste at moderate expansion levels (e.g., 0.12%) [13,14]. As ASR continues to further develop, the previously formed cracks reach the cement paste at both ends of the aggregate (e.g., 0.20% of expansion), which drastically impacts

the physical integrity and mechanical properties of the affected material [10]. Finally, at very high expansion levels (e.g., 0.30%), cracks developed at distinct aggregate particles start linking together, which creates an important crack network in the affected concrete, thus further reducing its durability and mechanical properties [12]. Although the aforementioned model was shown to be quite accurate to describe ASR-induced damage development under free expansion, its suitability to describe ASR-induced damage generation and propagation under restrained conditions is still unknown and should be further investigated.

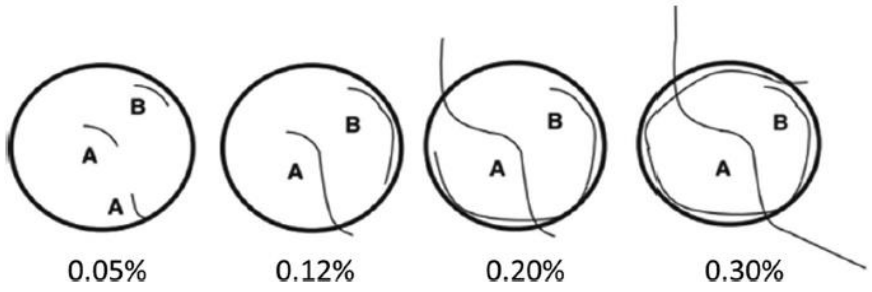

Figure 2: Qualitative model of crack propagation in ASR-affected concrete [12] *(Reproduced with permission of Elsevier).*

2.1.1 ASR gel production

Recently, several studies have been conducted to simplify the mechanism of ASR and explain the fundamentals of this reaction (e.g., [15–18]), where they commonly agreed that the reactive aggregate is simply represented by their metastable silica components (SiO_2). According to Varsheneya and Mauro [19], the interior part of the latter are mainly composed of a network of tetrahedral SiO_2 with one silicon atom is surrounded by four Oxygen atoms which are connected by the Oxygen vertices to form siloxane (≡Si–O–Si≡) bonds ("≡" indicate that each Si atom is connected to 3 other oxygen atoms). The exterior part of the abovementioned network ends with either Si^+ or O^- ions which cause siliceous material to be unstable [20,21], in which the hydrolysis takes place on the surface when such unstable material is exposed to water as per reaction 1[21]. Later, the siloxane bonds have been progressively attacked by the hydroxyl ions (OH^-) in an alkaline environment of pore solution to dissolve silica and form $Si(OH)_4$ following reaction 2 and as per Figure 3 [16,20,21].

$$(\equiv Si^+, \equiv Si - O^-)_S + H_2O \leftrightarrow 2(\equiv Si - OH)_S \qquad \text{Reaction 1}$$

$$(\equiv Si - OH)_S + 3(OH^-)_{aq} \leftrightarrow (Si(OH)_4)_{aq} \qquad \text{Reaction 2}$$

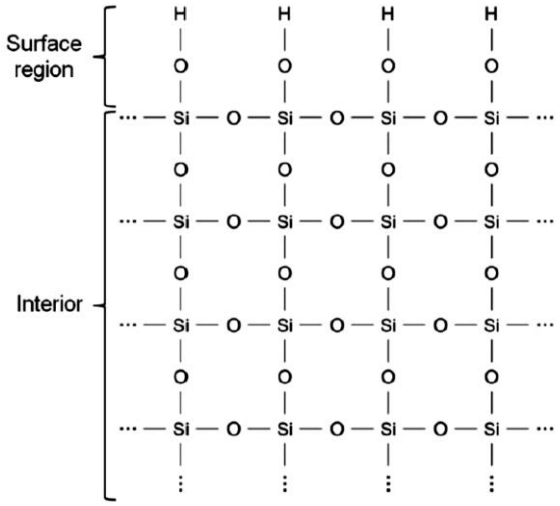

Figure 3: schematic diagram of silica structure that has undergone surface hydrolysis [21].

Hereafter, the alkali ions from the cement paste could replace hydrogen in $Si(OH)_4$ as per reaction 3 which is typically known as ion exchange, where A stands for alkalis (i.e., Na and K):

$$(Si(OH)_4)_{aq} + A^+ \leftrightarrow ((OH)_3 \equiv \mathrm{Si} - O^- - A^+)_{aq} + H^+{}_{aq} \qquad \text{Reaction 3}$$

Subsequently, the products of reaction 3 join together and undergo the condensation process as per reaction 4 and form nano-colloidal silica sol. This step is a very time-consuming process at high pH, since one of those reactants needs to donate one OH^-, which is a huge barrier due to the high concentration of hydroxyl ions in the aqueous solution.

$$2\,((OH)_3 \equiv \mathrm{Si} - O^- - A^+)_{aq} \leftrightarrow 2\,((OH)_3 \equiv \mathrm{Si} - O^- - A^+)_{sol} + H_2O \qquad \text{Reaction 4}$$

Lastly, the silica gel with a three-dimensional network could be formed through the polymerization process, however the presence of alkali ions would reduce the kinetics of condensation and polymerization. Conversely, the presence of calcium could significantly increase the kinetics of the condensation and polymerization of the silica species [22]; calcium from the pore solution could replace alkalis incorporated in silica gel which recycled the alkali ions back into the concrete pore solution and thus maintain a high pH in the latter [23], as per reaction 5. According to Rajabipour et al. [16], the final product of reaction 5 could be alternatively written as $H_6CaSi_2O_8$ or CS_2H_3 in cement chemistry notation.

$$2\,((OH)_3 \equiv \mathrm{Si} - O^-)_{aq} + Ca^{2+} \leftrightarrow ((OH)_3 \equiv \mathrm{Si} - O - \mathrm{Ca} - \mathrm{O} - \mathrm{Si} \equiv (OH)_3)_{sol} \qquad \text{Reaction 5}$$

Unlike the several studies conducted on the effect of calcium on ASR gel, there is still no agreement amongst researchers on the exact role of calcium in suppressing or escalating ASR deterioration [24]. On one hand, several authors suggested the essentiality of calcium for the formation of the ASR gel; the presence of calcium is necessary for the alkali silicate species condensation which leads to the gelation [25,26]. On the other hand, a few works observed the mitigation nature of calcium where a calcium-rich gel could be considered as non-swelling gel [24,27,28]. This clearly suggests that the mere presence of ASR gel does not always result in concrete deterioration; according to Kawamura and Iwahori [29], the different chemical compositions of ASR product can play an important role for the latter to be considered deleterious or innocuous.

2.1.2 Characteristics of ASR gel

ASR gel has a general composition of $(SiO_2)\cdot(Na_2O)_n\cdot(K_2O)_k\cdot(CaO)_c\cdot(H_2O)_x$, known as alkali–calcium–silicate–hydrate [30–34] (Figure 4). Although ASR gel consists of various chemical elements, the most important compositional parameters of an ASR gel are the atomic ratios of Ca/Si, K/Si, Na/Si and (Na + K)/Si, as per several authors (e.g., [7,31,35]). After reviewing several available literatures on the composition of ASR gel obtained from the laboratory made concrete/mortar specimens (e.g., [35–38]) as well as those retrieved from the real structures (e.g., [36,39–43]), the author concluded that the chemical composition of ASR gel in most of the studies comprise as follow: $0 < Na/Si < 0.55$, $0 < K/Si < 0.45$, $0 < Ca/Si < 1.2$, , $0.1 < (Na + K)/Si < 1.2$. Such a wide range of chemical compositions of ASR gel could clearly confirm that those ASR products with only certain compositions can be considered deleterious while other compositions might be innocuous. A deleterious gel is the one that has a high hydrophilic potential as well as a high free and restrained swelling capacity [32,33,44]. The free swelling capacity of ASR gel is the ability of the latter to swell when there is no resistance against its expansion, while the restrained swelling capacity is a measure of how much confining pressure the gel could withstand prior to flowing into adjacent capillary pores and microcracks of the surrounding paste [32,33,44]. As per Gholizadeh et al. [31–33], those hydrophile and expansive ASR gels, and at the same time have a high viscosity could be considered as the most deleterious ASR product [31–33]. Prezzi et al. [45] described the role of monovalent (i.e., Na^+ and K^+) and divalent (i.e., Ca^{2+} and Mg^{2+}) cations on the swelling behavior of ASR gel through the use of electric double-layer theory. The authors [45] suggested that relatively high swelling pressures in ASR gel can be observed after a diffuse layer containing monovalent cations offsets the negative charges on silica particles. Otherwise, Kawamura et al. [29] and Gholizadeh et al. [32] observed that a diluted ASR gel contained a high amount of alkali could expand freely, yet they might not be able to impose deleterious pressure to its surrounding environment because of slightly low viscosity which make them flow easily and relieve their stress.

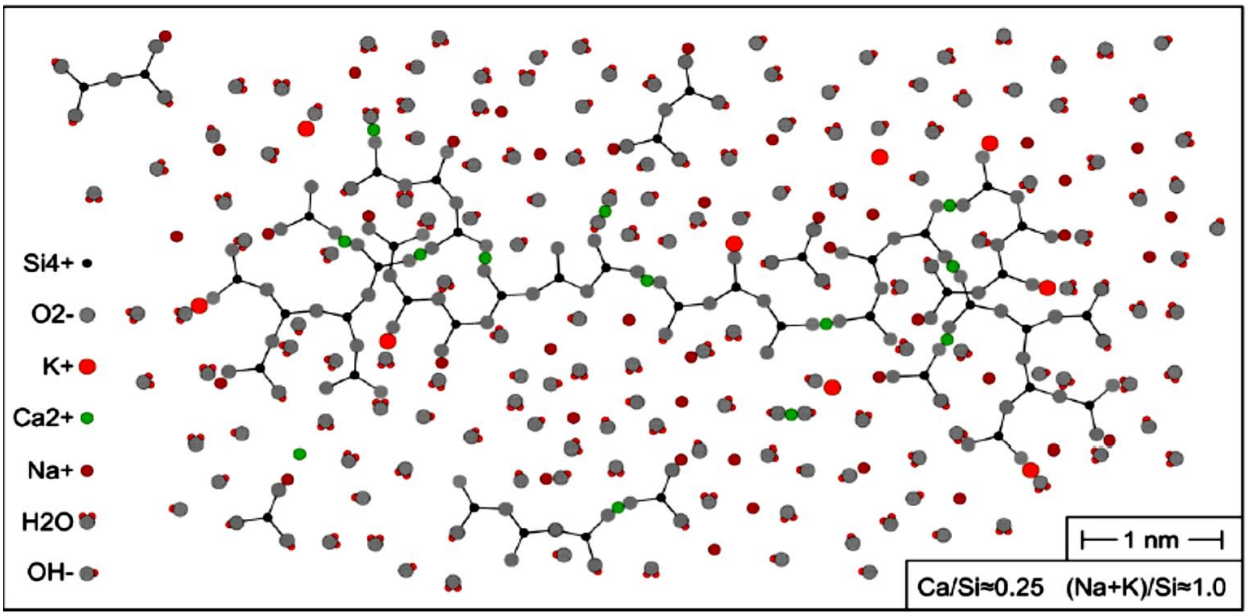

Figure 4: Schematic molecular model of a typical alkali-silica reaction gel [46] *(Reproduced with permission of Elsevier).*

Viscosity is the most important rheological property of ASR gel [32]; viscosity is generally known as the internal resistance of a fluid to flow [47]. Previously, several computer models have been developed for simulating the kinetics and mechanisms of ASR expansion [48–51]. Most of those assumed that ASR gel is a Newtonian fluid that could flow immediately upon formation into the bulk cement paste in the close vicinity of the aggregate particles. However, as per Gholizadeh et al. [32], ASR gel is deemed to display a non-Newtonian yield stress behavior where the latter showed an elastic behavior until the stress exceeds a certain limit. A direct way to measure the yield stress and thus the viscosity of ASR gel obtained from real concrete structures as well as laboratory made specimens has not yet been found, therefore, researchers intended to use synthesized ASR products which have been proved to have an identical molecular and nanoscale structures as the one retrieved from in-service concrete [52]. The studies on the synthesized gels with various chemical compositions, once again attested that monovalent and divalent cations are playing a crucial role in the various rheological properties of those gels [21,31,33]. As such Rajabipour et al. [16], suggested that increasing trend of calcium in ASR gels may increase the viscosity and yield strength of those gels.

The above information clearly confirms the effects of chemical composition and their molar ratio (primarily Ca/Si and Na or K/Si) on the rheological (e.g., yield stress) and swelling properties of ASR gels. As such, Gholizadeh et al. [32] proposed that the gel having intermediate calcium and high sodium contents could represent an ASR gel with the highest swelling capacity. Likewise, such chemical composition and molar ratios could significantly change the mechanical properties of ASR gel [44,53]. As such, those gels with

lower calcium and higher alkali content (i.e., generally could be found in the center of aggregate particles with a crystalline structure [20,30,34,35,53]- Figure 5), showed to have significantly lower modulus of elasticity and hardness compared to those have higher calcium and lower alkali content (i.e., can be found either at the edge of the aggregate particles or cement paste with amorphous structure- Figure 5) [30,53]. Accordingly, Leemann et al. [30] observed that the modulus of elasticity and Vickers hardness of crystalline ASR gel are range from 9-11 GPa and 13-18, respectively, while those properties increase significantly for the amorphous product to maximum values of 45 GPa and 270, respectively. Moreover, after reviewing the available literature investigating the modulus of elasticity of ASR gel [30,38,43,53–55], the authors observed a large variation among distinct works; while a range of 5-40 GPa was reported by Wu et al. [38] and Hu et al. [53], Zhang et al. [43] found that the modulus of elasticity of ASR gel is around 65 GPa. Such a huge variation in the modulus of elasticity of ASR gel could be attributed to the complex nanostructures of the latter (e.g., pores, defects, and cracks) or even the different testing procedures that they have used.

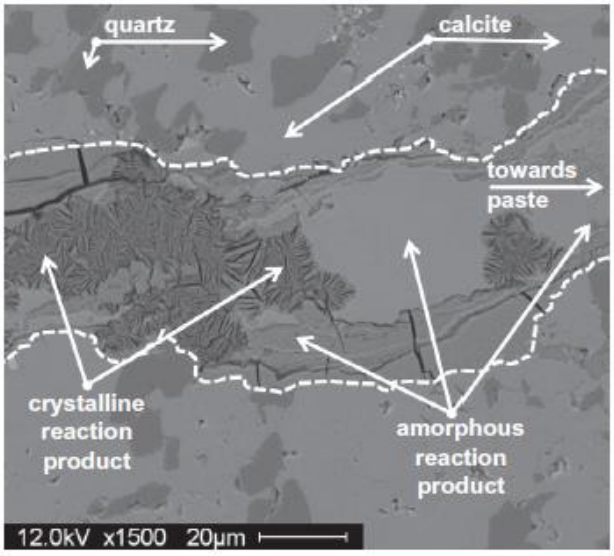

Figure 5: ASR product morphology: a rosette-like (or plate-like) micro-texture in the center of reactive aggregate particles and amorphous structure at the edge of the aggregate particle [30] *(Reproduced with permission of Elsevier)*.

2.2 ASR effects on the mechanical properties of affected concrete under free expansion

Conventional "sound" concrete is known to have a relatively high compressive strength and modulus of elasticity, yet a low tensile strength. However, the aforementioned mechanical properties may significantly change over time whether concrete is affected by damage mechanisms [10,11,56–59]. Therefore, understanding the impact of deterioration mechanisms on the mechanical properties of affected concrete is crucial while assessing the condition of aging infrastructure [60].

Research studies have shown a significant reduction of tensile strength (i.e., down to 65%- Figure 6A) and modulus of elasticity (i.e., down to 50%-Figure 6B) at low/moderate expansion levels (i.e., from 0.05% to

0.12%) in ASR-affected concrete [10]. Conversely, compressive strength only becomes significantly affected at high (i.e., 0.20%) or very high (i.e., 0.30%) expansion levels [1,10,58,61]. For instance, Esposito et. al. [59] and Ono [62] demonstrated that the reduction in compressive strength of ASR-affected concrete can be as high as 40–60% at expansion levels higher than 0.30%. Conversely, other studies reported a limited impact of ASR on the compressive strength of affected concrete [16–18]; this is attributed to the low reactivity of the aggregates used in the concrete mixtures which could likely not generate high levels of expansion [9].

The reduction of modulus of elasticity in ASR-affected concrete is influenced by the stiffness of the aggregate particles. ASR cracking is more likely to develop at the microscopic level within the aggregate particles; thus, stiffness reduction can be already observed at low expansion levels (i.e., 0.05%). Likewise, a significant reduction in tensile strength is verified at the early stages of ASR (i.e., from 0.05% to 0.12%) since porous media such as concrete are dependent on the existence and importance (i.e., size) of cracks as per fracture mechanics concepts. Thus, "stress concentration" peaks are developed at the tips of ASR-induced cracks in affected concrete under tension, leading to crack propagation and eventually failure [10]. On the other hand, the mechanism of failure in compression is much more ductile, being characterized by the failure of the "cement paste", where cracks are initially formed at the interfacial transition zone (ITZ) at distinct locations, propagating to the bulk cement paste and connecting to one another at later stages, causing instability and ultimately failure of the system [63]. Thus, since ASR-induced cracks are initially formed within the aggregate particles and only extend to the cement paste at later stages, ASR development causes a progressive compressive strength loss of affected concrete [10].

A)

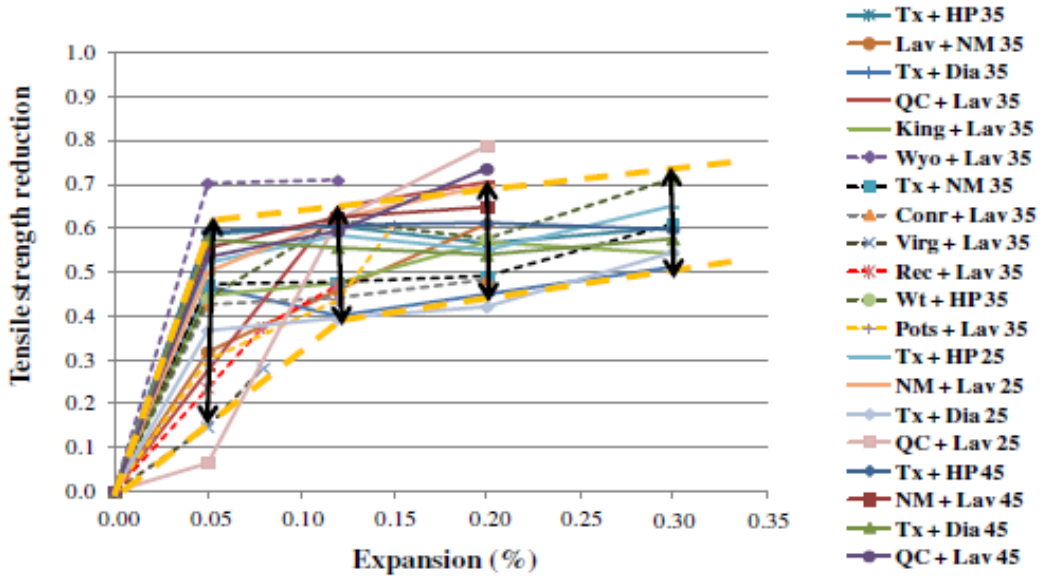

B)

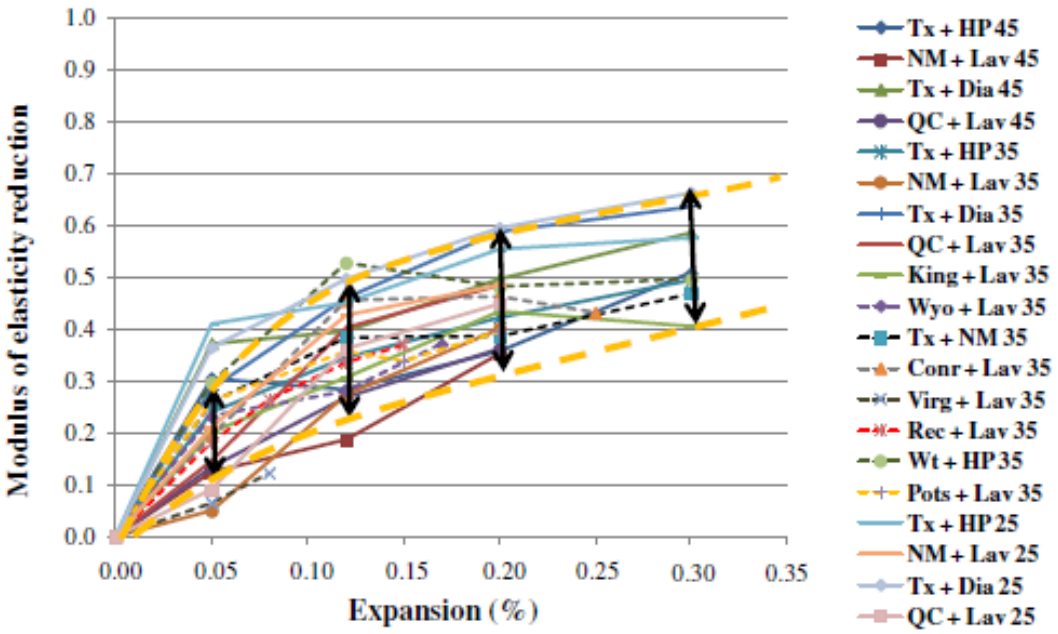

Figure 6: Mechanical properties reduction of ASR affected concrete. A) Tensile Strength reduction B) Modulus of Elasticity reduction [10] *(Reproduced with permission of Elsevier)*.

2.3 Effects of confinement on ASR-induced expansion

Although the vast majority of existing research on ASR has been performed using laboratory specimens under unrestrained (i.e., free expansion) conditions [10,56,61], a few works have been conducted to understand the effect of confinement on ASR-induced development. Some of these studies [64,65] observed no to negligible ASR-induced expansion in restrained directions; moreover, no transfer of induced

expansion and thus deterioration has been noticed to directions with less or no confinement [55,66]. However, according to Morenon et. al. [67] and Multon et. al. [68,69], the reduction of ASR-induced expansion in the confinement direction directly yields a transfer to unrestrained directions. The same observation has been made by a number of researchers [65,70–74]. These conflicting results can be attributed to numerous reasons, such as the specimen size (i.e., scale effect), casting direction, confinement ratio and orientation [75]. Generally, it is agreed that confinement helps to mitigate ASR-induced expansion of affected concrete [68]; accordingly, it has been observed that restrainment may decrease from 15 to 70% ASR-induced expansion in the direction of confinement [67,68,73,74,76]. Therefore, such an expansion reduction in the restrained direction results in anisotropic development of ASR-induced damage; the higher the ASR-induced advancement, the higher the anisotropic behaviour [77]. The latter means that the use of an average induced expansion (i.e. average value from distinct directions) observed in concrete members with non-symmetrical reinforcement configurations is not appropriate for analysis in most cases [73–75]. Moreover, anisotropy of ASR-affected restrained concrete could lead to major deformations [77]. As such, Allard et. al. [77] reported that heavily reinforced thick slabs displaying non-symmetrical configurations with a rectangular cross section deformed into trapezoidal sections after moderate to high (i.e., 0.20%) average ASR-induced expansion.

The ‘‘expansion transfer’’ phenomenon was initially reported on uniaxial specimens with two unrestrained directions [78]. They performed “the classical analysis” on ASR-induced expansion measurements where the transfer of expansion from restrained to both stress-free directions are equal. Although ASR-induced expansion of specimens under 3D confinement is reduced [79], “the classical analysis” cannot point out conclusions about real ASR-induced expansion [80]. Therefore, to have a more reliable assessment, investigating the multiaxial stress state of affected concrete is essential. Accordingly, Multon and Toutlemonde [68] carried out the ASR expansion measurements on the axially loaded concrete specimens restrained by steel rings in the radial directions (Figure 7). Although very promising, the specimens do not represent the real scenario of concrete under a multiaxial stress state, where the lateral confinement was only activated when concrete expanded laterally. Thus, the conclusion regarding the volumetric expansion may not be accurate and could not apply to concrete structures in which concrete has been subjected to stresses even before the reaction takes place [80].

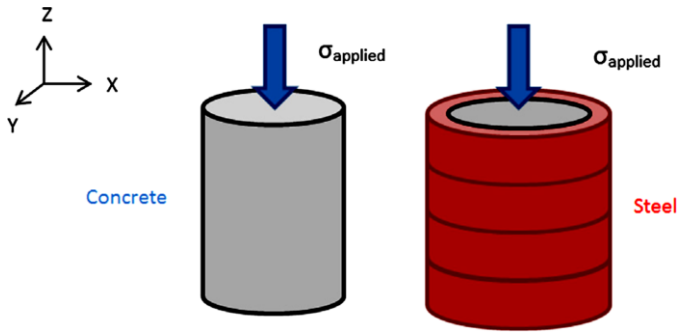

Figure 7: Scheme of Multon's [68] tests [67] *(Reproduced with permission of Elsevier)*.

2.3.1 Effects of confinement on ASR-induced crack orientation and mechanical properties

Although several studies have been carried out on the mechanical properties of ASR-affected unrestrained concrete [10,61], not many have considered the effects of confinement on the ASR-affected reinforced members [56,75]. Despite the fact that reinforcement could restrain the expansion caused by ASR, understanding of the effects of ASR on the structural behaviour of restrained concrete members is limited or often contradictory. Thus, improving the current knowledge on the rate of losses in mechanical properties is essential for a more reliable assessment of ASR-damaged concrete structures [81].

The progression and orientation of the induced cracks are significantly influenced by the boundary conditions and the reinforcement configuration of ASR-affected concrete structures/structural members. Confined reinforced concrete elastically restrained in the reinforcement direction causes tensile stresses in the reinforcement bars; thus, ASR-induced expansion is mostly suppressed in the main reinforcement direction [82]. Hence, most of ASR induced cracks in reinforced concrete members tend to be generated parallel to the main rebars [77,81–83] as observed by Hansen et. al. [84] in laboratory and field structural members.

Although limited, some works have addressed the effect of confinement on ASR-induced development and the reduction of mechanical properties such as compressive strength [67,75,83,85–88]. Some of these studies [86] observed little to no difference in the compressive strength of cores extracted perpendicular and/or parallel to the main confinement direction of ASR-affected concrete. Conversely, others have reported significant differences [67,75,83,85]: i.e., cores extracted perpendicular to the main confinement direction demonstrated significantly lower compressive strength than those cored parallel to the main reinforcing bars, with differences in the range of 7-35% [67,75,83,85]. Moreover, it has been verified by some authors that the modulus of elasticity is more sensitive to the confinement ratio and configuration, and crack orientation than the compressive strength [87]. Jones [89] observed that the modulus of elasticity of cores extracted perpendicular to the main confinement direction was significantly lower than those cored parallel to it. Such an observation can be due to the presence of higher amount of ASR cracks in cores

extracted perpendicular to the main confinement [90–92]. Likewise, Gautam et al. [87], after conducting research on the effect of distinct multi-axial stress applications (none, uniaxial, biaxial and triaxial) on the mechanical degradation of ASR affected concrete, observed that concrete members under triaxial conditions display lower mechanical degradation than all the other multi-axial stress applications.

Few works have been conducted on the impact of confinement on the distinct ASR petrographic distress features and crack orientation of reinforced members [83,85,86,93]. Barbosa et.al. [83] noticed various crack patterns and orientations on distinct concrete cores extracted from affected structures; in this work, cores were retrieved from bridge slabs in distinct directions (i.e., vertically and horizontally), where ASR-induced cracks perpendicular to loading were observed in vertically cored specimens (Figure 8A) while a network of cracks parallel to loading was noticed in the horizontally cored specimens (Figure 8B). Accordingly, cores extracted from distinct directions of affected concrete behave quite differently during compressive strength tests; several "splitting" cracks are generated perpendicular to the ASR-induced cracks over loading in vertically cored specimens (Figure 8A), while "inclined shear" cracks are formed in cores retrieved horizontally (Figure 8 B). Hence, it is expected that cores extracted from ASR-affected structures in distinct directions and displaying different cracks patterns and orientations present distinct mechanical responses.

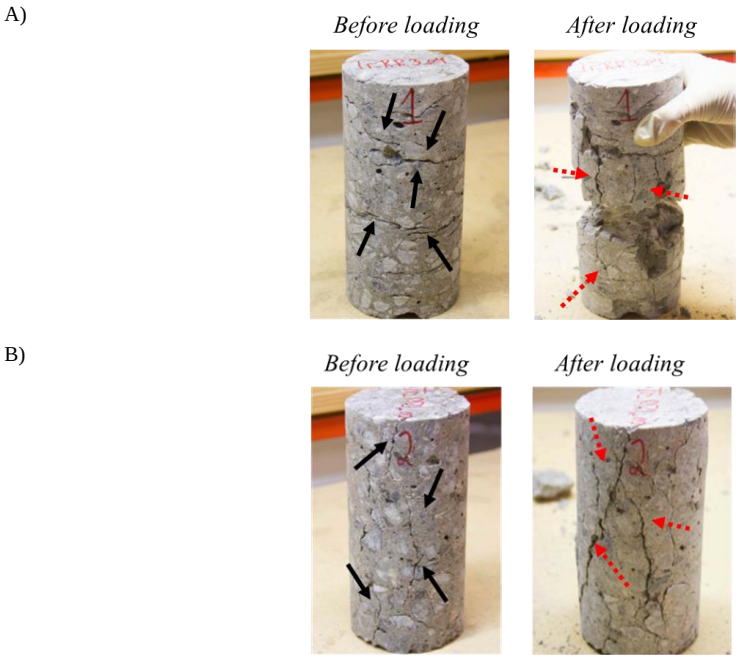

Figure 8: Distinct cracking orientation on A) vertically extracted core and B) horizontally extracted core having ASR induced cracks before loading (black arrows) and after loading (dashed red arrows) [83] *(Reproduced with permission of Elsevier).*

Moreover, very few studies [81,84] were performed to investigate the effects of different reactive aggregate types (i.e., fine vs coarse aggregate) on the development of ASR-induced deterioration in restrained concrete. Barbosa et. al. [81] and Hansen et. al. [84] observed that concrete members incorporating reactive fine aggregates displayed a much more pronounced deterioration degree when compared to those incorporating reactive coarse aggregates; moreover, the authors also reported significantly wider cracks in ASR-affected members bearing reactive fine aggregates. No further explanation has been addressed in this regard.

Although the current literature data are very useful and demonstrate the effect of reinforcement on the physicochemical development of ASR, to the best of the authors' knowledge, there is still a need to systematically and quantitatively evaluate this effect on the microscopic distress features and mechanical response of concrete samples having various reinforcement conditions, exhibiting different expansion levels and incorporating different reactive aggregate types (i.e., fine versus coarse aggregates).

2.4 Assessment of cause and extent of damage

As previous studies [94–97] have suggested, establishing a correlation between the ASR damage features and the reductions of mechanical properties and durability of the affected concrete members, is one of the biggest challenges for engineers. Therefore, a number of test protocols have been developed to determine the induced expansion and damage attained to date in the different locations of the structure (i.e., diagnosis). Among those, a comprehensive multi-level protocol (i.e., coupling of microscopic and mechanical test procedures, particularly the Stiffness Damage Test (SDT) and Damage Rating Index (DRI) respectively), are the most common and considered to be reliable.

2.4.1 Stiffness Damage Test (SDT)

The Stiffness Damage Test (SDT) is a mechanical and cyclic test procedure used to assess the condition of concrete affected by internal swelling reaction (ISR) mechanisms (e.g., ASR) [10,98]. The SDT was initially developed by Walsh who observed a good correlation between the crack density and the cycles of loading/unloading (i.e., stress/strain relationship) of rock specimens [99]; Crouch then adapted this procedure for concrete specimens in 1987 [100]. The test procedure, which is based upon five compression cycles of concrete specimens (cylinders or cores), was initially performed using fixed loads of 5.5 (Chrisp et. al. [101,102]) or 10 MPa (Smaoui et. al. [103]), at the loading rate of 0.10 MPa/s. The modulus of elasticity, dissipated energy (hysteresis area), plastic deformation (plastic strain) and the non-linearity index (NLI; the ratio of secant modulus at half of the maximum load and the secant modulus at the peak load) of the first and/or over the four last cycles were the selected outcomes of the test [98,104]. Later, Sanchez et al. [98,104] optimized the test procedure following an in-depth study using a wide variety of reactive aggregate types and concrete mixture proportions. Sanchez et al. [98,104] proposed that the SDT should be

performed using a percentage (40%) of the ultimate capacity (compressive strength) of the concrete under analysis instead of a fixed load; moreover, the authors suggested using indices as outcomes of the test procedure, namely the Stiffness Damage Index (SDI) and Plastic Deformation Index (PDI) to increase the diagnostic character of the test. The SDI and PDI represent, respectively, the ratio of dissipated energy to total energy, and plastic deformation to total deformation in the system (i.e., SI / (SI+SII) and DI / (DI+DII) over the five cycles as presented in [98,104,105] and Figure 2; where SI is the irreversible deformation energy, SII is the elastic deformation energy, and DI and DII represent the plastic deformation and elastic deformation, respectively, over the loading-unloading process). Moreover, the modulus of elasticity (average secant modulus of the 2nd and 3rd cycles) along with the NLI (Sec 1/Sec 2 in the first cycle and the average Sec1/Sec2 value of the last four cycles – Figure 2) as proposed by Chrisp et al. [101,102] were also considered efficient SDT outcomes for determining the damage extent and orientation (i.e., NLI is greater/lower than unity for cracks oriented perpendicular/parallel to loading) respectively, in affected concrete. Although, the SDT has been shown to be quite suitable to appraise ASR-induced expansion and deterioration in concrete under unrestrained (i.e., free expansion) conditions, the effect of confinement on mechanical properties reductions and SDT outcomes remains mostly unknown.

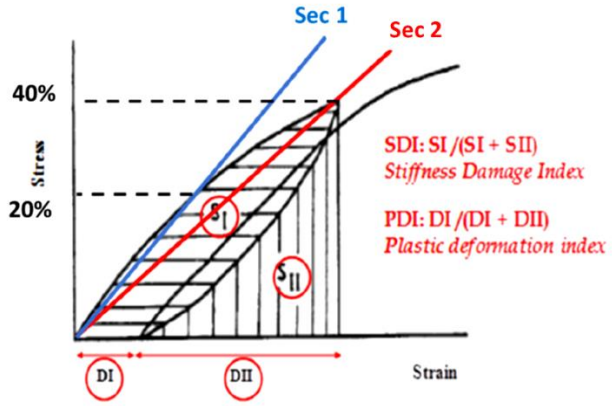

Figure 9: Calculation of the stiffness damage index (SDI) and Plastic Deformation (PDI) [105] *(Reproduced with permission of Elsevier)*.

2.4.2 Damage Rating Index (DRI)

Grattan-Bellew et. al. [106,107] proposed the Damage Rating Index method (DRI), a semi-quantitative microscopic tool used to appraise damage in concrete. Distress features are counted in 1 by 1 cm squares drawn on the surface of polished concrete sections using a stereomicroscope at 15-16x magnification. The damage features are then multiplied by weighing factors whose purpose is to balance their relative importance towards the corresponding distress mechanism (e.g., ASR), as proposed by Villeneuve & Fournier [108]. The DRI number is therefore calculated and the higher the DRI number, the higher the damage degree [10]. Ideally, a surface of at least 200 cm² should be assessed however, for comparative

purposes the final DRI value is always normalized to a 100 cm² area. DRI results are generally illustrated by the charts enabling easy visualization of the different distress features in affected specimens (Figure 10).

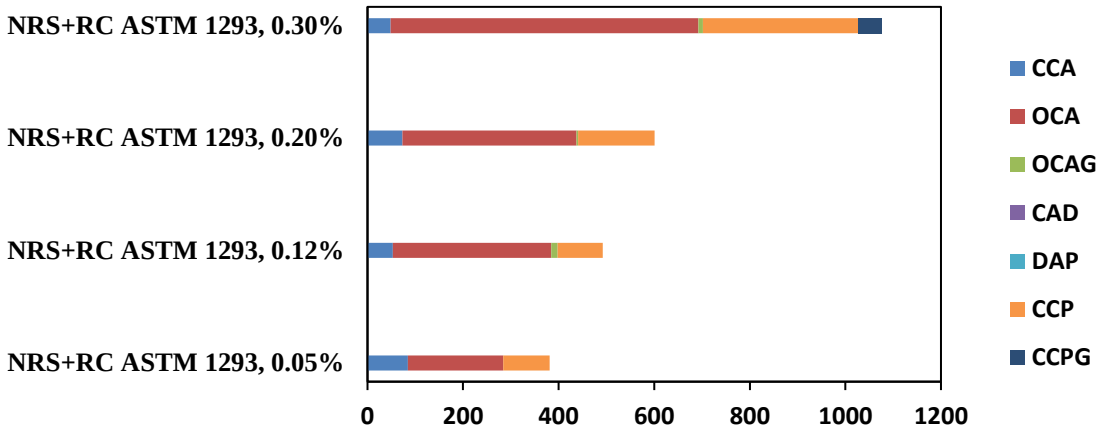

Figure 10: Example of DRI chart for damaged concretes with different levels of distress incorporating reactive coarse aggregate.

The petrographic features included in the DRI assessment are listed in Figure 11A along with their corresponding weighing factors; some of the distress features can be observed and identified in Figure 11B and Figure 12.

A

Petrographic features	Weighing factors
Cracks in aggregate (CCA)	0.25
Opened cracks in aggregates (OCA)	2
Crack with reaction product in aggregate (OCAG)	2
Coarse aggregate de-bonded (CAD)	3
Disaggregate/corroded aggregate particle (DAP)	2
Cracks in cement paste (CCP)	3
Cracks with reaction product in cement paste (CCPG)	3

B

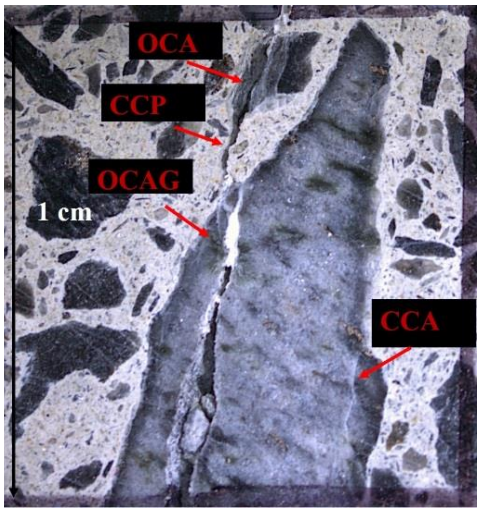

Figure 11: Damage Rating Index: A) Current weighing factors as per [108] and B) Micrograph illustrating a 1cm2 section where some of the petrographic features listed in A can be observed and identified *(Reproduced with permission of Elsevier)*.

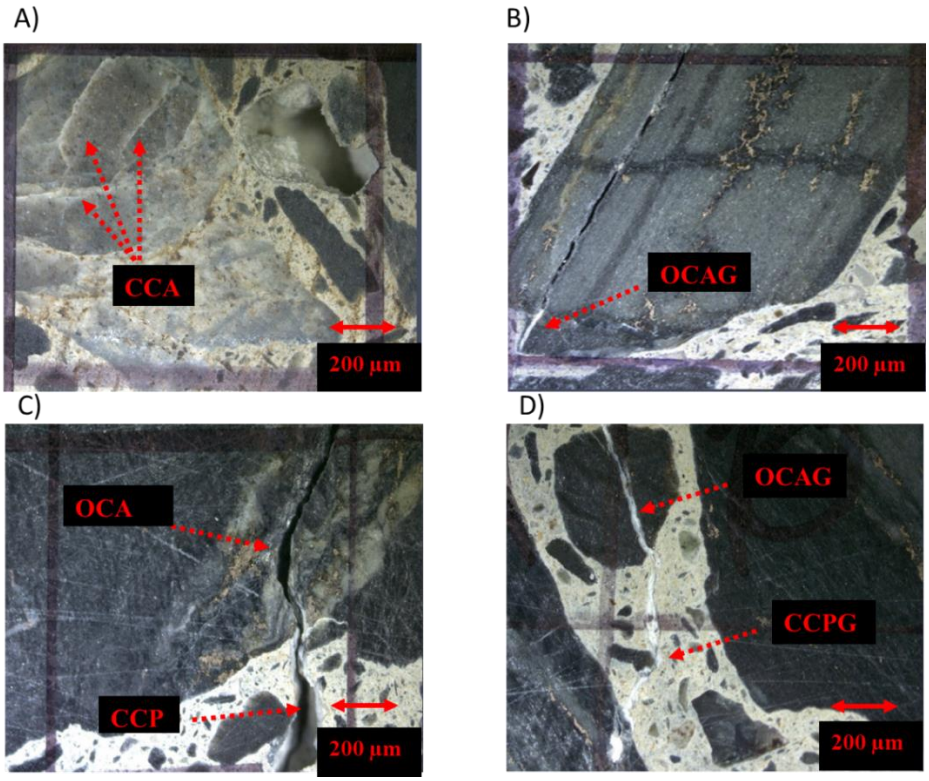

Figure 12: Petrographic features of ASR in concrete incorporating reactive coarse aggregates. The distance between the vertical lines is 1 cm as [108]. A. closed cracks in the coarse aggregate particle; B. opened crack with Gel in the coarse aggregate particle; C. open crack in the coarse aggregate particle propagates to cement paste, and D. cracks with reaction products in the coarse aggregate particles and the cement paste.

The proposed weighting factors as per Villeneuve & Fournier [108] aim not only to distinguish the importance of different types of features but rather reducing the variability between operators; for instance, the same weighing factor is given to a crack with or without reaction product (i.e., ASR gel) since its identification and interpretation may vary between operators [109]. Moreover, analyzing the distinct DRI petrographic features, one verifies that the closed crack in the aggregates (CCA) is a feature that may be caused by, for instance, ASR independent processes such as weathering or aggregates manufacturing; therefore a low importance is attributed to this feature (i.e., weighing factor of 0.25). Conversely, an increase in open cracks in the aggregate particles without or with gel (OCA and OCAG, respectively) is frequently observed as a function of ASR-induced development; thus, a weighing factor of 2 is given to such distress features. Lastly, a weighing factor of 3 is attributed to cracks in the cement paste without or with gel (CCP and CCPG, respectively), since those cracks reflect a more severely damaged concrete.

Besides the use of the conventional DRI method, Sanchez et. al. [12,110] proposed the utilization of supplementary petrographic analyses through the so-called “extended DRI version”, where the microscopic distress features presented in Figure 11 are evaluated in absolute (counts) and relative (%) manners, without the application of any weighing factors; it has been found that supplementary observations and evaluations

made through the extended DRI version may help towards a more comprehensive assessment and understanding of ASR-induced development of affected concrete. The extended DRI also allows the calculation of the crack density (CD), which represents the summation of the opened cracks in the aggregates and cement paste (with or without gel), in the system, and helps identifying the overall damage degree of the affected material. Finally, although the DRI has proven to be quite effective to appraise the extent of damage in ASR-affected concrete under unrestrained conditions, the effect of restraint on the ASR-induced petrographic distress features and thus DRI outcomes remains mostly unknown.

2.5 Potential for Further expansion of ASR affected concrete

As previously stated, monitoring the current condition and extent of damage, as well as the potential for future deterioration, are important for optimizing the rehabilitation strategies of ASR-affected concrete infrastructure. In order to better understand the potential of further damage in ASR-affected concrete, a combination of laboratory activities/investigations and field (in-situ) testing is proposed. The selection of the activities to be carried out will be depended on the condition and importance of the structure, the amount of time available to generate the data, and the degree of precision expected [111]. For instance, to develop a more comprehensive data for affected structures, obtaining data from in-situ monitoring of expansion is the most appropriate method. However, considering the seasonal and thermal effects, it will generally take a minimum of 2 to 3 years to obtain reliable data from that approach. Yet, detailed lab investigations on cores obtained from the structure will generate data in 6 to 12 months [111].

2.5.1 In-situ investigations

Detailed field investigations are carried out through site inspection and expansion, deformation and displacement measurements on the structure. Concrete members are regularly monitored by measuring their length change over time through the use of extensometers on installed metallic references/devices at the affected members' surface. Moreover, invar wires/rods and optical systems can also be used, with deformation measurements being performed and the data sent automatically to central servers for further treatment [111].

2.5.2 Detailed laboratory investigations

Laboratory investigations permit a relatively fast assessment of the concrete’s further potential expansion compared to the in-site monitoring of damaged structures. It also acts as an important tool to plan maintenance and costs involved. However, there are only few studies that deal with the subject up to date (e.g., [112–114]). This therefore causes several uncertainties on both the methodical approach for such measurements and the data analysis when compared to field structures exposed to complex environmental conditions [112,113]. Amongst the methods proposed to assess ASR-prognosis, the residual expansion

(RE) and Hot-Water Extraction (soluble alkali -SA) seems to be the simplest and most reliable procedures worldwide.

2.5.2.1 Residual Expansion (RE) Tests

As previously mentioned, the ability of laboratory procedures (i.e., RE test) to yield results in a relatively short period of time, e.g., 6 months to 1 year, promote them as fairly popular techniques for assessing the potential for further expansion of ASR-affected concrete (i.e., prognosis). Residual expansion tests derive from a generic concept that aims to assess the remaining expansion that might occur in affected structures [115]. Most RE tests are performed either under storage conditions of 38 °C and saturated air (100% RH) or in water or NaOH solutions [96]. Although RE test methods are quite easy and straightforward to be conducted, the vast majority of the results gathered from those tests have been found to be inaccurate when compared to the swelling behaviour of the respective structure in the field [96] and several potential issues have been raised with respect to adopted test setups (i.e. alkalis leaching or extremely aggressive solution). Moreover, concrete structures are often under different stress conditions (due to confinement effects, presence of reinforcement, loadings, etc.) when compared to laboratory tests, which make the physicochemical process to be different [116]. Another problem of the RE tests data analysis is the anisotropy between longitudinal and diametral expansions, which has often been observed and analyzed in detail [113,117]. Therefore, researchers aim to validate different test methods to obtain a more reliable testing protocol to predict the future of affected concrete elements, such as recovering aggregate particles from the cores extracted from the affected structures [116]. Even though the latter was found very promising, more reliable data is needed for the results obtained from that testing procedure to be considered reliable. Overall, while requiring further research, ‘‘classical” RE procedures have shown more reliable results both for laboratory research programs [113,115] and in-situ investigations [118,119]. Thus, the RE test's output is generally used to assess the prognosis of the affected structures and is sometimes used as input data in numerical tools to predict their mechanical behaviour [120].

2.5.2.2 Hot-Water Extraction (soluble alkali -SA)

As previously mentioned, in the presence of ASR, reaction products are formed that contain silica, calcium, and alkalis, which were originally present in the pore solution. As ASR progresses and more reaction products are formed, the alkali concentration in the solution progressively decreases, leading to the reduction of [OH^-] and the intensity of ASR. Some experiments suggest that ASR expansion in the presence of highly reactive natural aggregates can be minimized when the alkali concentration in the pore solution falls under 0.6N [NaOH + KOH] in the long term [2,111,121]. On the other hand, the higher the alkali concentration in the pore solution, the higher the OH- concentration (thus the pH), and the higher the risk for ASR. Therefore, the precise measurements of the above concentrations seem to be a promising tool to evaluate whether or not it is sufficiently high for ASR to maintain the deterioration process. The latter could

also play an important role in the process of selecting remedial actions. Moreover, since it is very difficult to extract pore solution from the concrete specimens, which could then be chemically analyzed for alkali and OH^- concentrations, an indirect way consists in measuring the active- or water-soluble alkali content of concrete, on a kg/m3 Na_2O_{eq} basis by subjecting a representative ground sample of concrete to hot-water extraction proposed by Rogers and Hooton [122] for the first time. Although very promising, the experimental variability of this test method is relatively high (i.e., 10 to 15%) even when using a control concrete, this may seem difficult to draw reliable conclusions from progressive measurements on the ASR damage development in a given ASR-affected concrete.

2.6 Tools for assessment of future damage caused by ASR

Recently, a number of test protocols have been developed to forecast the potential of ASR affected concrete for further distress over time (i.e. prognosis). Among the methods proposed to assess ASR-prognosis, the residual expansion techniques (RE) and Hot-Water Extraction (soluble alkali -SA) seem to be the simplest and the most widely used procedures around the globe.

2.6.1 Residual Expansion Test (RE)

As previously mentioned, Residual Expansion (RE) tests aim to assess the potential of further induced expansion that might occur in affected structures. Those tests are carried out on the cores extracted from ASR-affected structures and then the cores are monitored in terms of expansion over time. The specimens are stored in a controlled temperature (usually 38 °C for ASR) and moist environment in the laboratory and measured over one year. Usually, laboratory test setups and storage conditions are controlled, whereas concrete structures in the field are exposed to different environmental conditions. Therefore, the inner chemical reaction and swelling behaviour might be different under laboratory conditions, which may not represent the real scenario. Currently, to assess the residual expansion of ASR-affected concrete in Canada, two storage conditions are considered: a) 38ºC temperature and 100 RH and b) 38ºC temperature and 1M NaOH solution. Although these conditions may quickly trigger further ASR-development in the laboratory, the reliability of this approach is still unknown. It has been suggested that some RE laboratory conditions such as very aggressive and unrealistic environments (e.g., 1M NaOH), alkali leaching and stress relaxation (i.e., specimens are under non-restrained or free conditions in the laboratory) may endanger the test outcomes.

2.6.2 Hot-Water Extraction (soluble alkali -SA)

Hot-Water Extraction (soluble alkali -SA) is known as a method for predicting the further expansion of affected concrete through the chemical composition of specimens [121,123]. The latter may vary considerably within a given structure and even within a single member [121,123]. This may be due to variations in the concrete mixture proportioning, the extent of ASR (which consumes alkalis) and cracking (alkali concentration through evaporation or alkali leaching along cracks), and in the exposure conditions

which may greatly affect the water-soluble alkali content in the near-surface concrete (external sources of alkali, alkali migration in/out of the sampled zones, alkali concentration at the surface through evaporation, or alkali leaching by rain). Thus, it is suggested that the test method must be applied to concrete samples, usually cores, taken in different members exposed to various conditions. Later, the cored specimens should be wrapped in plastic film/sheets and placed in sealed plastic bags immediately after coring, to prevent any drying (or wetting). In order to find the soluble alkali content of a concrete specimen, an indirect way of measuring the chemical composition of concrete pore solutions may be used, where a representative sample of a minimum 2 kg (4.5 lbs) of concrete should be crushed with a hammer to < 25 mm (1 in) and allowed to dry immediately before testing. Later, two 10 gr subsamples of ground concrete (>160 μm) are taken as representative sub-samples. Two 10 gr representative sub-samples of a control concrete with a well-known water-soluble alkali content are also prepared and tested in parallel. Each10 gr sub-sample of the concrete are boiled in water for 10 minutes and the solution is left at room temperature to stand overnight. The next morning, the suspensions are filtered, and the solution volume topped to 100 mL by adding distilled water. Then, the Na and K concentrations of the solution are measured by using flame photometry or atomic absorption in accordance with Clause 17.1 ("Total Alkalis") of ASTM C 114 [124]. Finally, the average results are expressed on a kg/m^3 Na_2O_e basis.

2.7 Predicting ASR expansion and damage through modeling

Several analytical, numerical and empirical models have been proposed previously [125–132] to predict ASR-kinetics and induced expansion in the laboratory (i.e., materials level) and its impact on the mechanical properties and performance of affected structures/structural components in the field. Amongst those, Larive's analytical model [131] is probably one of the most accepted approaches by the ASR community [132]. Larive's model was initially proposed to determine the induced expansion behaviour of unrestrained concrete specimens in the laboratory but has also been used to predict the expansion rate of concrete structures in the field. It consists of a semi-empirical approach that was established based upon an extensive experimental campaign. In this model, ASR-induced expansion is demonstrated as a function of three main parameters: ultimate expansion (ε^{∞}), latency (τ_l), and characteristic (τ_c) times (Eq. 1). Latency time (τ_l) corresponds to the period of time that the reaction requires to kick off, whereas characteristic time (τc) corresponds to the rate of development of the swelling. Ultimate expansion (ε^{∞}) is the value of the strain at the end of the swelling process. Figure 13 illustrates an expansion curve resulting from Larive's analytical model.

$$\varepsilon(t,\theta) = \frac{1 - e^{-\frac{t}{\tau_c(\theta)}}}{1 + e^{-\frac{(t-\tau_l(\theta))}{\tau_c(\theta)}}} \times \varepsilon^{\infty}$$

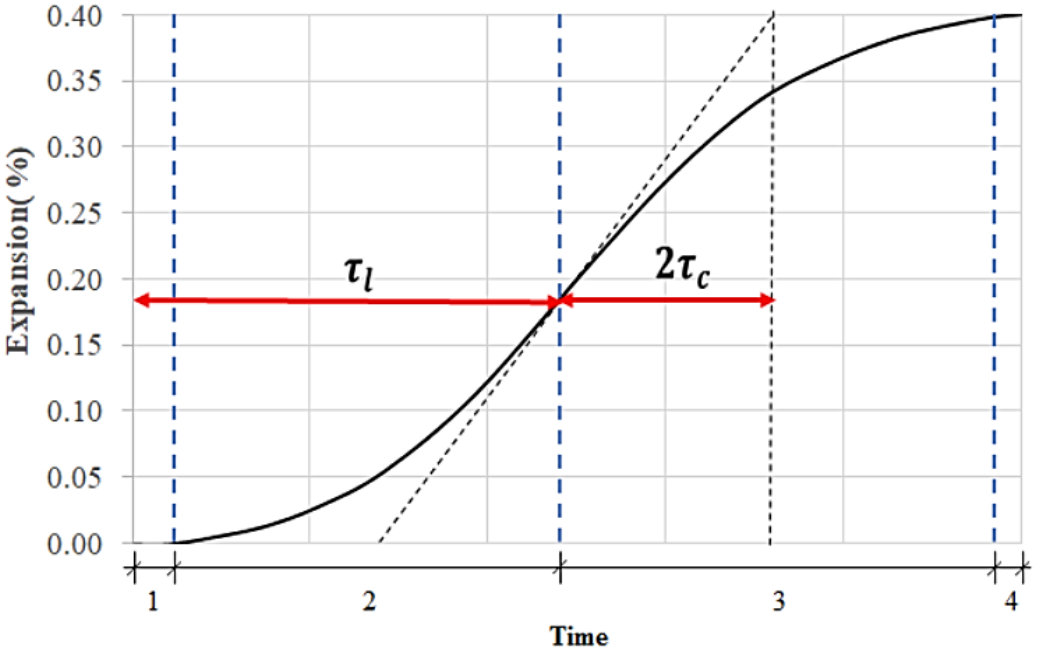

Figure 13: ASR-induced expansion curve obtained from Larive's model [131] *(Reproduced with permission of Elsevier)*.

Although interesting, the approaches proposed by Larive are only valid under constant conditions (i.e. temperature, moisture, exposure, etc.) [132]. Later, researchers aimed to develop a modified Larive's model accounting for the most important (and measurable) parameters that affect the physicochemical reaction (i.e., aggregate type and nature/reactivity, alkali content, temperature, and relative humidity) and thus be able to fully describe ASR-kinetics and unrestrained expansion in the laboratory. However, it is not yet appropriate to be used for real confined structures.

2.8 References

[1] N. Smaoui, B. Fournier, M. Bérubé, B. Bissonnette, B. Durand, Evaluation of the expansion attained to date by concrete affected by alkali silica reaction. Part II: Application to nonreinforced concrete specimens exposed outside, Can. J. Civ. Eng. 31 (2004) 997–1011. https://doi.org/10.1139/l04-074.

[2] B. Fournier, M. Bérubé, Alkali–Aggregate Reaction in Concrete: a Review of Basic Concepts and Engineering Implications, Can. J. Civ. Eng. 27 (2000) 167–191. https://doi.org/10.1139/l99-072.

[3] P. Akpinar, A. Zahedi, Comparison of the Alkali-Silica Reactivity of North Cyprus and South Cyprus aggregates ; preliminary studies using RILEM method, in: E3S Web Conf., 2021: p. 02001. https://doi.org/https://doi.org/10.1051/e3sconf/202130402001 ICECAE 2021.

[4] C. Trottier, R. Ziapour, A. Zahedi, L. Sanchez, F. Locati, Microscopic characterization of alkali-silica reaction (ASR) affected recycled concrete mixtures induced by reactive coarse and fine aggregates, Cem. Concr. Res. 144 (2021) 106426. https://doi.org/10.1016/j.cemconres.2021.106426.

[5] C. Trottier, A. Zahedi, R. Ziapour, L. Sanchez, F. Locati, Microscopic assessment of recycled concrete aggregate (RCA) mixtures affected by alkali-silica reaction (ASR), Constr. Build. Mater. 269 (2021) 121250. https://doi.org/10.1016/j.conbuildmat.2020.121250.

[6] P. Golterman, Mechanical predictions on concrete deterioration — part 2: classification on crack patterns, ACI Mater J. 92 (1995) 01–06.

[7] A. Leemann, T. Katayama, I. Fernandes, M.A. Broekmans, Types of alkali-aggregate reactions and the products formed,", Institut. Civ. Eng. - Constr. Mat. 169 (2016) 128.

[8] L.F.M. Sanchez, T. Drimalas, B. Fournier, Assessing Condition of Concrete Affected by Internal SwellingReactions (ISR) Through the Damage Rating Index (DRI), Cement. 1–2 (2020). https://doi.org/10.1016/j.cement.2020.100001.

[9] E. Boehm-courjault, A. Leemann, K.L. Scrivener, Microstructure, crystallinity and composition of alkali-silica reaction products in concrete determined by transmission electron microscopy, Cem. Concr. Res. 130 (2020). https://doi.org/10.1016/j.cemconres.2020.105988.

[10] L.F.M. Sanchez, B. Fournier, M. Jolin, D. Mitchell, J. Bastien, Overall assessment of Alkali-Aggregate Reaction (AAR) in concretes presenting different strengths and incorporating a wide range of reactive aggregate types and natures, Cem. Concr. Res. 93 (2017) 17–31. https://doi.org/http://dx.doi.org/10.1016/j.cemconres.2016.12.001.

[11] A. Mohammadi, E. Ghiasvand, M. Nili, Relation between mechanical properties of concrete and alkali-silica reaction (ASR); a review, Constr. Build. Mater. 258 (2020) 119567. https://doi.org/10.1016/j.conbuildmat.2020.119567.

[12] L.F.M. Sanchez, B. Fournier, M. Jolin, J. Duchesne, Reliable quantification of AAR damage through assessment of the Damage Rating Index (DRI), Cem. Concr. Res. 67 (2015) 74–92. https://doi.org/10.1016/j.cemconres.2014.08.002.

[13] F. Rajabipour, H. Maraghechi, G. Fischer, Investigating the alkali-silica reaction of recycled glass aggregates in concrete materials, J. Mater. Civ. Eng. 22 (2010) 1201–1208.

[14] J.M. Ponce, O.R. Batic, Different manifestations of the alkali-silica reaction in concrete according to the reaction kinetics of the reactive aggregate, Cem. Concr. Res. 36 (2006) 1148–1156.

[15] S. Diamond, A REVIEW OF ALKALI-SILICA REACTION AND EXPANSION MECHANISMS, Cem. Concr. Res. 6 (1976) 549–560.

[16] F. Rajabipour, E. Giannini, C. Dunant, J.H. Ideker, M.D.A. Thomas, Alkali-silica reaction: Current understanding of the reaction mechanisms and the knowledge gaps, Cem. Concr. Res. 76 (2015) 130–146. https://doi.org/10.1016/j.cemconres.2015.05.024.

[17] S. Chatterji, Chemistry of alkali-silica reaction and testing of aggregates, Cem. Concr. Compos. 27 (2005) 788–795. https://doi.org/10.1016/j.cemconcomp.2005.03.005.

[18] L.S.D. Glasser, N. Kataoka, The chemistry of "alkali-aggregate" reaction, Cem. Concr. Res. 11 (1981) 1–9.

[19] A.K. Varsheneya, J.C. Mauro, Fundamentals of Inorganic Glasses, Elsevier, 2019. https://doi.org/10.1016/b978-0-12-816225-5.09992-2.

[20] E. Boehm-Courjault, S. Barbotin, A. Leemann, K. Scrivener, Microstructure, crystallinity and composition of alkali-silica reaction products in concrete determined by transmission electron microscopy, Cem. Concr. Res. 130 (2020) 105988. https://doi.org/10.1016/j.cemconres.2020.105988.
[21] A. Gholizadeh Vayghan, Characterization of the Rheological and Swelling Properties of Synthetic Alkali Silicate Gels in Order To Predict Their Behavior in Asr Damaged Concrete, [PhD Thesis] Department of Civil and Environmental Engineering, The Pennsylvania State University, (2017) 245.
[22] H. Maraghechi, F. Rajabipour, C.G. Pantano, W.D. Burgos, Effect of calcium on dissolution and precipitation reactions of amorphous silica at high alkalinity, Cem. Concr. Res. 87 (2016) 1–13. https://doi.org/10.1016/j.cemconres.2016.05.004.
[23] M.D.A. Thomas, The role of calcium hydroxide in alkali recycling in concrete, in: J. Skalny, J. Gebauer, I. Odler (Eds.), Materials Science of Concrete Special Volume on Calcium Hydroxide in Concrete, American Ceramic Society, Westerville, OH, 2001.
[24] S. Diamond, A review of alkali-silica reaction and expansion mechanisms 1. Alkalies in cements and in concrete pore solutions, Cem. Concr. Res. 5 (1975) 329–345. https://doi.org/10.1016/0008-8846(75)90089-7.
[25] S.M.H. Shafaatian, A. Akhavan, H. Maraghechi, F. Rajabipour, How does fly ash mitigate alkali-silica reaction (ASR) in accelerated mortar bar test (ASTM C1567)?, Cem. Concr. Compos. 37 (2013) 143–153. https://doi.org/10.1016/j.cemconcomp.2012.11.004.
[26] R.F. Bleszynski, M.D.A. Thomas, Microstructural studies of alkali-silica reaction in fly ash concrete immersed in alkaline solutions, Adv. Cem. Based Mater. 7 (1998) 66–78. https://doi.org/10.1016/S1065-7355(97)00030-8.
[27] T.C. Powers, H.H. Steinour, An Interpretation of Some Published Researches on the Alkali-Aggregate Reaction Part 1-The Chemical Reactions and Mechanism of Expansion., J. Am. Concr. Inst. 26 (1955) 497–516.
[28] P.J.M. Monteiro, K. Wang, G. Sposito, M.C. Dos Santos, W.P. De Andrade, Influence of mineral admixtures on the alkali-aggregate reaction, Cem. Concr. Res. 27 (1997) 1899–1909. https://doi.org/10.1016/S0008-8846(97)00206-8.
[29] M. Kawamura, K. Iwahori, ASR gel composition and expansive pressure in mortars under restraint, Cem. Concr. Compos. 26 (2004) 47–56. https://doi.org/10.1016/S0958-9465(02)00135-X.
[30] A. Leemann, P. Lura, E -modulus of the alkali – silica-reaction product determined by micro-indentation, Constr. Build. Mater. 44 (2013) 221–227. https://doi.org/10.1016/j.conbuildmat.2013.03.018.
[31] A. Gholizadeh-Vayghan, F. Rajabipour, Quantifying the swelling properties of alkali-silica reaction (ASR) gels as a function of their composition, J. Am. Ceram. Soc. 100 (2017) 3801–3818. https://doi.org/10.1111/jace.14893.
[32] A. Gholizadeh Vayghan, F. Rajabipour, J.L. Rosenberger, Composition-rheology relationships in alkali-silica reaction gels and the impact on the Gel's deleterious behavior, Cem. Concr. Res. 83 (2016) 45–56. https://doi.org/10.1016/j.cemconres.2016.01.011.
[33] A. Gholizadeh-Vayghan, F. Rajabipour, The influence of alkali–silica reaction (ASR) gel composition on its hydrophilic properties and free swelling in contact with water vapor, Cem. Concr. Res. 94 (2017) 49–58. https://doi.org/10.1016/j.cemconres.2017.01.006.
[34] A. Leemann, T. Katayama, I. Fernandes, M. Broekmans, Types of alkali-aggregate reactions and the products formed, Proc. Inst. Civ. Eng. 169 (2016) 128–135. https://doi.org/10.1680/jcoma.15.00059.
[35] A. Leemann, Z. Shi, J. Lindgård, Characterization of amorphous and crystalline ASR products formed in concrete aggregates, Cem. Concr. Res. 137 (2020) 106190. https://doi.org/10.1016/j.cemconres.2020.106190.
[36] Š. Šachlová, R. Přikryl, Z. Pertold, Alkali-silica reaction products: Comparison between samples from concrete structures and laboratory test specimens, Mater. Charact. 61 (2010) 1379–1393. https://doi.org/10.1016/j.matchar.2010.09.010.
[37] C. Hu, B.P. Gautam, D. Shang, F. Wang, D.K. Panesar, Atomic force microscopy characterisation of alkali-silica reaction products to reveal their nanostructure and formation mechanism, Ceram. Int. 44 (2018) 7310–7314. https://doi.org/10.1016/j.ceramint.2018.01.069.

[38] H. Wu, J. Pan, J. Wang, Nano-scale structure and mechanical properties of ASR products under saturated and dry conditions, Sci. Rep. 10 (2020) 1–9. https://doi.org/10.1038/s41598-020-66262-9.
[39] I. Fernandes, F. Noronha, M. Teles, Examination of the concrete from an old Portuguese dam: Texture and composition of alkali-silica gel, Mater. Charact. 58 (2007) 1160–1170. https://doi.org/10.1016/j.matchar.2007.04.007.
[40] K. Peterson, D. Gress, T. Van Dam, L. Sutter, Crystallized alkali-silica gel in concrete from the late 1890s, Cem. Concr. Res. 336 (2006) 1523–1532.
[41] Niels Thaulow, U.H. Jakobsen, B. Clark, Composition of alkali-silica gel and ettringite in concrete railroad ties: SEM-EDX AND X-ray diffraction analysis, Cem. Concr. Res. 26 (1996) 309–318.
[42] Z. Shi, A. Leemann, D. Rentsch, B. Lothenbach, Synthesis of alkali-silica reaction product structurally identical to that formed in field concrete, Mater. Des. 190 (2020) 108562. https://doi.org/10.1016/j.matdes.2020.108562.
[43] C. Zhang, L. Sorelli, B. Fournier, J. Duchesne, J. Bastien, Z. Chen, Stress-relaxation of crystalline alkali-silica reaction products : Characterization by micro- and nanoindentation and simplified modeling, 148 (2017) 455–464.
[44] A. Gholizadeh-Vayghan, F. Rajabipour, M. Khaghani, M. Hillman, Characterization of viscoelastic behavior of synthetic alkali–silica reaction gels, Cem. Concr. Compos. 104 (2019) 103359. https://doi.org/10.1016/j.cemconcomp.2019.103359.
[45] M. Prezzi, P.J.M. Monteiro, G. Sposito, The alkali-silica reaction, part I: Use of the double-layer theory to explain the behavior of reaction-product gels, ACI Mater. J. 94 (1997) 10–17. https://doi.org/10.14359/280.
[46] A. Gholizadeh, F. Rajabipour, J.L. Rosenberger, Composition – rheology relationships in alkali – silica reaction gels and the impact on the gel's deleterious behavior, Cem. Concr. Res. 83 (2016) 45–56. https://doi.org/10.1016/j.cemconres.2016.01.011.
[47] N. Roussel, Understanding the Rheology of Concrete, A volume in Woodhead Publishing Series in Civil and Structural Engineering, 2012.
[48] L. Sun, X. Zhu, X. Zhuang, G. Zi, Chemo-mechanical model for the expansion of concrete due to alkali silica reaction, Appl. Sci. 10 (2020). https://doi.org/10.3390/app10113807.
[49] A.B. Giorla, K.L. Scrivener, C.F. Dunant, Influence of visco-elasticity on the stress development induced by alkali-silica reaction, Cem. Concr. Res. 70 (2015) 1–8. https://doi.org/10.1016/j.cemconres.2014.09.006.
[50] S. Multon, A. Sellier, M. Cyr, Chemo-mechanical modeling for prediction of alkali silica reaction (ASR) expansion, Cem. Concr. Res. 39 (2009) 490–500. https://doi.org/10.1016/j.cemconres.2009.03.007.
[51] Y. Zhuang, C. Qian, W. Xu, Calculation of alkali silica reaction (ASR) induced expansion before cracking of concrete, J. Wuhan Univ. Technol. Mater. Sci. Ed. 28 (2013) 110–116. https://doi.org/10.1007/s11595-013-0650-4.
[52] X. Hou, R.J. Kirkpatrick, L.J. Struble, P.J.M. Monteiro, Structural investigations of alkali silicate gels, J. Am. Ceram. Soc. 88 (2005) 943–949. https://doi.org/10.1111/j.1551-2916.2005.00145.x.
[53] C. Hu, B.P. Gautam, D.K. Panesar, Nano-mechanical properties of alkali-silica reaction (ASR) products in concrete measured by nano-indentation, Constr. Build. Mater. 158 (2018) 75–83. https://doi.org/10.1016/j.conbuildmat.2017.10.006.
[54] J. Moon, S. Speziale, C. Meral, B. Kalkan, S.M. Clark, P.J.M. Monteiro, Determination of the elastic properties of amorphous materials: Case study of alkali-silica reaction gel, Cem. Concr. Res. 54 (2013) 55–60. https://doi.org/10.1016/j.cemconres.2013.08.012.
[55] C.F. Dunant, K.L. Scrivener, Effects of uniaxial stress on alkali-silica reaction induced expansion of concrete, Cem. Concr. Res. 42 (2012) 567–576.
[56] N. Smaoui, M. Berube, B. Fournier, B. Bissonnette, B. Durand, Effects of alkali addition on the mechanical properties and durability of concrete, Cem. Concr. Res. 35 (2005) 203–212.
[57] R.S. Crouch, J.G.M. Wood, Damage evolution in ASR affected concretes., Eng. Fract. Mech. 35 (1990) 211–218.
[58] N. Smaoui, B. Bissonnette, M. Bérubé, B. Fournier, B. Durand, Mechanical properties of ASR-

affected concrete containing fine or coarse reactive aggregates, J. ASTM Int. 3 (2006) 1–16. https://doi.org/10.1520/jai12010.
[59] R. Esposito, C. Anaç, M.A.N. Hendriks, Influence of the Alkali-Silica Reaction on the Mechanical Degradation of Concrete, J. Mater. Civ. Eng. 28 (2016). https://doi.org/10.1061/(ASCE)MT.1943-5533.0001486.
[60] Y. Kubo, M. Nakata, Effect of reactive aggregate on mechanical properties of concrete affected by alkali-silica reaction., in: 14th ICAAR - Int. Conf. Alkali-Aggregate React. Concr., Austin (Texas), 2012.
[61] L.F.M. Sanchez, T. Drimalas, B. Fournier, D. Mitchell, J. Bastien, Comprehensive damage assessment in concrete affected by different internal swelling reaction (ISR) mechanisms, Cem. Concr. Res. 107 (2018) 284–303. https://doi.org/10.1016/j.cemconres.2018.02.017.
[62] K. Ono, Strength and stiffness of alkali–silica reaction concrete and concrete members., Struct Eng Rev. 2 (1990) 121–125.
[63] S. Mindess, J.F. Young, D. Darwin, Concrete, second edi, Pearson Education Ltd, 2003.
[64] A.E.K. Jones, L.A. Clark, The effects of restraint on ASR expansion of reinforced concrete, Mag Concr. Res. 48 (1996) 1–13.
[65] C. Gravel, G. Ballivy, K. K, Q. M, L. M, Expansion of AAR Concrete under Triaxial Stresses: Simulation with Instrumented Concrete Block., in: Proc. 11th Int. Conf. Alkali Aggreg. React., Québec, Canada, 2000.
[66] T.M.A. Ahmed, E. Burley, S.R. Rigden, The effect of alkali-silica reaction on the fatigue behaviour of plain concrete tested in compression, indirect tension and flexure, Mag Concr. Res. 51 (1999) 375–390.
[67] P. Morenon, S. Multon, A. Sellier, E. Grimal, F. Hamon, E. Bourdarot, Impact of stresses and restraints on ASR expansion, Constr. Build. Mater. 140 (2017) 58–74. https://doi.org/10.1016/j.conbuildmat.2017.02.067.
[68] S. Multon, F. Toutlemonde, Effect of applied stresses on alkali-silica reaction-induced expansions., Cem. Concr. Res. 36 (2006) 912–920.
[69] S. Multon, J.-F. Seignol, F. Toutlemonde, Structural behavior of concrete beams affected by alkali-silica reaction, ACI Mater. J. 102 (2005) 67–76.
[70] M. Noël, L. Sanchez, R. Martin, B. Fournier, J. Bastien, Structural Implications of Internal Swelling Reactions in Concrete : a Review, in: 15th Int. Conf. Alkali-Aggregate React., Sao Paulo, Brazil, 2016.
[71] H. Kagimoto, Y. Yasuda, M. Kawamura, ASR Expansion, Expansive Pressure and Cracking in Concrete Prisms under Various Degrees of Restraint, Cem. Concr. Res. 70 (2014) 1–15.
[72] M. Berra, G. Faggiani, T. Mangialardi, A. Paolini, Influence of Stress Restraint on the Expansive Behaviour of Concrete Affected by Alkali-Silica Reaction, Cem. Concr. Res. 40 (2010) 1403–1409.
[73] D. Wald, M.T. Allford, O. Bayrak, T.D. Hrynyk, Development and multiaxial distribution of expansions in reinforced concrete elements affected by alkali – silica reaction, Struct. Concr. 18 (2017) 914–928. https://doi.org/10.1002/suco.201600220.
[74] D. Wald, G. Arrieta, M. Oguzhan, Expansion behavior of a biaxially reinforced concrete member affected by alkali-silica reaction, Struct. Concr. 18 (2017) 550–560. https://doi.org/10.1002/suco.201600143.
[75] S. Sørgaard, O. Oseland, T. Kanstad, M.A.N. Hendriks, E. Rodum, Experimental investigation of ASR-affected concrete – The influence of uniaxial loading on the evolution of mechanical properties, expansion and damage indices, Constr. Build. Mater. 245 (2020) 118384–118398. https://doi.org/10.1016/j.conbuildmat.2020.118384.
[76] W. Koyangi, K. Rokugo, Y. Uchida, Properties of Concrete Deteriorated by Alkali Aggregate Reaction under Various Reinforcement Ratios, in: Proc. 9th Int. Conf. Alkali-Aggregate React. Concr., London, UK, 1992: pp. 556–563.
[77] A. Allard, S. Bilodeau, F. Pissot, B. Fournier, J. Bastien, B. Bissonnette, Expansive behavior of thick concrete slabs affected by alkali-silica reaction (ASR), Constr. Build. Mater. 171 (2018) 421–436. https://doi.org/10.1016/j.conbuildmat.2018.03.159.
[78] C. Larive, A. Laplaud, M. Joly, Behavior of AAR-affected concrete: experimental data, in: 10th Int. Conf. AAR, Melbourne, Australia, 1996: pp. 670–677.

[79] S. Multon, E. G. Leclainche, F. Bourdarot, Toutlemonde, Alkali–silica reaction in specimens under multi-axial mechanical stresses, in: 4th Int. Conf. CONSEC'04, Seoul, Korea, 2004: pp. 2004–2011.
[80] B.P. Gautam, D.K. Panesar, "A New Method of Applying Long-Term Multiaxial Stresses in Concrete Specimens undergoing ASR, and their Triaxial Expansions," Mater. Struct. 49 (2016) 3495–3508.
[81] R.A. Barbosa, K.K. Hansen, Alkali-Silica Reaction in Reinforced Concrete Structures Part II : Shear Strength of Severe ASR Damaged Concrete Beams, in: XXII Nord. Concr. Res. Symp., Iceland, 2014: pp. 69–72.
[82] A. McLeish, Structural implications of the alkali silica reaction in concrete, Report 177, Transport and Road Research Laboratory (TRRL), Wokingham, Berkshire United Kingdom, 1990.
[83] A.R. Barbosa, S. Gustenhoff, K. Kielsgaard, L. Cao, B. Grelk, Influence of alkali-silica reaction and crack orientation on the uniaxial compressive strength of concrete cores from slab bridges, Constr. Build. Mater. 176 (2018) 440–451. https://doi.org/https://doi.org/10.1016/j.conbuildmat.2018.03.096.
[84] S.G. Hansen, R.A. Barbosa, L.C. Hoang, Prestressing of reinforcing bars in concrete slabs due to concrete expansion induced by Alkali-Silica Reaction, in: Fib Symp., Cape Town, 2016.
[85] A.E.K. Jones, L.A. Clark, S. Amasaki, The suitability of cores in predicting the behaviour of structural members suffering from ASR, Mag. Concr. Res. 46 (1994) 145–150.
[86] A. Allard, S. Bilodeau, F. Pissot, B. Fournier, J. Bastien, B. Bissonnette, Performance Evaluation of Thick Concrete Slabs Affected by Alkali-Silica Reaction (ASR) – Part I: Materials Aspects, in: 15th Int. Conf. Alkali- Aggreg. React. Concr., São Paulo, 2016.
[87] P. Gautam, D.K. Panesar, S.A. Sheikh, F.J. Vecchio, Effect of Multiaxial Stresses on Alkali-Silica Reaction Damage of Concrete, ACI Mater. J. 114 (2017) 595–604. https://doi.org/10.14359/51689617.
[88] A. Zahedi, C. Trottier, L. Sanchez, M. Noël, Evaluation of the induced mechanical deterioration of alkali-silica reaction affected concrete under distinct confinement conditions through the Stiffness Damage Test, Cem. Concr. Compos. 126 (2021) 104343. https://doi.org/10.1016/j.cemconcomp.2021.104343.
[89] A.E.K. Jones, Cracking, Expansion and Strength of Concrete Subjected to Restrained Alkali Silica Reaction, PhD Thesis, The University of Birmingham, UK., 1994.
[90] E.R. Giannini, Evaluation of Concrete Structures Affected by Alkali-Silica Reaction and Delayed Ettringite Formation, PhD thesis, University of Texas at Austin, USA, 2012.
[91] K. Kobayashi, Load carrying behaviours of concrete structures and members affected by alkali-aggregate reactions, Concr. J. 24 (1986) 70–78.
[92] T. Ahmed, E. Burley, S. Rigden, The Static and Fatigue Strength of Reinforced Concrete Beams Affected by Alkali-Silica Reaction, ACI Mater. J. 95 (1999) 376–388.
[93] A. Zahedi, C. Trottier, L. Sanchez, M. Noël, Microscopic Assessment of ASR-Affected Concrete Under Confinement Conditions, Cem Concr Res. (2021) 106456. https://doi.org/https://doi.org/10.1016/j.cemconres.2021.106456.
[94] D. Palmer, The diagnosis of alkali silica reaction – report of a working party., Crowthorne, England, 1988.
[95] D.A. St-John, A.W. Poole, I. Sims, Concrete Petrography: A handbook of investigative techniques, Arnold, London, 1998.
[96] N. Zubaida, A. Zahedi, L. Sanchez, P. Rivard, Evaluation of the potential of residual expansion in concrete affected by Alkali Aggregate Reaction, in: 16th ICAAR, Int. Conferance Alkali Aggreg. React. Concr. 1-3 June, Lisboa, Portugal, 2020.
[97] A. Zahedi, N. Zubaida, L. Sanchez, P. Rivard, Effect of external confinement on Alkali-Silica Reaction (ASR)-induced expansion and damage, in: 16th ICAAR, Int. Conferance Alkali Aggreg. React. Concr. 1-3 June, Lisboa, Portugal, 2020.
[98] L.F.M. Sanchez, B. Fournier, M. Jolin, J. Bastien, Evaluation of the Stiffness Damage Test (SDT) as a tool for assessing damage in concrete due to alkali-silica reaction (ASR): Input parameters and variability of the test responses, Constr. Build. Mater. 77 (2015) 20–32. https://doi.org/10.1016/j.conbuildmat.2014.11.071.
[99] J. Walsh, The effects of cracks on the uniaxial elastic compression of rocks., J. Geophys. Res. 70 (1965) 339–411. https://doi.org/https://doi.org/10.1029/JZ070i002p00399.

[100] R.S. Crouch, Specification for the determination of stiffness damage parameters from the low cyclic uniaxial compression of plain concrete cores. Revision A, Mott, Hay & Anderson, Special services division, internal technical note, 1987.
[101] T.M. Chrisp, P. Waldron, J.G.M. Wood, Development of a non-destructive test to quantify damage in deteriorated concrete, Mag. Concr. Res. 45 (1993) 247–256. https://doi.org/10.1680/macr.1993.45.165.247.
[102] T.M. Crisp, J.G.M. Wood, P. Norris, Towards Quantification of Microstructural Damage in AAR Deteriorated Concrete. International Conference on Recent Developments on the Fracture of Concrete and Rock, The University of Wales, Cardiff, 1989.
[103] N. Smaoui, B. Fournier, M. Bérubé, B. Bissonnette, B. Durand, B. Fournier, B. Bissonnette, B. Durand, Evaluation of the expansion attained to date by concrete affected by alkali silica reaction. Part I:Experimental study, Can. J. Civ. Eng. 31 (2004) 826–845. https://doi.org/10.1139/L04-051.
[104] L.F.M. Sanchez, B. Fournier, M. Jolin, J. Bastien, D. Mitchell, Practical use of the Stiffness Damage Test (SDT) for assessing damage in concrete infrastructure affected by alkali-silica reaction, Constr. Build. Mater. 125 (2016) 1178–1188. https://doi.org/10.1016/j.conbuildmat.2016.08.101.
[105] Y. Zhu, A. Zahedi, L.F.M. Sanchez, B. Fournier, S. Beauchemin, Overall assessment of alkali-silica reaction affected recycled concrete aggregate mixtures derived from construction and demolition waste, Cem. Concr. Res. 142 (2021) 106350. https://doi.org/10.1016/j.cemconres.2020.106350.
[106] P.. Dunbar, P.E. Grattan-Bellew, Results of damage rating evaluation of condition of concrete from a number of structures affected by ASR, CANMET, in: ACI Int. Work. Alkali–Aggregate React. Concr., Darmouth, Canada, 1995: pp. 257–266.
[107] P.E. Grattan-Bellew, A. Danay, Comparison of Laboratory and Field Evaluation of AAR in Large Dams, in: Int. Conf. Concr. AAR Hydroelectr. Plants Dams, Canadian Electrical Association in association with Canadian National Committee of the International Commission on Large Dams, Frederiction, New Brunswick, Canada, 1992: p. 23.
[108] V. Villeneuve, B. Fournier, Determination of the damage in concrete affected by ASR — the damage rating index (DRI), in: 14th ICAR — Int. Conf. Alkali– Aggreg. React. Concr., Austin (Texas), 2012.
[109] V. Villeneuve, Détermination de l'endommagement du béton par méthode pétrographique quantitative, [MSc Thesis] Department of Geology and Geological Engineering, Université Laval, Québec, 2011, 2011.
[110] L.F.M. Sanchez, B. Fournier, M. Jolin, M.A.B. Bedoya, J. Bastien, J. Duchesne, Use of Damage Rating Index to quantify alkali-silica reaction damage in concrete: Fine versus coarse aggregate, ACI Mater. J. 113 (2016) 395–407. https://doi.org/10.14359/51688983.
[111] B. Fournier, A. Bérubé, J. Folliard, M. Thomas, Report on the Diagnosis, Prognosis, and Mitigation of Alkali-Silica Reaction (ASR) in Transportation Structures, Report No. FHWA-HIF-09-004, Federal Highway Administration, U. S. Department of Transportation, Washington, DC, 2010.
[112] C. Merz, A. Leemann, Assessment of the residual expansion potential of concrete from structures damaged by AAR, Cem. Concr. Res. 52 (2013) 182–189. https://doi.org/10.1016/j.cemconres.2013.07.001.
[113] S. Multon, J.-X. Barin, B. Godart, F. Toutlemonde, Estimation of the residual expansion of concrete affected by alkali silica reaction, ASCE, J.Mater. Civ. Eng. 20. (2008) 54–62.
[114] J.G.M. Wood, When does AAR stop: in the laboratory and in the field?, in: 12th ICAAR, Beijing, China, 2004: pp. 1016–1024.
[115] R.P. Martin, L. Sanchez, B. Fournier, F. Toutlemonde, Evaluation of different techniques for the diagnosis & prognosis of Internal Swelling Reaction (ISR) mechanisms in concrete, Constr. Build. Mater. 156 (2017) 956–964. https://doi.org/10.1016/j.conbuildmat.2017.09.047.
[116] A. Sellier, E. Bourdarot, S. Multon, M. Cyr, E. Grimal, Combination of Structural Monitoring and Laboratory Tests for Assessment of Alkali-Aggregate Reaction Swelling : Application to Gate Structure Dam, (2009).
[117] N. Smaoui, B. Fournier, B. Bissonnette, Influence of Specimen Geometry , Orientation of Casting Plane , and Mode of Concrete Consolidation on Expansion Due to ASR, Cem. Concr. Aggregates. 26 (2004)

1–13.
[118] M. Godart, B, Mahut, B, Fasseu, P, Michel, The guide for aiding to the management of structures damaged by concrete expansion in France, in: M. Tang, M. Deng (Eds.), Proc. 12th ICAAR, Beijing, China, M. Tang, M. Deng (Eds.), Proceedings of the 12th ICAAR, Beijing, China, 2004: pp. 1219–1228.
[119] O. Omikrine Metalssi, B. Kchakech, S. Lavaud, B. Godart, F. Beauvallet, A new model for the calculation of structures affected by DEF – application to a viaduct case, in: RILEM Int. Symp. Concr. Model. (CONMOD 2014), Beijing, China, 2014: pp. 460–469.
[120] J.-F. Seignol, N. Baghdadi, F. Toutlemonde, A macroscopic chemo-mechanical model aimed at re-assessment of delayed-ettringite-formation affected concrete structures, in: Proc. 1st Int. Conf. Comput. Technol. Concr. Struct., Jeju, Korea, 2009: pp. 422–440.
[121] M.A. Berube, J. Frenette, A. Pedneault, M. Rivest, Laboratory assessment of the potential rate of ASR expansion of field concrete, Cem. Concr. Aggregates. 24 (2002) 13–19. https://doi.org/10.1520/cca10486j.
[122] H.A. Rogers, R.D. Hooton, "Reduction in Mortar and Concrete Expansion with Reactive Aggregates Due to Alkali Leaching," Cem. Concr. Aggregates. 13 (1993) 42–49.
[123] M. Bérubé, J. Frenette, M. Rivest, D. Vézina, Measurement of the alkali content of concrete using hot-water extraction, Cem. Concr. Aggregates. 24 (2002) 28–36. https://doi.org/10.1520/cca10489j.
[124] American Association State Highway and Transportation Officials Standard, ASTM- C 144, Standard Specification for Aggregate for Masonry Mortar 1, 2002. https://doi.org/10.1520/C0144-18.2.
[125] V.E. Saouma, R.A. Martin, T. Hariri-Ardebili, M. A.Katayama, "A mathematical model for the kinetics of the alkali-silica chemical reaction.," Cem. Concr. Res. Elsevier Ltd. 68 (2015) 184–195.
[126] V. Saouma, L. Perotti, "Constitutive model for alkali-aggregate reactions.," ACI Mater. J. 103 (2006) 194–202.
[127] C. Comi, B. Kirchmayr, R. Pignatelli, "Two-phase damage modeling of concrete affected by alkali-silica reaction under variable temperature and humidity conditions.," Int. J. Solids Struct. Elsevier Ltd,. 49 (2012) 3367–3380.
[128] C. Comi, R. Fedele, U. Perego, "A chemo-thermo-damage model for the analysis of concrete dams affected by alkali-silica reaction.," Mech. Mater. Elsevier Ltd. 41 (2009) 210–230.
[129] E. Grimal, A. Sellier, S. Multon, Y. Le Pape, E. Bourdarot, "Concrete modelling for expertise of structures affected by alkali aggregate reaction.," Cem. Concr. Res. Elsevier Ltd. 40 (2010) 502–507.
[130] F. Bangert, D. Kuhl, G. Meschke, "Chemo-hygro-mechanical modelling and numerical simulation of concrete deterioration caused by alkali-silica reaction.," Int. J. Numer. Anal. Methods Geomech. 28 (2004) 689–714.
[131] C. Larive, "Combined contribution of experiments and modelling to the understanding of alkali-aggregate reaction and its mechanical consequences, 1997.
[132] N. Goshayeshi, Contribution to the development of analytical models to forecast alkali-aggregate reaction (AAR) kinetics and induced expansion in Civil Engineering, (2019).

3. OBJECTIVE

As previously stated in the sections above, there is a need to thoroughly and quantitatively understand the effect of restraint on ASR-induced expansion and damage (i.e., cracks generation and propagation) development, mechanical properties degradation as well as on the potential of further expansion of affected reinforced concrete. The multi-level assessment proposed by Sanchez et al. in 2017, was found to be an effective tool to assess damage development in ASR-affected concrete under free expansion and also to appraise the overall damage of affected concrete infrastructure. Yet, the impact of restraint on the damage generation and propagation and ultimately on the multi-level protocol outcomes needs further investigation. Furthermore, although somewhat criticized, some test procedures such as the residual expansion have been frequently used in various countries to assess the potential of further deterioration (i.e., prognosis) of concrete affected by ASR and should be further investigated. This work aims to answer the following questions through the use of the aforementioned tools to properly and reliably appraise ASR-affected concrete infrastructure:

- What is the difference between ASR-induced expansion and damage generation and propagation in "free" vs. "restrained" scenarios?
- How do distinct restraint configurations impact the reduction of mechanical properties of restrained members? What's the difference between mechanical degradation of concrete under unrestrained and restrained conditions as a function of ASR-induced development?
- How do the distinct type/nature of the reactive aggregate (i.e., fine versus coarse aggregate) impact on the damage development and mechanical properties losses of restrained ASR-affected concrete?
- How do the various restraint conditions affect the chemical composition and mechanical properties of ASR gel?
- How to reliably collect and use data from restrained and unrestrained members for a better condition assessment of affected infrastructure?

Hence, this work focuses on the improvement of the current knowledge and understanding of the effects of restraint on ASR physicochemical development (i.e., induced expansion and damage generation and propagation) as a function of the restraint configuration. It is also expected that this study develops a more reliable protocol to predict the potential for future induced development and distress in affected concrete, presenting distinct restraint scenarios. Therefore, concrete blocks incorporating reactive coarse and fine aggregates (Springhill coarse and Texas sand) and displaying distinct reinforcement configurations (i.e., none, 1D and 2 D) were fabricated in the laboratory and monitored over time. At distinct expansion levels (i.e., 0.08% and 0.15%) the blocks were cored in three distinct directions (i.e., longitudinal, transversal, and vertical) and the multi-level assessment and RE tests were conducted on each of those. Finally, comparisons

on the damage development and mechanical properties losses of restrained versus unrestrained concrete blocks at distinct deterioration levels are performed. In addition, the reliability of RE tests to predict the potential for further damage in restrained concrete will be appraised and discussed in the future.

4. RESEARCH PROGRAM

As mentioned before, the objective of this study is to improve the current knowledge and understanding of restraint effects on ASR-induced physicochemical and microstructural development. Upon completion, this work should enable infrastructure owners to develop better management protocols and optimized rehabilitation strategies of ASR-deteriorated concrete infrastructure. To achieve the proposed objectives, a series of studies were conducted on concrete cylinders and unrestrained/restrained concrete blocks manufactured in the laboratory. The work methodology proposed for this research is described in the following sections, as illustrated in Figure 14.

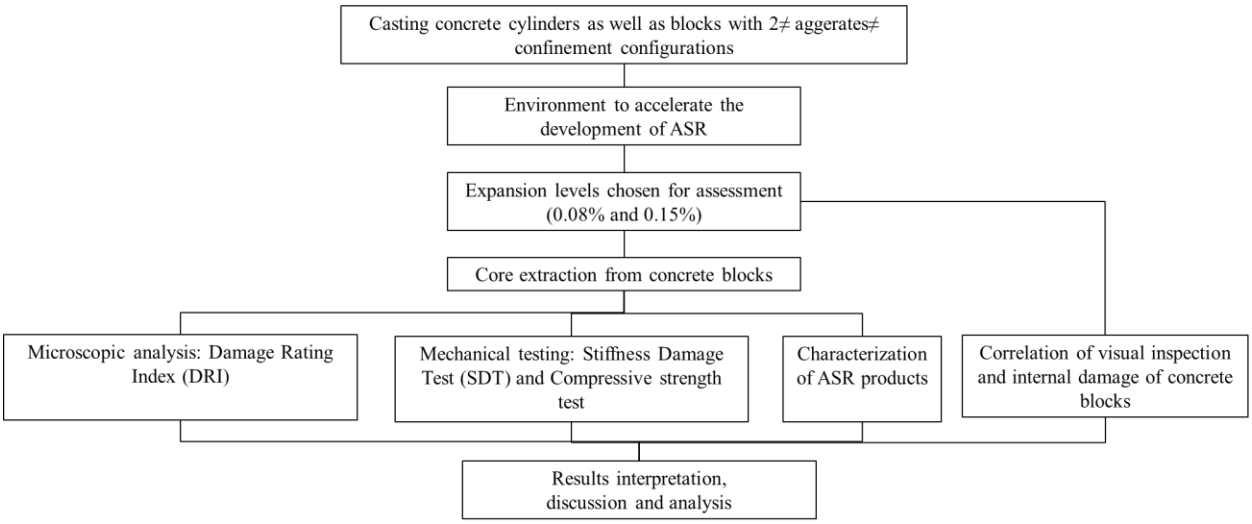

Figure 14: Structure of the PhD project.

4.1 Experimental procedures

A number of concrete blocks of 450 by 450 by 675 mm were manufactured using a concrete mix with a design strength of 35 MPa. A highly reactive sand [14] (i.e., Texas- Polymictic sand) and coarse aggregate (i.e., Springhill - Greywacke) in combination with non-reactive aggregate particles (i.e., Ottawa natural sand-OT and Ottawa limestone coarse aggregate-LS, respectively) from local quarries were used for concrete fabrication. It is worth noting that the reactivity level of non-reactivity aggregate particles was evaluated through ASTM C 1293 [1] and found to be less than 0.04% of expansion for both OT and LS aggregate particles. A conventional CSA Type GU (i.e., ASTM type 1) high alkali (0.88% Na2Oeq) Portland cement was used for both concrete mixtures. Moreover, the total alkali content of both mixtures was raised to 1.25% Na2Oeq, by cement mass, to accelerate ASR-induced development. The concrete mixtures were divided into the following two series: base series and complementary series. The mixture of the base series (Springhill-SP+ Ottawa natural sand-OT) was chosen to provide initial/base results/data to serve as the background for further analysis throughout the testing of the mixtures of the complementary

series. The base mixture was the subject of three scientific articles (Papers I, II, and V) of this PhD thesis (i.e., section 6.4.1). The results of the testing carried out on the test specimens of the complementary series were discussed in the other two scientific papers of this PhD thesis (Paper III and IV).

A total of 6 blocks from each reinforcement configuration (i.e., unrestrained, 1D and 2D) incorporating the SP coarse aggregate (eighteen concrete blocks) and 6 blocks bearing a 2D confinement configuration incorporating the TX fine aggregate were fabricated in the laboratory (i.e., a total of 24 concrete blocks). For comparative purposes, 40 concrete cylindrical specimens of 100 X 200 mm were also fabricated using the same highly reactive fine and coarse aggregates (i.e., 20 concrete cylinders per aggregate type) and using the same mix proportions as the concrete blocks. It is worth noting that for the restrained blocks, a reinforcement ratio of 2% was selected in each restrained direction, which is representative of a moderately high level of internal restraint in reinforced concrete members [15].

All concrete samples were demolded after one day and moist cured for another 24 hours at 20°C. Then, four holes with 10 mm in diameter by 55 mm in length, were drilled in the three main surfaces of the concrete blocks: a) top, b) longitudinal and c) transverse. Moreover, tiny holes of 8.5 mm in diameter by 19 mm in length, were also drilled at each end of all cylinders. Later, stainless-steel studs were placed using a fast-setting cement paste slurry for longitudinal expansion measurements in all concrete specimens. Forty-eight hours from manufacturing, the initial readings were recorded as follows: a) for concrete blocks, transverse, top longitudinal and side longitudinal expansion measurements (e.g., section 7.4.2), and b) longitudinal expansion measurements in the cylinders' case. All blocks were stored at 38ºC and 100% RH to accelerate ASR development. The concrete cylinders were stored in sealed buckets lined with a damp cloth and placed in the environmental chamber. All specimens were monitored for length changes regularly until they reached the expansion levels selected for this study, i.e., slight (i.e., 0.08% ± 0.01%) and moderate (i.e., 0.15% ± 0.01%). As per ASTM C 1293 [1], all concrete specimens were placed in 23°C conditions for 16 ± 4 hours before periodic expansion measurements. It is worth mentioning that the expansion level of 0.08% ± 0.01% (i.e., slightly deterioration) was selected since ASR-induced cracks are expected to be transitioning from the aggregate particles to the cement paste as per Sanchez et al [14] at this expansion level; on the other hand, the selection of 0.15% ± 0.01% (i.e., moderate deterioration) was based on the fact that most of the cracks are present in the cement paste at this expansion level [14].

Upon reaching the targeted expansion levels, concrete specimens were removed from the environmental chamber and three blocks from each distinct restraint configuration and aggregate type were cored to produce seven cores of 100 by 450 mm in the vertical and the transverse directions and four cores of 100 by 675 mm in the longitudinal direction for further analysis (e.g., section 6.4.2). Later, all concrete specimens were saw cut to lengths of 200 mm, wrapped in plastic film, and stored at 12°C until testing to

stop further ASR-development as per [6]. *Note: All characteristics of the aggregates and concrete mixture used in this PhD work are presented in the third scientific paper of the Thesis (e.g., section 8.4.1).*

The testing program performed on various concrete specimens of this study at different expansion levels included visual inspection, mechanical testing (SDT, modulus of elasticity, compressive strength determination and micro-indentation) and microscopic testing procedures (semi-quantitative petrographic analysis -DRI and SEM/EDS analysis). Table 1 and Table 2 demonstrate the typical testing program to be carried out on cores extracted from each set of distinct restrained concrete block and concrete cylinders respectively, in this part of the project. To compare the results obtained from the deteriorated concrete blocks under various restraint conditions with undamaged specimens, a number of control concrete cylinders were manufactured displaying the same mix-proportioning and ingredients (i.e., Portland cement and aggregates), and stored under 12°C over time for further analysis. The selection of 12°C has been made to stop further ASR-induced development as per Sanchez et al. [6]

Table 1: Testing matrix for cores obtained from each set of distinct restrained concrete blocks.

Test carried out	Coring direction	Number of specimens per direction for a given expansion level	
		0.08%	0.15%
SDT/CS	Vertical	3	3
	Transversal	3	3
	Longitudinal	3	3
DRI/SEM/Micro-indentation	Vertical	2	2
	Transversal	2	2
	Longitudinal	2	2
			Total Samples: 30

Table 2: Testing matrix for each family of concrete cylinders.

Test carried out	Number of samples per direction for a given expansion level		
	Control specimens	0.08%	0.15%
SDT/CS	3	3	3
DRI/SEM/ Micro-indentation	1	2	2
			Total Samples: 14

4.1.1 Visual inspection

Visual inspection is a non-destructive method for identifying potentially damaged members. ASR is typically identified on the concrete surface through its visual integrity (i.e., surface damage) such as map cracking, exudation of products on the surface, spalling, and discoloration [2]. Fournier et al. proposed the cracking index (CI) as an alternative to traditional qualitative visual inspection [3,4]. The cracking index (CI), a quantitative visual inspection technique, is a crack mapping process that averages out the crack

widths and frequencies along the vertical and horizontal directions on a grid with typical dimensions of 0.5 x 0.5 m [3,4]. First, a 0.5x0.5m grid is constructed (i.e., as a base length) on the surface of the most damaged face [3,4], with each segment divided into ten intervals. After recording the width of the largest crack intercepting each interval (i.e., along vertical and horizontal segments), the CI can be calculated by eq (2) as follows:

$$CI = \frac{\sum Crack\ opening}{Base\ length} \quad (2)$$

in which $\sum crack\ opening$ = the sum of all crack widths measured across the base length (i.e., generally 0.5 m). Such method gives a quantitative assessment of the extent of cracking in the affected members [3,4]; as per Fournier et. al. [3], a concrete member with CI > 0.5 mm/m (and/or cracks of width > 0.15 mm) require more detailed investigations to identify the extent of cracking.

4.1.2 Stiffness Damage Test (SDT)

Three specimens from distinct coring directions per set of concrete blocks (i.e., vertical, longitudinal and transverse; a total of 9 specimens per distinct directions per expansion level) as well as three concrete cylinders displaying the same expansion levels were subjected to five cycles of loading/unloading at the controlled loading rate of 0.10 MPa/s. Prior to conducting the SDT, all specimens were reconditioned in the moist curing room for 48h (enabling the samples rewetting and thus lessening the test's variability) according to CSA23.2-14C [5], and as per Sanchez et al. works [6]. Moreover, both ends of all concrete specimens (cylinders and cores) were mechanically ground to generate appropriate flatness of the specimen's end surfaces for mechanical tests in compression as per CSA23.2-9C [7]. The SDT was performed then following the procedure proposed by Sanchez et. al. [6,8]; i.e., loading up to 40% of the 28-day concrete strength of the specimens tested.

4.1.3 Compressive strength

In this research, the compressive strength was measured using two distinct approaches with different and specific goals. First, the 28-day compressive strength of the mixture used to manufacture both the blocks and cylinders was determined on control samples. Considering that the concrete mixture contained a highly reactive coarse aggregate, one could not follow ASTM C 39 [9] since some ASR might have been generated while moist curing. Thus, in order to avoid ASR-induced development, the control specimens were wrapped in the plastic film upon demoulding and placed at 12°C for 47 days as per Sanchez et al. [6], which is equivalent to 28 days at 20°C according to the maturity concept (i.e., ASTM C 1074 [10]). This approach has proven to be effective to suppress ASR development in the laboratory [6]. The "equivalent" 28-day compressive strength collected from this procedure was then used to determine the SDT loading level (i.e.,

40% of this value). Second, compressive strength measurements were also conducted on the concrete cylinders/cores following the SDT to verify the compressive strength losses of the material as a function of ASR-induced development. The SDT using 40% of the 28-day compressive strength has been found to be non-destructive by Sanchez et al. [6]; thus, mechanical results such as compressive strength obtained following the SDT are considered valid [6]. Finally, the compressive strength losses were calculated in this work (for both cylinders and cores) as the difference between the results obtained after the SDT (for distinct expansion levels, restraint conditions, and directions) and the "equivalent" 28-day values obtained on control samples.

4.1.4 Damage Rating Index (DRI)

Before the microscopic evaluation, two consecutive specimens per the direction of the blocks (i.e., 6 specimens per restraint configuration) and two cylinders per damage degree were initially cut axially in two followed by subsequent mechanical polishing with grits of 30, 60, 140, 280 (80–100 µm), 600 (20–40 µm), 1200 (10–20 µm) and 3000 (4–8µm). Once the surface of the polished concrete section was properly polished, a 1 x 1 cm grid was drawn on the surface of the samples before the microscopic evaluation. Distress features of 1mm in size or higher observed in the cement paste and aggregate particles were evaluated using the weighting factors proposed by Villeneuve et. al. [37] (Figure 11) to compute the DRI numbers. Ultimately, it is worth mentioning that the damage orientation of concrete specimens has been evaluated using an image analysis protocol following the procedure proposed by Zahedi et al. [16], where the observed damage features in each 1x1 cm DRI grid (Figure 11) drawn on the polished concrete specimens were highlighted through the use of a commercial software.

4.1.5 SEM/EDS and micro-indentation

Two concrete cores per coring direction of each concrete block was initially cut longitudinally into 10 mm-thick slabs with the aid of a diamond bladed masonry saw followed by subsequent mechanical polishing using liquid paraffin oil with grits of 30 (coarse), 60, 140, 280, 600, 1200 and 3000 (very fine). The slabs were then evaluated through a stereomicroscope to find some cracks filled with ASR gel, and further cutting was performed to produce a proper size sample for further testing. Later, the proper cut specimens were finely polished (i.e., up to 0.25µm) based on the procedure proposed by Leemann et al. [11] and Zhang et al. [12] as shown in Table 3. Finally, the finely polished specimens were protected in air-tight plastic bags and subjected to SEM/EDS and micro-indentation within 24h after the completion of the polishing operations:

Table 3: Polishing procedure used in this study [11-12].

Sandpaper	Microns (μm)	Methods	Durations (mins)
SiC sandpaper 400-400	22	with liquid paraffin oil	10
SiC sandpaper 400-800	12	with liquid paraffin oil	10
SiC sandpaper 400-1200	6.5	with liquid paraffin oil	15
Oil based Diamond suspension	6	Acetone flush, air gun dry	40
Oil based Diamond suspension	1	Acetone flush, air gun dry	30
Diamond paste	0.25	Acetone flush, air gun dry	60

- **SEM/ EDS analysis**

Backscattered electrons (BEC) imaging was performed on two specimens containing propagated ASR filled cracks within aggregate particle to cement paste per direction of each concrete block using scanning electron microscopy (SEM- JEOL 6610LV) with operating parameters set at 15 kV and a beam current of 200–220 mA. Energy-dispersive X-ray spectroscopy (EDX) was also used to analyze the chemical composition of the reaction product (i.e., ASR gel). It is worth mentioning that the concrete specimens were placed in 50^{o} C for one day (24 hours) and then a thin layer of Au-Pd was used to coat them.

- **Micro indentation**

Indentation measurements were performed on similar specimens as per SEM analysis (i.e., two samples with ASR gel formed in aggregate particles and propagate into cement paste per direction of each concrete block) with a Vickers micro-hardness tester (Struers Duramin-1 micro-hardness). The latter has an indenter with a square-based pyramid shape with an angle of 136 (Figure 15A) [13]. The Vickers hardness value, HV, is generally calculated using the indenter load L and the actual surface area of the impression Ac [13] as shown in Figure 15B. The load used in this study is either 12.5mN, 25mN (only for cracks in aggregate particles) or 50 mN (for cracks in aggregate particles and cement paste) similar to the one proposed by Leemann et al. [11]. As the authors [11] suggested, the increase of linear loading takes 20 s and then the maximum load is kept constant for 5 s and later linear unloading takes 20 s (Figure 15C). After conducting the indentation procedure, the diagonal width (i.e., d- Figure 15A) is measured under a microscope at 400X which helps to find the hardness of the material. It is worth noting that the indentation procedure was carried out on aggregate particles and cement paste as per the distance shown in Figure 16.

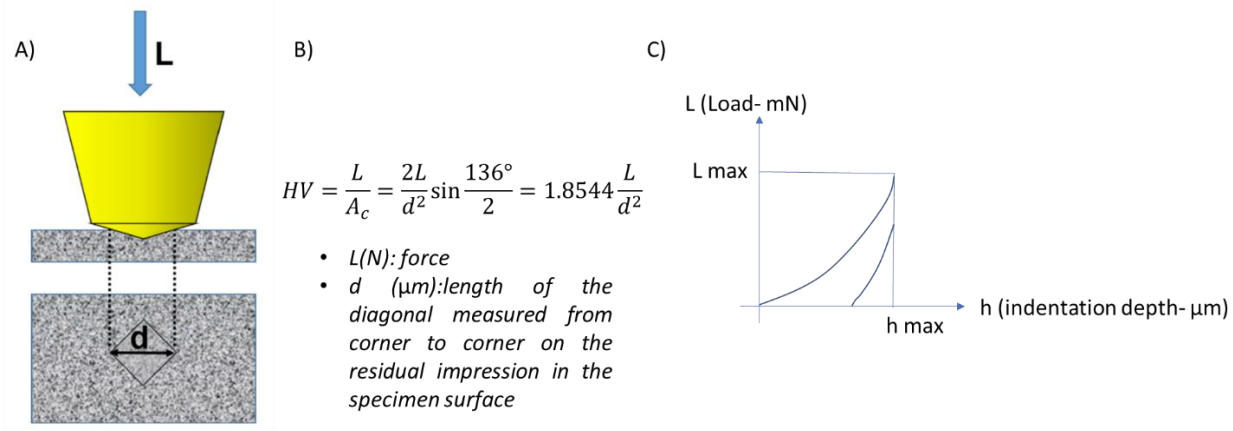

Figure 15: A) Schematic of Vickers hardness [13], B) Vickers hardness calculation [13] and C) typical load-indentation depth (P-h) curve.

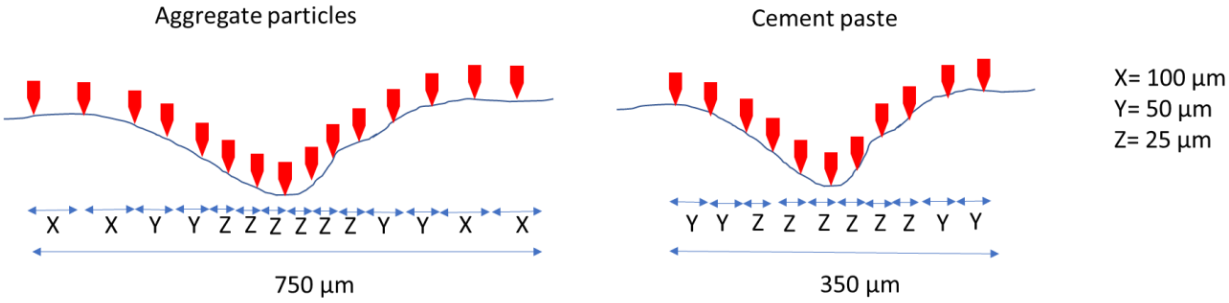

Figure 16: Indentation distance profile across a crack in aggregate particles and cement paste.

4.2 References

[1] ASTM C1293, Standard test method for determination of length change of concrete due to alkali-silica reaction, Annu. B. ASTM Stand. (2015) 1–7. https://doi.org/10.1520/C1293-08B.2.

[2] B. Fournier, M. Bérubé, Alkali–Aggregate Reaction in Concrete: a Review of Basic Concepts and Engineering Implications, Can. J. Civ. Eng. 27 (2000) 167–191. https://doi.org/10.1139/l99-072.

[3] B. Fournier, A. Bérubé, J. Folliard, M. Thomas, Report on the Diagnosis, Prognosis, and Mitigation of Alkali-Silica Reaction (ASR) in Transportation Structures, Report No. FHWA-HIF-09-004, Federal Highway Administration, U. S. Department of Transportation, Washington, DC, 2010.

[4] B. Fournier, M.A. Berube, K.J. Folliard, M. Thomas, Report on the Diagnosis, Prognosis, and Mitigation of Alkali-Silica Rection (ASR) in Transportation Structures, Austin, 2010.

[5] Standard Counsil of Canada, CSA23.2-14C: Obtaining and testing drilled cores for compressive strength testing, in: CSA A23.119/CSA A23.219 Natl. Stand. Canada, 2019: pp. 774–778.

[6] L.F.M. Sanchez, B. Fournier, M. Jolin, J. Bastien, Evaluation of the Stiffness Damage Test (SDT) as a tool for assessing damage in concrete due to alkali-silica reaction (ASR): Input parameters and variability of the test responses, Constr. Build. Mater. 77 (2015) 20–32. https://doi.org/10.1016/j.conbuildmat.2014.11.071.

[7] Standard Counsil of Canada, CSA23.2-9C: Compressive strength of cylindrical concrete specimens, in: CSA A23.119/CSA A23.219 Natl. Stand. Canada, 2019: pp. 733–748.

[8] L.F.M. Sanchez, B. Fournier, M. Jolin, J. Bastien, D. Mitchell, Practical use of the Stiffness Damage Test (SDT) for assessing damage in concrete infrastructure affected by alkali-silica reaction, Constr. Build. Mater. 125 (2016) 1178–1188. https://doi.org/10.1016/j.conbuildmat.2016.08.101.

[9] ASTM C39, Standard Test Method for Compressive Strength of Cylindrical Concrete Specimens, West Conshohocken (USA), 2012.

[10] ASTM C1074-19, Standard Practice for Estimating Concrete Strength by the Maturity Method, West Conshohocken (USA), 2019.
[11] A. Leemann, P. Lura, E -modulus of the alkali – silica-reaction product determined by micro-indentation, Constr. Build. Mater. 44 (2013) 221–227. https://doi.org/10.1016/j.conbuildmat.2013.03.018.
[12] C. Zhang, L. Sorelli, B. Fournier, J. Duchesne, J. Bastien, Z. Chen, Stress-relaxation of crystalline alkali-silica reaction products : Characterization by micro- and nanoindentation and simplified modeling, 148 (2017) 455–464.
[13] E. Broitman, Indentation Hardness Measurements at Macro-, Micro-, and Nanoscale: A Critical Overview, Tribol. Lett. 65 (2017) 1–18. https://doi.org/10.1007/s11249-016-0805-5.
[14] L.F.M. Sanchez, B. Fournier, M. Jolin, D. Mitchell, J. Bastien, Overall assessment of Alkali-Aggregate Reaction (AAR) in concretes presenting different strengths and incorporating a wide range of reactive aggregate types and natures, Cem. Concr. Res. 93 (2017) 17–31. https://doi.org/http://dx.doi.org/10.1016/j.cemconres.2016.12.001.
[15] Standard Counsil of Canada, CSA A23.3:19:Design of concrete structures, 2019.

5. CORE OF THE THESIS – SCIENTIFIC PAPERS

5.1 General overview

In order to analyze the results gathered from the various experimental procedures implemented in this PhD work, five scientific papers were prepared. They cover all the major themes of the research, thus enabling them to fully meet the various objectives of the PhD project. Figure 17 display the links between the papers.

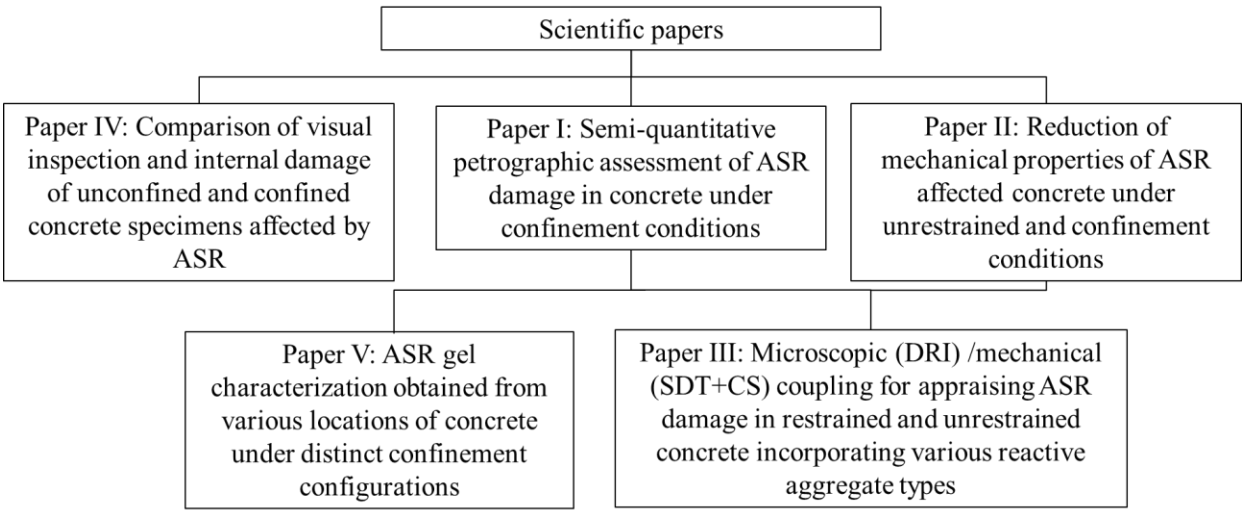

Figure 17: Core of the PhD Thesis – links between the scientific papers.

Generally, the scientific paper I and II, investigate the effects of restraint on ASR physicochemical development and ultimately on the DRI and SDT outcomes after conducting various testing procedures on affected concrete specimens under restrained and unrestrained conditions

Then paper III deals with a global appraisal (i.e., using a microscopic/mechanical coupling) of ASR development through the study of various aggregate types (i.e., fine vs coarse) and restraint configurations. For paper III of this PhD project, the diagnostic potential of DRI and SDT has already been demonstrated (i.e., after the first two scientific papers) so that a full understanding of the coupling between "micro features of damage and macro mechanical behavior" of concretes incorporated various aggregate types, restraint conditions and affected by ASR is possible. Paper IV presents the deterioration data obtained from various visual inspection techniques and expansion measurements (i.e., internal- through steel bar's strain gauges vs external- Stainless steel gauge studs /demec gauges) of various concrete blocks of this project. Also, Paper IV proposed a correlation between the crack size (i.e., width) obtained through visual inspection and the damage degree of affected concrete blocks obtained through the paper I. Finally, paper V deals with the microscopic and mechanical characterization of ASR gel obtained from aggregate particles, ITZ and cement paste of various directions of concrete blocks of this study.

5.2 Scope and objectives of the scientific papers

A summary description of the content of each scientific paper, as well as their specific objectives, is given hereafter.

5.2.1 Paper I (Chapter 6): *Microscopic Assessment of ASR-Affected Concrete Under Restraint Conditions*

Initially, a brief literature review on the use of the Damage Rating Index (DRI) on ASR-affected concrete as well as the impact of restraint on the ASR-induced damage development is presented in this scientific paper. Then, it focuses on the analysis of the results of DRI gathered from distinct concrete specimens extracted from un/reinforced concrete blocks, stored under highly controlled conditions, and incorporating a highly reactive coarse aggregate (SP coarse aggregate- base series)

Three different restraint conditions (i.e., none, 1D and 2D) were selected for this study, from which a number of concrete blocks (450 by 450 by 675 mm in size) were manufactured and then stored under conditions enabling ASR development. Upon reaching the two expansion levels chosen for this work (i.e., 0.08% and 0.15%), they were cored in three main directions (i.e., vertical, transverse and longitudinal) and two consecutive specimens per direction of each block were tested through damage rating index (DRI). The effect of restraint on ASR-induced expansion, damage generation and propagation has been thoroughly investigated through the conventional and extended DRI versions. The development of the petrographic features of ASR distress (crack pattern and orientation) was then evaluated as a function of expansion and restraint configurations.

5.2.2 Paper II (Chapter 7): *Evaluation of Alkali-Silica Reaction (ASR)-Induced Mechanical Deterioration Under Unrestrained and Restraint Conditions*

This paper first presents a brief literature review on the effect of ASR on the mechanical properties of affected concrete under unrestrained and restraint Conditions. Then, it focuses on the analysis of the results of stiffness damage testing and compressive strength of a series of laboratory-made concrete blocks, stored under highly controlled conditions, and incorporating a highly reactive coarse aggregate (SP coarse - base series).

The specimens used for this work were gathered from the same test blocks used for the first paper of this thesis. Three cored specimens per direction of each block were tested through stiffness damage test (SDT) and compressive strength test. The effect of restraint on the mechanical properties of ASR affected concrete under various restraint configurations as well as the diagnostic potential of various output parameters of SDT (SDI, PDI and Modulus of elasticity - ME) was thus evaluated. The Damage Rating Index (DRI) was

also performed on companion concrete samples in order to validate the mechanical response of various cored specimens. In addition, a statistical analysis (i.e., two-variable ANOVA and complementary "t-test") was also performed in order to determine whether the conclusions drawn through the analysis of the data could be considered statistically significant.

5.2.3 Paper III (Chapter 8): *Overall Assessment of Alkali-Silica Reaction Affected Concrete Under Restraint Conditions: Reactive Sand Versus Reactive Coarse Aggregate*

This scientific paper presents a global analysis of the results obtained in the first two papers of PhD research through the coupling of the microscopic features of deterioration (DRI observations) against the mechanical responses obtained on companion specimens tested through SDT, modulus of elasticity and compressive test. Moreover, the different deterioration mechanisms of ASR when it is triggered by a reactive coarse (i.e., SP) or a reactive fine (i.e., TX) aggregate in affected concrete under various restraint configurations is thoroughly investigated. Finally, a comprehensive quantitative AAR damage chart is proposed.

5.2.4 Paper IV (Chapter 9): *Improving the Knowledge of Visual Inspection on ASR Affected Unrestrained and Restrained Concrete*

Initially, a brief literature review on distinct visual inspection methods used for condition assessment of deteriorated concrete as well as the impact of ASR on the external surfaces of affected concrete have been presented in this scientific paper. Then, it focuses on the analysis of the results obtained through various visual inspection techniques, expansion measurements (gathered from steel bars and concrete surface) as well as the Damage Rating Index (DRI) performed on the surface of concrete blocks and the cored specimens used in paper 3. Later, this paper compared the expansion results obtained from the steel bars and surface of concrete elements as well as the external damage (obtained through visual inspection and performing DRI on the external surfaces of concrete blocks) and internal deterioration (obtained through DRI on the cored specimens) of ASR affected concrete under various restraint conditions. Finally, at the end of this paper, a correlation between the visual inspection (cracking index - C.I) and the expansion levels of distinct surfaces of concrete specimens as well as the qualitative ASR distress models on the surface of the concrete have been proposed.

5.2.5 Paper V (Chapter 10): *Influence of the restraint configuration on alkali-silica reaction (ASR) reaction product's features*

This paper first presents a brief literature review on the chemical composition and mechanical properties of ASR gel obtained from various concrete elements. Then, it focuses on the analysis of the SEM/EDS and micro-indentation results obtained from the concrete blocks used for the first two papers of this PhD study (a highly reactive coarse aggregate -SP coarse - base series).

The cored specimens reached the higher expansion level of this study (0.15%) were properly cut and polished and prepared for the abovementioned tests. Comparison of the chemical composition and mechanical properties of ASR gel obtained from concrete blocks with various restraint configurations as well as those obtained from the distinct directions of each concrete block has been conducted.

6. MICROSCOPIC ASSESSMENT OF ASR-AFFECTED CONCRETE UNDER RESTRAINT CONDITIONS

Andisheh Zahedi [1], Cassandra Trottier [2], Leandro Sanchez [3], Martin Noël [4]

Abstract

The Damage Rating Index (DRI), a semi-quantitative microscopic procedure, has been successfully used to describe alkali-silica reaction (ASR) damage development of concrete under "free expansion" conditions. Yet, the restraint impact on ASR-induced cracks' generation and propagation has not been fully investigated. This work aims to understand the influence of restraint on ASR development through the DRI. Eighteen concrete blocks incorporating a highly reactive coarse aggregate and distinct reinforcement configurations were manufactured, stored in conditions enabling ASR development, and monitored over time. Two expansion levels were selected for analysis (0.08% and 0.15%) and once reached, cores were extracted from three different directions (longitudinal, transverse and vertical) and the DRI conducted on those. Results demonstrate that ASR-induced expansion and deterioration change according to the direction and restraint configuration. Moreover, distinct crack features and orientations are generated in restrained concrete, which attests that ASR displays different damage mechanisms under free and restraint conditions.

Keywords: Alkali-Silica Reaction (ASR), Damage Rating Index (DRI), Expansion, Damage transfer, Restraint, Crack orientation.

6.1 Introduction

Alkali-Silica Reaction (ASR) is one of the most important damage mechanisms affecting the durability and serviceability of concrete infrastructure worldwide [1]. Over the last years, a number of test procedures have been developed to assess the current condition (i.e., diagnosis) and the potential for further expansion/distress (i.e., prognosis) of ASR-affected concrete; those are fundamental steps towards the optimization of management protocols and rehabilitation strategies of deteriorated concrete infrastructure. Amongst the proposed techniques, the Damage Rating Index (DRI), a semi-quantitative microscopic procedure, was found to be quite suitable to appraise ASR-induced expansion and deterioration in concrete under unrestrained (i.e., free expansion) conditions, which does not reflect the real scenario of reinforced concrete members in the field [1,2]. Although few recent works have suggested the efficiency of the DRI to appraise condition of affected aging infrastructure [3–6], there is currently a lack of "quantitative" information of the effects of restraint (e.g., reinforcement) on ASR-induced physicochemical development (i.e., kinetics and induced expansion, damage generation and propagation, crack pattern and orientation) and ultimately on the DRI outcomes. This work aims to use the DRI to assess the condition of ASR-affected

concrete blocks displaying distinct reinforcement configurations (i.e., none, 1D and 2D) and expansion levels (i.e., 0.08% and 0.15%).

6.2 Background

6.2.1 ASR-induced development under free expansion

ASR is a complex physicochemical reaction between the alkali hydroxides (i.e., Na^+, K^+, OH^-) from the concrete pore solution and certain unstable mineral phases found in the aggregates used to make concrete; ASR produces a secondary reaction product (ASR gel) that swells upon moisture uptake, leading to expansion and cracking of the affected material [7,8]. ASR-induced expansion generates tensile stresses within the reactive aggregate particles along with compressive stresses at the particles' edges [9]. Hence, ASR cracks are initially generated within the aggregate particles and propagate to the cement paste with the increase in induced expansion [9,10]. Moreover, the ITZ often remains intact during ASR development, except in locations close to the radial cracks formed within the particles (Figure 1) [11,12]. The degree of deterioration of ASR-affected concrete is normally expressed by its level of expansion; although the relationship between expansion and deterioration is not necessarily linear, it is anticipated that the higher the expansion level, the higher the overall deterioration (i.e., loss of mechanical properties, physical integrity and stiffness) of affected concrete [13,14].

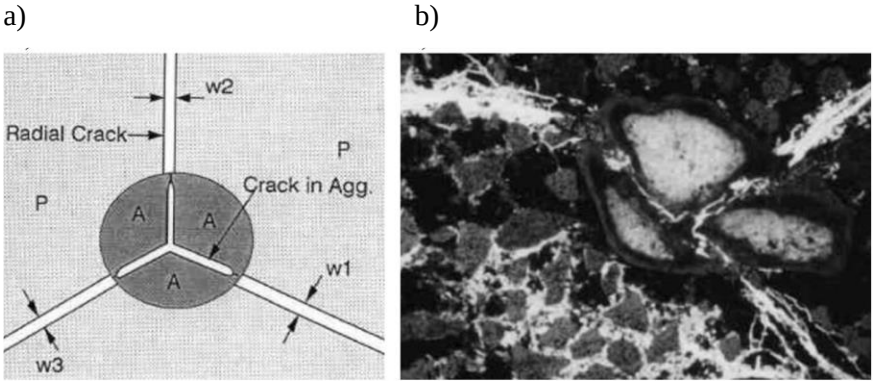

Figure 1: Signatures of concrete damage due to alkali–silica reaction (ASR): a) a model and b) 2 mm size aggregate under thin section microscopy [9] *(Reproduced with permission of Elsevier).*

Regardless of the aggregate type, Sanchez et. al. [1] developed a qualitative and descriptive model to describe ASR-induced damage generation and propagation under unrestrained conditions (Figure 2) [1]. At low expansion levels (e.g., 0.05%), sharp and onion skin type cracks (represented by A and B in Figure 2, respectively) are generated within the reactive aggregate particles. As the reaction progresses, not only are new cracks formed in the aggregate particles but, more importantly, the previously developed cracks increase in length and width and may even begin to slightly extend into the cement paste at moderate expansion levels (e.g., 0.12%) [15,16]. As ASR continues to further develop, the previously formed cracks

reach the cement paste at both ends of the aggregate (e.g., 0.20% of expansion), which drastically impacts the physical integrity and mechanical properties of the affected material [13]. Finally, at very high expansion levels (e.g., 0.30%), cracks developed at distinct aggregate particles start linking together, which creates an important crack network in the affected concrete, thus further reducing its durability and mechanical properties [1]. Although the aforementioned model was shown to be quite accurate to describe ASR-induced damage development under free expansion, its suitability to describe ASR-induced damage generation and propagation under restrained conditions is still unknown and should be further investigated.

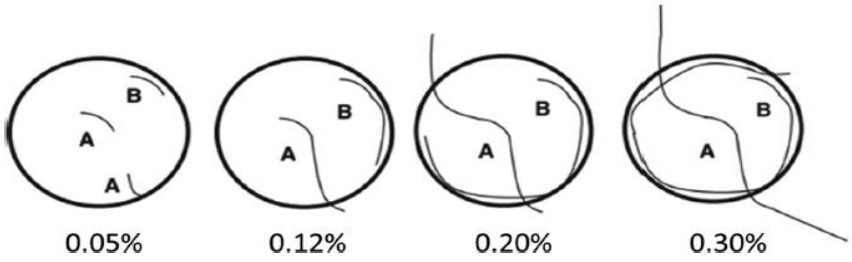

Figure 2: Qualitative model of crack propagation in ASR-affected concrete [1] *(Reproduced with permission of Elsevier)*.

6.2.2 Effect of confinement on ASR-induced development

Although the vast majority of existing research on ASR has been performed using laboratory specimens under unrestrained (i.e., free expansion) conditions [13,17,18], a few works have been conducted to understand the effect of confinement on ASR-induced development. Some of these studies [19,20] observed no or negligible ASR-induced expansion in restrained directions; moreover, no transfer of induced expansion and thus deterioration was noticed to directions with less or no confinement [21,22]. Conversely, according to Morenon et. al. [23] and Multon et. al. [24,25], the reduction of ASR-induced expansion in the confinement direction directly yields a transfer to unrestrained directions. The same observation has been made by a number of researchers [20,26–30]. These conflicting results can be attributed to numerous reasons, such as the specimen size (i.e., scale effect), casting direction, confinement ratio and orientation [31].

Generally, it is agreed that confinement helps to mitigate ASR-induced expansion of affected concrete [24]; accordingly, it has been observed that various forms of restraint may decrease ASR-induced expansion in the direction of confinement by 15 to 70% [23,24,29,30,32]. Therefore, such an expansion reduction in the restrained direction results in anisotropic development of ASR-induced damage; the more advanced the stage of ASR development, the higher the degree of anisotropy [33]. The latter means that the use of an average/overall induced expansion (i.e. average value from distinct directions) observed in concrete members with concentrated (i.e. non-uniformly distributed) or anisotropic reinforcement configurations, boundary conditions, or sustained loading may not be appropriate for analysis in some cases [29–31]. Yet,

there is current a lack of discussion in the literature on how ASR anisotropic effect might change the induced damage generation and propagation of affected concrete.

It has been found that anisotropy of ASR-affected restrained concrete could lead to major deformations due to increase of expansion in other directions [33]. Allard et. al. [33] reported that thick slabs with asymmetrically distributed longitudinal reinforcement about the centroidal axis of the rectangular cross-section deformed into trapezoidal sections after moderate to high (i.e., 0.20%) average ASR-induced expansion. Likewise, the progression and orientation of the induced cracks are significantly influenced by the boundary conditions and the reinforcement configuration of ASR-affected concrete structures/structural members. Confined reinforced concrete elastically restrained in the reinforcement direction causes tensile stresses in the reinforcing bars; thus, ASR-induced expansion is mostly suppressed in the main reinforcement direction [34]. Hence, most ASR-induced cracks in reinforced concrete members tend to be generated parallel to the main rebars [33–36] as observed by Hansen et. al. [37] in laboratory and field structural members.

Very few studies have been conducted to date on the effects of confinement on the distinct ASR petrographic distress features, crack patterns, and crack orientation of reinforced concrete members [35,36,38–41]. Barbosa et.al. [35,36] observed distinct crack patterns and orientation on various concrete cores extracted from affected structures; cores were retrieved from reinforced slab bridges in different directions (i.e., vertically and horizontally - Figures 3A and 3B, respectively), where perpendicular ASR-induced cracks to the loading were observed in vertically cored specimens while parallel cracks to the loading were verified in horizontally cored specimens.

A) 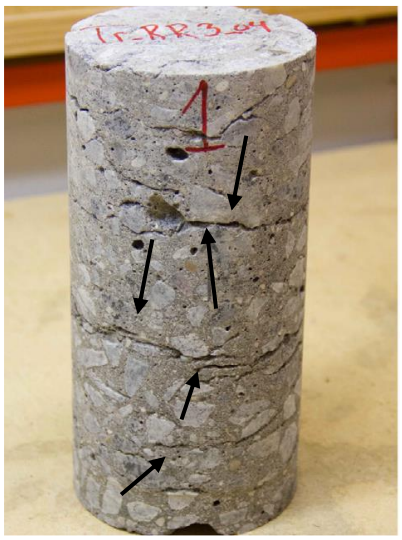

B) 

Figure 3: A) Vertically extracted cores having perpendicular ASR-induced cracks to the loading (black arrows) and B) horizontally extracted cores having parallel ASR-induced cracks to the loading (red arrows) [36] *(Reproduced with permission of Elsevier)*.

Although the above results are very interesting and indeed indicate an important impact of restraint on ASR-induced damage development, to the authors' best knowledge, there is a lack of studies quantitatively and systematically appraising this impact on concrete members displaying distinct reinforcement ratios and configurations, and presenting distinct damage degrees (i.e., induced expansion levels).

6.2.3 Damage Rating Index (DRI)

Grattan-Bellew et. al. [42,43] proposed the Damage Rating Index method (DRI), a semi-quantitative microscopic tool used to appraise damage in concrete. Distress features are counted in 1 by 1 cm squares drawn on the surface of polished concrete sections using a stereomicroscope at 15-16x magnification. The damage features are then multiplied by weighting factors whose purpose is to balance their relative importance towards the corresponding distress mechanism (e.g., ASR), as proposed by Villeneuve & Fournier [44]. The DRI number is therefore calculated and the higher the DRI number, the higher the damage degree [13]. Ideally, a surface of at least 200 cm^2 should be assessed however, for comparative purposes the final DRI value is always normalized to a 100 cm^2 area. The petrographic features included in the DRI assessment are listed in Figure 4A along with their corresponding weighting factors; some of the distress features can be observed and identified in Figure 4B.

A B

Petrographic features	Weighting factors
Closed cracks in aggregates (CCA)	0.25
Opened cracks in aggregates (OCA)	2
Opened crack with reaction product in aggregate (OCAG)	2
Coarse aggregate de-bonded (CAD)	3
Disaggregate/corroded aggregate particle (DAP)	2
Cracks in cement paste (CCP)	3
Cracks with reaction product in cement paste (CCPG)	3

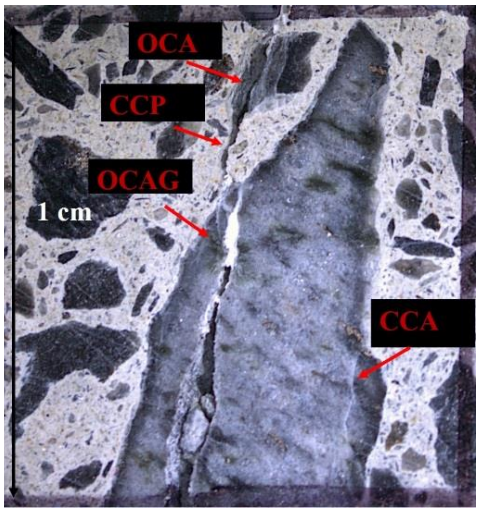

Figure 4: Damage Rating Index: A) Current weighting factors as per [44] and B) Micrograph illustrating a 1cm^2 section where some of the petrographic features listed in A can be observed and identified *(Reproduced with permission of Elsevier)*.

The proposed weighting factors as per Villeneuve & Fournier [44] aim not only to distinguish the importance of different types of features but rather reducing the variability between operators; for instance, the same weighting factor is given to a crack with or without reaction product (i.e., ASR gel) since its identification and interpretation may vary between operators [45]. Moreover, analysing the distinct DRI petrographic features, one verifies that the closed crack in the aggregates (CCA) is a feature that may be caused by, for instance, ASR-independent processes such as weathering or aggregates manufacturing; therefore a low importance is attributed to this feature (i.e., weighting factor of 0.25). Conversely, an increase in open cracks in the aggregate particles without or with gel (OCA and OCAG, respectively) is frequently observed as a function of ASR-induced development; thus, a weighting factor of 2 is given to such distress features. Lastly, a weighting factor of 3 is attributed to cracks in the cement paste without or with gel (CCP and CCPG, respectively), since those cracks reflect a more severely damaged concrete.

Besides the use of the conventional DRI method, Sanchez et. al. [1,2] proposed the utilization of supplementary petrographic analyses through the so-called "extended DRI version", where the microscopic distress features presented in Figure 4 are evaluated in absolute (counts) and relative (%) manners, without the application of any weighting factors; it has been found that supplementary observations and evaluations made through the extended DRI version may help towards a more comprehensive assessment and understanding of ASR-induced development of affected concrete. The extended DRI also allows the calculation of the crack density (CD), which represents the summation of the opened cracks in the aggregates and cement paste (with or without gel), in the system, and helps to identify the overall damage degree of the affected material. Finally, although the DRI has proven to be quite effective to appraise the

extent of damage in ASR-affected concrete under unrestrained conditions, the effect of restraint on the ASR-induced petrographic distress features and thus DRI outcomes remains mostly unknown.

6.3 Scope of the work

As stated in the previous sections, there is a need of a thorough, quantitative and systematic evaluation of the restraint effects on ASR-induced expansion and microscopic deterioration (i.e., kinetics and induced expansion, damage generation and propagation, crack pattern and orientation). Therefore, concrete blocks incorporating a highly reactive coarse aggregate and displaying distinct reinforcement configurations (i.e., none, 1D and 2D) were fabricated in the laboratory, stored in conditions enabling ASR-induced development (i.e., 38 °C and 100% R.H.) and monitored over time. At distinct expansion levels (i.e., 0.08% and 0.15%) the blocks were cored in three directions (i.e., longitudinal, transverse, and vertical) and the conventional and extended DRI versions were conducted on each of those. Finally, comparisons on the damage development, extent, pattern and orientation of restrained versus unrestrained concrete blocks at distinct deterioration levels were performed.

6.4 Materials and methods

6.4.1 Materials and mixture proportions

Eighteen concrete blocks of 450 by 450 by 675 mm (Figure 5) were fabricated in the laboratory using a concrete mixture with a design compressive strength of 35 MPa. A highly reactive coarse aggregate (i.e., Springhill - Sp) combined with a non-reactive fine aggregate (Ottawa natural sand - Ot) from a local natural pit were selected for concrete manufacturing. Table 1 provides information on the different aggregates used in this study, including the mineralogical composition of the aggregates. The coarse aggregates ranged in size from 5 to 20 mm. A conventional Portland cement (CSA Type GU, ASTM type 1) containing a high alkali content (0.88% Na_2O_{eq}) was used in the mixture. Reagent grade sodium hydroxide pellets were used to raise the total alkali content to 1.25% Na_2O_{eq}, by cement mass, to accelerate ASR-induced expansion. The concrete blocks were proportioned using the Concrete Prism Test (CPT) standard mixture proportion as per ASTM C 1293 [46] and displayed in Table 2.

Table 1: Aggregate properties selected for this study.

Aggregate				Rock type	Specific gravity (g/cm^3)	Absorption (%)	AMBT [a] 14 days expansion (%)
Type	Reactivity	Location	Name				
Coarse	Reactive	New Brunswick	Sp	Crushed greywacke	2.72	0.602	0.69
Fine	Non-reactive	Ottawa	Ot	Natural, derived granite	2.65	1.18	0.07

a) Typical expansion of ASTM C 1260.

Table 2: Concrete mix design.

Materials	Quantities in the mix (kg/m^3)
Cement	420
Fine aggregate (Ot)	681
Coarse aggregate (Sp)	1044
Water	176

6.4.2 Manufacture of concrete blocks and cylinders

To investigate the effect of restraint on ASR-induced expansion, damage generation and propagation, distinct confinement conditions/configurations were selected for this study: 1) unrestrained blocks, 2) 1D confined blocks and, 3) 2D confined blocks (Figures 5 and 6). Restraint was introduced to the blocks using internal steel reinforcing bars at a reinforcement ratio of 2% in a) the longitudinal direction (i.e., 1D confined blocks), or b) both the longitudinal and transverse directions (i.e., 2D confined blocks). This reinforcement ratio is considered moderately high, and not uncommon for certain reinforced concrete member types such as columns or wall boundary elements. Hence, for most structural member types this may be viewed as a reasonable upper limit to the degree of restraint provided by internal reinforcement where the reinforcing bars are primarily oriented along one or two orthogonal directions. Embedded 35M steel reinforcing bars, having a nominal diameter of 35 mm, were selected in order to achieve a sufficiently large bar spacing to accommodate core extraction (Figure 6). Moreover, In the case of restrained concrete, the concrete cover and spacing between the top and bottom steel rebars is 50 mm and 280 mm, respectively (Figure 6C). In the case of 2D confined blocks, the longitudinal and transverse steel reinforcing bars were professionally welded to facilitate construction (Figure 6A). It is important to notice that the reinforcement was equally distributed between the top and bottom portions of each block to avoid curvatures associated with non-uniform expansion. Effects of reinforcement distribution, external boundary conditions, and sustained loads are not considered here and are recommended topics for future work.

All blocks were demoulded after 24 hours and moist cured (i.e., 20°C) for over 24 hours. Four small holes, 10 mm in diameter by 55 mm long, were then drilled in the three main sides of the blocks: a) top (Figure 7A - points 1 and 2), b) longitudinal (Figure 7A - points 3 and 4) and c) transverse (Figure 7A - points 5 and 6). Stainless steel gauge studs were then glued in place with a fast-setting cement slurry for longitudinal expansion measurements.

Figure 5: Concrete blocks presenting: A) 2D confinement (Top View), B) 2D confinement (Side View), C) 2D confinement (Front View) and, D) Environmental chamber at 38ºC and 100% RH.

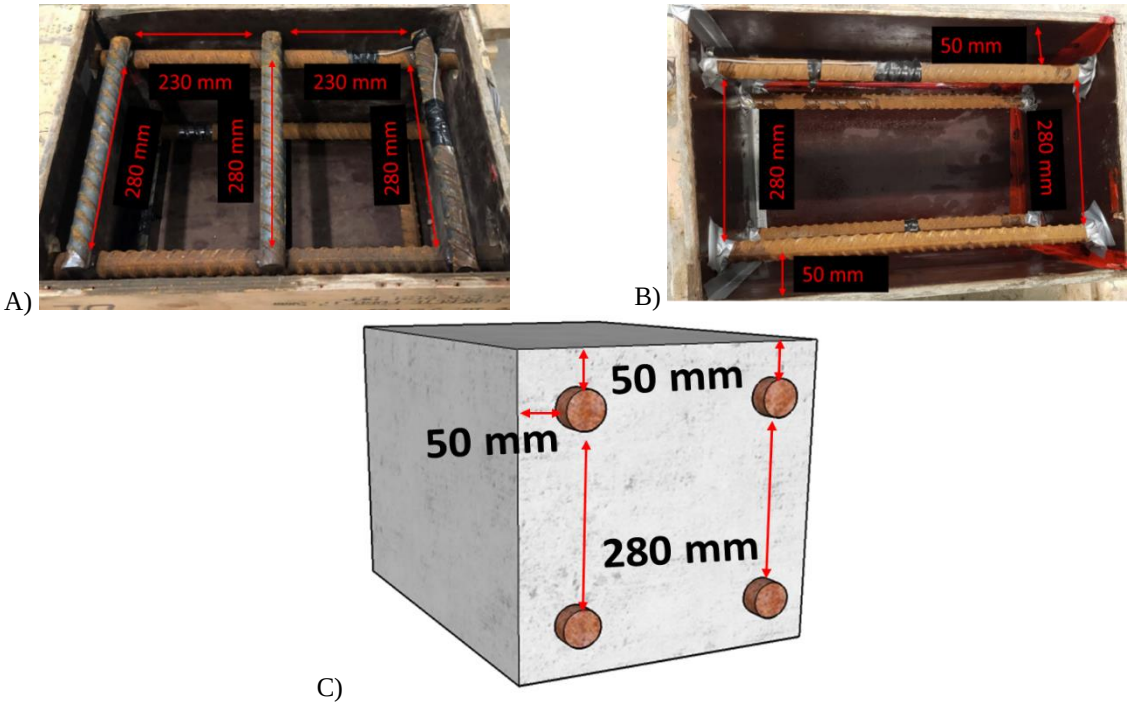

Figure 6: Confinement orientations: A) 2D confinement, B) 1D confinement and C) schematic of restrained blocks with 50 mm concrete cover and 280 mm distance between top and bottom steel bars.

For comparison purposes, 20 concrete cylinders (i.e., 100 by 200 mm) were also manufactured incorporating the same highly reactive coarse aggregate and using the same mixture proportion as the concrete blocks. The cylindrical specimens were demoulded after 24 hours and moist cured (i.e., 20°C) for 24 hours. Small holes, 8.5 mm in diameter by 19 mm long, were then drilled in both ends of each test cylinder and stainless-steel gauge studs were glued in place with a fast setting cement slurry for longitudinal expansion measurements.

After 48 hours (i.e., two days from casting), the zero reading was taken (i.e., in case of concrete blocks: top longitudinal, side longitudinal and transverse expansion measurements as per Figure 7A, and in case of cylinders: longitudinal/axial expansion measurements) and all concrete blocks were stored in an environmental chamber enabling and accelerating ASR-induced development (i.e., 38ºC and 100% RH). Likewise, the concrete cylinders were placed in sealed plastic containers of 22 liters lined with a damp cloth (Figure 7B and C) and stored in the same conditions as the concrete blocks. All specimens (i.e., blocks and cylinders) were regularly monitored over time and were placed at 23°C for 16 ± 4 hours prior to periodic expansion measurements. Upon reaching low (i.e., 0.08%) and moderate (i.e., 0.15%) expansion levels, the test cylinders and blocks were removed from the environmental chamber for the DRI analyses. Following the removal, three blocks per restraint configuration were cored to produce seven 100 by 450 mm cores (Figure 8 D) from the vertical (Figure 8 A) and transverse (Figure 8 B) directions, along with four 100 by 675 mm cores from the longitudinal (Figure 8 C) direction.

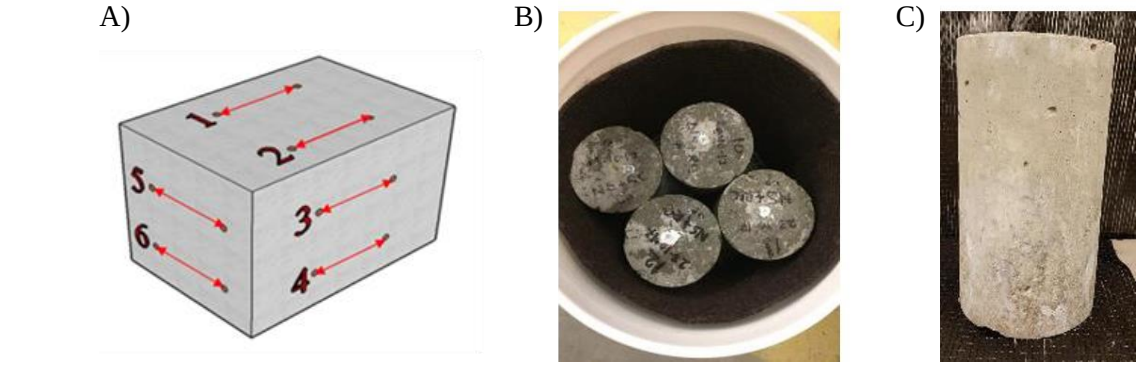

Figure 7: A) Gauge studs orientation for blocks, B) sealed bucket arrangement for the 38°C and 100% RH test and, C) affected test cylinder.

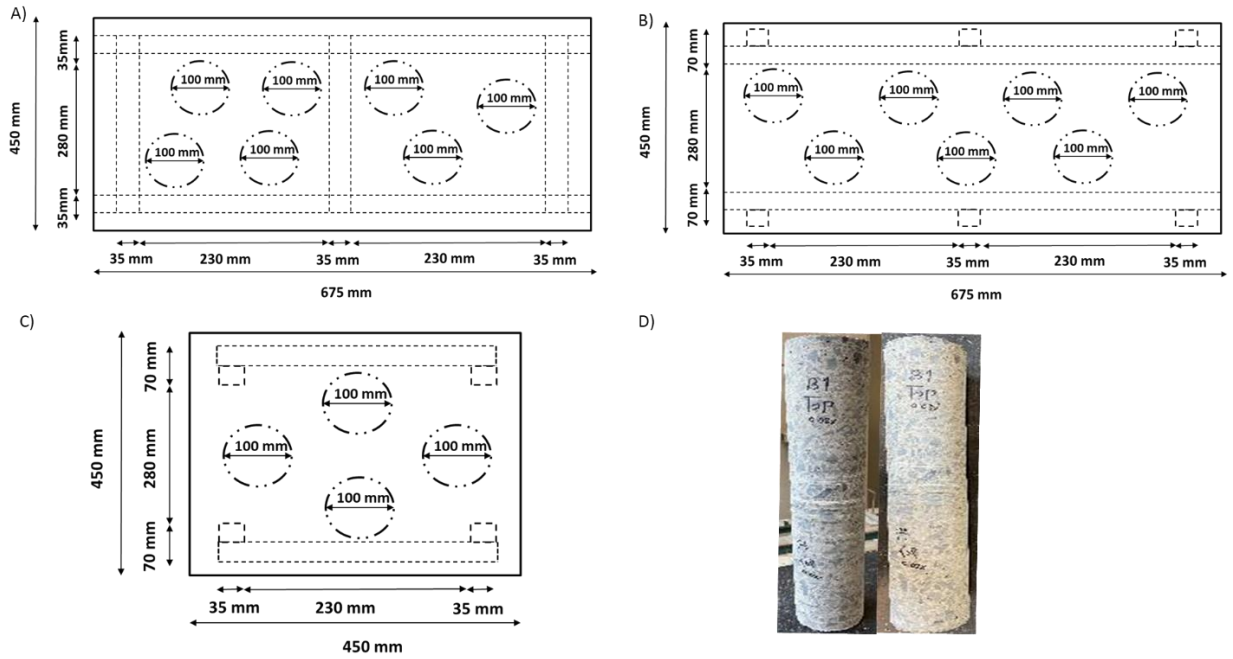

Figure 8: Qualitative sketch of the cores extracted from 2D Blocks A) vertical, B) transverse, C) longitudinal and D) core specimens of 100 mm by 450 mm.

6.4.3 Experimental procedures

The conventional and extended DRI versions were conducted on concrete cylinders and cores from ASR-affected blocks at distinct expansion levels (i.e., 0.08% and 0.15%). Prior to the microscopic assessment, two consecutive core samples from each of the three coring directions (i.e., vertical, longitudinal and transverse; total of 6 specimens per restraint condition per expansion level) and two cylinders per expansion level were cut in half longitudinally using a diamond bladed masonry saw followed by subsequent mechanical polishing with grits of 30 (coarse), 60, 140, 280, 600, 1200 and 3000 (very fine). Once the surface of the polished section was considered suitable for analysis, a 1 by 1 cm grid was drawn on the polished surface of the specimens. The distress features were then appraised as per Villeneuve and Fournier (i.e., conventional method - Figure 4) [44] and Sanchez et. al. (i.e., extended version) [1,2]. The DRI has been conducted in two different, yet related ways. First, the microscopic results were averaged from the three coring orientations (i.e., longitudinal, transverse and vertical) to assess the influence of the restraint on the "overall deterioration" of ASR-affected blocks (i.e., *Results section*). Second, the DRI was evaluated as per the coring direction (i.e., longitudinal, transverse and vertical) to appraise and quantify ASR anisotropic behaviour as a function of the restraint effect (i.e., *Discussion section*).

6.5 Results

6.5.1 ASR kinetics and development

Figure 9 presents the average induced expansions (i.e., average value of four consecutive measurements per specimen per direction over time with standard deviations ranging from 0.02% to 0.06%) as a function of time of the distinct directions of the ASR-affected concrete blocks displaying different reinforcement configurations. Figure 9A also displays the average axial expansions of concrete cylinders (standard deviation of 0.03%). Analyzing the plots, one observes that all specimens (i.e., concrete cylinders and blocks, restrained and unrestrained), were able to reach the two induced expansion levels selected for this work (i.e., 0.08% and 0.15%). Yet, the expansion kinetics (i.e., induced expansion rate) of concrete cylinders was much faster than the blocks, regardless of their reinforcement configuration (i.e., none, 1D and 2D). Furthermore, all concrete blocks presented some shrinkage (i.e., all directions) at the beginning of ASR-induced development. The induced expansions from the distinct directions as a function of time followed a similar trend (i.e., parallel curves) for all blocks. However, different values were obtained as per the distinct directions (i.e., top longitudinal, side longitudinal and transverse - Figure 7A). Moreover, the higher the restraint effect, the higher the degree of anisotropy and thus the higher the expansion scattering amongst distinct directions.

In the case of the unrestrained blocks (Figure 9A), the expansion curves are very close to each other, although the expansions are slightly higher in the transverse direction, followed by the longitudinal top and side directions. The 0.15% expansion level was reached after 175, 190, and 212 days at 38°C and 100% R.H on the transverse, longitudinal top and longitudinal side directions, respectively. Otherwise, as Figures 9B and 9C illustrate, the 1D and 2D restrained blocks displayed a much slower ASR-induced expansion development than unrestrained blocks, where a 0.15% expansion was achieved after 190, 212 and 255 days by 1D blocks, compared to 235, 275, and 340 days by 2D blocks on the transverse, longitudinal top and longitudinal sides, respectively. Furthermore, concrete cylinders showed considerably faster expansion levels when compared to all concrete blocks, where an expansion of 0.15% was reached after 70 days on average (Figure 9A). The difference between cylinders and blocks could be attributed to the size of the samples, which directly affects the moisture transfer and thus may decrease the rate of ASR-induced development in larger specimens [47,48]. Moreover, comparing the expansion levels attained by the concrete blocks as a function of time, it is clear that the restraint plays an important role on ASR-induced development (kinetics and expansion amplitude) since the higher the overall degree of restraint, the slower the expansion rate and the lower the amplitude over time. As such, averaging all directions, one observes that a 0.15% expansion level is attained by the unrestrained concrete at 190 days followed by the 1D and 2D concrete blocks at 235 and 270 days, respectively. Likewise, the non-restrained blocks reached (on

average) a maximum expansion of 0.27% at 340 days, while the 1D and 2D blocks attained respectively expansions of 0.23% and 0.18% (on average) at the same time period. The above influence of restraint on ASR-induced expansion kinetics and amplitude has already been reported in the literature [23,49,50].

The expansion measurements on distinct surfaces of the restrained blocks revealed the transfer of induced expansion from restrained directions to directions with less or no restraint resulting in higher expansion levels. As Figures 9B and 9C illustrate, the transverse face reached higher expansion levels followed by the top surface then the longitudinal side. This shows that a higher amount of ASR-induced expansion has been generated in the non/less-restrained direction of the reinforced blocks (i.e., transverse direction), possibly revealing an effect of restraint on constitutive anisotropy of the specimens as previously reported in the literature [23,31,50]. Moreover, although the 2D blocks present the same reinforcement ratio in the longitudinal and transverse directions (i.e., 2%), the reinforcement configuration is different in these two directions (i.e., 2 bars of 35 mm in the longitudinal direction and 3 bars of 35 mm in the transverse direction). This difference along with geometric features (i.e., longer size and thus friction per unit width for the longitudinal direction) might be among the causes the of the higher expansion obtained for the transverse faces. As such, while the side longitudinal surface of 1D confinement (i.e., restrained direction) reached 0.15% of expansion at 255 days, the top longitudinal and the transverse surfaces reached 0.17% and 0.21% of expansion at the same time period, respectively. Likewise, the longitudinal surface of the 2D blocks reached 0.15% at 340 days, while the top longitudinal and the transverse reached 0.18% and 0.22% respectively at the same age. The above confirms that the relative expansion levels achieved by the different blocks' faces are influenced by the restraint direction (i.e., transverse > longitudinal top > longitudinal side) along with reinforcement configuration and geometric features as per [51]. Furthermore, these results clearly demonstrate that the longitudinal side of all concrete blocks represents the lowest expansion level among all other surfaces as previously observed by [51] since they are not (or at least less) influenced by local effects [23,29,30] (i.e., the top drying/wetting cycles, differential restriction between bottom and top surfaces) and/or are parallel to the main reinforcement. Therefore, for the sake of further microscopic analysis, the expansion level adopted as "representative" of a given damage degree was measured on the longitudinal side for all concrete blocks (as Figure 7A -longitudinal measurements starting from points 3 and 4).

A)

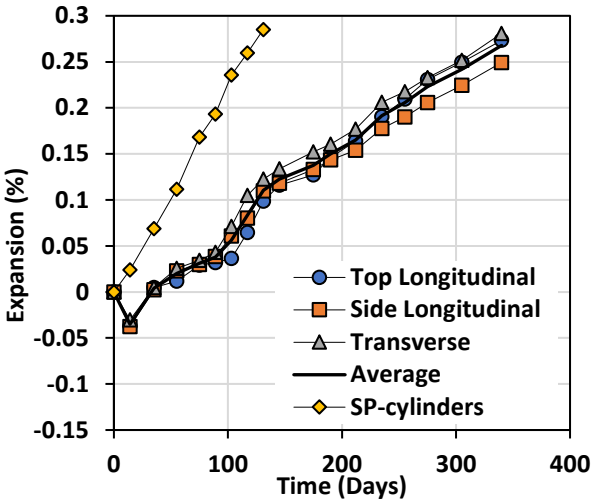

B)

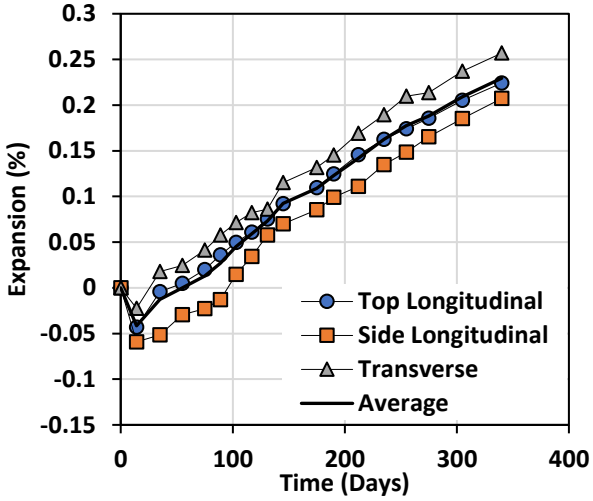

C)

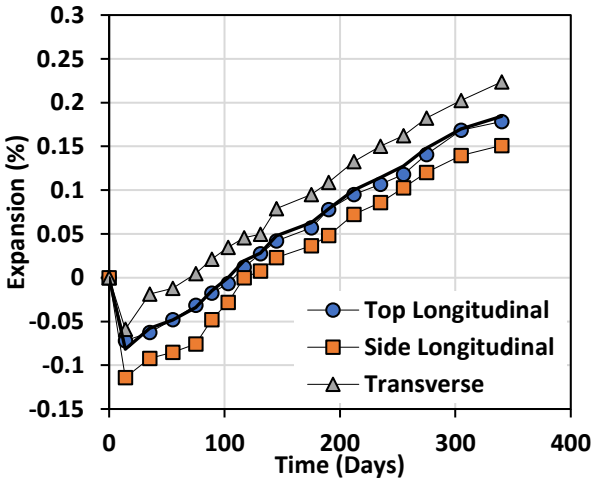

Figure 9: ASR kinetics (expansion vs. time) for: A) unrestrained concrete specimens, B) 1D concrete blocks and, C) 2D concrete blocks incorporating distinct surfaces of the blocks.

6.5.2 Microscopic distress features and crack density

The ASR microscopic distress features and crack density (CD) of the concrete specimens as a function of expansion were evaluated using the extended version of the DRI as proposed by Sanchez et al. [1,2]. It is worth noting that the results presented hereafter are the "overall" microscopic distress features and CD values (i.e., average of six specimens, two per direction) from the ASR-affected blocks at each expansion level tested.

Figure 10A illustrates the distinct microscopic features appraised in a relative (i.e., as counts, normalized to 100 cm^2) manner, without the use of the proposed DRI weighting factors. The most common microscopic feature in all concrete specimens appraised corresponds to the group of closed cracks in the aggregates

(CCA), for both given expansion levels. Although for each concrete type the counts of open cracks in the aggregates and cracks in the cement paste increase with expansion, the difference remains in the total counts of cracks. The unrestrained concrete blocks present 442 counts at 0.08%; yet, a higher count at 0.15% (i.e., 565) is observed. Moreover, the 1D and 2D blocks display 463 and 438 counts at 0.08% of expansion, while they raise to 512 and 508 at 0.15%, respectively. The latter demonstrates that the microscopic features (counts) are affected by the restraint configuration (i.e., counts of unrestrained concrete > 1D > 2D). Noticeably, the concrete cylinders present the highest counts of cracks of 502 and 570 for 0.08% and 0.15% of expansion, respectively. It is worth noting that the data in brief can be found in Table 4 of the supplementary materials section.

The relative proportions (%) of the microscopic features as a function of the expansion for all concrete specimens are illustrated in Figure 10B. The proportions are nearly identical for each concrete type, with the proportions of open cracks in the aggregate and cracks in the cement paste increasing with expansion. For the slightly damaged (i.e., expansion level of 0.08%) concrete, the groups of closed cracks in aggregate and open cracks in aggregate represent between 70 to 80% and 7 to 15% of the microscopic features, respectively. On the other hand, for the moderately damaged (i.e., expansion level of 0.15%) concrete, the group of closed cracks in aggregate decreases, ranging from 45 to 55%, and the proportion of open cracks in aggregate increases, representing between 15 to 25%. The proportion of the group of cracks in cement paste however remains quite low for all concrete types at both given expansion levels, being less than 10% for the majority of the concrete specimens in this study.

A)

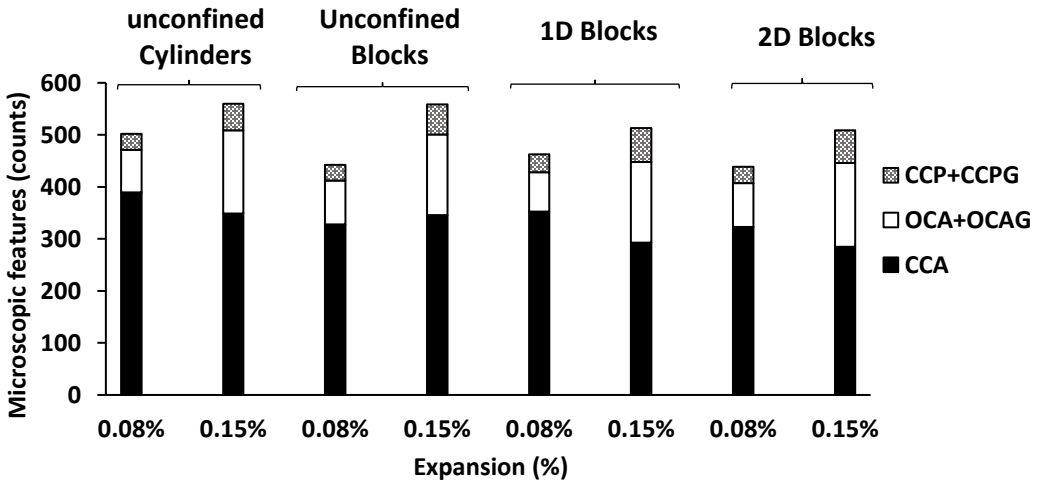

B)

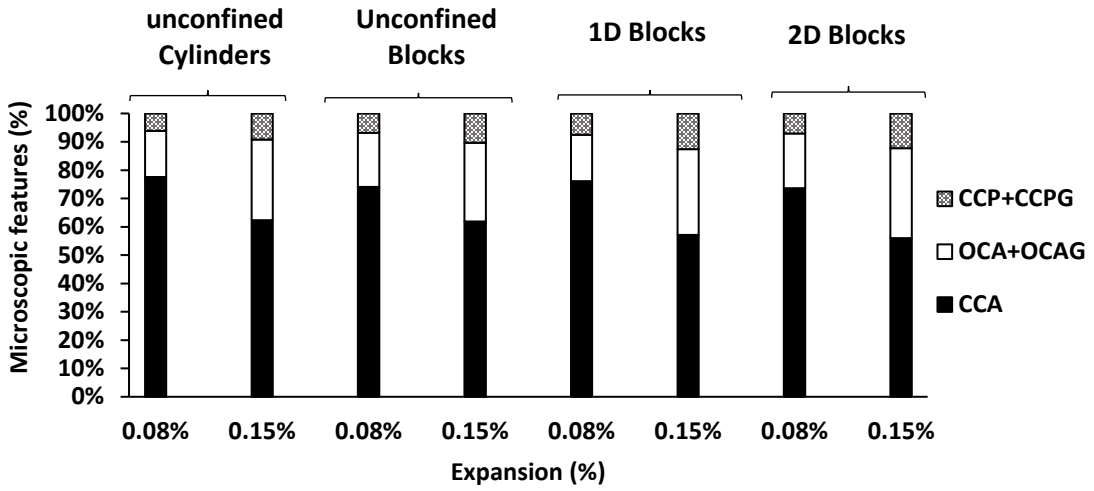

Figure 10: Microscopic features of deterioration as: A) Counts normalized for 100 cm^2 surface area and B) Percentage without using the weighting factors.

Figure 11 displays the crack density (CD – crack counts/cm^2) obtained from the distinct concrete specimens studied in this research without the use of the DRI weighting factors. At 0.08% of expansion, the unrestrained concrete block yielded a CD of 2.59 counts/cm^2 while the 1D and 2D concrete blocks displayed a CD of 2.55 counts/cm^2 and 2.62 counts/cm^2, respectively. Noticeably, the CD increases with increasing expansion for each type of concrete where, at 0.15% of expansion, the CD is slightly higher for the 2D concrete blocks (i.e., 5.10 counts/cm^2) followed by the 1D concrete blocks (i.e., 5.05 counts/cm^2) then the unrestrained concrete blocks (i.e., 4.83 counts/cm^2). Similar to the microscopic features, the achieved crack density is influenced by the direction of restraint (i.e., CD 2D > CD 1D > CD unrestrained). Furthermore, concrete cylinders showed the CD of 2.56 counts/cm^2 for slightly damaged concrete (i.e., expansion level of 0.08%) and reached 4.73 counts/cm^2 for moderately damaged concrete (i.e., expansion level of 0.15%). It is worth noting that the data in brief can be found in Table 4 of the supplementary materials section.

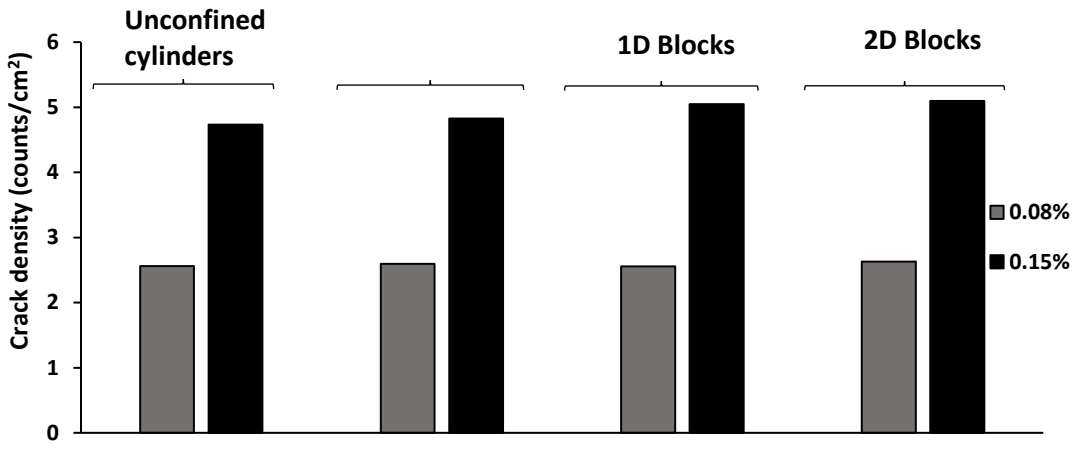

Figure 11: Crack density as a function of expansion.

6.5.3 Crack widths/lengths versus degree of expansion/damage

The maximum length and widths of cracks as a function of expansion may act as indicators to assess the development/progress of ASR-induced deterioration in concrete (Figure 12). As proposed by Sanchez et. al. [2], the maximum length of cracks (L_{max}) was measured for cracks in the cement paste only or cracks in aggregates extending into the cement paste. The maximum crack width (W_{max}) was measured for cracks within the aggregate particles only, as this is considered a more readily/reliably measure than in the case of cracks in the cement paste. The maximum lengths and widths of cracks were measured manually using a clear comparator card. In this section, the "overall" crack length and width results (i.e., average of six specimens, two per direction) from the ASR-affected specimens are presented.

Analyzing the results, one observes that the maximum crack length increases with expansion for each of the restraint conditions. At an expansion level of 0.08%, the maximum crack length of 12 mm was measured for the unrestrained and restrained concrete blocks while a maximum crack length of 14 mm was seen in the concrete cylinders (Figure 12A). At an expansion level of 0.015%, the unrestrained concrete block presented the longest crack at 18 mm followed by 1D concrete blocks displaying a maximum crack length of 17 mm, while the 2D concrete blocks presented the shortest crack at 16 mm (i.e., L_{max} unrestrained > L_{max} 1D > L_{max} 2D). Likewise, the maximum crack width was found to increase with expansion for all specimens (Figure 12B); the maximum crack width measured was 0.10 mm at 0.08% expansion for all specimens (blocks and cylinders), while different yet quite similar maximum widths of 0.15 mm, 0.14 mm and 0.16 mm were gathered for the unrestrained concrete blocks, 1D and 2D blocks (respectively), at 0.15% of expansion (i.e., W_{max} 2D > W_{max} unrestrained > W_{max} 1D). Moreover, the concrete cylinders presented a maximum crack length and width of 17 mm and 0.15 mm respectively, at 0.15% of expansion. It is worth mentioning that the data in brief can be found in Table 4 of the supplementary materials section.

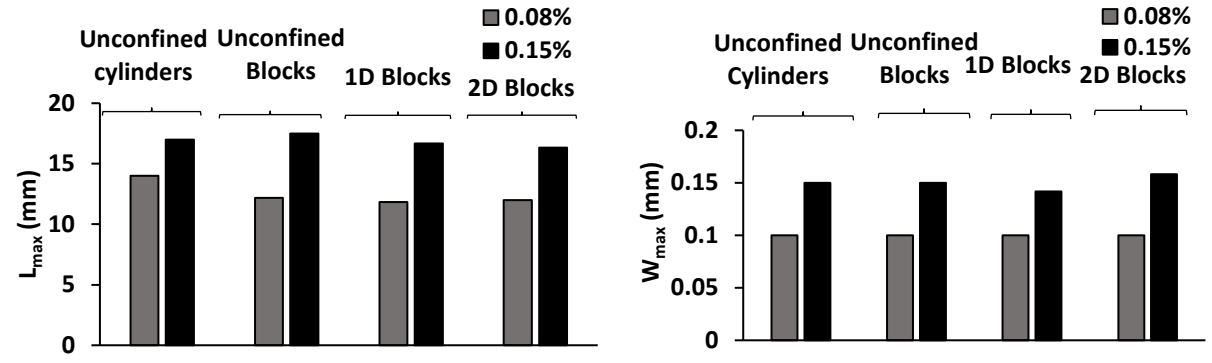

Figure 12: A) Maximum length and B) Maximum width of cracks for all concrete specimens as function of expansion.

6.5.4 Quantitative assessment of damage through DRI

Figure 13 represents the "overall" DRI values (i.e., average of six specimens, two per direction) for all concrete specimens incorporating the Springhill reactive coarse aggregate. In general, microscopic investigations verified that the opened cracks (i.e., in the aggregates and in the cement paste) increase with expansion, leading to an increase of the DRI number in all concrete specimens. One interesting point to notice is that all specimens generally follow the same trend with increasing expansion. As such, the DRI numbers for unrestrained concrete were 340 and 575 for slightly damaged (i.e., expansion level of 0.08%) and moderately damaged concrete (i.e., expansion level of 0.15%), respectively. The 1D and 2D-confined concrete presented similar DRI numbers of 368 and 343 at 0.08%, as well as 579 and 574 at 0.15% expansion, respectively. The above suggests that although the microscopic distress features (in counts - see section 5.2) are slightly different for distinct restraint conditions, the "overall" damage obtained through the DRI, that accounts for not only the number of counts but rather the number and importance of the crack counts (i.e., counts x weighing factors), is quite similar for the distinct concrete blocks appraised in this study. Comparing the DRI numbers of blocks and cylinders, one notices that they generally show similar trends with the concrete cylinders displaying a slightly larger DRI number at 0.08% (i.e., 353) and similar DRI value to unrestrained concrete blocks at 0.15% (i.e., 575). It is worth saying that the data in brief can be found in Table 4 of the supplementary materials section.

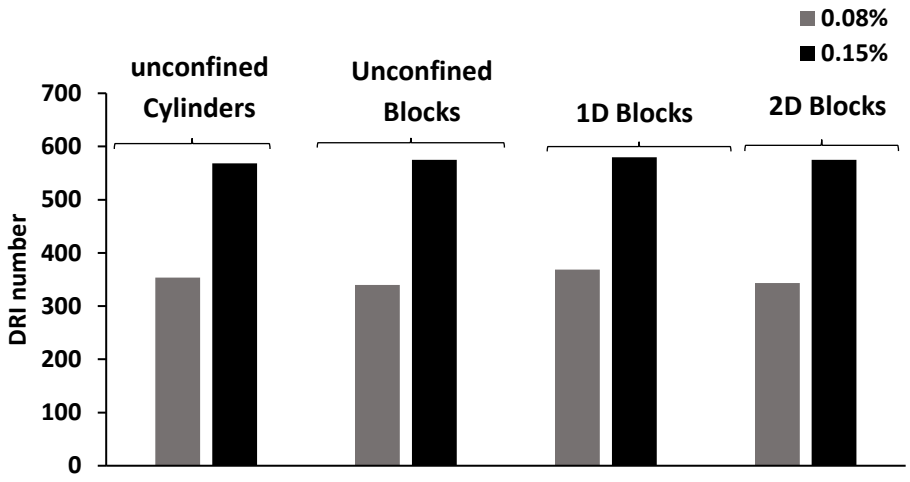

Figure 13: DRI number as a function of expansion.

6.6 Discussion

6.6.1 Effect of restraint on the "overall" ASR-induced expansion and damage development

The microscopic assessment (i.e., overall results, disregarding the cores direction) performed during this study enabled some key observations to better understand ASR-induced damage features and their propagation in restrained concrete. The microscopic features of deterioration (in counts – Figure 10A), cracking density (Figure 11) and maximum cracks lengths and widths (Figure 12A and B) clearly demonstrate the influence of the restraint on ASR damage development; i.e., the higher the restraint, the slightly lower the cracks counts and maximum lengths, and the slightly higher the crack density. Conversely, the crack pattern displayed through the microscopic features of deterioration (in % - Figure 10B) and DRI number look like very similar for all specimens, regardless of their restraint condition. The above means that the overall deterioration of the distinct specimens evaluated is roughly similar, although some microscopic distress features seem to "change" according to the restraint configuration. For instance, closed cracks in the aggregates (CCA) were more observed in unrestrained specimens; this implies that some closed cracks in the aggregates (CCA) might reopen due to ASR-development under restraint. Nevertheless, regardless of the restraint condition, the distinct types of cracks and thus overall damage increased as a function of ASR-induced expansion, as expected and verified in previous studies [1,3,13,17]

To better visualize the above discussion, Figure 14 illustrates the detailed overall DRI charts (i.e., average of six specimens, two per direction), displaying all the petrographic features identified in the method obtained from the distinct unrestrained/restrained specimens. Analyzing the charts, one observes that all specimens show a general increase in the number of open cracks in the aggregates without and with gel (i.e., OCA and OCAG, respectively) and cracks in the cement paste without and with gel (i.e., CCP and

CCPG, respectively) from 0.08% to 0.15% of expansion. Even though the DRI numbers are quite similar at 0.15% of expansion for all specimens, the most noticeable differences in damage features between unrestrained and restrained concrete are the closed cracks in the aggregates (CCA – blue chart), open cracks in the aggregates (OCA – red chart) and the cracks in the cement paste (CCP - orange chart). The closed cracks in the aggregates (CCA) and the open cracks in the aggregates (OCA) are higher for the unrestrained specimens (i.e., ≈86 vs ≈72 and ≈310 vs ≈280 on average, respectively) whereas the cement paste cracks are higher for the restrained concrete (i.e., ≈190 vs ≈163, on average). Moreover, open cracks in the non-reactive fine aggregate particles start to be observed at 0.15% of expansion, which accounts for almost 16% of the total number of open cracks in the aggregates. Cracking of non-reactive particles and the increase in cracks in the cement paste of restrained concrete could be due to the anisotropic character of ASR under restraint (i.e., decrease in induced expansion and deterioration in the main reinforcement direction and transfer to less restrained directions).

As Figures 13 and 14 illustrate, the average DRI values for the slightly damaged concrete ranges from 340 to 370, followed by 560 to 580 for the moderately damaged concrete. Notably, the results gathered in this study from restrained concrete follow the same trend as proposed by Sanchez et. al. [13] while evaluating concrete under unrestrained expansion (Table 3). The latter was proposed with a confidence level of 95% after the appraisal of 20 different concrete mixtures presenting distinct mechanical properties (i.e., 25, 35 and 45 MPa) and incorporating 13 different reactive aggregate lithotypes. It was therefore revealed that the distress features and crack propagation in ASR-affected concrete are similar despite the concrete and aggregate type; hence, the DRI value correlates quite well (almost linearly) with the amount of ASR-induced expansion [13].

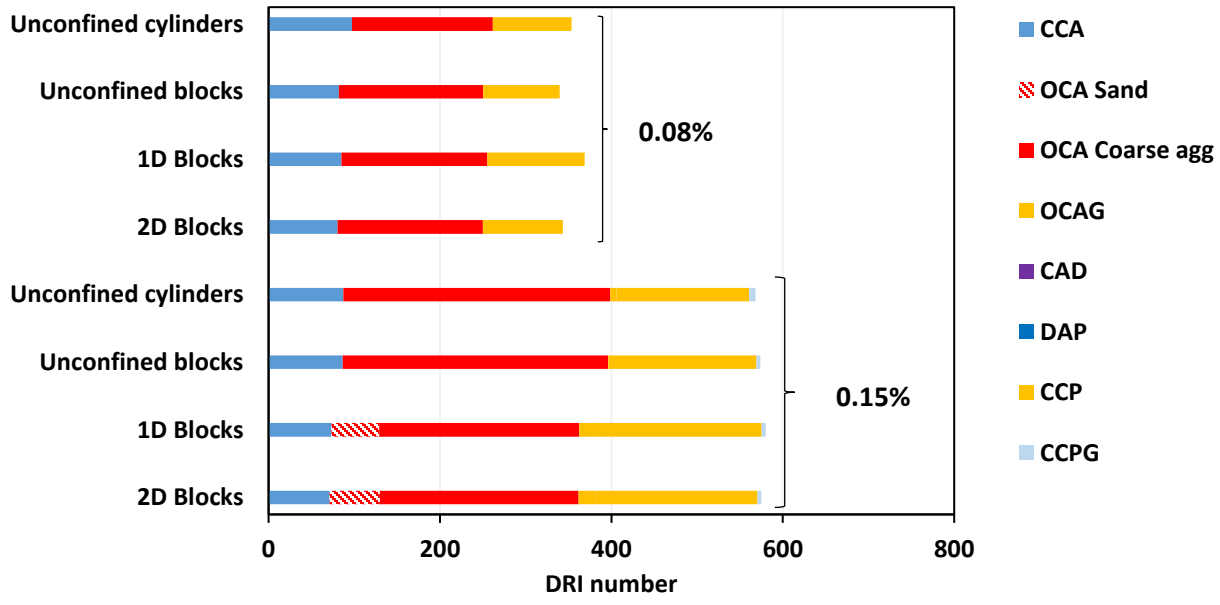

Figure 14: DRI charts all concrete specimens.

The present results indicate that the chart as per Sanchez et. al. [13] can be used to evaluate the "overall" (i.e., average results from distinct directions) ASR-induced damage development regardless of the restraint condition. In other words, ASR-induced damage does not seem to significantly change the "overall quantitative" DRI number as a function of the restraint condition, although some differences in crack features (pattern and orientation) were found and will be discussed in the next sections. Nevertheless, from Figure 9 one could notice that ASR-induced expansion indeed changes with the restraint configuration; i.e., the higher the restraint, the slower the induced expansion (i.e., lower expansion rate) and the lower the expansion amplitude at a given time period. Furthermore, the results presented in Figure 9 also indicate that expansion transfer takes place in the direction of less restraint (i.e., distinct measured expansions from different directions). Hence, a thorough study on ASR anisotropy is required to fully understand the effect of restraint on ASR-induced damage generation and propagation.

Table 3: Classification of the damage degree in concrete due to ASR [13] *(Reproduced with permission of Elsevier)*.

Classification of ASR damage degree (%)	Reference expansion level (%) [13]	Assessment of ASR (DRI number)				
		Conventional Concrete [13]	Expansion level from this study	Unrestrained concrete blocks	1D concrete blocks	2D concrete blocks
Negligible	0.00–0.03	100–155		-	-	-
Marginal	0.04 ± 0.01	210–400	0.08%	330-350	328-350	330-355
Moderate	0.11 ± 0.01	330–500	0.15%	565-580	540-580	520-580
High	0.20 ± 0.01	500–765				
Very high	0.30 ± 0.01	600–925				

6.6.2 Effect of restraint on ASR anisotropy

It has been observed that the restraint configuration could affect on ASR-induced damage features (i.e., pattern and orientation) [36] and their perceived development in affected restrained concrete. To further understand this effect, Figures 15, 16 and 17 display the CD, maximum crack length and width, and DRI chart, respectively, for concrete cores obtained from distinct directions (i.e., coring orientations – vertical, longitudinal and transverse). It is worth noting that the data in brief of the CD, maximum crack length and width, and DRI chart can be found in Table 5 of the supplementary materials section. For unrestrained concrete, there is no significant variation of CD, maximum crack length and width, and DRI values for distinct coring orientations for both slightly damaged (0.08%) and moderately damaged (0.15%) concrete. The 1D concrete blocks' vertical and transverse cores (i.e., unrestrained/ less restrained directions) on the other hand present a 38% higher CD, 37% longer cracks, and 30% and 33% higher DRI values, respectively, when compared to the longitudinal cores (i.e., restrained direction) for both slightly damaged and moderately damaged concrete. Moreover, even though similar maximum crack widths were verified in distinct directions for slightly damaged 1D concrete (0.08%), 25% wider cracks (on average) were observed in the vertical and transverse cores (i.e., unrestrained direction) when compared to the longitudinal cores

(i.e., restrained direction) for moderately damaged 1D blocks (0.15%). Comparing the average CD, maximum crack length and width, and DRI values of 1D concrete blocks with distinct coring orientations for both slightly damaged (0.08%) and moderately damaged (0.15%) concrete, one notices that vertical and transverse cores demonstrate higher values than the average, while the longitudinal specimens display lower results. This shows that using the average values (or "overall deterioration values") clearly underestimates ASR-induced damage in unrestrained directions while overestimates restrained orientations. Likewise, for 2D-confined concrete blocks, the vertical cores (i.e., unrestrained direction) presented the highest amount of induced damage, while the transverse and longitudinal cores (i.e., restrained directions) did only display a slight difference between them. The vertical 2D cores demonstrated an increase of almost 28% and 69% for CD, 60% and 38% for the maximum length, and 29% and 62% for the DRI number for both slightly and moderately damaged concrete, respectively, compared to the transverse and longitudinal samples. Yet, no significant difference in the crack width for slightly damaged concrete was observed; on average 48% wider cracks are identified in the vertical cores (i.e., unrestrained direction) when compared to the transverse and longitudinal cores (i.e., restrained direction) for moderately damaged 2D concrete blocks. As for the 1D blocks, if one uses the average values (or "overall deterioration values") for evaluation of ASR-induced deterioration of 2D blocks, one may underestimate the deterioration in unrestrained directions while overestimating it in restrained orientations.

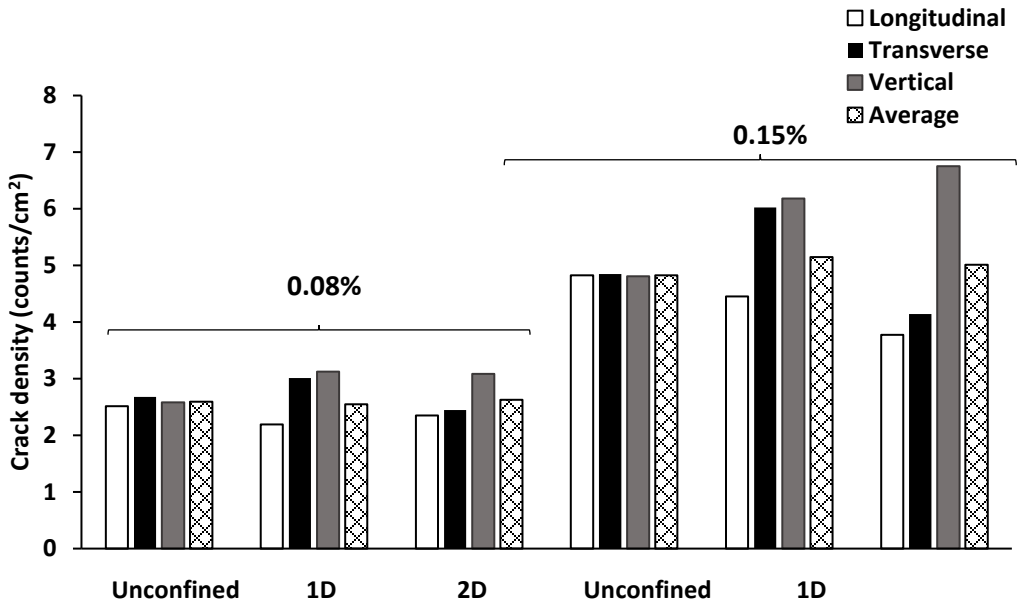

Figure 15: Crack density as a function of coring direction for specified expansion in concrete blocks.

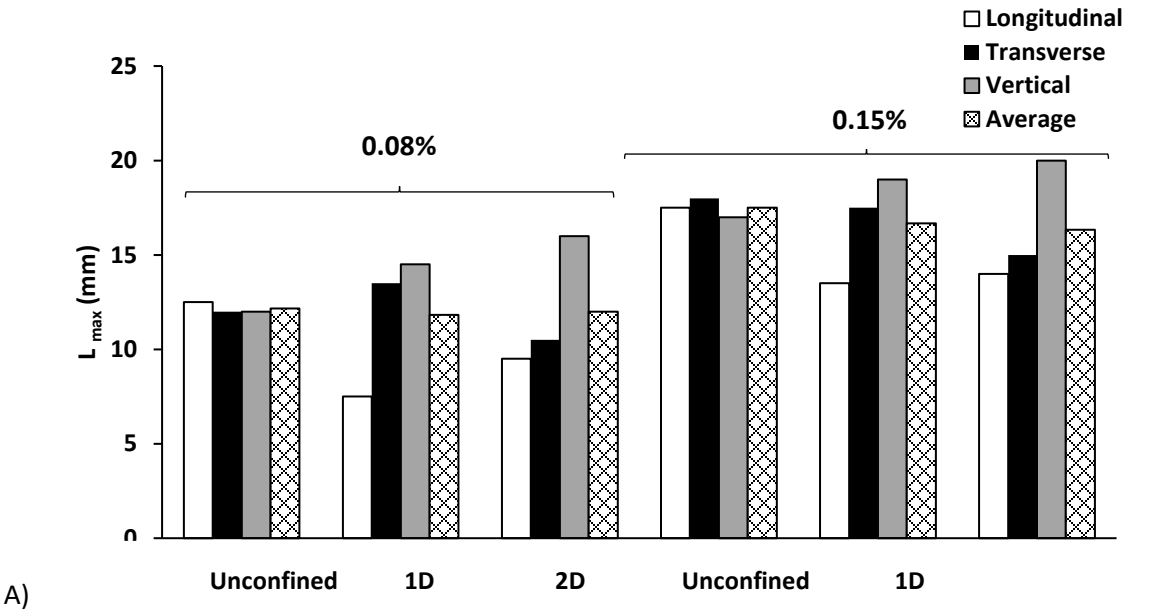

A)

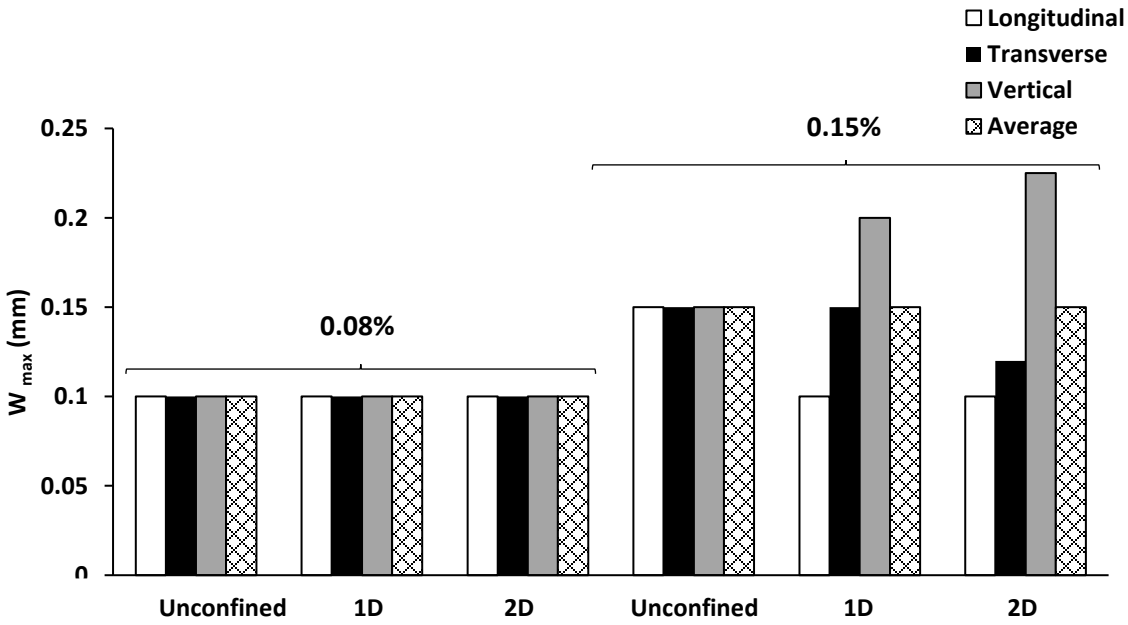

B)

Figure 16: Maximum length (A), and width (B) of cracking as a function of coring direction for specified expansion in concrete blocks.

A) unrestrained blocks B)1D blocks

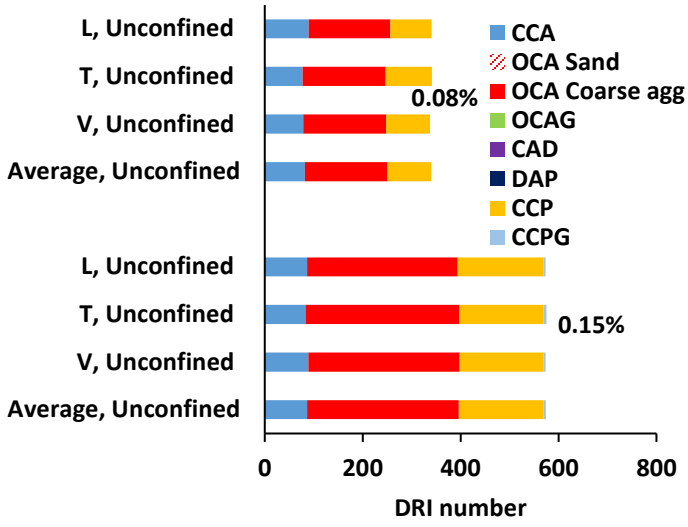

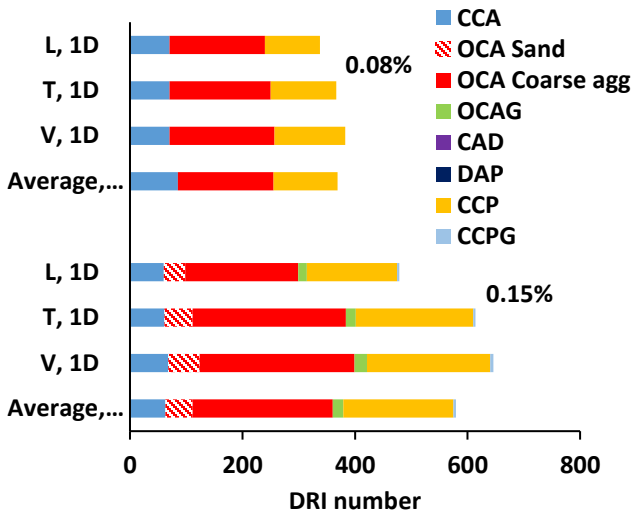

C) 2D blocks

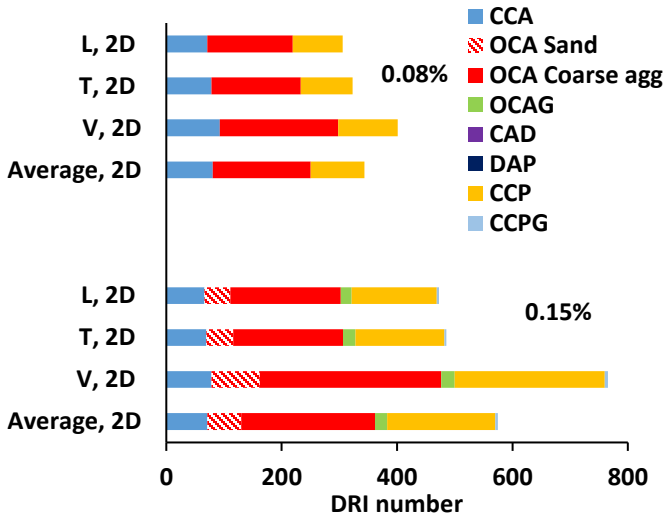

Figure 17: DRI charts as a function of coring direction for specified expansion in concrete blocks.

6.6.3 Understanding ASR-induced damage development of unrestrained and restrained concrete

Previous sections discussed the use of "overall damage values" for appraising ASR affected unrestrained and restrained concrete along with the importance of anisotropic effects generated by members displaying different restraint configurations. With this previous understanding, the current section aims to describe and compare ASR-induced damage development (i.e., cracks generation and propagation) of unrestrained and restrained concrete.

- *Unrestrained concrete specimens*

As illustrated by the DRI charts (Figure 17A), there is no considerable difference amongst the various damage features in distinct coring directions of both slightly damaged (0.08%) and moderately damaged

(0.15%) unrestrained concrete. These results attest that the distinct coring directions follow a similar damage development (i.e., cracks generation and propagation) than the one proposed by Sanchez et. al. [1] for concrete under "free expansion conditions" and displayed in Figure 2. According to Sanchez et al [1], ASR-induced cracks ("sharp" and "onion skin" crack types) are initially developed within the aggregates at low expansion levels (e.g., 0.05%); these cracks enhance in length and width with an increase in expansion and start extending to the cement paste at moderate expansion levels (e.g., 0.12%). Finally, the cracks reach the cement paste completely at high expansion levels (e.g., 0.20%), linking to each other later on, at very high levels of expansion (0.30%). In this work, damage features similar to those proposed by Sanchez et. al. [1], including "sharp" and "onion skin" crack types were identified in all concrete specimens. Figures 18A and 18B illustrate these two crack types, respectively at 0.15% of expansion. Figures 18C and 18D display open cracks in the aggregates (OCA) slightly extending into the cement paste along with open cracks in the aggregates (OCA) with ASR products (i.e., ASR gel), respectively.

A) Sharp crack in unrestrained concrete blocks (close and open cracks in aggregate)

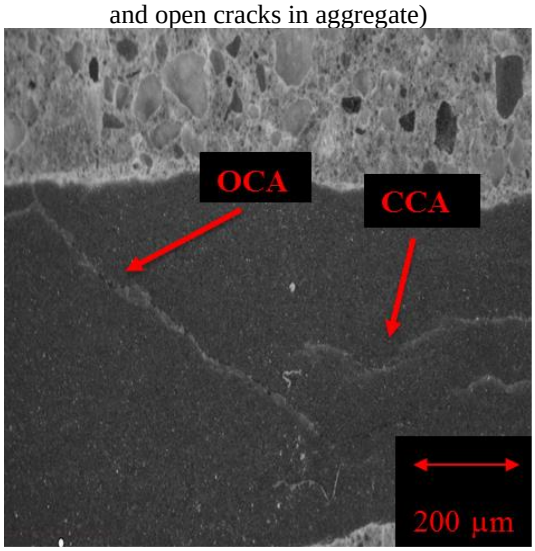

B) Onion skin crack in unrestrained concrete blocks (close crack in aggregate)

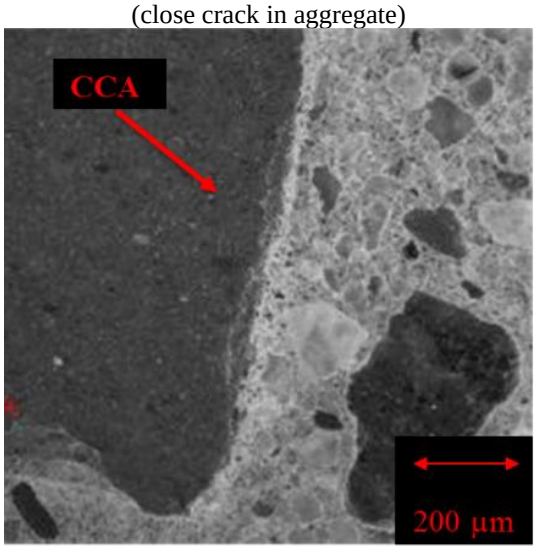

C) Open cracks in aggeregate run into cement paste

D) Open crack in the aggregate with gel in unrestrained concrete block

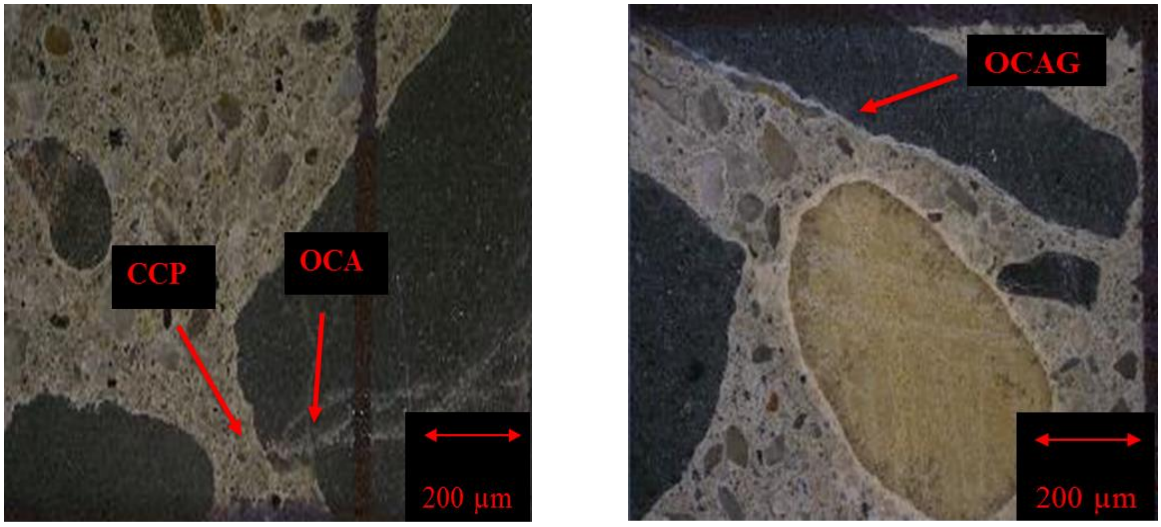

Figure 18: Typical cracking features in the unrestrained concrete cylinders/blocks.

- *Restrained concrete specimens*

In the case of restrained concrete, ASR-induced development (i.e., cracks generation and propagation) was found to be considerably different from unrestrained concrete (especially at moderate expansion levels) due to the important anisotropic effects taking place under restraint conditions. Figures 17B and C display the DRI charts for 1D and 2D confined blocks, respectively. For slightly damaged concrete (e.g., 0.08%), ASR-induced cracks seem to have a similar pattern in restrained and unrestrained blocks (i.e., majority of cracks within the aggregates - OCA, with some of them extending to the cement paste). This means that the descriptive damage development model proposed by Sanchez et al. [1] might still be applied to slightly damage concrete under restraint. Conversely, for moderately damaged concrete (0.15%, Figures 17B and C), different damage features are observed in restrained concrete (1D and 2D blocks), as follows: a) different damage degrees are observed as per the different coring directions (i.e., anisotropic effect) as thoroughly discussed in the section 6.2; b) a lower number of closed cracks in the aggregates and open cracks in the reactive coarse aggregate particles (CCA and OCA – blue and red charts from Figure 17, respectively) is found in the restrained blocks; c) some non-reactive fine aggregates start displaying opened cracks (OCA sand – white with red stripes chart, Figure 19A) which is not observed in unrestrained concrete and; d) a higher number of open cracks presenting ASR products (i.e., OCAG – green chart, Figures 19B and 19C) is identified in restrained concrete. These distress features were observed in all directions of restrained specimens. Furthermore, both “sharp” and “onion skin” cracks were verified in the distinct directions of restrained concrete (Figures 19D and 19E, respectively, at 0.15% of expansion).

The above differences in distress features observed in restrained concrete emphasizes that ASR-induced damage generation and propagation under restraint differs from the model proposed by Sanchez et al [1] under “free expansion” conditions, especially from moderate expansion levels and onwards. Hence, the

microscopic results from Figure 17 seem to indicate that besides the previously reported [20,23–30] and currently identified ASR anisotropy, affected concrete under restraint may develop important (and higher) tensile stresses within the aggregates, which could accelerate the process of increasing (in length) ASR pre-existing cracks, causing the observed reduction of open cracks in the reactive aggregate particles (OCA – red chart from Figure 17) along with the increase of cracks in the cement paste (CCP- orange chart from Figure 17). In other words, once ASR is triggered and cracks are initially developed at low expansion levels, the stresses generated under restraint may primarily increase ASR previously generated cracks than creating new ones in the system from moderate expansion levels. Moreover, these important tensile stresses generated under restraint may even reduce the closed cracks in the aggregates (CCA - blue chart from Figure 17), transforming then into fast tracks for open cracks in the aggregates (OCA) and developing further cracks in the non-reactive fine aggregate particles (OCA sand, white with red stripes chart from Figure 17). This clearly suggests that the impact of ASR on the mechanical properties of affected concrete might be different from restrained and non-restrained concrete and should be thoroughly investigated in future studies.

A) Open cracks in non- reactive fine aggregate

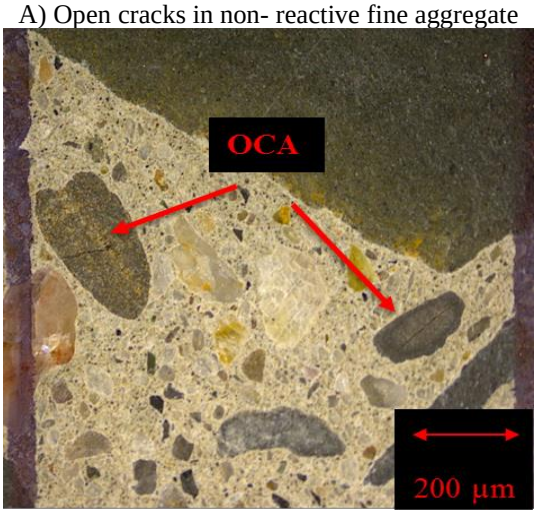

B) Open crack with gel in 1D blocks at 0.15%

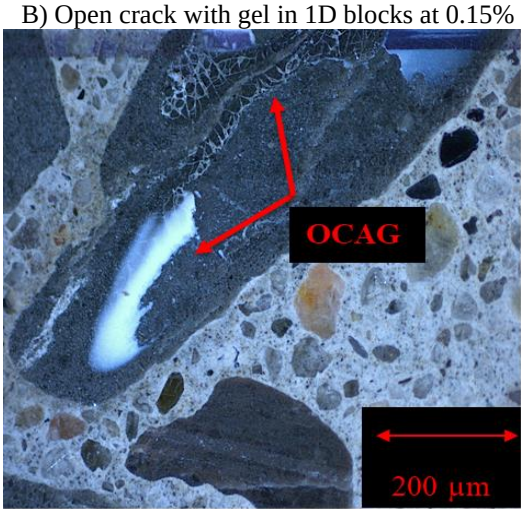

C) Open crack with gel in 2D blocks at 0.15% with 1: Magnified sector

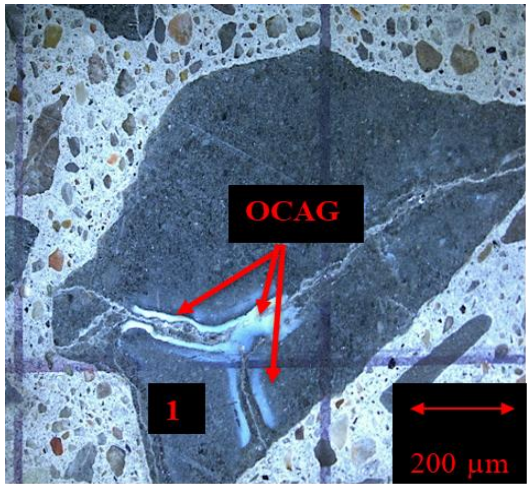

D) Sharp cracks in restrained concrete blocks (close crack in aggregate)

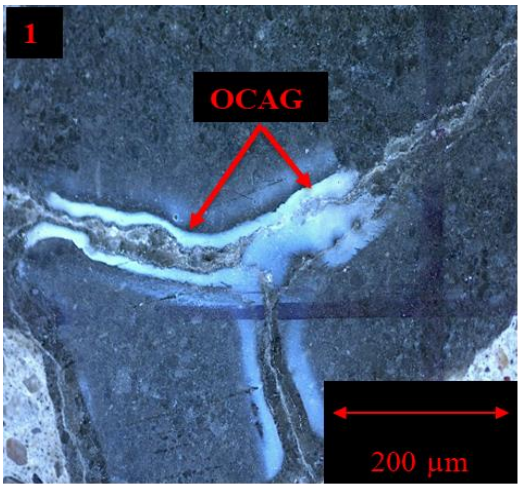

E) Onion skin crack in aggregate (Open crack in aggregate)

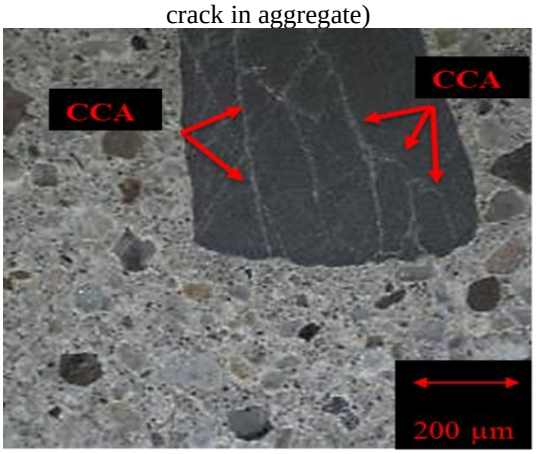

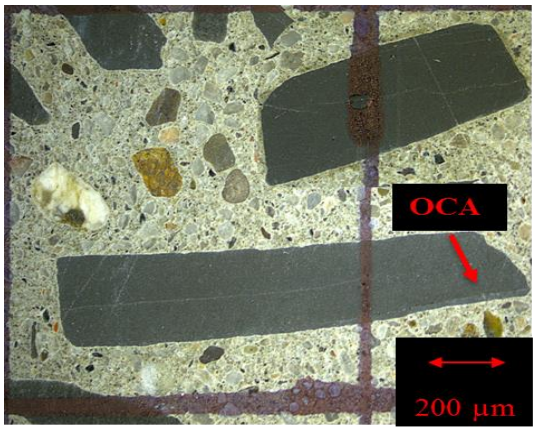

Figure 19: Typical cracking features in the restrained concretes incorporating the variety of restraint configurations.

6.6.4 Evaluating ASR-induced damage development as a function of the depth of restrained and unrestrained concrete

The microscopic analyses conducted in this work enable the evaluation of ASR-induced deterioration as a function of the blocks' depth for restrained and unrestrained concrete. Figure 20 illustrates the results gathered from the "surface" cores (i.e., 50-250 mm in depth) and "inner" cores (i.e., 250-450 mm in depth) of all concrete blocks. Analyzing the plots, one verifies that "surface" cores tend to have a slightly higher DRI number and thus damage than "inner" cores. This scattering is more pronounced for restrained concrete blocks (as expected) due to the restraint provided by the reinforcement which in turn generates an ASR-induced expansion and deterioration gradient between the blocks' surface and core. The latter has been previously reported by other researchers [3]. However, the differences observed in this work between "surface" and "inner" cores for both confined and unconfined concrete are deemed very minor (< 10%), since the typical variability amongst distinct operators while conducting the DRI is about 15% [44]. Hence, the DRI numbers from "surface" and "inner" cores may be treated equally in this work and averaging "surface" and "inner" cores results is deemed thus reasonable.

To further understand the differences between “surface” and “inner” cores, yet in a more detailed fashion (i.e., not as an average DRI value of cores extracted from distinct depths but as a function of the depth itself), Figure 21 displays a heating map (i.e., damage obtained from the numerous 1cm^2 squares evaluated through the DRI on two consecutive cores extracted from the 2D blocks in each direction). It is worth noting that the damage numbers obtained per 1cm^2 from the heat map are classified as follows: 2.25-4.125 (green – negligible/low damage), 4.125-6.00 (yellow – low/moderate damage), 6.00-7.876 (orange – moderate/high damage) and 7.876-9.75 (red – high/very high). Analyzing the heat maps from the three directions (i.e., vertical, transverse and longitudinal), one observes some interesting points: a) the vertical direction presents a much higher ASR-induced damage (i.e., represented by the amount of red and orange 1cm^2 squares), followed by the transverse and longitudinal directions (close results, yet the transverse deterioration is slightly higher), as previously reported in past sections of this work and; b) the first 50 mm of the cores (i.e., concrete cover - Figure 6C), experiences a higher damage degree when compared to the other portions of the specimen. This indicates a higher amount of cracks on the surface due to the so-called ASR-induced expansion gradient (i.e., lower restraint and higher alkali leaching at the surface) as verified by [52].

A) Unrestrained blocks

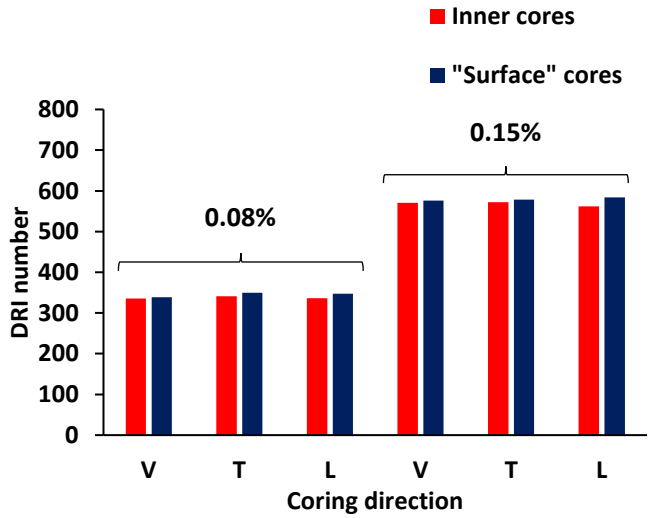

B) 1D blocks

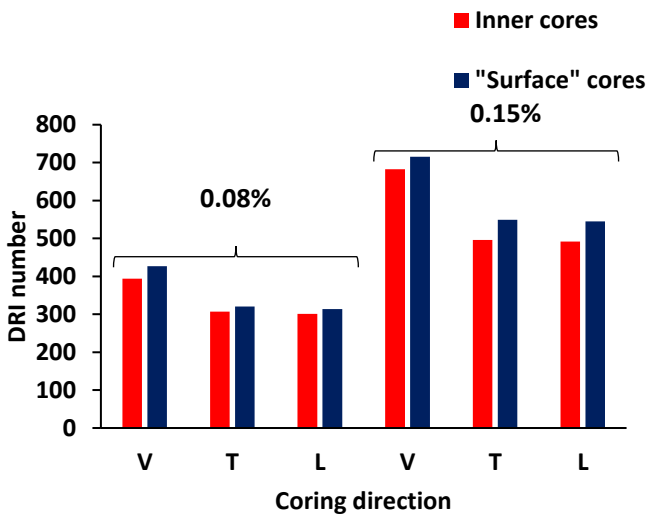

C) 2D blocks

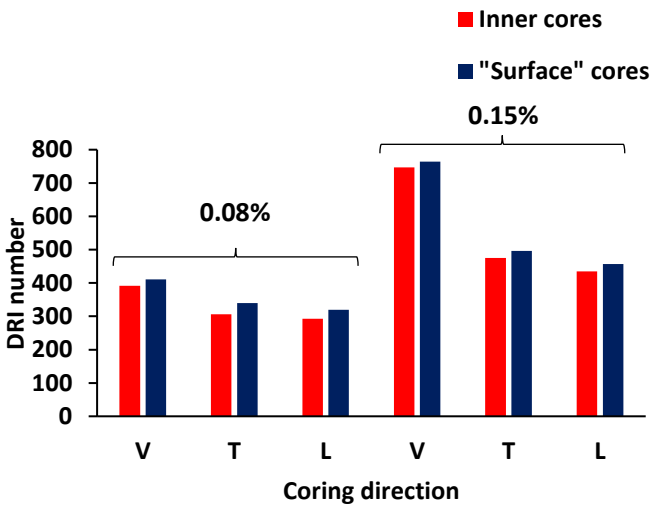

Figure 20: DRI number as a function of coring depth for specified coring direction and expansion level in concrete blocks.

A)

	1	2	3	4	5	6	7	8	9	10	11	12	13	14	15	16	17	18	19	20	21	22	23	24	25	26	27	28	29	30
A	9.5	9.5	8.75	7.25	8.5	7.25	7.25	7.25	6.5	7.75	6.75	6.752	6.75	7.75	6.75	6.75	6	6.25	7.75	7.5	5.75	7.75	6.5	6.75	6.5	6.25	7	6.75	6.75	7.25
B	8	8.5	8.5	8.75	7.75	7.25	6.5	6.5	6.5	6.75	6.5	6.75	6.5	6.5	5.75	6.5	6.5	7.5	6.5	7	6.75	6.75	7.25	6.75	6.5	6.75	7.75	6.75	6.25	6.75
C	9.75	9.25	8.25	9.5	7.45	6.75	6.5	6.5	6.5	6.25	7.5	7.25	6.5	7.5	6.75	6.5	6.75	6.75	6.75	6.75	6.75	7	7.25	6.75	6.5	6.25	6.75	6.75	7	7.5
D	8.5	8.25	9.25	8	8.75	7.25	7.25	7	6.25	7.75	6.75	7.25	6.75	6.5	7.25	6.5	7.25	6.75	7.75	6.75	7.75	6.75	6.75	6.5	7	6.75	6.25	6.75	6.75	7.25
E	9.25	8.75	8	9.25	8.75	8	8.25	6.75	6.75	6.75	7	7	6.75	6.5	6.5	6.5	6.5	6.75	6.75	6.75	6.75	7.25	7.25	7.5	7.5	6.75	6.5	7.75	6.75	6.75
F	9.5	8.5	8.5	7.75	7.25	8.25	7.25	6.5	7.5	6.75	7.5	6.75	7.75	7	7.25	7	6.5	7.75	6.5	7.25	6.75	6.5	6.75	6.75	7.75	6.75	5.75	6.75	7.75	6.75
G	8.25	8.5	8	8.5	7.5	7.5	6.5	6.5	6.5	6.5	7.25	6.5	6.75	6.75	7	6.75	7	6.75	6.25	7.75	6.5	7.75	5.75	7.5	6.75	6.75	7.25	6.5	6.75	6.5

B)

	1	2	3	4	5	6	7	8	9	10	11	12	13	14	15	16	17	18	19	20	21	22	23	24	25	26	27	28	29	30
A	7.5	8.5	7.5	6.5	5.5	6	3.5	6	3.5	4	5.5	4	4	4.5	4	5	3.75	4.5	3	4.5	4.5	4.25	3.5	4.25	5.25	4.25	4.5	4.25	4.25	4.25
B	8.25	8.5	8	6.5	6	5	4	5.25	2.75	3.5	3.5	4	3	5.25	4.5	4.25	4.25	4.25	4	4.25	4	4.5	4.25	2.75	4.25	5.25	2.75	4.5	4.75	4.25
C	7.5	8.25	6.5	6	5.25	5.5	4.5	4	3.75	4.5	4	4.5	4.5	5.25	4.25	4.25	3.65	5.25	4.5	3.75	4	3.5	5.25	4.25	2.25	4.5	3.25	5	3.5	5.25
D	9	7	7.25	6	5.5	5.25	4.5	3.5	5	4.5	4.75	4.25	4.25	3.5	3.75	4.25	4.5	3.25	4	4.5	4.25	3.5	4	3.75	4.25	4.25	4.25	4.25	3.75	5
E	7.25	8.25	7	6	5.5	5	3	4	4	4.5	3.75	4	4.5	4.5	3.5	5	5.25	4.5	4.25	3.75	4	4.25	2.75	4.25	4.5	3.25	4.25	2.75	5.25	3.5
F	8.5	7	8	7.5	5.5	5	3.5	4.5	3	3.5	4.25	3.5	5	3.5	4.25	4.25	3.5	5.25	3.25	4.25	4	3.25	4.25	3.75	4.5	4.5	4.5	4.25	4.5	4.25
G	8.5	8	6.75	5.5	5.5	5	4	3	3.75	3.75	3.25	4	4	3.5	3	4.25	5.25	4.25	4.75	4.25	3.75	4.25	5.25	4.25	3.5	4.25	4.25	5.25	4.25	3.75

C)

	1	2	3	4	5	6	7	8	9	10	11	12	13	14	15	16	17	18	19	20	21	22	23	24	25	26	27	28	29	30
A	6.5	8	6.75	4.25	4.5	4.5	4	3.5	3.5	4	3.5	3.5	4	4.5	4	4.5	4	4.25	4.25	3.25	4.25	4.25	4.25	4.25	4.25	3.25	4.25	3.75	4.5	4.25
B	8.5	5.75	5.75	5.25	4.25	5	4.25	3.75	4.25	3.5	3.5	4	4.75	3	4.5	4	4.5	4.25	4.25	4.25	5	3.75	3.75	3.25	4.5	4	4.25	4.25	3.75	3.25
C	7.75	7.25	8.25	4.75	4	4.5	4.5	4	3.75	4.5	4.5	4.5	4.5	3.5	3	3.5	3.5	4.25	4.5	3.25	4.25	4.25	4.25	4.25	4	4.25	5.25	4.5	4.5	3.25
D	7	6.75	4.75	5.25	4.75	5	4	3.5	5	4	4.75	3.25	3.75	4.5	4.25	4.5	4.25	4.25	3.75	4.5	3.75	3.75	3.25	3.25	4	4.25	2.75	4.25	4.25	4.25
E	9	6.5	4.75	4.25	4.75	4	4.5	4	4	4.25	3.75	4.25	4.25	4	3.5	4.5	3.75	3.25	3	4.25	4.25	4.25	4.25	4.25	3.25	4.25	3.25	3.25	4	4.25
F	6.5	6.75	8.25	4.5	4.75	4.5	3.5	4	4.25	3.5	3.75	3.5	4.25	4.25	4	3.75	4	4.5	4.25	3.25	4.75	4.25	4	4.75	4.5	3.5	4.25	4.25	4.5	3.5
G	8.25	8	5.75	5.5	5.5	5	4	3	3.75	3.75	3.25	4.5	3	3.5	3	3.5	5	4.25	3.25	4.5	3.25	3.5	4.5	3.25	5	4.25	4.25	4.25	4.25	4.25

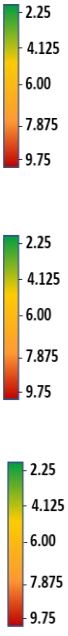

Figure 21: Heat map of damage distribution for 2D concrete blocks in: A) vertical cores, B) transverse and C) longitudinal.

6.6.5 Evaluating cracks orientation in unrestrained and restrained concrete

In reinforced concrete members affected by ASR, not only the overall deterioration (i.e., number of cracks) matters but also the cracks orientation. The study of the cracks orientation has been performed in this research through an image analysis system where the distinct crack features observed and identified in each

1 cm^2 DRI grid (Figure 4) drawn on the surface of ASR-affected cores were highlighted using a commercial software. Two hundred squares were highlighted (one hundred squares per core - two cores per direction) and then attached to each other, so that 100 by 400 mm cores could be entirely evaluated. This procedure was conducted on cores from the unrestrained and restrained blocks, for comparison purposes. As previously reported in the literature [8,25,52,53], the cracks observed in the cores extracted from the unrestrained block demonstrated a random distribution; in other words, a common crack pattern described as "map-cracking", often displayed on the surface of ASR-affected unrestrained/less restrained field members, was found on cores extracted from the unrestrained block regardless of their coring direction (Figures 22A). Conversely, a thorough analysis on restrained blocks displaying 1D and 2D reinforcement configurations demonstrated that ASR-induced cracks are predominantly oriented parallel to the longitudinal reinforcements. This observation has been made by a number of researchers in the past [33–37]. Figures 22B and C presents the crack patterns observed in the longitudinal and transverse directions (top view) and longitudinal and vertical directions (side/longitudinal view) respectively, of restrained blocks displaying a 2D reinforcement configuration. Evaluating the crack orientations, one verifies that the vast majority of cracks are aligned parallel to the longitudinal reinforcement bars. Such an observation once again confirms the fact that ASR-induced deterioration has been transferred from restrained to unrestrained/less restrained areas. As previously stated in 6.3, the aforementioned information will require further investigation of the changes in mechanical properties and ultimately structural implications of ASR-affected reinforced concrete displaying distinct reinforcement configurations as a function of induced expansion and deterioration.

A – Unrestrained block (Top view)

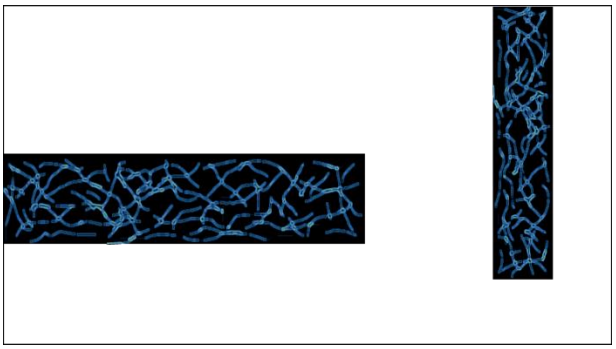

B – 2D Confined block (Top view)

C– 2D Confined block (Side/Longitudinal view)

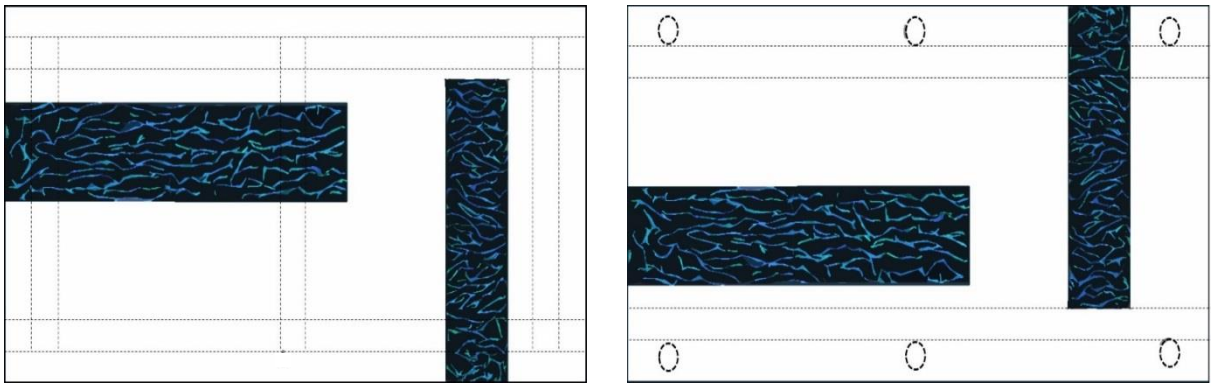

Figure 22: Typical ASR-induced crack orientation obtained through image analysis on cores extracted from: A) Unrestrained block (Top view), B) 2D Confined block (Top view) and, C) 2D Confined block (Side/Longitudinal view).

6.7 Conclusions

The purpose of this study was to microscopically appraise ASR-induced development in concrete blocks displaying distinct restraint configurations (i.e., none, 1D and 2D). The results obtained in this research demonstrate that restraint affects ASR-induced development (i.e., induced expansion and deterioration) of affected concrete. The following conclusions can be drawn from the findings of this work:

- ASR-induced expansion kinetics (i.e., expansion rate) and amplitude are influenced by the specimen's size. Concrete blocks (restrained and unrestrained) displayed slower expansion rate and lower expansion amplitude as a function of time when compared to concrete cylinders. These results indicate that the moisture transfer is likely affected in larger specimens, decreasing the rate of ASR-induced development within the time periods (1 year) and expansion levels (0.15%) evaluated in this research.

- The higher the restraint degree, the slower the expansion rate and the lower the expansion amplitude as a function of time. Moreover, an investigation of ASR-induced expansion as per the different directions/surfaces of the blocks (i.e., longitudinal top, longitudinal side and transverse) demonstrated that ASR development (i.e., expansion and deterioration) under restraint displays an anisotropic behaviour; i.e., induced expansion is transferred from restrained to unrestrained/less restrained areas, which emphasizes the results obtained in this research (i.e., transverse > longitudinal top > longitudinal side).

- The Damage Rating Index (DRI), as per its conventional and extended approaches, showed to be a quite reliable and valuable tool for assessing condition of ASR-affected unrestrained/restrained

concrete. Regardless of the restraint configuration, the use of an "overall" damage degree (i.e., average of three distinct directions at a given expansion level) showed to be in accordance with the range of values previously proposed for concrete specimens under "free expansion".

- Similar to the induced expansion, an important anisotropic behaviour in terms of crack development has also been observed for both 1D and 2D confined concrete blocks, where greater damage features and DRI numbers were more observed in the non-restrained directions than in the directions with confinement restrictions. Moreover, the higher the restraint degree, the higher the induced damage in the unrestrained directions, while less deterioration is observed in the restrained direction(s), especially for the 2D configuration.

- Besides anisotropy, ASR-affected concrete under restraint displays a different induced crack development (i.e., generation and propagation) when compared to unrestrained concrete. Among the differences, which start being visible from moderate expansion levels, one observes the reduction of open cracks in the reactive aggregate particles (OCA) and the increase of cracks in the cement paste (CCP) as a function of induced expansion. Furthermore, a slight decrease in the closed cracks in the aggregates (CCA) along with the generation of open cracks in the non-reactive fine aggregate particles (OCA sand) are also observed under restraint. This clearly suggests that the impact of ASR on the mechanical properties of affected restrained concrete might be different from unrestrained concrete and should be further investigated.

- Image analysis on cores extracted from restrained and unrestrained blocks from distinct orientations revealed that ASR-induced cracks in unrestrained concrete remain randomly distributed, whereas they are predominantly oriented parallel to the longitudinal reinforcement bar for restrained members. The latter indicates that the mechanical performance and ultimately structural implications of ASR-affected concrete bearing distinct reinforcement configurations might differ from studies based upon unrestrained conditions and should be further studied.

Acknowledgments

The authors would like to thank Drs. Gamal Elnabelsya and Muslim Majeed, technical officers of Materials and Structures laboratory in the Department of Civil Engineering at the University of Ottawa, as well as the undergraduate research assistants (UROPs) who helped with the manufacturing and testing of the test specimens used in this project. Likewise, the authors would like to thank Mr. Matthew McDonald and his team from Advance Cutting & Coring Ltd. for facilitating the crucial process of drilling and extracting core

specimens from the studied concrete blocks. Lastly, M. Zahedi benefits from the prestigious University of Ottawa entrance scholarship for international PhD students.

References

[1] L.F.M. Sanchez, B. Fournier, M. Jolin, J. Duchesne, Reliable quantification of AAR damage through assessment of the Damage Rating Index (DRI), Cem. Concr. Res. 67 (2015) 74–92. https://doi.org/10.1016/j.cemconres.2014.08.002.
[2] L.F.M. Sanchez, B. Fournier, M. Jolin, M.A.B. Bedoya, J. Bastien, J. Duchesne, Use of Damage Rating Index to quantify alkali-silica reaction damage in concrete: Fine versus coarse aggregate, ACI Mater. J. 113 (2016) 395–407. https://doi.org/10.14359/51688983.
[3] L.F.M. Sanchez, B. Fournier, D. Mitchell, J. Bastien, Condition assessment of an ASR-affected overpass after nearly 50 years in service, Constr. Build. Mater. 236 (2020) 117554. https://doi.org/10.1016/j.conbuildmat.2019.117554.
[4] R. Rivard, Quantitative Petrographic Technique for Concrete Damage Due to ASR : Experimental and Application, (2000) 63–72.
[5] M. Thomas, K. Folliard, B. Fournier, P. Rivard, T. Drimalas, Methods for Evaluating and Treating ASR-Affected Structures: Results of Field Application and Demonstration Projects I, 2013.
[6] B. Fournier, M.. Berube, K.. Folliard, M. Thomas, Report on the Diagnosis, Prognosis, and Mitigation of Alkali-Silica Reaction (ASR) in Transportation Structures, 2004.
[7] N. Smaoui, B. Fournier, M.-A. Bérubé, B. Bissonnette, B. Durand, Evaluation of the expansion attained to date by concrete affected by alkali silica reaction. Part II: Application to nonreinforced concrete specimens exposed outside, Can. J. Civ. Eng. 31 (2004) 997–1011. https://doi.org/10.1139/l04-074.
[8] B. Fournier, M.-A. Bérubé, Alkali–Aggregate Reaction in Concrete: a Review of Basic Concepts and Engineering Implications, Can. J. Civ. Eng. 27 (2000) 167–191. https://doi.org/10.1139/l99-072.
[9] P. Golterman, Mechanical predictions on concrete deterioration — part 2: classification on crack patterns, ACI Mater J. 92 (1995) 01–06.
[10] A. Leemann, T. Katayama, I. Fernandes, M.A. Broekmans, Types of alkali-aggregate reactions and the products formed,", Institut. Civ. Eng. - Constr. Mat. 169 (2016) 128.
[11] L.F.M. Sanchez, T. Drimalas, B. Fournier, Assessing Condition of Concrete Affected by Internal SwellingReactions (ISR) Through the Damage Rating Index (DRI), Cement. 1–2 (2020). https://doi.org/10.1016/j.cement.2020.100001.
[12] E. Boehm-courjault, A. Leemann, K.L. Scrivener, Microstructure, crystallinity and composition of alkali-silica reaction products in concrete determined by transmission electron microscopy, Cem. Concr. Res. 130 (2020). https://doi.org/10.1016/j.cemconres.2020.105988.
[13] L.F.M. Sanchez, B. Fournier, M. Jolin, D. Mitchell, J. Bastien, Overall assessment of Alkali-Aggregate Reaction (AAR) in concretes presenting different strengths and incorporating a wide range of reactive aggregate types and natures, Cem. Concr. Res. 93 (2017) 17–31. https://doi.org/http://dx.doi.org/10.1016/j.cemconres.2016.12.001.
[14] A. Mohammadi, E. Ghiasvand, M. Nili, Relation between mechanical properties of concrete and alkali-silica reaction (ASR); a review, Constr. Build. Mater. 258 (2020) 119567. https://doi.org/10.1016/j.conbuildmat.2020.119567.
[15] F. Rajabipour, H. Maraghechi, G. Fischer, Investigating the alkali-silica reaction of recycled glass aggregates in concrete materials, J. Mater. Civ. Eng. 22 (2010) 1201–1208.
[16] J.M. Ponce, O.R. Batic, Different manifestations of the alkali-silica reaction in concrete according to the reaction kinetics of the reactive aggregate, Cem. Concr. Res. 36 (2006) 1148–1156.
[17] L.F.M. Sanchez, T. Drimalas, B. Fournier, D. Mitchell, J. Bastien, Comprehensive damage assessment in concrete affected by different internal swelling reaction (ISR) mechanisms, Cem. Concr. Res. 107 (2018) 284–303. https://doi.org/10.1016/j.cemconres.2018.02.017.
[18] N. Smaoui, M.A. Berube, B. Fournier, B. Bissonnette, B. Durand, Effects of alkali addition on the

mechanical properties and durability of concrete, Cem. Concr. Res. 35 (2005) 203–212.
[19] A.E.K. Jones, L.A. Clark, The effects of restraint on ASR expansion of reinforced concrete, Mag Concr. Res. 48 (1996) 1–13.
[20] C. Gravel, G. Ballivy, K. K, Q. M, L. M, Expansion of AAR Concrete under Triaxial Stresses: Simulation with Instrumented Concrete Block., in: Proc. 11th Int. Conf. Alkali Aggreg. React., Québec, Canada, 2000.
[21] T.M.A. Ahmed, E. Burley, S.R. Rigden, The effect of alkali—silica reaction on the fatigue behaviour of plain concrete tested in compression, indirect tension and flexure, Mag Concr. Res. 51 (1999) 375–390.
[22] C.F. Dunant, K.L. Scrivener, Effects of uniaxial stress on alkali–silica reaction induced expansion of concrete, Cem. Concr. Res. 42 (2012) 567–576.
[23] P. Morenon, S. Multon, A. Sellier, E. Grimal, F. Hamon, E. Bourdarot, Impact of stresses and restraints on ASR expansion, Constr. Build. Mater. 140 (2017) 58–74. https://doi.org/10.1016/j.conbuildmat.2017.02.067.
[24] S. Multon, F. Toutlemonde, Effect of applied stresses on alkali-silica reaction-induced expansions., Cem. Concr. Res. 36 (2006) 912–920.
[25] S. Multon, J.-F. Seignol, F. Toutlemonde, Structural behavior of concrete beams affected by alkali-silica reaction, ACI Mater. J. 102 (2005) 67–76.
[26] M. Noël, L. Sanchez, R. Martin, B. Fournier, J. Bastien, Structural Implications of Internal Swelling Reactions in Concrete : a Review, in: 15th Int. Conf. Alkali-Aggregate React., Sao Paulo, Brazil, 2016.
[27] H. Kagimoto, Y. Yasuda, M. Kawamura, ASR Expansion, Expansive Pressure and Cracking in Concrete Prisms under Various Degrees of Restraint, Cem. Concr. Res. 70 (2014) 1–15.
[28] M.. Berra, G.. Faggiani, T.. Mangialardi, A.E. Paolini, Influence of Stress Restraint on the Expansive Behaviour of Concrete Affected by Alkali-Silica Reaction, Cem. Concr. Res. 40 (2010) 1403–1409.
[29] D.M. Wald, M.T. Allford, O. Bayrak, T.D. Hrynyk, Development and multiaxial distribution of expansions in reinforced concrete elements affected by alkali – silica reaction, (2017) 914–928. https://doi.org/10.1002/suco.201600220.
[30] D. Wald, G. Arrieta, M. Oguzhan, Expansion behavior of a biaxially reinforced concrete member affected by alkali-silica reaction, (2017) 550–560. https://doi.org/10.1002/suco.201600143.
[31] S. Sørgaard, O. Oseland, T. Kanstad, M.A.N. Hendriks, E. Rodum, Experimental investigation of ASR-affected concrete – The influence of uniaxial loading on the evolution of mechanical properties, expansion and damage indices, 245 (2020). https://doi.org/10.1016/j.conbuildmat.2020.118384.
[32] Koyanagi, R. W., and U. K., Y. Mechanical, Properties of Concrete Deteriorated by Alkali Aggregate Reaction under Various Reinforcement Ratios, in: Proc. 9th Int. Conf. Alkali-Aggregate React. Concr., London, UK, 1992: pp. 556–563.
[33] A. Allard, S. Bilodeau, F. Pissot, B. Fournier, J. Bastien, B. Bissonnette, Expansive behavior of thick concrete slabs affected by alkali-silica reaction (ASR), Constr. Build. Mater. 171 (2018) 421–436. https://doi.org/10.1016/j.conbuildmat.2018.03.159.
[34] A. McLeish, Structural implications of the alkali silica reaction in concrete, 1990.
[35] R.A. Barbosa, K.K. Hansen, Alkali-Silica Reaction in Reinforced Concrete Structures Part II : Shear Strength of Severe ASR Damaged Concrete Beams, in: XXII Nord. Concr. Res. Symp., Iceland, 2014: pp. 69–72.
[36] A.R. Barbosa, S. Gustenhoff, K. Kielsgaard, L. Cao, B. Grelk, Influence of alkali-silica reaction and crack orientation on the uniaxial compressive strength of concrete cores from slab bridges, 176 (2018) 440–451.
[37] S.G. Hansen, R.A. Barbosa, L.C. Hoang, Prestressing of reinforcing bars in concrete slabs due to concrete expansion induced by Alkali-Silica Reaction, in: Fib Symp., Cape Town, 2016.
[38] A.E.K. Jones, L.A. Clark, S. Amasaki, The suitability of cores in predicting the behaviour of structural members suffering from ASR, Mag. Concr. Res. 46 (1994) 145–150.
[39] Y. Hiroi, T. Yamamoto, Y. Toda, H. Manabe, T. Miyagawa, Experimental and analytical studies

on flexural behavior of post-tensioned concrete beam specimen deteriorated by alkali-silica reaction (ASR), in: 15th Int. Conf. Alkali-Aggregate React. Concr., São Paulo, 2016.
[40] F. Bach, T.S. Thorsen, M.P. Nielsen, Load-carrying capacity of structural members subjected to ASR, Constr. Build. Mater. 7 (1993) 109–115.
[41] A. Allard, S. Bilodeau, F. Pissot, B. Fournier, J. Bastien, B. Bissonnette, Performance Evaluation of Thick Concrete Slabs Affected by Alkali-Silica Reaction (ASR) – Part I: Materials Aspects, in: 15th Int. Conf. Alkali- Aggreg. React. Concr., São Paulo, 2016.
[42] P.A. Dunbar, P.E. Grattan-Bellew, Results of damage rating evaluation of condition of concrete from a number of structures affected by ASR, CANMET, in: ACI Int. Work. Alkali–Aggregate React. Concr., Darmouth, Canada, 1995: pp. 257–266.
[43] P.E. Grattan-Bellew, A. Danay, Comparison of Laboratory and Field Evaluation of AAR in Large Dams, in: Int. Conf. Concr. AAR Hydroelectr. Plants Dams, Canadian Electrical Association in association with Canadian National Committee of the International Commission on Large Dams, Frederiction, New Brunswick, Canada, 1992: p. 23.
[44] V. Villeneuve, B. Fournier, Determination of the damage in concrete affected by ASR — the damage rating index (DRI), in: 14th ICAR — Int. Conf. Alkali– Aggreg. React. Concr., Austin (Texas), 2012.
[45] V. Villeneuve, Determination de l'endommagement du béton par méthode pétrographique quantitative, Université Laval, 2011.
[46] ASTM C1293, Standard test method for determination of length change of concrete due to alkali-silica reaction, Annu. B. ASTM Stand. (2015) 1–7. https://doi.org/10.1520/C1293-08B.2.
[47] N. Smaoui, B. Fournier, B. Bissonnette, Influence of Specimen Geometry , Orientation of Casting Plane , and Mode of Concrete Consolidation on Expansion Due to ASR, Cem. Concr. Aggregates. 26 (2004) 1–13.
[48] Y. Zhang, H. Li, A. Abdelhady, J. Yang, H. Wang, Effects of specimen shape and size on the permeability and mechanical properties of porous concrete, Constr. Build. Mater. 266 (2021) 121074. https://doi.org/10.1016/j.conbuildmat.2020.121074.
[49] B.P. Gautam, D.K. Panesar, "A New Method of Applying Long-Term Multiaxial Stresses in Concrete Specimens undergoing ASR, and their Triaxial Expansions," Mater. Struct. 49 (2016) 3495–3508.
[50] J. Liaudat, I. Carol, M.L. Carlos, ASR expansions in concrete under triaxial confinement, Cem. Concr. Compos. 86 (2018) 160–170. https://doi.org/10.1016/j.cemconcomp.2017.10.010.
[51] B. Fournier, P.C. Nkinamubanzi, R. Chevrier, Comparative field and laboratory investigations on the use of supplementary cementing Materials to control alkali-silica reaction in concrete, in: 12th Int. Conf. Alkali-Aggregate React., Beijing, China, 2004.
[52] S.W. Forster, R.L. Boone, M.S. Hammer, J.F. Lamond, D.S. Lane, R.E. Miller, S.E. Parker, A. Pergalsky, J.S. Pierce, M.Q. Robert, J.W. Schmitt, R.E. Tobin, State-of-the-Art Report on Alkali-Aggregate Reactivity Reported by ACI Committee 221, 98 (1998) 1–31.
[53] S. Fan, J.M. Hanson, Effect of alkali silica reaction expansion and cracking on structural behavior of reinforced concrete beams, ACI Struct. J. 95 (1998) 498–505.

SUPPLEMENTARY MATERIALS

Table 4: Data in brief for the "overall" analysis.

Concrete Specimens	Features (Counts)		CD (Counts/cm2)		Lmax (mm)		W max (mm)		DRI Number	
	0.08%	0.15%	0.08%	0.15%	0.08%	0.15%	0.08%	0.15%	0.08%	0.15%
Unconfined cylinders	502.058805	559.9073	2.562609	4.7338	14	17	0.1	0.15	353.5809	568.216
Unconfined blocks	442.367862	558.2572	2.593212	4.8276	12.16667	17.5	0.1	0.15	339.8161	575.136
1D blocks	462.89119	512.8892	2.55615	5.046417	11.83333	16.66667	0.1	0.141667	368.731	579.5717
2D blocks	438.561526	508.4734	2.62715	5.097212	12	16.33333	0.1	0.158333	343.3996	574.7309

Table 5: Data in brief for the “anisotropic” analysis.

Restratinment types	Core orientation	CD (Counts/cm^2)		Lmax (mm)		w max (mm)		DRI Number	
		0.08%	0.15%	0.08%	0.15%	0.08%	0.15%	0.08%	0.15%
Unconfined Blocks	Vertical	2.58473	4.807931	12	17	0.1	0.15	337.199	573.1576
	Transverse	2.680952	4.850195	12	18	0.1	0.15	341.1905	575.136
	Longitudinal	2.513954	4.824674	12.5	17.5	0.1	0.15	341.0588	573.2605
1D Block	Vertical	3.1242	6.18415	14.5	19	0.1	0.2	382.75	646.07
	Transverse	3.01	6.022	13.5	17.5	0.1	0.15	366.55	613.92
	Longitudinal	2.1951	4.4513	7.5	13.5	0.1	0.1	337.831	478.725
2D Block	Vertical	3.085149	6.74978	16	20	0.1	0.225	401.2283	765.8121
	Transverse	2.44575	4.14323	10.5	15	0.1	0.12	323.0195	485.488
	Longitudinal	2.35055	3.775575	9.5	14	0.1	0.1	305.951	472.8925

7. Evaluation of The Induced Mechanical Deterioration Of Alkali-Silica Reaction Affected Concrete Under Distinct Restraint Conditions Through The Stiffness Damage Test

Andisheh Zahedi [1], Cassandra Trottier [2], Leandro Sanchez [3], Martin Noël [4]

Abstract

The Stiffness Damage Test (SDT), a mechanical and cyclic test procedure, has been successfully used to appraise alkali-silica reaction (ASR) deterioration under unrestrained conditions. However, the effects of restraint on ASR-induced mechanical damage have not been fully investigated. This work aims to understand the influence of restraint on ASR-damage development through mechanical protocols (SDT and compressive strength). Eighteen concrete blocks incorporating a highly reactive coarse aggregate and displaying distinct reinforcement configurations were fabricated and monitored over time. Two expansion levels were selected for analysis (0.08% and 0.15%) and once reached, cores were extracted from three different directions (longitudinal, transverse and vertical) and the mechanical tests conducted on those. Results show that the SDT is a reliable procedure to assess damage under restrained conditions. Moreover, ASR-induced mechanical distress varies according to the coring direction and restraint configuration. Finally, microscopic analyses validate the mechanical responses obtained as per the distinct coring orientations.

Keywords: Alkali-Silica Reaction (ASR), Mechanical properties, Stiffness Damage Test (SDT), Expansion, Damage transfer, Restraint, ASR-induced damage.

7.1 Introduction

Alkali-Silica Reaction (ASR), a chemical reaction between some unstable siliceous mineral phases within coarse and/or fine aggregates and the alkali hydroxides (Na^+, K^+, OH^-) from the concrete pore solution, is the precursor of one of the most deleterious damage mechanisms deteriorating the structural integrity, and shortening the service life of concrete infrastructure worldwide [1]. ASR produces a reaction product (i.e., *alkali-silica gel*), which leads to expansive pressure within the reactive aggregate particles and adjacent cement paste upon water uptake from the surroundings; this induced expansion causes the loss in the material's physical integrity (i.e., mechanical/durability) and, in some cases, functionality of affected structures [2]. Over the past years, a number of test protocols and recommendations have been developed, including a variety of laboratory test procedures (i.e., chemical, microscopic and mechanical) to appraise the current and predict the future condition of ASR-affected concrete; i.e., to assess the cause and extent of damage (diagnosis) and the potential for further deterioration (prognosis) of ASR-affected concrete. These

developments led to the implementation of better management protocols and more suitable rehabilitation strategies for ASR-affected concrete infrastructure [3].

Among the promising tools proposed, the Stiffness Damage Test (SDT), a mechanical and cyclic test procedure, was found to be quite suitable to appraise ASR-induced expansion and deterioration in concrete under unrestrained (i.e., free expansion) conditions, which does not reflect the real scenario of reinforced concrete members in the field [4]. Although few recent works have suggested the efficiency of the SDT to assess condition of affected concrete infrastructure [3,5–7], there is currently a lack of "quantitative" information about the influence of restraint (e.g., reinforcement) on ASR-induced physicochemical development (i.e., kinetics and induced expansion, damage development and mechanical response) and ultimately on the SDT outcomes. Thus, this work aims to use the SDT to assess the condition of ASR-affected concrete blocks displaying distinct reinforcement configurations (i.e., none, 1D and 2D) and expansion levels (i.e., 0.08% and 0.15%).

7.2 Background

7.2.1 Influence of ASR-induced development on mechanical properties of concrete under free expansion

Conventional "sound" concrete is known to have a relatively high compressive strength and modulus of elasticity, yet a low tensile strength. However, the aforementioned mechanical properties may significantly change over time whether concrete is affected by damage mechanisms [4,8–12]. Therefore, understanding the impact of deterioration mechanisms on the mechanical properties of affected concrete is crucial while assessing condition of aging infrastructure [13].

Research studies have shown a significant reduction of tensile strength (i.e., down to 65%) and modulus of elasticity (i.e., down to 50%) at low/moderate expansion levels (i.e., from 0.05% to 0.12%) in ASR-affected concrete [4]. Conversely, compressive strength only becomes significantly affected at high (i.e., 0.20%) or very high (i.e., 0.30%) expansion levels [2,4,11,14]. For instance, Esposito et. al. [12] and Ono [15] demonstrated that the reduction in compressive strength of ASR-affected concrete can be as high as 40–60% at expansion levels higher than 0.30%. Conversely, other studies reported a limited impact of ASR on the compressive strength of affected concrete [16–18]; this is attributed to the low reactivity of the aggregates used in the concrete mixtures which could likely not generate high levels of expansion [9].

The reduction of modulus of elasticity in ASR-affected concrete is influenced by the stiffness of the aggregate particles. ASR cracking is more likely to develop at the microscopic level within the aggregate particles; thus, stiffness reduction can be already observed at low expansion levels (i.e., 0.05%). Likewise, a significant reduction in tensile strength is verified at early stages of ASR (i.e., from 0.05% to 0.12%)

since porous media such as concrete are dependent on the existence and importance (i.e., size) of cracks as per fracture mechanics concepts. Thus, “stress concentration” peaks are developed at the tips of ASR-induced cracks in affected concrete under tension, leading to crack propagation and eventually failure [4]. On the other hand, the mechanism of failure in compression is much more ductile, being characterized by the failure of the “cement paste”, where cracks are initially formed at the interfacial transition zone (ITZ) at distinct locations, propagating to the bulk cement paste and connecting to one another at later stages, causing instability and ultimately failure of the system [19]. Thus, since ASR-induced cracks are initially formed within the aggregate particles and only extend to the cement paste at later stages, ASR development causes a progressive compressive strength loss of affected concrete [4].

7.2.2 Influence of restraint on ASR-induced development and mechanical properties

Most of the existing studies on ASR were conducted using laboratory specimens under “free expansion” conditions [4,8,14]; thus, limited research has been performed to understand the effects of confinement on ASR-induced development. Some studies [20,21] reported no or negligible ASR-induced expansion in confined/restrained directions; hence, no transfer of induced expansion and damage was observed to directions with less or no confinement [22,23]. However, as Multon and coworkers [24–26] observed, ASR-induced expansion decreases in the confinement direction, yielding transfer in unrestrained/less restrained directions. The same observation has been reported by other researchers [27–30]. These conflicting results may be attributed to various reasons, such as the specimen size (i.e., specimen size effect), casting direction and confinement configurations [7].

It is commonly agreed that confinement helps to mitigate ASR-induced expansion of affected concrete [25,31–33]; as such, Liaudat et al. [32] reported an almost 80% reduction of induced expansion in the restrained direction of concrete cubes (i.e., 150mm) asymmetrically confined. Thus, such an expansion reduction in the direction of confinement might lead to an anisotropic development of ASR-induced deterioration [34,35]. According to Allard et. al. [36], the higher the ASR-induced expansion, the higher the degree of anisotropy in affected reinforced concrete. This confirms that the use of an average induced expansion (i.e., average value from distinct directions) observed in ASR-affected concrete members with non-uniformly distributed reinforcement configurations, boundary conditions, or sustained loading may not be a suitable approach for analysis in some cases [7,30,37]. Yet, the available literature on the impact of anisotropy on ASR-induced expansion and mechanical degradation is currently fairly limited.

Although limited, some works have addressed the effect of confinement on ASR-induced development and the reduction of mechanical properties such as compressive strength [7,24,34,38–40]. Some of these studies [40] observed little to no difference in the compressive strength of cores extracted perpendicular and/or

parallel to the main confinement direction of ASR-affected concrete. Conversely, others have reported significant differences [7,24,38,39]: i.e., cores extracted perpendicular to the main restraint direction demonstrated significantly lower compressive strength than those cored parallel to the main reinforcing bars, with differences in the range of 7-35% [7,24,38,39]. Moreover, it has been verified by some authors that the modulus of elasticity is more sensitive to the restraint ratio and configuration, and crack orientation than the compressive strength [34]. Jones [41] observed that the modulus of elasticity of cores extracted perpendicular to the main restraint direction was significantly lower than those cored parallel to it. Such an observation can be due to the presence of higher amount of ASR cracks in cores extracted perpendicular to the main restraint [42–44]. Likewise, Gautam et al. [34], after conducting research on the effect of distinct stress configurations (none, uniaxial, biaxial and triaxial) on the mechanical degradation of ASR affected concrete, observed that concrete members under triaxial conditions display lower mechanical degradation than all the other stress configurations.

Few works have been conducted on the impact of restraint on the distinct ASR petrographic distress features and crack orientation of reinforced members [38–40]. Barbosa et.al. [38] noticed various crack patterns and orientations on distinct concrete cores extracted from affected structures; in this work, cores were retrieved from bridge slabs in distinct directions (i.e., vertically and horizontally), where ASR-induced cracks perpendicular to loading were observed in vertically cored specimens (Figure 1A) while a network of cracks parallel to loading was noticed in the horizontally cored specimens (Figure 1B). Accordingly, cores extracted from distinct directions of affected concrete behave quite differently during compressive strength tests; several “splitting” cracks are generated perpendicular to the ASR-induced cracks over loading in vertically cored specimens (Figure 1A), while “inclined shear” cracks are formed in cores retrieved horizontally (Figure 1B). Hence, it is expected that cores extracted from ASR-affected structures in distinct directions and displaying different cracks patterns and orientations present distinct mechanical responses.

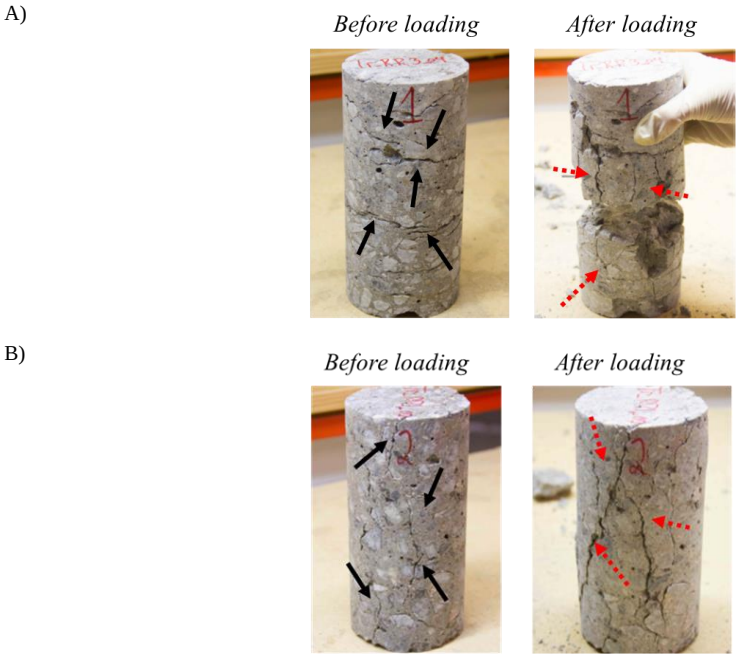

Figure 1: Distinct cracking orientation on A) vertically extracted core and B) horizontally extracted core having ASR induced cracks before loading (black arrows) and after loading (dashed red arrows) [38] *(Reproduced with permission of Elsevier).*

Although limited yet important results on the effects of confinement/restrainment on ASR-induced damage development are displayed in the literature, to the authors' best knowledge, there is a lack of studies quantitatively and systematically assessing this impact on concrete members displaying distinct reinforcement ratios and configurations, and presenting different damage degrees (i.e., induced expansion levels).

7.2.3 Mechanical tools to assess damage of ASR-affected concrete

7.2.3.1. Tensile, compressive and shear strength tests

Tensile and especially compressive strength tests are mainly used for design purposes of concrete members, as well as for the condition assessment of affected concrete. It has been observed that tensile strength is significantly affected by ASR [4,11]; however, depending on the test procedure implemented, ASR impact on tensile strength may be completely different. Among the methods used to evaluate tensile strength of ASR-affected concrete, the direct tensile strength, the splitting tensile strength and the gas pressure tension tests are the most used. All of them display some strengths and drawbacks. Studies on ASR-affected concrete involving direct tensile strength tests are fairly limited; such a test setup is expensive and susceptible to some challenges such as elimination of load eccentricity, stress-strain non-uniform distribution along with stress concentrations at the specimen ends that may lead to premature failure [11,45]. Conversely, the splitting tensile strength is a much simpler, easier to implement and non-expensive procedure; while the majority of authors agree that the test outcomes of the splitting test are not "direct"

tensile strength values and may not accurately represent the “pure” or “true” tensile strength of concrete [11,46]. Moreover, since a failure plane of the tested specimen is selected in the procedure, the test may become less diagnostic to appraise ASR-induced damage, besides enhancing variability amongst companion samples [47]. The gas pressure tension is a relatively new technique which aims to measure the “pure” or “true” tensile strength of concrete. It has demonstrated promising results to assess deterioration due to ASR, especially at low to moderate expansion levels [4]. However, the gas pressure test seems to be unable to identify ASR-impact on the tensile response of affected concrete for expansion levels above and beyond moderate degrees [4].

Compressive strength is known to be much less influenced by ASR than tensile strength [4]; in general, compressive strength is seen as a technique to appraise the actual state and residual capacity of affected concrete rather than a diagnostic protocol to evaluate ASR-induced deterioration over time. On the other hand, it has been found that the evaluation of shear strength (i.e., a property governed by tension and compression forces) might be a diagnostic approach to assess ASR-induced development in concrete. Various test protocols have been proposed over the years to appraise the direct shear capacity and shear friction of reinforced and unreinforced concrete; among those, the direct shear test proposed by De Souza et. al. [47] showed promising results to capture ASR-induced damage under “free-expansion” conditions. Further analysis is still required to evaluate the impact of confinement/restraint on the direct shear results as well as its efficiency to assess condition of affected concrete structures. If on the one hand the aforementioned mechanical test procedures display some shortcomings or require further analysis, on the other hand, the Stiffness Damage Test (SDT) has been shown as an efficient technique to assess condition of ASR-affected concrete [4,48].

7.2.3.2. Stiffness Damage Test (SDT)

The Stiffness Damage Test (SDT) is a mechanical and cyclic test procedure used to assess condition of concrete affected by internal swelling reaction (ISR) mechanisms (e.g., ASR) [4,48]. The SDT was initially developed by Walsh who observed a good correlation between the crack density and the cycles of loading/unloading (i.e., stress/strain relationship) of rock specimens [49]; Crouch then adapted this procedure for concrete specimens in 1987 [50]. The test procedure, which is based upon five compression cycles of concrete specimens (cylinders or cores), was initially performed using fixed loads of 5.5 (Chrisp et. al. [51,52]) or 10 MPa (Smaoui et. al. [53]), at the loading rate of 0.10 MPa/s. The modulus of elasticity, dissipated energy (hysteresis area), plastic deformation (plastic strain) and the non-linearity index (NLI; the ratio of secant modulus at half of the maximum load and the secant modulus at the peak load) of the first and/or over the four last cycles were the selected outcomes of the test [48,54]. Later, Sanchez et al. [48,54] optimized the test procedure following an in-depth study using a wide variety of reactive aggregate types

and concrete mixture proportions. Sanchez et al. [48,54] proposed that the SDT should be performed using a percentage (40%) of the ultimate capacity (compressive strength) of the concrete under analysis instead of a fixed load; moreover, the authors suggested using indices as outcomes of the test procedure, namely the Stiffness Damage Index (SDI) and Plastic Deformation Index (PDI) to increase the diagnostic character of the test. The SDI and PDI represent, respectively, the ratio of dissipated energy to total energy, and plastic deformation to total deformation in the system (i.e., SI / (SI+SII) and DI / (DI+DII) over the five cycles as presented in [48,54,55] and Figure 2; where SI is the irreversible deformation energy, SII is the elastic deformation energy, and DI and DII represent the plastic deformation and elastic deformation, respectively, over the loading-unloading process). Moreover, the modulus of elasticity (average secant modulus of the 2nd and 3rd cycles) along with the NLI (Sec 1/Sec 2 in the first cycle and the average Sec1/Sec2 value of the last four cycles – Figure 2) as proposed by Chrisp et al. [51,52] were also considered efficient SDT outcomes for determining the damage extent and orientation (i.e., NLI is greater/lower than unity for cracks oriented perpendicular/parallel to loading) respectively, in affected concrete. Although, the SDT has been shown to be quite suitable to appraise ASR-induced expansion and deterioration in concrete under unrestrained (i.e., free expansion) conditions, the effect of restraint on mechanical properties reductions and SDT outcomes remains mostly unknown.

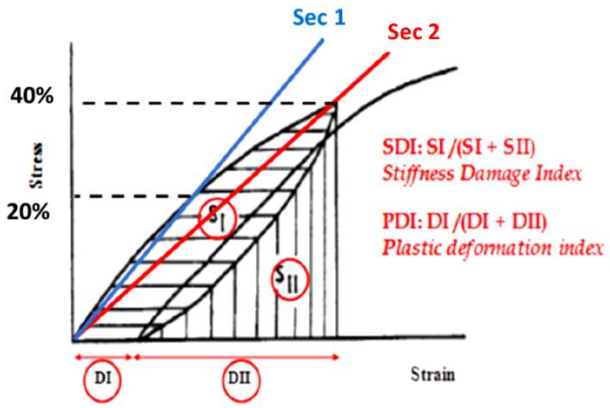

Figure 2: Calculation of the stiffness damage index (SDI) and Plastic Deformation (PDI) [55] *(Reproduced with permission of Elsevier).*

7.3 Research significance

As stated in the previous sections, there is a need for improving the current knowledge along with developing a thorough understanding of the effect of restraint on ASR-induced expansion and mechanical deterioration of affected concrete. Therefore, concrete blocks incorporating a highly reactive coarse aggregate and displaying distinct reinforcement configurations (i.e., none, 1D and 2D) were fabricated in the laboratory, stored in conditions enabling ASR-induced development (i.e., 38 °C and 100% R.H.) and monitored over time. At distinct expansion levels (i.e., 0.08% and 0.15%) the blocks were cored in three directions (i.e., longitudinal, transverse, and vertical) and mechanical test procedures (i.e., SDT, modulus

of elasticity and compressive strength) were conducted on each of those. Finally, comparisons on the extent of mechanical damage (i.e., physical integrity and mechanical properties reductions) of restrained versus unrestrained concrete are performed. It is worth noting that the word "confinement" is defined in this work as any restraint provided by the reinforcement bars to ASR-induced development in a given direction.

7.4 Experimental investigation

7.4.1 Concrete ingredients and mix design

Eighteen concrete blocks displaying a prismatic geometry (i.e., 450 by 450 by 675 mm - Figure 3) were fabricated in the laboratory using a concrete mixture with a design compressive strength of 35 MPa. This prismatic geometry was selected because 1) concrete blocks presenting similar geometry were manufactured in past researches [56], and 2) it allowed the extraction of a reasonable number of cores per specimen per direction without being excessively large and difficult to maneuver. A highly reactive coarse aggregate (i.e., Springhill - SP) was used in combination with a non-reactive fine aggregate (Ottawa natural sand - Ot) for concrete fabrication. Table 1 provides information on the different aggregates used in this study. A conventional CSA Type GU (i.e., ASTM type 1) high alkali (0.88% Na_2O_{eq}) Portland cement was selected for this research; moreover, reagent grade NaOH was used to raise the total alkali content of the cement to 1.25% Na_2O_{eq} (by mass), to accelerate ASR-induced expansion. The mix-proportion selected for this study is based on the Concrete Prism Test (CPT) standard mixture proportion as per ASTM C 1293 [57] and presented in Table 2.

Table 1: Aggregate properties selected for this study.

Aggregate				Rock type	Specific gravity (g/cm^3)	Absorption (%)	AMBT [a] 14 days expansion (%)
Type	Reactivity	Location	Name				
Coarse	Reactive	New Brunswick	Sp	Crushed greywacke	2.72	0.602	0.69
Fine	Non-reactive	Ottawa	Ot	Natural, derived granite	2.65	1.18	0.07

a) Typical expansion of ASTM C 1260.

Table 2: Concrete mixture proportion.

Materials	Quantities in the mix (kg/m^3)
Cement	420
Fine aggregate (Ot)	681
Coarse aggregate (Sp)	1044
Water	176

7.4.2 Concrete specimens manufacturing

To investigate the effect of restraint on ASR-induced expansion and mechanical properties of concrete, distinct concrete restraint conditions were selected for this study: 1) unrestrained blocks, 2) 1D confined

blocks and, 3) 2D confined blocks (Figures 3 and 4). For the confined blocks, a reinforcement ratio of 2% was selected, which is representative of a moderately high level of internal restraint in typical reinforced concrete members. For reference, several standards and design codes specify a minimum reinforcement ratio in slabs of 0.2% and a maximum practical limit in columns of 4% (e.g., CSA A23.3 [58]). Relatively large steel reinforcing bars with a nominal diameter of 35 mm (35M) were used as reinforcement in the 1D and 2D confined blocks in order to achieve the desired reinforcement ratio while ensuring sufficient space between bars to allow for concrete core extraction. It is worth noting that, in the case of 2D confined blocks, longitudinal and transverse steel reinforcing bars were professionally welded together to facilitate the construction (Figure 4B). Moreover, in the case of restrained concrete, the concrete cover and spacing between the top and bottom reinforcing bars, as well as spacing between transverse steel reinforcing bars (in the case of 2D concrete blocks) were 50 mm, 280 mm and 230 mm, respectively (Figure 3C and 4A and B). The spacing of the reinforcement used in this study is not considered excessive when compared to that of real concrete structures as per CSA A23.3:19 [58] (i.e., the max reinforcement spacing in a wall or slab is three times of the slab thickness or 500 mm-whichever is smaller; e.g., a 100 mm thick slab has a max spacing of 300 mm while a 200 mm slab has a max spacing of 500 mm). After 24 hours, all blocks were demoulded and moist cured at 20°C for over 24 hours. Stainless steel gauges were then glued in place with a fast-setting slurry for longitudinal expansion measurements following the drilling of four small holes (i.e., 10 mm in diameter by 55 mm long) in the three main sides of the blocks: a) top (Figure 5A-points 1 and 2), b) longitudinal (Figure 5A- points 3 and 4) and c) transverse (Figure 5A-points 5 and 6).

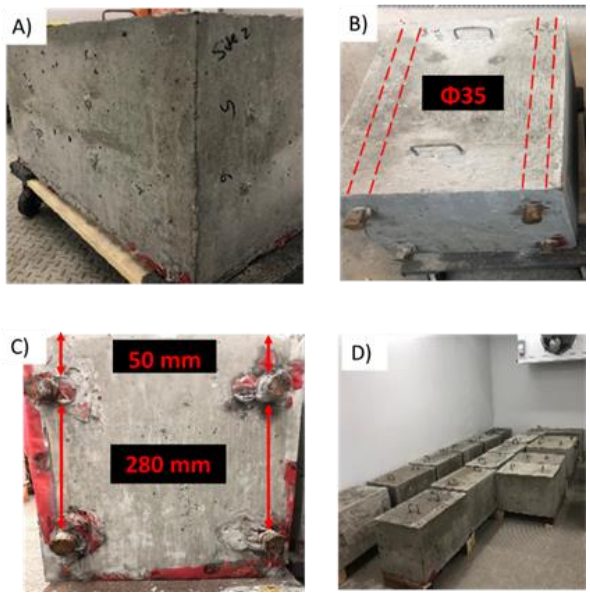

Figure 3: Concrete blocks presenting: A) unrestrained concrete block, B) 1D confined concrete block, C) 2D confined concrete block and, D) environmental chamber with 38ºC and 100% RH.

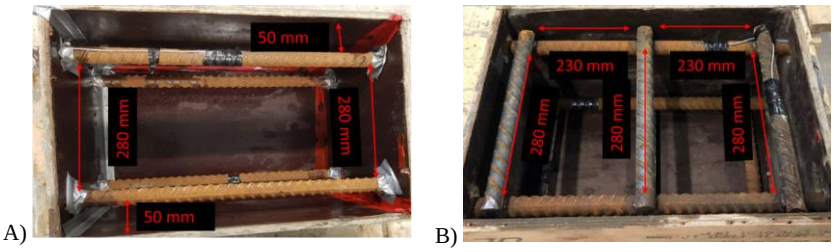

Figure 4: Restraint orientations: A) 1D confinement and, B) 2D confinement.

For comparison purposes, 20 concrete cylinders of 100 mm by 200 mm were also fabricated incorporating the same highly reactive aggregate and using the same mixture proportion as the concrete blocks. The cylindrical specimens were demoulded after 24 hours and moist cured at 20°C for 24 hours. Stainless steel gauge studs were glued in place with a fast setting cement slurry in small holes of 8.5 mm in diameter by 19 mm in length drilled in both ends of each concrete cylinder for periodic longitudinal expansion measurements. The "0" length readings were taken after 48h (i.e., two days from casting) as follows: a) in the case of concrete blocks, top longitudinal, side longitudinal and transverse expansion measurements as per Figure 5A and 5B, and b) longitudinal expansion measurements in the cylinders' case. All concrete blocks were subsequently placed in an environmental chamber enabling ASR development (i.e., 38ºC and 100% RH). The concrete cylinders were stored in sealed plastic (22 liters) buckets lined with damp cloth (Figure 5C and 5D) and placed in the same conditions as the concrete blocks. All specimens (i.e., cylinders and blocks) were regularly monitored over time and were stored at 23°C for 16 ± 4 hours prior to periodic expansion measurements as per ASTM C 1293 [57]. Upon reaching the selected expansion levels for this research (i.e., 0.08% and 0.15%), the concrete cylinders and blocks were removed from the environmental chamber for mechanical testing. Following their removal, three blocks from each distinct restraint configuration per expansion level were cored to produce seven cores of 100 mm by 450 mm (Figure 6D) from the vertical (Figure 6A) and the transverse (Figure 6B) directions as well as four 100 mm by 675 mm cores in the longitudinal (Figure 6C) direction. Afterward, all specimens were wrapped in plastic film and stored at 12°C (since not all specimens could be tested at the same time due to testing capacity issues) to stop further ASR-induced development as per Sanchez et al. [4] prior to testing.

Figure 5: A) Gauge studs' orientation for blocks, B) expansion measurements on distinct direction of concrete blocks with a micrometer, C) sealed bucket arrangement for the 38°C and 100% RH test and, D) affected concrete cylinder.

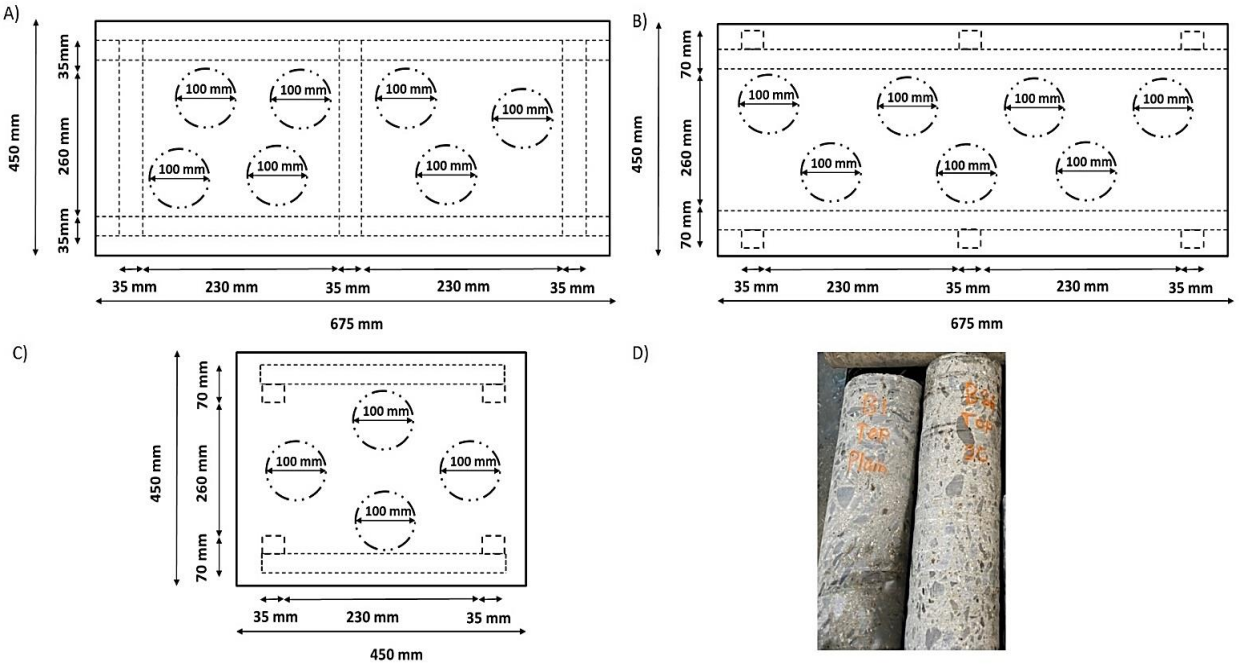

Figure 6: Qualitative sketch of the cores extracted from 2D Blocks: A) top view (vertical), B) longer side view (transverse), C) shorter side view (longitudinal) and D) cores of 100 mm by 450 mm.

7.4.3 Experimental procedures

The mechanical testing was conducted in two different, yet related ways in this work. First, the mechanical results were averaged from the three coring directions/orientations (i.e., longitudinal, transverse and vertical) to evaluate the impact of the restraint on the "overall deterioration" of ASR-affected blocks (i.e., *Results section*). Second, the mechanical properties were appraised as per the coring direction to assess and quantify ASR anisotropic behaviour as a function of the restraint configuration (i.e., *Discussion section*).

7.4.3.1. Stiffness Damage Test (SDT)

Three specimens from distinct coring directions per set of concrete blocks (i.e., vertical, longitudinal and transverse; total of 9 specimens per distinct directions per expansion level) as well as three concrete cylinders displaying the same expansion levels were subjected to five cycles of loading/unloading at the controlled loading rate of 0.10 MPa/s. Prior to conducting the SDT, all specimens were reconditioned in the moist curing room for 48h (enabling the samples rewetting and thus lessening the test's variability) according to CSA23.2-14C [59], and as per Sanchez et al. works [48]. Moreover, both ends of all concrete specimens (cylinders and cores) were mechanically ground to generate appropriate flatness of the specimen's end surfaces for mechanical tests in compression as per CSA23.2-9C [60]. The SDT was performed then following the procedure proposed by Sanchez et. al. [48,54]; i.e., loading up to 40% of the 28-day concrete strength of the specimens tested.

7.4.3.2. Compressive Strength

In this research, the compressive strength was measured using two distinct approaches with different and specific goals. First, the 28-day compressive strength of the mixture used to manufacture both the blocks and cylinders was determined on control samples. Considering that the concrete mixture contained a highly reactive coarse aggregate, one could not follow ASTM C 39 [61] since some ASR might have been generated while moist curing. Thus, in order to avoid ASR-induced development, the control specimens were wrapped in plastic film upon demoulding and placed at 12°C for 47 days as per Sanchez et al. [48], which is equivalent to 28 days at 20°C according to the maturity concept (i.e., ASTM C 1074 [62]). This approach has proven to be effective to suppress ASR development in the laboratory [48]. The "equivalent" 28-day compressive strength collected from this procedure was then used to determine the SDT loading level (i.e., 40% of this value). Second, compressive strength measurements were also conducted on the concrete cylinders/cores following the SDT to verify the compressive strength losses of the material as a function of ASR-induced development. The SDT using 40% of the 28-day compressive strength has been found to be non-destructive by Sanchez et al. [48]; thus mechanical results such as compressive strength obtained following the SDT are considered valid [48]. Finally, the compressive strength losses were calculated in this work (for both cylinders and cores) as the difference between the results obtained after the SDT (for distinct expansion levels, restraint conditions, and directions) and the "equivalent" 28-day values obtained on control samples.

7.5 Results

7.5.1 ASR kinetics and development

Figure 7 presents the average induced expansions (i.e., average value of four consecutive measurements per specimen per direction over time with standard deviations ranging from 0.02% to 0.06%) as a function of time for the various directions of the ASR-affected concrete blocks incorporating different reinforcement configurations. Figure 7A also displays the average longitudinal expansions of concrete cylinders (standard deviation of about 0.03%). Analyzing the plots, one notices that all concrete blocks and cylinders were able to reach the given expansion levels selected for this work (i.e., 0.08% and 0.15%). However, the rate of expansion of the concrete cylinders was significantly faster than the blocks, regardless of the reinforcement condition (i.e., none, 1D and 2D). Moreover, all concrete blocks presented some amount of shrinkage at the beginning of ASR-induced development. It took 35, 75, and 105 days on average for the unrestrained concrete blocks, 1D concrete blocks and 2D concrete blocks, respectively, to recover from shrinkage.

Generally, the expansion curves of the unrestrained blocks (Figure 7A) are almost identical regardless of the direction, where 0.15% expansion was achieved at 175, 190, and 212 days on transverse, longitudinal

top and longitudinal side directions, respectively. Otherwise, as Figures 7B and 7C illustrate, the 1D and 2D confined blocks displayed a much slower ASR-induced expansion development than the unrestrained blocks, where 0.15% expansion was achieved after 190, 212 and 255 days by 1D blocks and 235, 275, and 340 days by 2D blocks on transverse, longitudinal top and longitudinal side, respectively. Comparing the reached expansion levels for the concrete blocks at a given time, the unrestrained concrete blocks demonstrate a significantly faster and higher expansion level than the confined blocks, which establishes the effect of restraint on ASR-induced development since the higher the reinforcement level, the slower the expansion rate and the lower the ultimate expansion for the same time period. As such, averaging all directions, it was found that the unrestrained blocks reached (on average) a maximum expansion of 0.27% at 340 days followed by 1D and 2D concrete blocks which achieved the expansion levels of 0.23% and 0.18% (on average) at the same time period. Similarly, this behaviour has previously been observed in the literature [24,32,63] and confirms that the relative expansion levels reached by the different blocks' surfaces are influenced by the restraint direction (i.e., transverse > longitudinal top > longitudinal side) along with reinforcement configuration and geometric features. In addition, the 100 mm by 200 mm concrete cylinders presented faster ASR kinetics and a higher ultimate expansion than all of the concrete blocks, reaching 0.15% within 70 days on average (Figure 7A).

It is worth noting that for the sake of further mechanical analysis, the expansion adopted as "representative" of a given damage degree was assumed to be the one from the longitudinal side for all concrete blocks (as Figure 5A-points 3 and 4), which represents the lowest expansion level among all surfaces since this direction is parallel to the main reinforcement and is not (or at least less) influenced by local effects [24,30,37] (i.e., the top drying/wetting cycles, differential restriction between bottom and top surfaces).

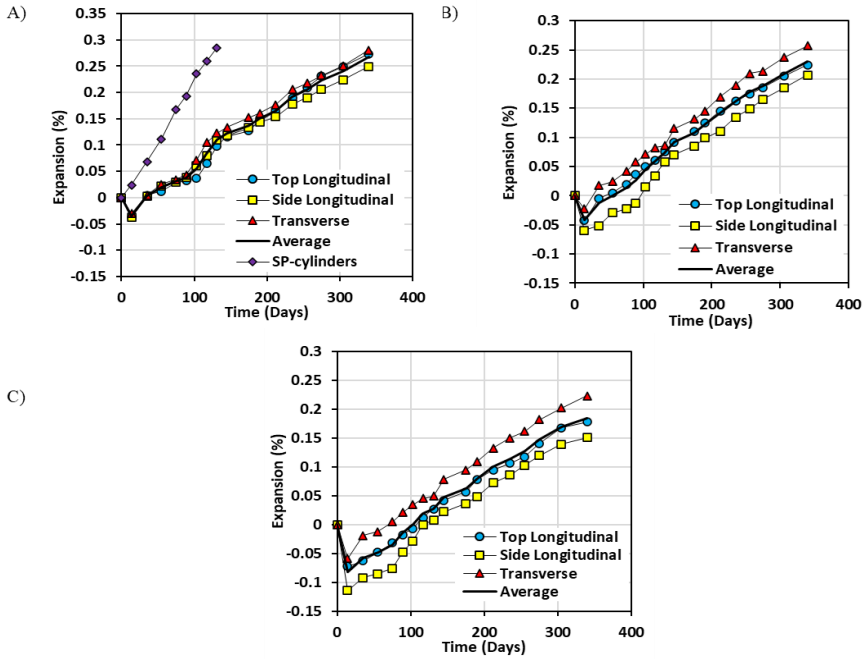

Figure 7: ASR kinetics (expansion vs. time) for the 35 MPa concrete mixtures at various restraint configurations: A) unrestrained cylinders and blocks, B) 1D and C) 2D.

7.5.2 Stiffness Damage Test (SDT)

The results presented in this section are the average values obtained on all nine core specimens from each of the ASR-affected blocks (i.e., regardless of the coring direction) and three concrete cylinders at each expansion level tested (including the control samples, showing no deterioration). Evaluating the data, one observes that the higher the ASR-induced expansion level, the higher the SDI and PDI indices and the lower is the modulus of elasticity (ME), as expected, for both cylinders and concrete blocks. As such, SDI values (standard deviations presented in the plot) of the unrestrained and restrained concrete blocks showed similar results (i.e., about 0.18- Figure 8A) at 0.08% expansion, while at 0.15% of expansion, the unrestrained and 1D confined blocks displayed an SDI of 0.27 and the 2D confined blocks exhibited a slightly lower SDI of 0.25. Likewise, similar results were obtained for the concrete cylinders, where SDI values of 0.18 and 0.26 were found for 0.08% and 0.15% of expansion, respectively. It is worth noting that the control specimens (i.e., undamaged concrete) demonstrated an initial SDT value of 0.12.

Figure 8B illustrates the PDI values (standard deviations added to the plot) gathered from cylinders and concrete blocks with distinct restraint configurations at low and moderate expansion levels. At 0.08% expansion, the cylinders and unrestrained blocks displayed a PDI of 0.13, while the 1D and 2D confined blocks exhibited a PDI of 0.15. At 0.15% expansion, the results obtained were quite close for all specimens, where the cylinders, unrestrained and 1D confined blocks yielded a PDI of 0.24 whereas the 2D confined block presented a PDI of 0.23. The initial PDI for the control/sound samples was 0.08.

Figure 8C displays the modulus of elasticity (ME- including their standard deviations) for all specimens and expansion levels studied in this work. Analyzing the data, one notices that an initial ME of 30 GPa has been obtained for the undamaged/sound samples; then, a decreasing trend is observed for all specimens, where 25 GPa results were gathered from cylinders and unrestrained blocks at 0.08% of expansion, while 24 GPa was attained for the 1D and 2 D confined blocks at the same expansion level. At 0.15% of expansion, all specimens yielded an ME of 19 GPa, attesting an important lessening in modulus of elasticity due to ASR-induced development. In order to improve the understanding and visualization of the ASR impact on the ME of affected concrete, Figure 8D presents the modulus of elasticity reductions (with their standard deviations) of all ASR-affected concrete specimens (cylinders and blocks, in %) at low and moderate expansion levels. At 0.08% of expansion, the cylinders and unrestrained concrete blocks presented a reduction of 17% while the 1D and 2D concrete blocks show an ME reduction of 20%. At 0.15% of expansion, all specimens (cylinders and blocks) displayed a 36% ME loss. Finally, comparing the SDT outcomes above discussed (i.e., SDI, PDI, ME and ME reductions), one notices that the "overall" damage (i.e., disregarding the coring direction) is quite similar for all specimens evaluated (i.e., cylinders and blocks) at a given induced expansion level, regardless of their restraint configuration. The data in brief can be found in Table 9 of the supplementary materials section.

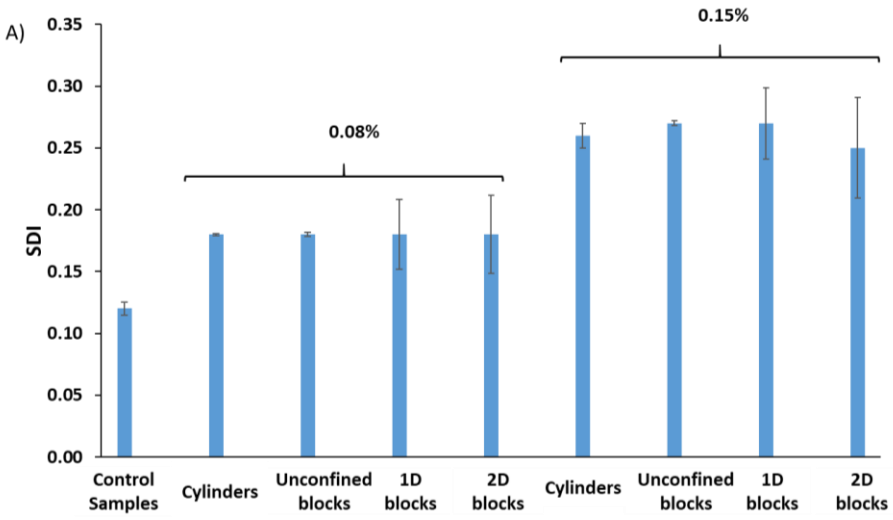

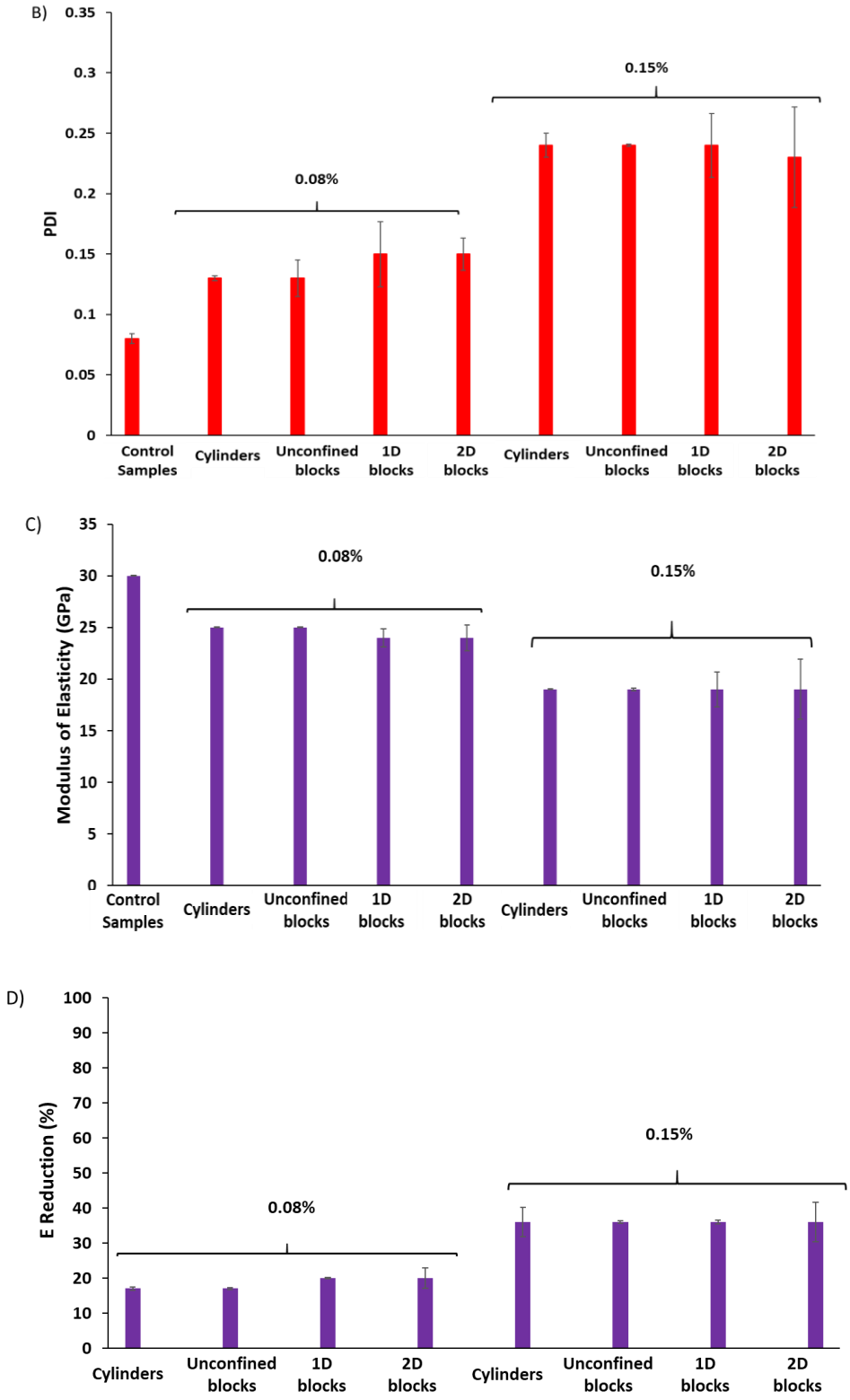

Figure 8: Results of A) SDI, B) PDI, C) ME (GPa) and D) ME reduction (%) from distinct concrete specimens.

7.5.3 Compressive Strength

The compressive strength results as a function of ASR-induced expansion are displayed in Figure 9A. As for the SDT, this section presents the "overall" compressive strength results of concrete blocks (i.e., average values obtained on all nine core specimens from each of the ASR-affected blocks with their standard deviations - regardless of the coring direction) and three concrete cylinders at each expansion level tested (including the control samples, bearing no previous deterioration). Analyzing the data, one observes a decreasing trend in compressive strength as a function of ASR-induced development. However, this reduction is less important than the loss in modulus of elasticity, as expected. The compressive strength obtained in the control/sound samples was 35 MPa; at 0.08% of expansion, all specimens yielded the compressive strength value of 31 MPa, while 28 MPa and 29 MPa have been gathered for the cylinders and block specimens at 0.15% of expansion, respectively.

Figure 9B illustrates the compressive strength reductions (%) of all concrete specimens (standard deviations added to the plot) as a function of the expansion. All the specimens (cylinders and blocks) displayed 11% loss in compressive strength at 0.08% of expansion, while the cylinders presented a reduction of 20% and the unrestrained, 1D and 2D blocks displayed 17% loss in compression at 0.15% of expansion. Lastly, similar to the SDT results, the "overall" damage (i.e., disregarding the coring direction) obtained through compressive strength for all specimens appraised (i.e., distinct reinforcement configurations) was quite similar at a given induced expansion level. The data in brief can be found in Table 4 of the supplementary materials section.

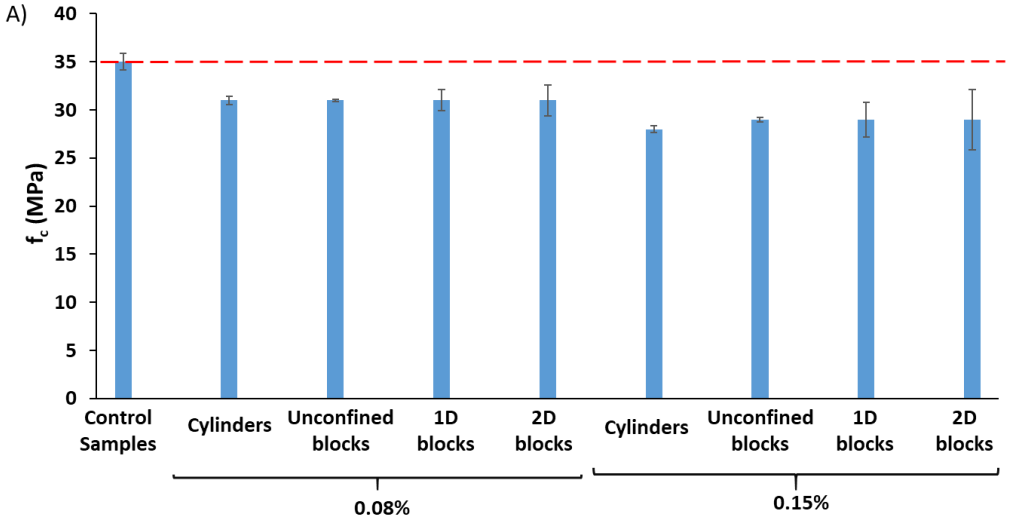

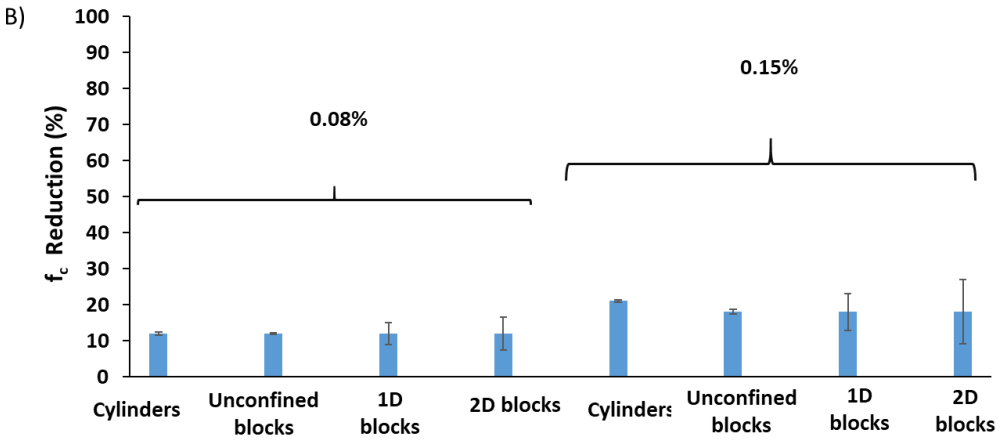

Figure 9: A) Compressive strength (CS) and B) CS reduction (%) as a function of expansion.

7.6 Discussion

7.6.1 Effect of restraint on the kinetics and magnitude of ASR-induced expansions

As Figure 7A illustrates, a significant difference was observed between concrete cylinders and concrete blocks with respect to ASR kinetics. The concrete cylinders presented considerably higher expansion levels as a function of time than all blocks, possibly due to the influence of size on moisture transfer [64]; therefore, significantly higher (and faster) expansion levels were observed when compared to the blocks.

On the other hand, comparing the achieved expansion level of distinct surfaces of unrestrained concrete blocks (Figure 7A), one notices that almost an identical expansion level attained by various surfaces of the latter with the side longitudinal having a slightly lower expansion level when compared to the other two surfaces. This slightly lower induced expansion may be attributed to boundary [24,30] and local friction [65] conditions at the base of the blocks, which may provide a higher restraint against expansion in the longitudinal direction. However, the expansion levels attained on the distinct surfaces of the restrained blocks demonstrate the presence of an anisotropic behaviour, the so-called “expansion transfer”, where ASR-induced expansion transfers from restrained to unrestrained/less restrained directions. Therefore, the transverse surface yields a higher induced expansion, followed by the top surface and then the side longitudinal (Figure 7B and 7C). Moreover, even though the 2D blocks present the same reinforcement ratio in the longitudinal and transverse directions (i.e., 2%), the reinforcement configuration is different in these two directions (i.e., 2 bars of 35 mm in the longitudinal direction with 280 mm spacing and 3 bars of 35 mm in the transverse direction with 230 mm spacing in each plane layer - top and bottom - for a total of 4 or 6 bars per cross-section, respectively). This difference as well as geometric features (i.e., longer size and thus friction per unit width for the longitudinal direction) could be among the causes of the higher expansion obtained for the transverse faces in the 2D blocks. As such, although the side longitudinal direction of 1D confinement (i.e., restrained direction) reached 0.15% of expansion at 255 days, the

transverse and top longitudinal directions (i.e., unrestrained/less restrained directions) displayed 0.21% and 0.17% of expansion at the same time period, respectively. Likewise, while the side longitudinal surface of 2D concrete blocks achieved 0.15% after 340 days, the top longitudinal and the transverse reached 0.18% and 0.22% respectively at the same period. The above results confirm that the anisotropic behavior observed in the blocks is more pronounced with the increase of reinforcement, which results in higher expansion scattering amongst distinct directions.

7.6.2 Understanding the influence of ASR deterioration on the "overall" mechanical properties of unrestrained/restrained concretes

The experimental campaign performed in this study contributes to a better understanding of the effect of ASR-induced expansion and deterioration on the mechanical properties of restrained concrete. As the SDT (i.e., SDI, PDI, and ME) and compressive strength outcomes display (Figure 8 and 9, respectively), all concrete specimens, demonstrate a roughly similar "overall" (i.e., disregarding the distinct directions evaluated) mechanical behaviour where higher SDI, PDI and lower ME and compressive strength values are observed with increasing induced expansion. Analyzing the "overall" results obtained from restrained concrete, one sees that they follow the same trend as proposed by Sanchez et. al. [4] while evaluating concrete specimens under "free expansion" conditions (Table 3). Sanchez et. al. [4] proposed a chart of values composed of data envelopes with confidence level of 95%, after studying 20 different concrete mixtures presenting distinct mechanical properties (i.e., 25, 35 and 45 MPa) and incorporating 13 different reactive aggregate lithotypes, to classify the damage degree (mechanical and microscopic) of ASR-affected concrete. It has been verified that ASR-induced mechanical deterioration measured through the SDT outcomes follows a similar trend regardless of the concrete strength and reactive aggregate lithotype used; hence, the SDT outcomes correlate quite well with ASR-induced expansion and deterioration (i.e., physical integrity and stiffness reduction) [4]. The above indicates that, although the chart values developed by Sanchez et al. [4] has been initially generated using concrete specimens under free expansion conditions, it can also be used to appraise the "overall" mechanical deterioration (i.e., average results from the three orthogonal orientations) of affected restrained concrete. In other words, ASR-induced damage does not seem to significantly change the "overall" mechanical deterioration of concrete incorporating distinct restraint conditions, although differences in mechanical properties as per the distinct directions were indeed observed and will be discussed in the next sections.

In order to assess the statistical validity and significance of the results obtained through the SDT (i.e., SDI, PDI and ME) and compressive strength, a two-way analysis of variance (ANOVA) with a confidence level of 95% was performed as a function of ASR-induced expansion on the "overall" results obtained in this study. As per Table 4, the SDT outcomes (i.e., SDI, PDI and ME) are statistically significant for all concrete

specimens appraised, since all the “F values” are greater than the “Fcritic” and the “p values” are lower than 0.05. However, the results obtained through the compressive strength test were not considered statistically significant towards ASR development. Therefore, a complementary “t-test” was conducted to check the significance of the “overall” compressive strength results separately at each expansion level studied (0.08% and 0.15%) by comparing with those gathered from sound concrete specimens (Table 5). Evaluating the results, one sees that the compressive strength results are not significant at 0.08% expansion but are indeed statistically significant at 0.15%. The findings above attest the “diagnostic” nature of SDT to assess the “overall” mechanical deterioration of unrestrained and restrained ASR-affected specimens. Conversely, the compressive strength test seems to be only effective to appraise the degree of ASR-induced deterioration at moderate expansion levels (i.e., 0.15%) as previously observed by Sanchez et al. [4], regardless of the restrainment condition.

The current results disagree with the recent findings reported by Sørgaard et. al. [7], where the SDT was found a somewhat unreliable/incomplete tool to appraise the damage degree of ASR-affected concrete under restrained conditions. Nevertheless, as Figure 7 illustrates, ASR-induced expansion is significantly affected by the restraint configuration where the higher the restraint, the slower the induced expansion (i.e., lower expansion rate) and the lower the expansion amplitude at a given time period. In addition, the results presented in Figure 7 along with the ones available in the literature as per Gautam et al. [34] and Multon et. al. [24–26] indicate that “expansion transfer” takes place from restrained to the non/less restrained directions (i.e., distinct measured expansions from different directions). Therefore, a comprehensive study on ASR anisotropy is required to fully understand the effect of restraint on the mechanical degradation of ASR-affected reinforced concrete.

Table 3: Classification of the damage degree in concrete due to ASR [4] *(Reproduced with permission of Elsevier)*.

Classification of ASR damage degree	Reference expansion level (%) [4]	Assessment of ASR												
		Conventional Concrete [4]			-	unconfined concrete blocks			1D concrete blocks			2D concrete blocks		
		ME loss (%)	CS loss (%)	SDI	Expansion level from this study	ME loss (%)	CS loss (%)	SDI	ME loss (%)	CS loss (%)	SDI	ME loss (%)	CS loss (%)	SDI
Negligible	0.00–0.03	-	-	0.06–0.16										
Marginal	0.04 ± 0.01	5–37	10–15	0.11–0.25	0.08%	15	13	0.17	19	12	0.18	19	12.5	0.18
Moderate	0.11 ± 0.01	20–50	0–20	0.15–0.31	0.15%	35	18.5	0.26	36	18	0.26	36	17.5	0.25
High	0.20 ± 0.01	35–60	13–25	0.19–0.32										
Very high	0.30 ± 0.01	40–67	20–35	0.22–0.36										

Table 4: Two-variable ANOVA on the "overall" mechanical testing results (SDT-SDI, PDI and ME as well as CS) for all concrete specimens of this study.

ANOVA analysis			SDI						PDI						ME						CS					
Specimens type	Load (%)	Expansion (%)	SDI-F	SDI-Fcritic	F>Fcritic	SDI_P value	α	P<α	PDI-F	PDI-Fcritic	F>Fcritic	PDI_P value	α	P<α	ME-F	ME-Fcritic	F>Fcritic	ME_P value	α	P<α	CS-F	CS-Fcritic	F>Fcritic	CS_P value	α	P<α
Cylinders	40	0.08%-0.15%	92.11	7.71	√	0.0006	0.05	√	112.48	7.71	√	0.000424	0.05	√	71.98	7.71	√	0.001041	0.05	√	2.21	7.71	X	0.0710	0.05	X
Unconfined blocks	40	0.08%-0.15%	77.66	4.75	√	7.56E-11	0.05	√	119.66	4.75	√	2.86E-10	0.05	√	97.11	4.75	√	2.14E-12	0.05	√	2.54	4.75	X	0.061	0.05	X
1D blocks	40	0.08%-0.15%	58.66	4.75	√	1.08E-14	0.05	√	74.52	4.75	√	5.12E-15	0.05	√	53.55	4.75	√	9.14E-13	0.05	√	4.06	4.75	X	0.063	0.05	X
2D blocks	40	0.08%-0.15%	49.85	4.75	√	2.27E-10	0.05	√	52.3	4.75	√	3E-12	0.05	√	46.55	4.75	√	3.7E-12	0.05	√	4.43	4.75	X	0.054	0.05	X

Table 5: t-Test analysis on the "overall" compressive strength results of all concrete specimens of this study.

t-Test analysis - compressive strength loss									
Blocks type	Strength (MPa)	Expansion level	CS_P value	α	P<α	Expansion level	CS_P value	α	P<α
Cylinders	35	0.08	0.09522	0.05	X	0.15%	0.03452	0.05	√
Unconfined blocks	35	0.08	0.09244	0.05	X	0.15%	0.041225	0.05	√
1D blocks	35	0.08	0.08835	0.05	X	0.15%	0.03869	0.05	√
2D blocks	35	0.08	0.09687	0.05	X	0.15%	0.02766	0.05	√

7.6.3 Understanding the effect of restraint orientation on the mechanical properties of ASR-affected concrete

As Gautam et al. [34] and other researchers [24–26,38] suggested, the confinement configuration could considerably affect the resulting mechanical properties of ASR-affected concrete in distinct directions, leading to important anisotropy in mechanical properties reductions. Therefore, Figure 10 and 11 illustrate the SDT and compressive strength results respectively (i.e., average of three cores per direction with their standard deviations), from the distinct directions (i.e., coring orientations). The data in brief can be found in Table 10 of the supplementary materials section.

For unrestrained concrete, a slight difference is noticed for the SDT and compressive strength results from distinct coring orientations for both given expansion levels (i.e., 0.08% and 0.15%). Conversely, the situation is completely different for the restrained blocks. The 1D concrete blocks' vertical and transverse cores (i.e., unrestrained directions) display 30% and 35% higher SDI and PDI, respectively, when compared to the longitudinal cores (i.e., restrained direction) for both slightly damaged (0.08%) and moderately damaged (0.15%) concrete. The modulus of elasticity and compressive strength of those cores obtained from unrestrained directions (i.e., vertical and transverse cores) on the other hand, present 17% and 12% lower values respectively, when compared to the longitudinal cores (i.e., restrained direction) for both slightly and moderately damage levels. Comparing the average SDI, PDI along with ME and compressive strength reductions of the 1D concrete blocks with distinct coring orientations for both slightly damaged (0.08%) and moderately damaged (0.15%) concrete, it is observed that although vertical and transverse cores display higher values than the average, longitudinal cores demonstrate lower results. The latter clearly confirms that using the average values (or "overall deterioration values") of the aforementioned parameters underestimates (i.e., 3 to 12%) the induced damage in unrestrained directions while overestimates (i.e., 5 to 25%) restrained orientations.

In the 2D concrete blocks, while the vertically extracted cores (i.e., unrestrained direction) display the highest amount of damage, the transverse and longitudinal cores (i.e., restrained directions) do not demonstrate a considerable variation among themselves. As such, the vertical 2D cores show an increase of almost 27% and 25% of the SDI, 29% and 16% of the PDI along with a decrease of 29% and 10% of modulus of elasticity, and 21% and 9% of compressive strength for both slightly and moderately damaged concrete, respectively, compared to transverse and longitudinal specimens. Similar to 1D concrete blocks, using the average values (or "overall deterioration values") of the aforementioned parameters, one would underestimate (i.e., 7 to 21%) ASR-induced damage in unrestrained directions while overestimating (i.e., 3 to 21%) it in restrained orientations of 2D concrete blocks.

Analyzing all the results obtained through the mechanical testing from unrestrained/restrained concrete blocks, one may notice that a lower damage level has been reached in the restrained directions of all reinforced blocks (i.e.,

longitudinal specimens in case of 1D and longitudinal and transverse in case of 2D concrete blocks) for the given expansion levels (i.e., 0.08% and 0.15%) of this research. Moreover, if one compares the distinct restraint configurations studied (i.e., 1D vs 2D), higher SDI and PDI values along with lower ME and compressive strength results were obtained for the unrestrained direction (i.e., vertical), whereas a lower SDI and PDI and higher ME and compressive strength in the restrained direction (i.e., transverse and longitudinal) are detected in the 2D configuration compared to the 1D concrete blocks. The above discussion illustrates the impact of restraint configuration on ASR-induced damage that is clearly transferred from restrained to the less/no restraint directions. The latter results in higher damage degrees along unrestrained directions of concrete specimens displaying higher overall degree of restraint.

To evaluate the statistical validity of the results obtained, a two-way ANOVA was conducted on the mechanical results (i.e., SDT and CS) obtained from the distinct blocks directions as a function of ASR development. As Tables 6 and 7 display, the SDI, PDI and ME parameters obtained from the distinct blocks directions are statistically significant (with a confidence level of 95%) for all concrete specimens of this study, where all the "F values" are greater than the "Fcritic" and the "p values" are lower than 0.05. However, as previously observed by Sanchez et al. [4], the results of compressive strength gathered from the various directions of the blocks were not considered statistically significant as a function of ASR development (Table 7). Therefore, a complementary "t-test" was performed to verify the significance of compressive strength results gathered at each expansion level (0.08% and 0.15%) when compared to the control samples (Table 8). Analyzing the results, one sees that only three out of nine conditions are considered significant at 0.08%, whereas all the twelve conditions are considered significant at 0.15% of expansion. These results prove the analysis and discussions prior conducted in this section and demonstrate the efficiency of the SDT to assess ASR-induced deterioration and anisotropy in restrained concrete, while the compressive strength is only effective after moderate levels of deterioration.

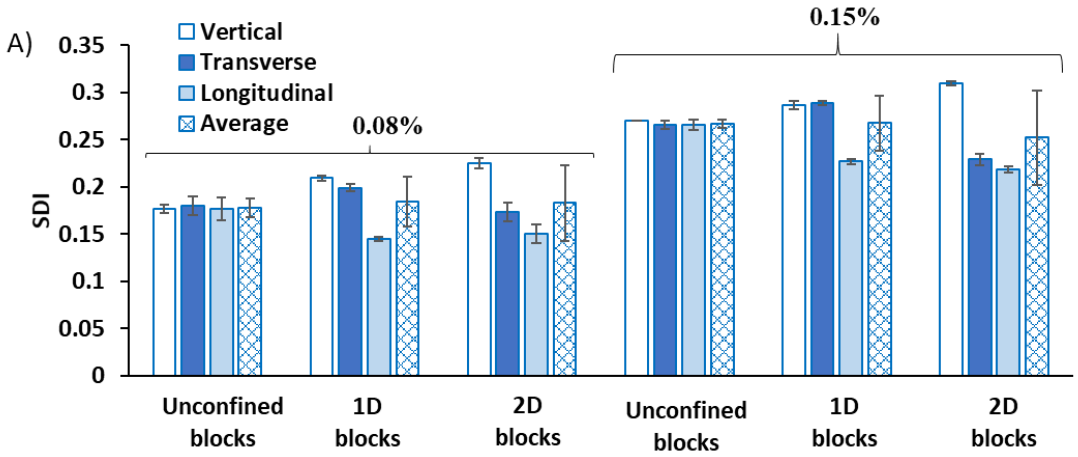

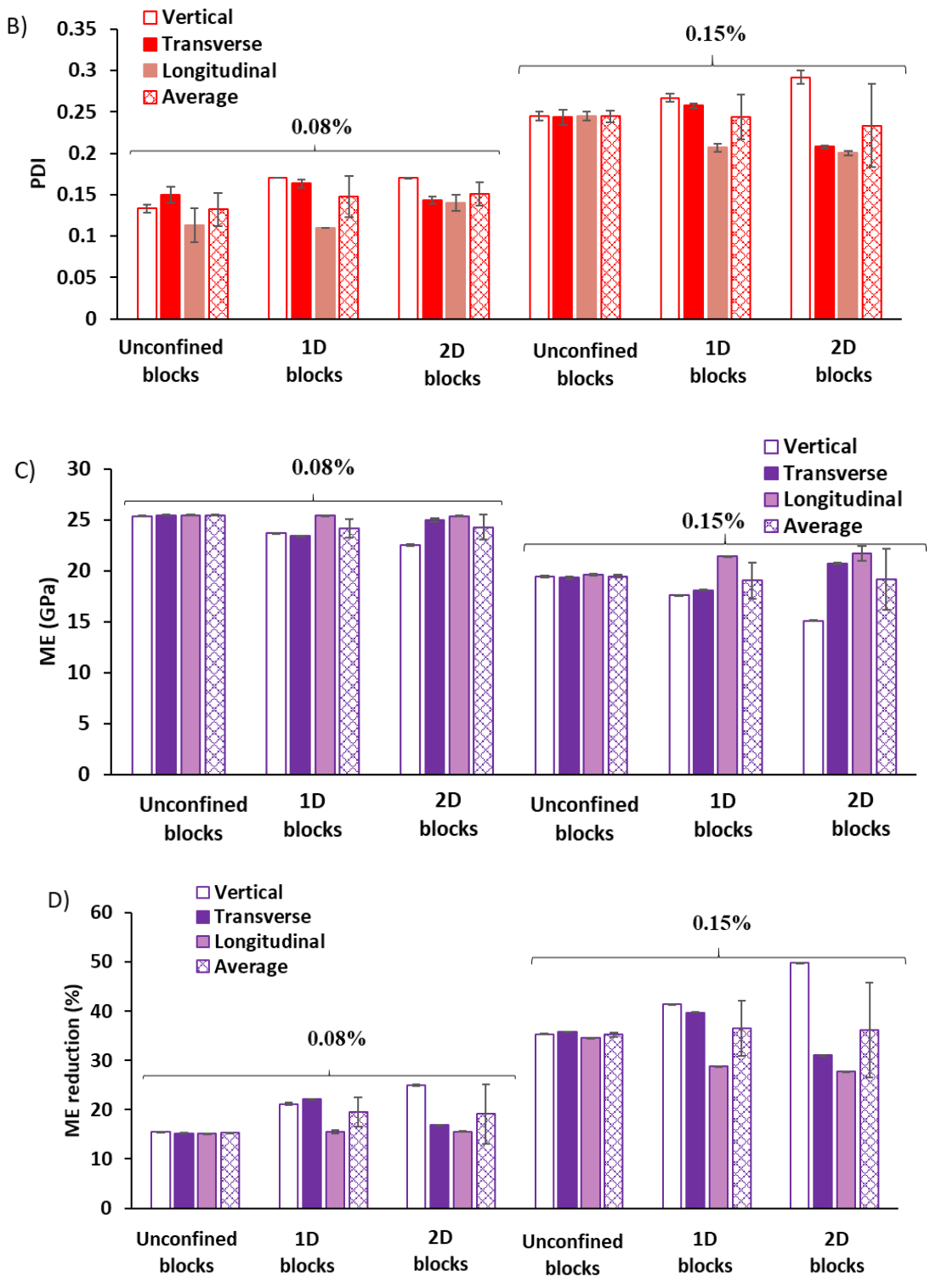

Figure 10: A) SDI, B) PDI, C) ME Reduction (%) and, D) ME values (GPA) from blocks considering various coring orientations.

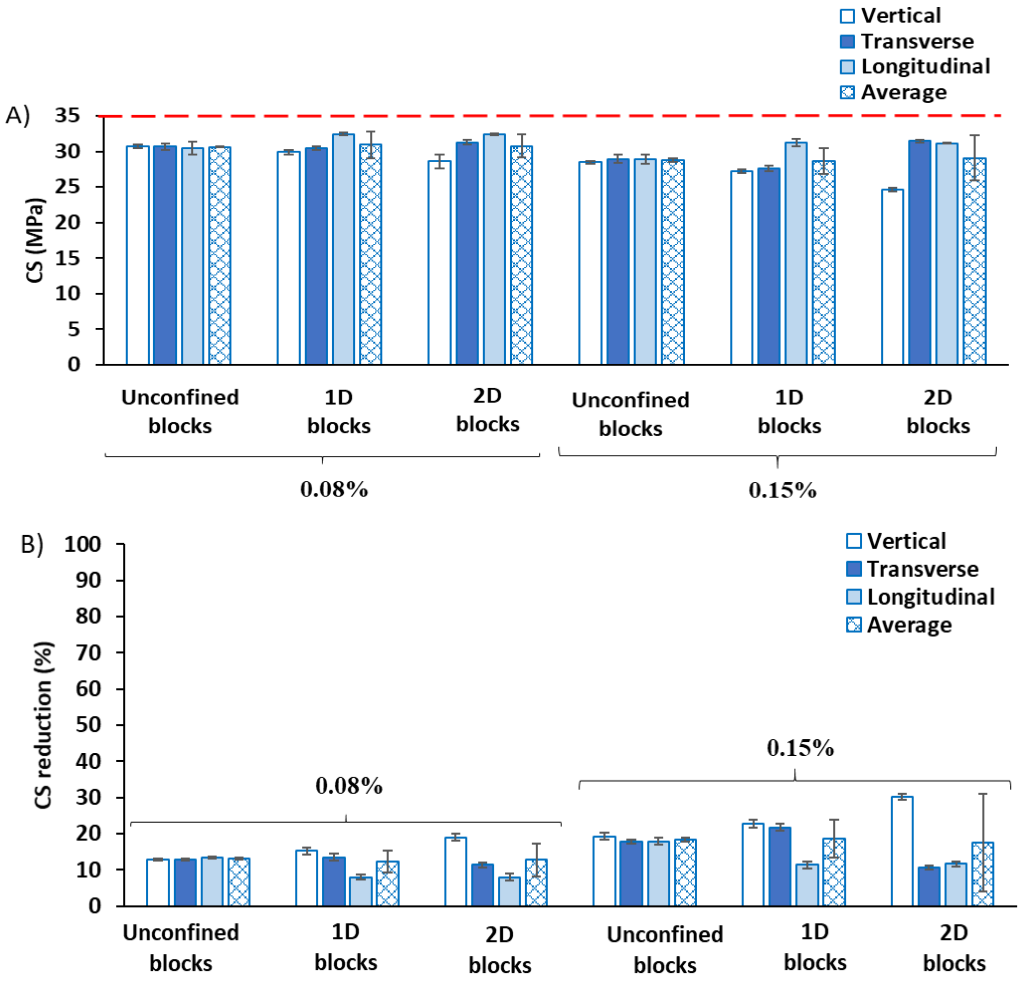

Figure 11: A) Compressive strength results (MPa) and, B) Compressive strength reductions (%) considering various coring orientations.

Table 6: Two-variable ANOVA on the SDT results (SDI and PDI parameters) considering various coring orientations.

ANOVA analysis				SDI						PDI					
Blocks type	Coring direction	Load (%)	Expansion (%)	SDI-F	SDI-Fcritic	F>Fcritic	SDI_P value	α	P<α	PDI-F	PDI-Fcritic	F>Fcritic	PDI_P value	α	P<α
Unconfined blocks	Vertical	40	0.08%-0.15%	676.00	7.71	✓	1.3E-05	0.05	✓	578.00	7.71	✓	1.78E-05	0.05	✓
	Transverse	40	0.08%-0.15%	150.09	7.71	✓	0.000255	0.05	✓	105.13	7.71	✓	0.00051	0.05	✓
	Longitudinal	40	0.08%-0.15%	82.81	7.71	✓	0.000809	0.05	✓	80.00	7.71	✓	0.000864	0.05	✓
1D blocks	Vertical	40	0.08%-0.15%	393.81	7.71	✓	3.8E-05	0.05	✓	841.00	7.71	✓	8.42E-06	0.05	✓
	Transverse	40	0.08%-0.15%	745.14	7.71	✓	1.07E-05	0.05	✓	607.21	7.71	✓	1.61E-05	0.05	✓
	Longitudinal	40	0.08%-0.15%	327.05	7.71	✓	3.9E-06	0.05	✓	841.00	7.71	✓	8.42E-06	0.05	✓
2D blocks	Vertical	40	0.08%-0.15%	424.19	7.71	✓	3.28E-05	0.05	✓	511.30	7.71	✓	2.27E-05	0.05	✓
	Transverse	40	0.08%-0.15%	51.14	7.71	✓	0.002023	0.05	✓	310.19	7.71	✓	6.1E-05	0.05	✓
	Longitudinal	40	0.08%-0.15%	119.84	7.71	✓	0.000396	0.05	✓	99.12	7.71	✓	0.000572	0.05	✓

Table 7: Two-variable ANOVA on the mechanical properties results (ME and CS) considering various coring orientations.

ANOVA analysis				ME						CS					
Blocks type	Coring direction	Load (%)	Expansion (%)	ME-F	ME-Fcritic	F>Fcritic	ME_P value	α	P<α	CS-F	CS-Fcritic	F>Fcritic	CS_P value	α	P<α
Unconfined blocks	Vertical	40	0.08%-0.15%	205.75	7.71	✓	1.35E-06	0.05	✓	120.19	7.71	✓	0.000393	0.05	✓
	Transverse	40	0.08%-0.15%	163.35	7.71	✓	0.000216	0.05	✓	6.97	7.71	X	0.059592	0.05	X
	Longitudinal	40	0.08%-0.15%	232.83	7.71	✓	0.000108	0.05	✓	3.84	7.71	X	0.121666	0.05	X
1D blocks	Vertical	40	0.08%-0.15%	166.32	7.71	✓	2.29E-08	0.05	✓	82.04	7.71	✓	0.000823	0.05	✓
	Transverse	40	0.08%-0.15%	149.01	7.71	✓	0.000259	0.05	✓	7.62	7.71	X	0.0949	0.05	X
	Longitudinal	40	0.08%-0.15%	262.54	7.71	✓	8.49E-05	0.05	✓	6.36	7.71	X	0.054453	0.05	X
2D blocks	Vertical	40	0.08%-0.15%	477.94	7.71	✓	2.59E-05	0.05	✓	3.65	7.71	X	0.05491	0.05	X
	Transverse	40	0.08%-0.15%	134.19	7.71	✓	0.000317	0.05	✓	0.63	7.71	X	0.47254	0.05	X
	Longitudinal	40	0.08%-0.15%	196.39	7.71	✓	0.00015	0.05	✓	131.78	7.71	✓	0.000329	0.05	✓

Table 8: t-Test analysis on the compressive strength results obtained from distinct directions of concrete blocks.

t-Test analysis - compressive strength loss										
Blocks type	Coring direction	Strength (MPa)	Expansion level	CS_P value	α	P<α	Expansion level	CS_P value	α	P<α
Unconfined blocks	Vertical	35	0.08%	0.04866	0.05	✓	0.15%	0.045766	0.05	✓
	Transverse	35	0.08%	0.06235	0.05	X	0.15%	0.025504	0.05	✓
	Longitudinal	35	0.08%	0.07422	0.05	X	0.15%	0.03646	0.05	✓
1D blocks	Vertical	35	0.08%	0.04866	0.05	✓	0.15%	0.047241	0.05	✓
	Transverse	35	0.08%	0.07966	0.05	X	0.15%	0.025701	0.05	✓
	Longitudinal	35	0.08%	0.09122	0.05	X	0.15%	0.025597	0.05	✓
2D blocks	Vertical	35	0.08%	0.06658	0.05	X	0.15%	0.029605	0.05	✓
	Transverse	35	0.08%	0.08369	0.05	X	0.15%	0.020781	0.05	✓
	Longitudinal	35	0.08%	0.4955	0.05	✓	0.15%	0.04852	0.05	✓

Figures 10 and 11 clearly demonstrate ASR anisotropic behaviour and its impact on the mechanical responses of affected concrete for distinct restrainment and induced expansion levels. However, it is important to notice that the above plots were generated assuming the side longitudinal expansion of the blocks as the "representative" of a given damage degree, since the side longitudinal direction is parallel to the main reinforcement and is not/less influenced by local effects such as drying/wetting cycles, differential restriction, etc. Nevertheless, it would be interesting to verify whether the SDT outcomes correlate well not only with the "representative" expansion but rather with the "real" expansion measured from the distinct surfaces evaluated. It worth noting that since vertical expansion measurements have not been conducted in this study, the correlation between vertical cored specimens and vertical expansion could not be obtained. Thus, Figure 12 illustrates the correlation between the SDI results obtained from the side longitudinal and transverse cored specimens and the measured expansions from the same blocks' surfaces (Figure 7). Analyzing the data, one verifies an almost linear trend between the SDI and the measured expansions from distinct directions. This plot confirms the anisotropic behaviour discussed above using a "representative" expansion level and attest once more the efficiency and diagnostic character of the SDT to assess damage in affected concrete regardless of its restraint configuration, as opposed to what has been previously reported by Sørgaard et. al. [7], and in accordance with previous works on concrete under unrestrained conditions [4] and while the condition assessment of critical infrastructure [6]. Finally, it is worth mentioning that the aggregate selected for concrete manufacturing in this work and similar studies [34,35] is a highly reactive coarse aggregate; according to past research, this aggregate generates a thin and low-viscosity ASR gel [66]. Therefore, a comprehensive experimental investigation through the use of slower reactivity aggregates, which may generate higher viscosity ASR gels and deterioration, is required and may be a topic of interest for future works.

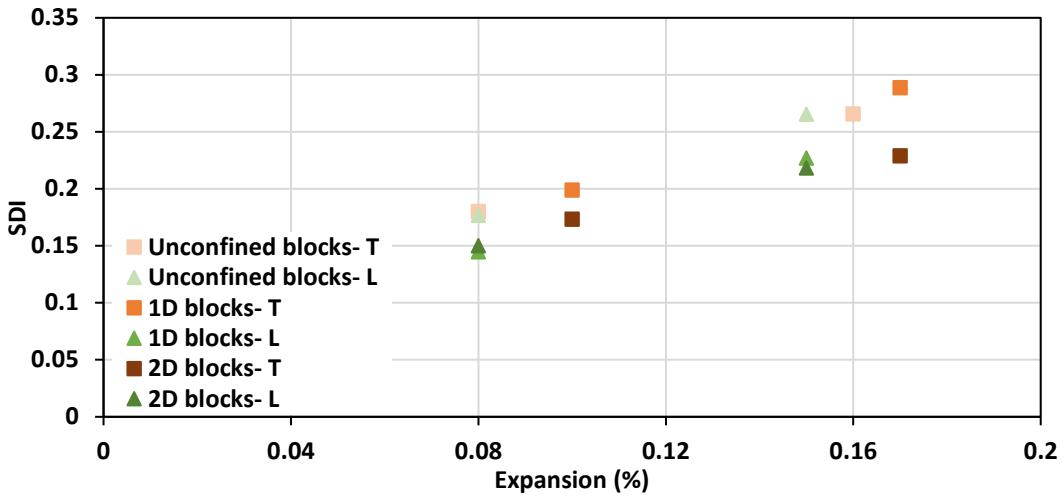

Figure 12: Correlation between SDI and measured expansion levels as per the distinct coring orientations evaluated.

7.6.4 Effect of restraint on the cracks' orientation of ASR-affected concrete

The Non-Linearity Index (NLI) has been reported by Chrisp et al. [51,52] as a useful parameter to appraise the cracks' orientation of ASR-affected concrete. As such, Figure 13A and 13B illustrate a typical stress-strain curve of vertical and transverse specimens (i.e., concave shaped curve) and longitudinal cores (i.e., convex shaped curve) of the 2D blocks, respectively, while Figure 13C displays the NLI values corresponding to distinct coring orientations for both slightly damaged (i.e., 0.08% of expansion) and moderately damaged (i.e., 0.15% of expansion) concrete. Analyzing these plots, one notices that the longitudinally cored specimens (convex shaped curves) from both restrained concrete blocks present an NLI parameter (i.e., Sec 1/Sec 2 of the first cycle – Figure 2) "lower than unity", indicating a cracking network parallel to the loading as per Chrisp et al. [51,52]. On the other hand, transverse and vertically cored specimens (concave shaped curves) demonstrate a NLI parameter "higher than unity" representing a cracking network perpendicular to the loading (i.e., longitudinal specimens present parallel ASR-induced cracks to the main steel rebars, while the cracks are perpendicular to the coring direction for vertical and transverse cores). The results gathered in this research show a strong correlation with previous works (e.g., [35,38,67]) and demonstrate the importance of computing the NLI for assessing ASR-affected reinforced concrete members and thus understanding the main orientation of induced cracks. The validation of the aforementioned results through image analysis might be a topic of interest for future works. The data in brief can be found in Table 12 of the supplementary materials section.

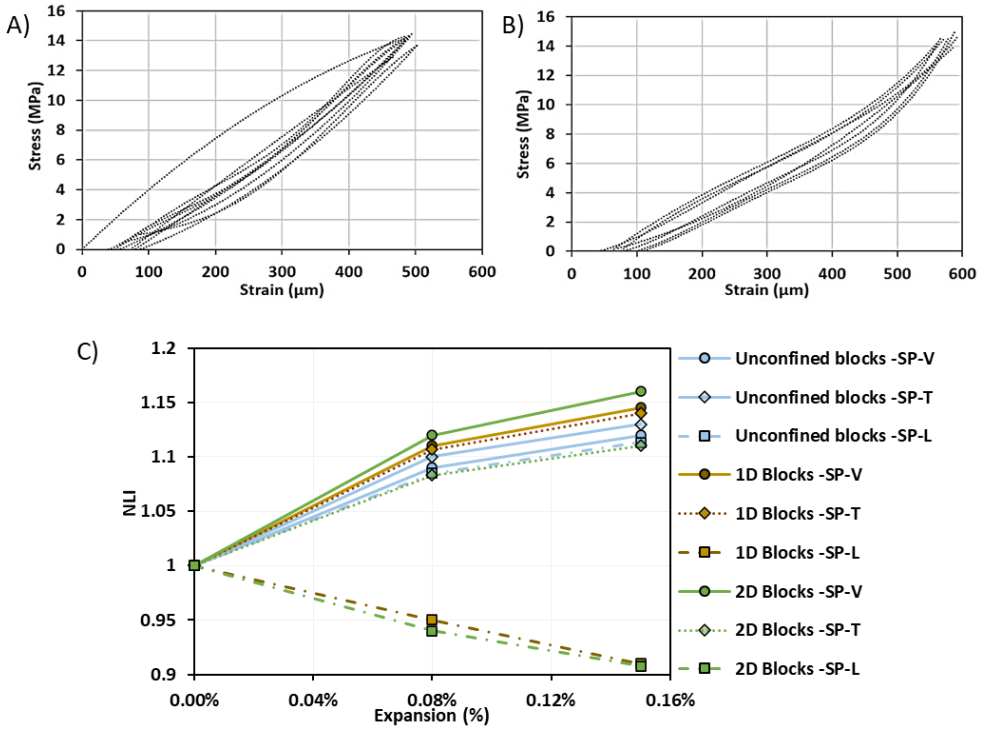

Figure 13: A) concave SDT graph (i.e. vertical and transverse cores), B) convex SDT graph (i.e. longitudinal cores) and, C) NLI graph for various coring directions.

7.6.5 Validation of the SDT for assessing damage in concrete

In order to validate the results obtained from the mechanical experimental campaign, semi-quantitative microscopic analyses through the Damage Rating Index (DRI) were conducted on specimens extracted from companion blocks presenting the same concrete mixture, expansion levels and reinforced configurations. Upon extraction, two consecutive core specimens from each of the three coring directions (i.e., vertical, longitudinal and transverse; total of 6 specimens per restraint condition per expansion level) were cut in half longitudinally using a diamond bladed masonry saw followed by subsequent mechanical polishing with grits of 30, 60, 140, 280 (80–100 µm), 600 (20–40 µm), 1200 (10–20 µm) and 3000 (4–8µm). Once the polished surface of the concrete section was deemed ready, a 1×1 cm grid was drawn on the surface of the specimens and the DRI was then conducted. The DRI is a microscopic technique where distinct damage features (Figure 14) are counted in each 1 cm^2 square drawn on polished concrete specimens using a stereomicroscope at 15-16x magnification. The damage features counted are then multiplied by weighting factors whose purpose is to balance their relative importance towards the corresponding distress mechanism (e.g., ASR in this case), as proposed by Villeneuve and Fournier [68] (Figure 14). The DRI number is therefore calculated; the higher the DRI number, the higher the induced damage in the material [4]. Ideally, a surface of at least 200 cm^2 should be assessed per member per direction, yet for comparative purposes, the final DRI value is normalized to a 100 cm^2 area.

A)

Petrographic features	Weighting factors
Closed cracks in aggregates (CCA)	0.25
Opened cracks in aggregates (OCA)	2
Opened crack with reaction product in aggregate (OCAG)	2
Coarse aggregate de-bonded (CAD)	3
Disaggregate/corroded aggregate particle (DAP)	2
Cracks in cement paste (CCP)	3
Cracks with reaction product in cement paste (CCPG)	3

B)

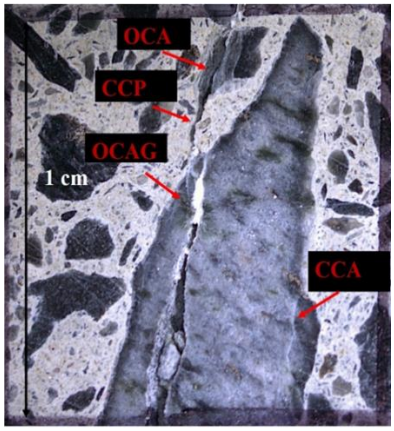

Figure 14: Damage Rating Index: A) current weighting factors as per [68] and, B) micrograph illustrating a 1cm^2 section where some of the petrographic features listed in A can be observed and identified [35] *(Reproduced with permission of Elsevier)*.

Previously, Gautam et al. [34] investigated the effect of distinct confinement conditions on the microstructure of ASR-affected restrained concrete through the DRI. According to the authors [34], it was important to specify not only the direction but rather the plane from which the specimens were extracted before the microscopic analysis. However, the current work follows the procedure proposed by Zahedi et al. [35] where the DRI evaluations were effectively and reliably (i.e., very low variability) conducted as per the distinct blocks' directions; further information can be found in [35]. Following their procedure, Figure 15 illustrates the distinct DRI numbers obtained from all specimens evaluated in this research (standard deviations added to the plot). Evaluating the data below, one notices that as for the SDT outcomes (e.g., SDI and PDI), there is not a significant difference in DRI values for the unrestrained concrete specimens as per the distinct directions; i.e., DRI numbers of 342, 341 and 337 were obtained at 0.08% of expansion, while DRI numbers of 578, 575 and 573 were gathered at 0.15% of expansion for the vertical, transverse and longitudinal cores, respectively. Conversely, the 1D and 2D confined blocks displayed quite different values as per the specimens' orientation, illustrating through a "microscopic point of view" ASR anisotropic behaviour. DRI numbers of 382, 366 and 337 at low expansion (0.08%), and 646, 613 and 479 at moderate expansion (0.15%) were obtained from the vertical, transverse and longitudinal directions of the 1D blocks. Furthermore, the cores extracted from the restrained directions of the 2D concrete blocks (i.e., transverse and longitudinal core specimens) did not show a noticeable difference in DRI number; yet, they demonstrated significantly lower DRI number (and thus induced damage) when compared to vertical specimens (i.e., unrestrained direction). As such, DRI numbers of 401, 310 and 305 were gathered at 0.08% of expansion and 766, 485 and 479 were obtained at 0.15% of expansion on the vertical, transverse and longitudinal cores, respectively.

The DRI results obtained in this work validate the mechanical assessment (i.e., SDT outcomes and compressive strength) previously discussed since cores presenting higher DRI values also yielded higher SDI and PDI and lower ME and compressive strength results. Moreover, the microscopic observations made on the cores extracted from the

1D and 2D ASR-affected blocks confirm the existence of the so-called expansion (and damage) transfer since higher induced deterioration is found on unrestrained/less restrained directions when compared to restrained orientations. The data in brief can be found in Table 12 of the supplementary materials section.

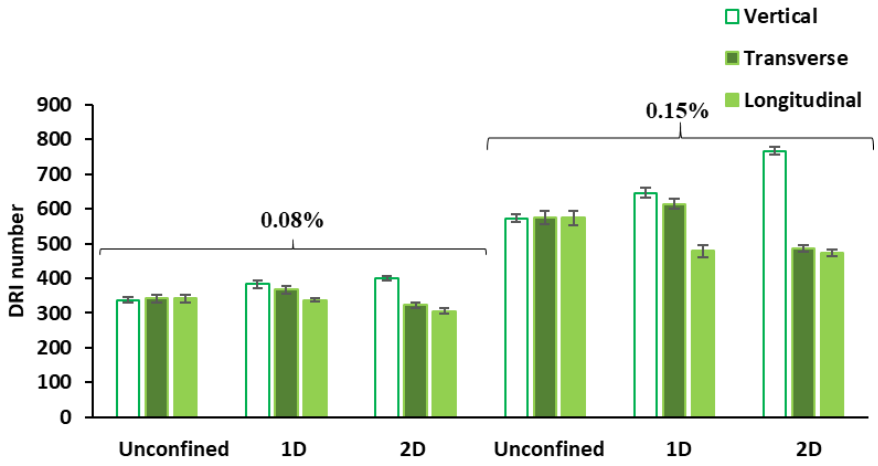

Figure 15: DRI charts as a function of coring direction for specified expansion.

7.7 Conclusion

The purpose of this study was to appraise ASR-induced physicochemical development in concrete blocks with distinct restraint configurations (i.e., none, 1D and 2D) through mechanical testing procedures (i.e., stiffness damage test-SDT and compressive strength). Based on the results obtained in this study, it is verified that confinement/restrainment influences the development of ASR in terms of induced expansion and mechanical distress. The main conclusions of the above investigations are presented hereafter:

- ASR-induced expansion was significantly lower for all concrete blocks when compared to the concrete cylinders; the latter could be attributed to the size of specimens, since moisture transfer is likely affected in larger members (i.e., blocks), thus decreasing ASR-induced development;

- Comparing the expansion levels reached by the distinct concrete blocks, one may observe that the higher the restraint degree, the slower the expansion rate and the lower the expansion level as a function of time. Furthermore, measuring induced expansion from distinct directions of the concrete blocks (i.e., longitudinal top, longitudinal side and transverse) demonstrated ASR anisotropic behaviour and the so-called “expansion transfer” from restrained to unrestrained/less restrained directions;

- The “overall” ASR-induced deterioration (i.e., average of three distinct directions at a given expansion level) obtained from the distinct blocks suggests that whether anisotropy is disregarded, the “overall” damage of ASR-affected specimens does not significantly change as a function of the restraint degree and configuration for the same expansion level. Moreover, the “overall” results acquired in this work on confined/restrained

concrete are in accordance with the data ranges proposed by Sanchez et al. [4] to classify damage in ASR-affected concrete under "free-expansion" conditions. However, it is clear from the results obtained that whether the "overall" deterioration is used to assess and classify damage of restrained concrete, underestimation and overestimation of unrestrained and restrained directions, respectively, are made;

- Statistical analysis (two-way analysis of variance - ANOVA) confirmed the significance of the SDT as a diagnostic tool for assessing the condition (i.e., physical integrity and stiffness reductions) of ASR-affected concrete under distinct confinement/restrainment configurations. Furthermore, the anisotropic character of ASR under confinement could be gathered by the distinct SDT outcomes (i.e., SDI, PDI and ME); higher SDI and PDI along with lower modulus of elasticity values were obtained from non/less restrained directions of the reinforced concrete blocks. Also, one sees that the higher the restraint, the higher the induced damage in unrestrained/less restrained directions, and the lower the deterioration in restrained directions. Furthermore, the NLI was shown to be an effective parameter to appraise the cracks orientation of ASR-affected concrete. NLI greater/lower than 1 indicates cracking networks mainly perpendicular/parallel to the reinforcing bars;

- The compressive strength results obtained on the distinct ASR-affected specimens in this study showed that although less influenced than the modulus of elasticity (as expected), significant reductions of compressive strength (e.g., 15-30%) may be gathered at low to moderate expansion levels (0.15%). Moreover, the compressive strength reductions could be even exacerbated in some directions due to anisotropy. The latter raises concerns not only on the serviceability but also on the ultimate capacity of ASR-affected structures withstanding service loads. Further studies should be conducted in this regard.

- The DRI, a semi-quantitative microscopic procedure, has been used to validate the mechanical results gathered in this research along with the anisotropic behaviour observed for the distinct restrained concrete blocks. According to the microscopic analyses, not only the SDT data was completely validated but also the "expansion transfer" phenomenon observed microscopically.

Acknowledgments

The authors would like to thank Drs. Gamal Elnabelsya and Muslim Majeed, technical officers of Materials and Structures Laboratory in the Department of Civil Engineering at the University of Ottawa, as well as the undergraduate research assistants (UROPs) who helped with the manufacturing and testing of the test specimens used in this project. Likewise, the authors would like to thank Mr. Matthew McDonald and his team from Advance Cutting & Coring Ltd. for facilitating the crucial process of drilling and extracting core specimens from the studied

concrete blocks. Lastly, Mr. Zahedi benefits from the prestigious University of Ottawa admission scholarship for international Ph.D. students.

References

[1] B. Fournier, M. Bérubé, Alkali–Aggregate Reaction in Concrete: a Review of Basic Concepts and Engineering Implications, Can. J. Civ. Eng. 27 (2000) 167–191. https://doi.org/10.1139/l99-072.

[2] N. Smaoui, B. Fournier, M. Bérubé, B. Bissonnette, B. Durand, Evaluation of the expansion attained to date by concrete affected by alkali silica reaction. Part II: Application to nonreinforced concrete specimens exposed outside, Can. J. Civ. Eng. 31 (2004) 997–1011. https://doi.org/10.1139/l04-074.

[3] B. Fournier, A. Bérubé, J. Folliard, M. Thomas, Report on the Diagnosis, Prognosis, and Mitigation of Alkali-Silica Reaction (ASR) in Transportation Structures, Report No. FHWA-HIF-09-004, Federal Highway Administration, U. S. Department of Transportation, Washington, DC, 2010.

[4] L.F.M. Sanchez, B. Fournier, M. Jolin, D. Mitchell, J. Bastien, Overall assessment of Alkali-Aggregate Reaction (AAR) in concretes presenting different strengths and incorporating a wide range of reactive aggregate types and natures, Cem. Concr. Res. 93 (2017) 17–31. https://doi.org/http://dx.doi.org/10.1016/j.cemconres.2016.12.001.

[5] L.F.M. Sanchez, B. Fournier, D. Mitchell, J. Bastien, Condition assessment of an ASR-affected overpass after nearly 50 years in service, Constr. Build. Mater. 236 (2020) 117554. https://doi.org/10.1016/j.conbuildmat.2019.117554.

[6] M. Thomas, K. Folliard, B. Fournier, P. Rivard, T. Drimalas, Methods for Evaluating and Treating ASR-Affected Structures: Results of Field Application and Demonstration Projects I, Report No. FHWA-HIF-14-0002, Federal Highway Administration, U. S. Department of Transportation, Washington, DC, 2013.

[7] S. Sørgaard, O. Oseland, T. Kanstad, M.A.N. Hendriks, E. Rodum, Experimental investigation of ASR-affected concrete – The influence of uniaxial loading on the evolution of mechanical properties, expansion and damage indices, Constr. Build. Mater. 245 (2020) 118384–118398. https://doi.org/10.1016/j.conbuildmat.2020.118384.

[8] N. Smaoui, M. Berube, B. Fournier, B. Bissonnette, B. Durand, Effects of alkali addition on the mechanical properties and durability of concrete, Cem. Concr. Res. 35 (2005) 203–212.

[9] A. Mohammadi, E. Ghiasvand, M. Nili, Relation between mechanical properties of concrete and alkali-silica reaction (ASR); a review, Constr. Build. Mater. 258 (2020) 119567. https://doi.org/10.1016/j.conbuildmat.2020.119567.

[10] R.S. Crouch, J.G.M. Wood, Damage evolution in ASR affected concretes., Eng. Fract. Mech. 35 (1990) 211–218.

[11] N. Smaoui, B. Bissonnette, M. Bérubé, B. Fournier, B. Durand, Mechanical properties of ASR-affected concrete containing fine or coarse reactive aggregates, J. ASTM Int. 3 (2006) 1–16. https://doi.org/10.1520/jai12010.

[12] R. Esposito, C. Anaç, M.A.N. Hendriks, Influence of the Alkali-Silica Reaction on the Mechanical Degradation of Concrete, J. Mater. Civ. Eng. 28 (2016). https://doi.org/10.1061/(ASCE)MT.1943-5533.0001486.

[13] Y. Kubo, M. Nakata, Effect of reactive aggregate on mechanical properties of concrete affected by alkali-silica reaction., in: 14th ICAAR - Int. Conf. Alkali-Aggregate React. Concr., Austin (Texas), 2012.

[14] L.F.M. Sanchez, T. Drimalas, B. Fournier, D. Mitchell, J. Bastien, Comprehensive damage assessment in concrete affected by different internal swelling reaction (ISR) mechanisms, Cem. Concr. Res. 107 (2018) 284–303. https://doi.org/10.1016/j.cemconres.2018.02.017.

[15] K. Ono, Strength and stiffness of alkali–silica reaction concrete and concrete members., Struct Eng Rev. 2 (1990) 121–125.

[16] F. Saint-Pierre, P. Rivard, G. Ballivy, Measurement of alkali-silica reaction progression by ultrasonic waves attenuation, Cem. Concr. Res. 37 (2007) 948–956. https://doi.org/https://doi.org/10.1016/j.cemconres.2007.02.022.

[17] F. Bektas, K. Wang, Performance of ground clay brick in ASR-affected concrete: Effects on expansion, mechanical properties and ASR gel chemistry, Cem.Concr. Compos. 34 (2012) 273–278. https://doi.org/https://doi.org/10.1016/j. cemconcomp.2011.09.012.

[18] P. Rivard, G. Ballivy, C. Gravel, F. Saint-Pierre, Monitoring of an hydraulic structure affected by ASR: a

case study, Cem. Concr. Res. 40 (2010) 676–680.
[19] S. Mindess, J.F. Young, D. Darwin, Concrete, second edi, Pearson Education Ltd, 2003.
[20] A.E.K. Jones, L.A. Clark, The effects of restraint on ASR expansion of reinforced concrete, Mag Concr. Res. 48 (1996) 1–13.
[21] C. Gravel, G. Ballivy, K. K, Q. M, L. M, Expansion of AAR Concrete under Triaxial Stresses: Simulation with Instrumented Concrete Block., in: Proc. 11th Int. Conf. Alkali Aggreg. React., Québec, Canada, 2000.
[22] T.M.A. Ahmed, E. Burley, S.R. Rigden, The effect of alkali-silica reaction on the fatigue behaviour of plain concrete tested in compression, indirect tension and flexure, Mag Concr. Res. 51 (1999) 375–390.
[23] C.F. Dunant, K.L. Scrivener, Effects of uniaxial stress on alkali-silica reaction induced expansion of concrete, Cem. Concr. Res. 42 (2012) 567–576.
[24] P. Morenon, S. Multon, A. Sellier, E. Grimal, F. Hamon, E. Bourdarot, Impact of stresses and restraints on ASR expansion, Constr. Build. Mater. 140 (2017) 58–74. https://doi.org/10.1016/j.conbuildmat.2017.02.067.
[25] S. Multon, F. Toutlemonde, Effect of applied stresses on alkali-silica reaction-induced expansions., Cem. Concr. Res. 36 (2006) 912–920.
[26] S. Multon, J.-F. Seignol, F. Toutlemonde, Structural behavior of concrete beams affected by alkali-silica reaction, ACI Mater. J. 102 (2005) 67–76.
[27] M. Noël, L. Sanchez, R. Martin, B. Fournier, J. Bastien, Structural Implications of Internal Swelling Reactions in Concrete : a Review, in: 15th Int. Conf. Alkali-Aggregate React., Sao Paulo, Brazil, 2016.
[28] H. Kagimoto, Y. Yasuda, M. Kawamura, ASR Expansion, Expansive Pressure and Cracking in Concrete Prisms under Various Degrees of Restraint, Cem. Concr. Res. 70 (2014) 1–15.
[29] M. Berra, G. Faggiani, T. Mangialardi, A. Paolini, Influence of Stress Restraint on the Expansive Behaviour of Concrete Affected by Alkali-Silica Reaction, Cem. Concr. Res. 40 (2010) 1403–1409.
[30] D. Wald, M.T. Allford, O. Bayrak, T.D. Hrynyk, Development and multiaxial distribution of expansions in reinforced concrete elements affected by alkali – silica reaction, Struct. Concr. 18 (2017) 914–928. https://doi.org/10.1002/suco.201600220.
[31] N. Smaoui, Contribution à l'évaluation du comportement structural des ouvrages d'arts affectés de réaction alcalis-silice., Département Génie Civil, Univ. Laval, Quebec, Canada. (2003).
[32] J. Liaudat, I. Carol, M.L. Carlos, ASR expansions in concrete under triaxial confinement, Cem. Concr. Compos. 86 (2018) 160–170. https://doi.org/10.1016/j.cemconcomp.2017.10.010.
[33] A. Zahedi, L. Sanchez, M. Noël, Effect of Confinement on AAR-induced expansion and damage, in: 16th ICAAR, Int. Conferance Alkali Aggreg. React. Concr. 1-3 June, Lisboa, Portugal, 2020.
[34] P. Gautam, D.K. Panesar, S.A. Sheikh, F.J. Vecchio, Effect of Multiaxial Stresses on Alkali-Silica Reaction Damage of Concrete, ACI Mater. J. 114 (2017) 595–604. https://doi.org/10.14359/51689617.
[35] A. Zahedi, C. Trottier, L. Sanchez, M. Noël, Microscopic Assessment of ASR-Affected Concrete Under Confinement Conditions, Cem Concr Res. (2021) 106456. https://doi.org/https://doi.org/10.1016/j.cemconres.2021.106456.
[36] A. Allard, S. Bilodeau, F. Pissot, B. Fournier, J. Bastien, B. Bissonnette, Expansive behavior of thick concrete slabs affected by alkali-silica reaction (ASR), Constr. Build. Mater. 171 (2018) 421–436. https://doi.org/10.1016/j.conbuildmat.2018.03.159.
[37] D. Wald, G. Arrieta, M. Oguzhan, Expansion behavior of a biaxially reinforced concrete member affected by alkali-silica reaction, Struct. Concr. 18 (2017) 550–560. https://doi.org/10.1002/suco.201600143.
[38] A.R. Barbosa, S. Gustenhoff, K. Kielsgaard, L. Cao, B. Grelk, Influence of alkali-silica reaction and crack orientation on the uniaxial compressive strength of concrete cores from slab bridges, Constr. Build. Mater. 176 (2018) 440–451. https://doi.org/https://doi.org/10.1016/j.conbuildmat.2018.03.096.
[39] A.E.K. Jones, L.A. Clark, S. Amasaki, The suitability of cores in predicting the behaviour of structural members suffering from ASR, Mag. Concr. Res. 46 (1994) 145–150.
[40] A. Allard, S. Bilodeau, F. Pissot, B. Fournier, J. Bastien, B. Bissonnette, Performance Evaluation of Thick Concrete Slabs Affected by Alkali-Silica Reaction (ASR) – Part I: Materials Aspects, in: 15th Int. Conf. Alkali-Aggreg. React. Concr., São Paulo, 2016.
[41] A.E.K. Jones, Cracking, Expansion and Strength of Concrete Subjected to Restrained Alkali Silica Reaction, PhD Thesis, The University of Birmingham, UK., 1994.

[42] E.R. Giannini, Evaluation of Concrete Structures Affected by Alkali-Silica Reaction and Delayed Ettringite Formation, PhD thesis, University of Texas at Austin, USA, 2012.
[43] K. Kobayashi, Load carrying behaviours of concrete structures and members affected by alkali-aggregate reactions, Concr. J. 24 (1986) 70–78.
[44] T. Ahmed, E. Burley, S. Rigden, The Static and Fatigue Strength of Reinforced Concrete Beams Affected by Alkali-Silica Reaction, ACI Mater. J. 95 (1999) 376–388.
[45] A. Abrishambaf, J.A.O. Barros, V.M.C.F. Cunha, Tensile stress-crack width law for steel fibre reinforced self-compacting concrete obtained from indirect (splitting) tensile tests, Cem. Concr. Compos. 57 (2015) 153–165. https://doi.org/10.1016/j.cemconcomp.2014.12.010.
[46] S.F. Resan, S.M. Chassib, S.K. Zemam, M.J. Madhi, New approach of concrete tensile strength test, Case Stud. Constr. Mater. 12 (2020) 1–13. https://doi.org/10.1016/j.cscm.2020.e00347.
[47] D.J. De Souza, L.F.M. Sanchez, M.T. De Grazia, Evaluation of a direct shear test setup to quantify AAR-induced expansion and damage in concrete, Constr. Build. Mater. 229 (2019) 116806. https://doi.org/10.1016/j.conbuildmat.2019.116806.
[48] L.F.M. Sanchez, B. Fournier, M. Jolin, J. Bastien, Evaluation of the Stiffness Damage Test (SDT) as a tool for assessing damage in concrete due to alkali-silica reaction (ASR): Input parameters and variability of the test responses, Constr. Build. Mater. 77 (2015) 20–32. https://doi.org/10.1016/j.conbuildmat.2014.11.071.
[49] J. Walsh, The effects of cracks on the uniaxial elastic compression of rocks., J. Geophys. Res. 70 (1965) 339–411. https://doi.org/https://doi.org/10.1029/JZ070i002p00399.
[50] R.S. Crouch, Specification for the determination of stiffness damage parameters from the low cyclic uniaxial compression of plain concrete cores. Revision A, Mott, Hay & Anderson, Special services division, internal technical note, 1987.
[51] T.M. Chrisp, P. Waldron, J.G.M. Wood, Development of a non-destructive test to quantify damage in deteriorated concrete, Mag. Concr. Res. 45 (1993) 247–256. https://doi.org/10.1680/macr.1993.45.165.247.
[52] T.M. Crisp, J.G.M. Wood, P. Norris, Towards Quantification of Microstructural Damage in AAR Deteriorated Concrete. International Conference on Recent Developments on the Fracture of Concrete and Rock, The University of Wales, Cardiff, 1989.
[53] N. Smaoui, B. Fournier, M. Bérubé, B. Bissonnette, B. Durand, B. Fournier, B. Bissonnette, B. Durand, Evaluation of the expansion attained to date by concrete affected by alkali silica reaction. Part I:Experimental study, Can. J. Civ. Eng. 31 (2004) 826–845. https://doi.org/10.1139/L04-051.
[54] L.F.M. Sanchez, B. Fournier, M. Jolin, J. Bastien, D. Mitchell, Practical use of the Stiffness Damage Test (SDT) for assessing damage in concrete infrastructure affected by alkali-silica reaction, Constr. Build. Mater. 125 (2016) 1178–1188. https://doi.org/10.1016/j.conbuildmat.2016.08.101.
[55] Y. Zhu, A. Zahedi, L.F.M. Sanchez, B. Fournier, S. Beauchemin, Overall assessment of alkali-silica reaction affected recycled concrete aggregate mixtures derived from construction and demolition waste, Cem. Concr. Res. 142 (2021) 106350. https://doi.org/10.1016/j.cemconres.2020.106350.
[56] B. Fournier, J. Lindgård, B.J. Wigum, I. Borchers, Outdoor exposure site testing for preventing Alkali-Aggregate Reactivity in concrete-a review., MATEC Web Conf. 199 (2018). https://doi.org/10.1051/matecconf/201819903002.
[57] ASTM C1293, Standard test method for determination of length change of concrete due to alkali-silica reaction, Annu. B. ASTM Stand. (2015) 1–7. https://doi.org/10.1520/C1293-08B.2.
[58] Standard Counsil of Canada, CSA A23.3:19:Design of concrete structures, 2019.
[59] Standard Counsil of Canada, CSA23.2-14C: Obtaining and testing drilled cores for compressive strength testing, in: CSA A23.119/CSA A23.219 Natl. Stand. Canada, 2019: pp. 774–778.
[60] Standard Counsil of Canada, CSA23.2-9C: Compressive strength of cylindrical concrete specimens, in: CSA A23.119/CSA A23.219 Natl. Stand. Canada, 2019: pp. 733–748.
[61] ASTM C39, Standard Test Method for Compressive Strength of Cylindrical Concrete Specimens, West Conshohocken (USA), 2012.
[62] ASTM C1074-19, Standard Practice for Estimating Concrete Strength by the Maturity Method, West Conshohocken (USA), 2019.
[63] B.P. Gautam, D.K. Panesar, “A New Method of Applying Long-Term Multiaxial Stresses in Concrete

Specimens undergoing ASR, and their Triaxial Expansions," Mater. Struct. 49 (2016) 3495–3508.
[64] N. Smaoui, B. Fournier, B. Bissonnette, Influence of Specimen Geometry , Orientation of Casting Plane , and Mode of Concrete Consolidation on Expansion Due to ASR, Cem. Concr. Aggregates. 26 (2004) 1–13.
[65] M.D. Champiri, M. Mohammad, R. Mousavi, K.J. Willam, Effect of Alkali-Silica Reactivity Damage to Tip-Over Impact Performance of Dry Cask Storage Structures, Int. J. Concr. Struct. Mater. (2018). https://doi.org/10.1186/s40069-018-0248-5.
[66] A. Gholizadeh Vayghan, F. Rajabipour, J.L. Rosenberger, Composition-rheology relationships in alkali-silica reaction gels and the impact on the Gel's deleterious behavior, Cem. Concr. Res. 83 (2016) 45–56. https://doi.org/10.1016/j.cemconres.2016.01.011.
[67] S.G. Hansen, R.A. Barbosa, L.C. Hoang, Prestressing of reinforcing bars in concrete slabs due to concrete expansion induced by Alkali-Silica Reaction, in: Fib Symp., Cape Town, 2016.
[68] V. Villeneuve, B. Fournier, Determination of the damage in concrete affected by ASR — the damage rating index (DRI), in: 14th ICAR — Int. Conf. Alkali– Aggreg. React. Concr., Austin (Texas), 2012.

SUPPLEMENTARY MATERIALS

Table 9: Data in brief for the “overall” analysis.

Block Type	SDI		PDI		E (GPa)		E Reduction (%)		CS (MPa)		CS Reduction (%)	
	0.08%	0.15%	0.08 %	0.15 %	0.08 %	0.15 %	0.08%	0.15%	0.08%	0.15%	0.08%	0.15%
Cylinder	0.18	0.26	0.13	0.24	25	19	17	36	31	28	12	21
unrestrained Blocks	0.18	0.27	0.13	0.24	25	19	17	36	31	29	12	18
1D Blocks	0.18	0.27	0.15	0.24	24	19	20	36	31	29	12	18
2D Blocks	0.18	0.25	0.15	0.23	24	19	20	36	31	29	12	18

Table 10: Data in brief for the “anisotropic” analysis.

Block Type	Core orientation	SDI		PDI		E (GPa)		E Reduction (%)		CS (MPa)		CS Reduction (%)	
		0.08%	0.15%	0.08%	0.15%	0.08%	0.15%	0.08%	0.15%	0.08%	0.15%	0.08%	0.15%
Unrestrained Block	Vertical	0.18	0.27	0.13	0.25	25.36	19.39	15.47	35.38	30.74	28.45	12.75	19.25
	Transverse	0.18	0.27	0.15	0.24	25.44	19.28	15.20	35.74	30.69	28.95	12.90	17.82
	Longitudinal	0.18	0.27	0.11	0.25	25.45	19.62	15.16	34.60	30.51	28.93	13.42	17.88
1D Block	Vertical	0.21	0.29	0.17	0.27	23.65	17.59	21.17	41.38	29.89	27.22	15.16	22.74
	Transverse	0.20	0.29	0.16	0.26	23.37	18.09	22.09	39.70	30.48	27.58	13.48	21.71
	Longitudinal	0.14	0.23	0.11	0.21	25.37	21.38	15.45	28.73	32.43	31.25	7.95	11.31
2D Block	Vertical	0.23	0.31	0.17	0.29	22.52	15.06	24.95	49.79	28.59	24.61	18.86	30.16
	Transverse	0.17	0.23	0.14	0.21	24.95	20.70	16.83	31.01	31.25	31.46	11.30	10.71
	Longitudinal	0.15	0.22	0.14	0.20	25.35	21.67	15.52	27.77	32.44	31.13	7.92	11.64

Table 11: Data in brief for the NLI analysis.

Block Type	Core orientation	0.08%	0.15%
Unrestrained Block	Vertical	1.09	1.12
	Transverse	1.1	1.13
	Longitudinal	1.085	1.1132
1D Block	Vertical	1.11	1.145
	Transverse	1.1069	1.14
	Longitudinal	0.95	0.91
2D Block	Vertical	1.12	1.16
	Transverse	1.083	1.11
	Longitudinal	0.94	0.9075

Table 12: Data in brief for the DRI analysis.

Block Number	Core orientation	DRI Number	
		0.08%	0.15%
Unrestrained Blocks	Vertical	337.199	573.1576
	Transverse	341.1905	575.136
	Longitudinal	341.0588	573.2605
1D Block	Vertical	382.75	646.07
	Transverse	366.55	613.92
	Longitudinal	337.831	478.725
2D Block	Vertical	401.2283	765.8121
	Transverse	323.0195	485.488
	Longitudinal	305.951	472.8925

8. CONDITION ASSESSMENT OF ALKALI-SILICA REACTION AFFECTED CONCRETE UNDER RESTRAINT CONDITIONS INCORPORATING DISTINCT REACTIVE AGGREGATE TYPES

Andisheh Zahedi [1], Cassandra Trottier [2], Leandro Sanchez [3], Martin Noël [4]

Abstract

The multi-level assessment, combining microscopic (i.e., Damage Rating Index) and mechanical (i.e., Stiffness Damage Test) techniques, has been effectively used to appraise the deterioration cause by alkali-silica reaction (ASR) in unconfined concrete. However, the impact of restrainment on ASR-induced deterioration originated from reactive fine and coarse aggregates has not been fully explored. This study intends to evaluate the effect of the restraint degree and reactive aggregate type on ASR damage development through the multi-level assessment. Twenty-four concrete blocks incorporating two different reactive aggregate types (fine and coarse) and three restraint configurations (unrestrained, 1D, and 2D) were produced and monitored over time. Upon reaching the desired expansion levels (0.08% and 0.15%), cores were retrieved from three main directions (vertical, longitudinal and transverse) and the multi-level assessment was performed. Results indicate that ASR-induced expansion and damage are influenced by the reactive aggregate type, restraint configuration and coring direction.

Keywords: Restraint, Alkali-Silica Reaction (ASR), Multi-level assessment, Damage Rating Index (DRI), Stiffness Damage Test (SDT), Aggregate type.

8.1. Introduction

Alkali-silica reaction (ASR), a complex physicochemical reaction between certain mineral phases in the aggregates and the alkali hydroxides from the concrete pore solution, is one of the main deleterious processes influencing the durability and serviceability of concrete infrastructure around the world [1]. ASR produces a secondary product (i.e., silica gel) that generates expansion and internal pressure upon moisture uptake from its surrounding environment, causing a loss in the material's mechanical properties and, in some cases, functionality of affected structures [1,2]. Most of Canada's concrete infrastructure is currently suffering from deterioration mechanisms such as ASR, freeze-thaw and steel corrosion [3–5]; thus, serious concerns have been raised about the structural performance and safety of those structures [3]. Since ASR is an active and ongoing process, obtaining information on the actual damage degree along with the potential for further deterioration of affected structures is critical when designing effective rehabilitation strategies and management protocols. In this context, several test procedures have been developed over the

past decades to determine the induced expansion and deterioration attained to date (i.e., diagnosis), as well as to forecast the potential of future distress (i.e., prognosis) of concrete infrastructure damaged by ASR. Among those, a comprehensive multi-level protocol, through the use of microscopic and mechanical test procedures (particularly the Stiffness Damage Test- SDT and the Damage Rating Index- DRI, respectively), has shown to be effective to appraise the condition of ASR-affected unreinforced concrete [6]. Nevertheless, such condition does not typically represent field concrete structures [7,8]. Although past studies have reported the reliability of the multi-level assessment to assess the condition of deteriorated concrete structures [9,10], there is currently a lack of "extensive" data on the impact of reinforcement (e.g., confinement) on ASR physicochemical development and ultimately on the multi-level assessment outcomes. Therefore, this study intends to appraise the condition of ASR-affected concrete blocks incorporating different types of reactive aggregates (i.e., fine and coarse aggregates), having different reinforcement conditions (i.e., unrestrained, 1D and 2D) and expansion levels (i.e., 0.08% and 0.15%) through the use of the multi-level protocol. It is worth noting that the term "confinement" is used in this work to describe any type of restraint that prevents the concrete from freely expanding, such as the presence of steel reinforcement.

8.2. Effects of confinement on physicochemical development of ASR

Literature suggests that ASR-induced expansion of affected concrete is lessened due to confinement [11–13]; Smaoui [12] reported a reduction of almost 60% of the induced expansion in the direction parallel to the reinforcing bars of concrete beams (810 x 228 x 228 mm) with a reinforcement ratio of 1.53% when compared to similar beams without any reinforcement. According to the authors, this expansion reduction in the restrained direction might result in an increase of damage development in the directions with less or no confinement [11,14–16]. As such, Multon and coworkers [11,14] confirmed the redistribution of expansion amongst distinct directions of restrained concrete where ASR-induced expansion decreased from 15% to 70% in the direction of confinement and has been transferred to the unrestrained directions; such an expansion transfer results in anisotropic ASR-induced development [16], which has been found to be dependent on the reinforcing ratio and configuration [3]. Deschenes et al. [17] and Bracci et al. [18] made observations on the rate and ultimate expansion achieved by various ASR-affected concrete members displaying distinct restraint configurations; they reported that higher expansion levels and rates were observed in lightly reinforced members when compared those heavily reinforced [19].

Abd-Elssamd et al. [20] verified that the modulus of elasticity (ME) and compressive strength (CS) reductions of ASR-affected restrained and unrestrained concrete follow similar degradation trends. However, similar to the expansion behavior, the progression and orientation of the induced microcracking and degradation of mechanical properties of restrained concrete members are affected by the anisotropic

ASR-induced development [21]. Therefore, dissimilar mechanical properties reductions are expected in the three principal directions [20,22,23], where the compressive strength and modulus of elasticity of specimens extracted perpendicular to the main restraint direction demonstrate significantly higher degradation than those cored parallel to the main reinforcement bars [21,24,25]. As such, it has been observed that the compressive strength of cores extracted perpendicular to the main restraint direction may have higher reductions from 7-35% when compared to those retrieved parallel to the main steel bars [14,19,21,24,25]. Such an observation can be due to the presence of a higher amount of ASR cracks in the cores retrieved perpendicular to the main rebars [16,26,27].

Very few studies [21,28] were performed to investigate the effects of different reactive aggregate types (i.e., fine vs coarse aggregate) on the development of ASR-induced deterioration in restrained concrete. Barbosa et. al. [21] and Hansen et. al. [28] observed that concrete members incorporating reactive fine aggregates displayed a much more pronounced deterioration degree when compared to those incorporating reactive coarse aggregates; moreover, the authors also reported significantly wider cracks in ASR-affected members bearing reactive fine aggregates. No further explanation has been addressed in this regard.

Although the current literature data are very useful and demonstrate the effect of reinforcement on the physicochemical development of ASR, to the best of the authors' knowledge, there is still a need to systematically and quantitatively evaluate this effect on the microscopic distress features and mechanical response of concrete samples having various reinforcement conditions, exhibiting different expansion levels and incorporating different reactive aggregate types (i.e., fine and coarse aggregates).

8.2.1 Tools for appraising concrete damaged by ASR

Several microscopic and mechanical test procedures were proposed in the past decades to evaluate the cause and extent of damage in ASR-affected concrete. Among them, the multi-level protocol as per [6], using microscopic and mechanical test procedures, particularly the Stiffness Damage Test (SDT) and Damage Rating Index (DRI) respectively, was found to be quite effective.

8.2.1.1. Stiffness Damage Test (SDT)

The Stiffness Damage Test (SDT) was initially developed by Walsh who observed a good correlation between the crack density and the cycles of loading/unloading (i.e., stress/strain relationship) of rock specimens [29,30]. Crisp et al. [31,32] used this test method to evaluate ASR-induced damage in affected concrete. Later, Sanchez et al. [29,30] optimized the test procedure by conducting a large experimental campaign on test specimens manufactured from concrete mixtures of various mixture proportions (i.e., 25, 35 and 45 MPa) and incorporating a wide range of reactive aggregates (i.e., coarse vs fine aggregates, and distinct lithotypes and reactivity degrees). They proposed that the SDT should be conducted through five

loading/unloading cycles at 40% of the design (28-day) concrete strength, as well as adapting indices as the test outcomes, namely the Stiffness Damage Index (SDI) and Plastic Deformation Index (PDI), representing, respectively, the ratio of dissipated energy/plastic deformation to the total energy/deformation implemented in the system (i.e., SI / (SI+SII) and DI / (DI+DII) over the five cycles as presented in [29,30]- Figure 1). Furthermore, the modulus of elasticity (average secant modulus of the 2nd and 3rd cycles) and the Non-Linearity Index (NLI- Sec 1 divided by Sec 2 in the first cycle– Figure 1) as proposed by Crisp et al. [31,33] could also be considered as efficient SDT outcomes for determining the damage extent and cracks orientation (i.e., NLI is greater/lower than unity for cracks oriented perpendicular/parallel to loading) respectively, in affected concrete.

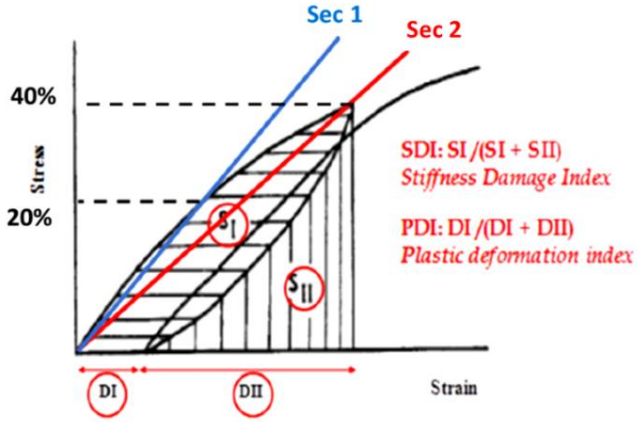

Figure 1: Calculation of the Stiffness Damage Index (SDI) and Plastic Deformation Index (PDI) [34] *(Reproduced with permission of Elsevier)*.

8.2.1.2. Damage Rating Index (DRI)

In the early 1990′s, Grattan-Bellew and coworkers [35,36] developed the Damage Rating Index (DRI) method, a semi-quantitative microscopic tool where distinct petrographic features (Figure 2B) are counted in each 1 cm^2 square drawn on the surface of polished concrete specimens through the use of a stereomicroscope at 15-16x magnification [7]. The number of counts associated with each type of petrographic feature is then multiplied by a weighting factor proposed by Villeneuve et al. [37] (Figure 2A), whose purpose is to balance their relative importance towards the mechanism of distress (e.g., ASR). The final DRI value is thus calculated, and a higher DRI number represents a higher degree of deterioration in affected concrete [6]. Ideally, a surface of at least 200 cm² should be used for analysis, yet for comparison purposes, the final DRI value is normalized to a 100 cm² area. The detailed test procedure of DRI is presented in [7,8].

A)

Petrographic features	Weighting factors
Closed cracks in aggregates (CCA)	0.25
Opened cracks in aggregates (OCA)	2
Opened crack with reaction product in aggregate (OCAG)	2
Coarse aggregate de-bonded (CAD)	3
Disaggregate/corroded aggregate particle (DAP)	2
Cracks in cement paste (CCP)	3
Cracks with reaction product in cement paste (CCPG)	3

B)

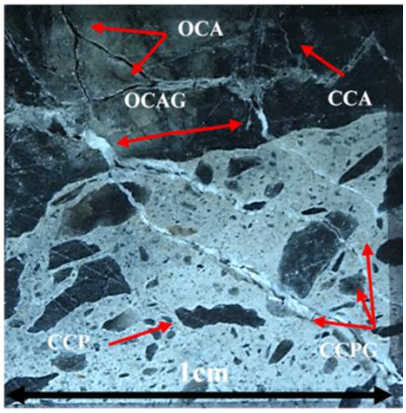

Figure 2: Damage Rating Index: A) distress features and corresponding weighting factors as per [37] and, B) some of the petrographic features listed in A can be identified in a 1cm ^{2} section *(Reproduced with permission of Elsevier)*.

8.3. Scope of work

As previously mentioned in the above sections, there is still a need to thoroughly and quantitatively understand the impact of reinforcement on the physicochemical development of ASR. Thus, twenty-four concrete blocks incorporating reactive fine and coarse aggregates and having various restraint conditions (i.e., unrestrained, 1D and 2D) were manufactured and monitored over time. After reaching the targeted expansion levels (i.e., slight - 0.08% and moderate - 0.15%), core specimens were extracted from three main directions (i.e., longitudinal, vertical and transverse) of the concrete blocks and the multi-level assessment as per [6] was performed on those. Ultimately, the damage development and mechanical properties reductions of concrete members incorporating different aggregate types and displaying distinct restraint configurations have been compared.

8.4. Materials and methods

8.4.1 Materials and mix proportions

Twenty-four concrete blocks with dimensions of 450 X 450 X 675 mm (Figure 3) were manufactured in the laboratory using a concrete mix with a design strength of 35 MPa. A highly reactive sand (i.e., Texas-Polymictic sand) and a reactive coarse aggregate (i.e., Springhill - Greywacke) in combination with non-reactive aggregate particles (i.e., Ottawa natural sand-OT and Ottawa limestone coarse aggregate-LS, respectively) from local quarries were used for concrete fabrication. Table 1 presents information on the various aggregates selected for this work. A conventional CSA Type GU (i.e., ASTM type 1) high alkali (0.88% Na_2O_{eq}) Portland cement was used for both concrete mixtures. Moreover, the total alkali content of both mixtures was raised to 1.25% Na_2O_{eq}, by cement mass, to accelerate ASR-induced development. Table

2 presents the mixture proportions selected for this study based on the concrete prism test (CPT) test as per ASTM C 1293 [38].

Table 1: Reactive and non-reactive aggregates used in the study.

Aggregate				Rock type	Specific gravity (g/cm^3)	Absorption (%)	AMBT [a] 14 days expansion(%)
Type	Reactivity	Location	Name				
Coarse	Reactive	New Brunswick	SP	Greywacke	2.72	0.60	0.69
	Non-reactive	Ottawa	LS	Limeston derived from quarries	2.68	0.53	0.05
Fine	Reactive	Texas (USA)	TX	Polymictic sand	2.60	0.55	0.76
	Non-reactive	Ottawa	OT	Natural derived from granite	2.65	1.18	0.07

a) Typical expansion cf. ASTM C1260.

Table 2: Concrete mixtures proportioned using the same amount of aggregates (i.e., fine and coarse) and cement paste in volume.

Materials	Mix proportions (kg/m^3)	
	OT+SP	TX+LS
Cement	420	420
Fine aggregate	681	732
Coarse aggregate	1044	1072
Water	176	176
Air content (%)	2	2

8.4.2 Production of concrete specimens

Three different restraint scenarios were selected for this study: 1) unreinforced concrete blocks (Figure 3A), 2) 1D confined blocks (Figures 3B and 4A) and, 3) 2D confined blocks (Figures 3C and 4B). For the restrained blocks, a reinforcement ratio of 2% was selected in each restrained direction, which is representative of a moderately high level of internal restraint in reinforced concrete members. For instance, several standards and design codes indicate a minimum reinforcement ratio in slabs of 0.2% and a maximum practical limit in columns of 4% (e.g., CSA A23.3 [39]). Relatively large steel bars with a nominal diameter of 35 mm were used to reinforce the restrained blocks to achieve the desired reinforcement ratio while ensuring sufficient space between bars to allow for concrete core extraction. It is worth noting that the transverse and longitudinal steel bars of the 2D concrete blocks were welded together to facilitate the manufacturing of the reinforcement cages (Figure 4B). Moreover, the concrete cover of the reinforced concrete blocks and spacing between the bottom and top steel bars are 50 mm and 280 mm, respectively (Figure 4C). A total of 6 blocks from each reinforcement configuration (i.e., unrestrained, 1D and 2D) incorporating the SP coarse aggregate (eighteen concrete blocks) and 6 blocks bearing a 2D confinement configuration incorporating the TX fine aggregate were fabricated in the laboratory. For comparative purposes, 40 concrete cylindrical specimens of 100 X 200 mm (Figure 5D) were also fabricated using the same highly reactive fine and coarse aggregates (i.e., 20 concrete cylinders per aggregate type) and using the same mix proportions as the concrete blocks.

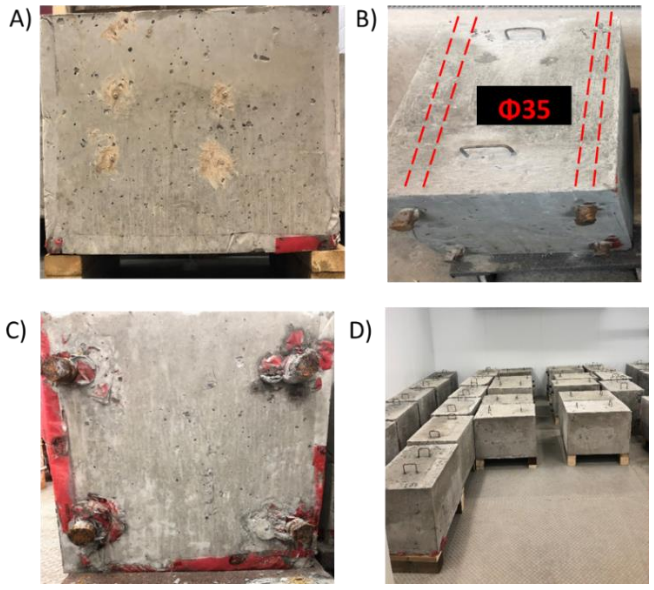

Figure 3: Concrete blocks fabricated presenting A) unreinforced concrete; B) 1D block; C) 2D block; D) Specimens placed in an environmental chamber with 38ºC and 100% RH.

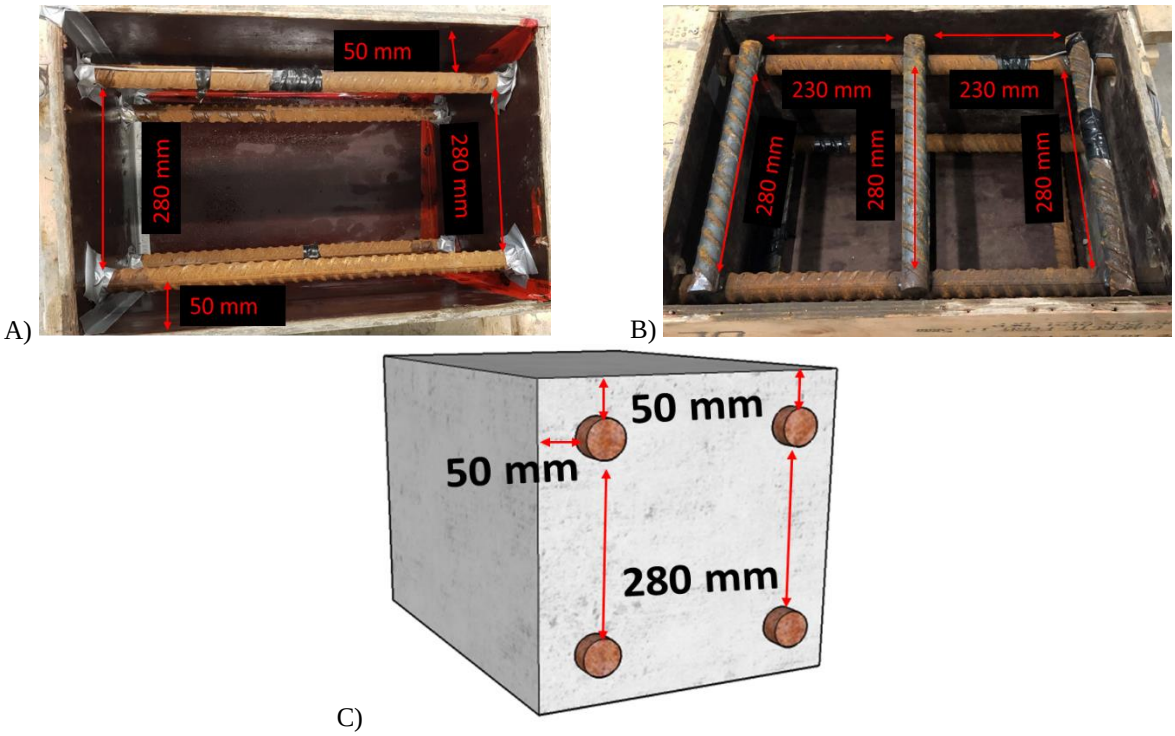

Figure 4: Reinforcement configurations: A) 1D reinforced blocks B) 2D reinforced blocks C) schematic of reinforced blocks.

All concrete samples were demolded after one day and moist cured for another 24 hours at 20°C. Then, four holes with 10 mm in diameter by 55 mm in length, were drilled in the three main surfaces of the concrete blocks: a) Top (Figure 5A points 1 and 2), b) Longitudinal (Figure 5A points 3 and 4) and c) Transverse (Figure 5A points 5 and 6). Moreover, tiny holes of 8.5 mm in diameter by 19 mm in length,

were also drilled at each end of all cylinders. Later, stainless-steel studs were placed using a fast-setting cement paste slurry for longitudinal expansion measurements in all concrete specimens. Forty-eight hours from manufacturing, the initial readings were recorded as follows: a) for concrete blocks, transverse, top longitudinal and side longitudinal expansion measurements as per Figure 5A and 5B, and b) longitudinal expansion measurements in the cylinders' case. All blocks were stored at 38ºC and 100% RH (Figure 3D) to accelerate ASR development. The concrete cylinders were stored in sealed buckets lined with a damp cloth (Figure 5C) and placed in the environmental chamber. All specimens were monitored for length changes regularly until they reached the expansion levels selected for this study, i.e., slight (i.e., 0.08% ± 0.01%) and moderate (i.e., 0.15% ± 0.01%). As per ASTM C 1293 [38], all concrete specimens were placed in 23°C conditions for 16 ± 4 hours before periodic expansion measurements. Upon reaching the targeted expansion levels, concrete specimens were removed from the environmental chamber and three blocks from each distinct restraint configuration and aggregate type were cored to produce seven cores of 100 by 450 mm in the vertical (Figures 6A and 6E) and the transverse (Figures 6B and 6E) directions and four cores of 100 by 675 mm in the longitudinal (Figures 6C and 6D) direction for further analysis. Later, all concrete specimens were saw cut to lengths of 200 mm, wrapped in plastic film, and stored at 12°C until testing to stop further ASR-development as per [6]. It is important to note that after retrieving the cores from the affected concrete blocks, the latter are no longer subjected to the same stress level as the in-situ concrete. Such stress relieve might change the characteristics of damage developed by ASR during the condition assessment performed in this study. While this effect has not been explicitly quantified in this work, it is worth noting that such phenomenon is also true for the cores retrieved from the real concrete structures, and thus the findings of this work are expected to be applicable to such cases.

A) B) C) D)

Figure 5: A) Schematic of concrete block's expansion measurements, B) expansion measurements of concrete blocks with a micrometer, C) Sealed container for storage in the environmental chamber and, D) concrete cylinder.

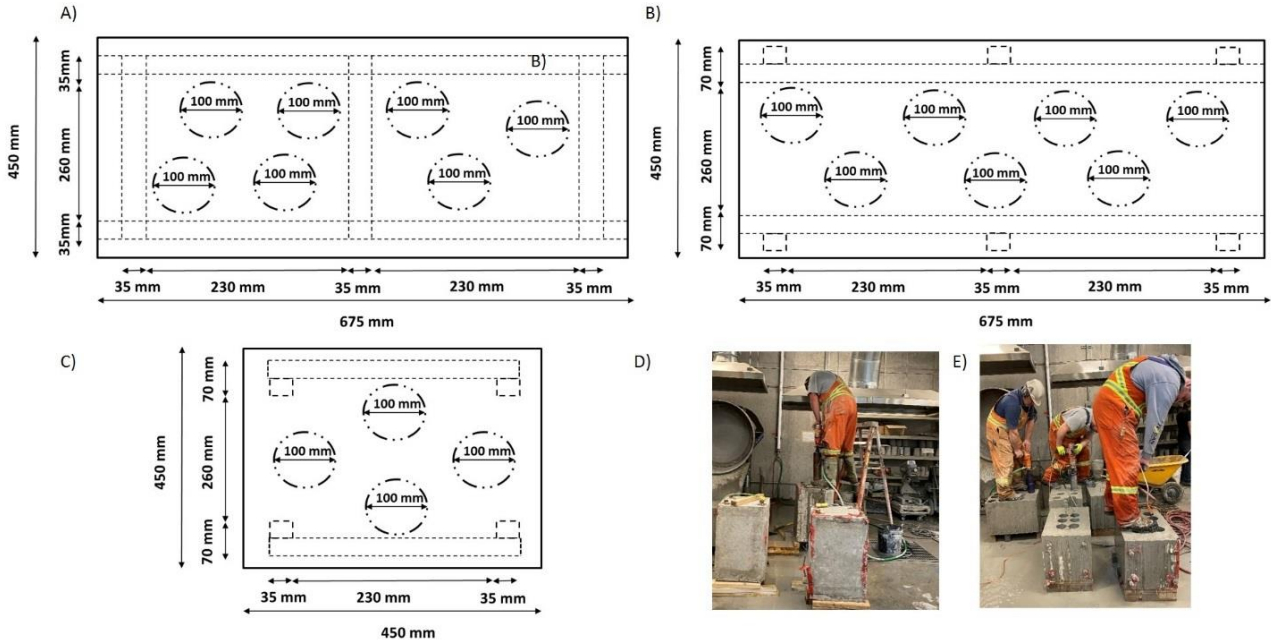

Figure 6: Sketch of the cores retrieved from the concrete blocks (i.e., 2D): A) top view (vertical), B) longer side view (transverse) C) shorter side view (longitudinal) D) longitudinally coring E) vertically and transversally coring.

8.4.3. Experimental procedures

Table 3 displays the testing matrix developed in this study. The testing protocols performed on the cores extracted from distinct concrete blocks and concrete cylinders at the selected expansion levels include mechanical testing and semi-quantitative microscopic assessment.

Table 3: Testing matrix.

Aggregate type	Types of concrete specimens	Test methods	Coring direction	Number of specimens for a given expansion level	
				0.08%	0.15%
Springhill coarse and Texas sand aggregate	Cylinders	**SDT/ CS**	-	3	3
		DRI	-	2	2
	Concrete blocks	**SDT/ CS**	Vertical	3	3
			Transverse	3	3
			Longitudinal	3	3
		DRI	Vertical	2	2
			Transverse	2	2
			Longitudinal	2	2
Minimum number of specimens tested for each concrete block: 30					
Total samples: 140					

8.4.3.1. Stiffness Damage Test (SDT)

Three specimens from the distinct coring directions of each set of concrete blocks (i.e., transverse, longitudinal and vertical) as well as three concrete cylinders at given expansion levels (Table 3), were subjected to five cycles of loading/unloading at a controlled loading rate of 0.10 MPa/s. Prior to performing the SDT, all specimens were reconditioned for 48h in the moist curing room (and protected from running water) to lessen the test's variability according to CSA23.2-14C [40] and as per Sanchez et al. [29]. Moreover, both ends of all concrete specimens were mechanically ground in order to avoid any interference from the stainless-steel studs used for expansion measurements. The SDT was conducted following the procedure proposed by [29,30]; i.e., loading up to 40% of the 28-day concrete strength of the specimens tested.

8.4.3.2. Compressive Strength (CS)

Compressive strength tests were first performed to characterize the concrete mixtures at 28 days to determine the 40% value for stiffness damage testing. The conventional standard method (i.e., ASTM C 39 [41]) could not be adapted for concrete specimens containing highly reactive coarse and fine aggregates as some ASR might have been generated while moist curing. Thus, the specimens were wrapped and stored at 12°C for a 47-day period, representing an equivalent maturity as concrete cured for 28 days at 20 °C according to ASTM C 1074 [42]. Compression strength tests were also conducted after reaching target expansions to determine the strength reduction caused by ASR. Previous research [29] has demonstrated that the SDT is non-destructive while using 40% of the 28-day compressive strength; thus mechanical results such as compressive strength obtained following the SDT are considered valid. The compressive strength losses were obtained in this work as the difference between the results gathered after the SDT and the "equivalent" 28-day values obtained from the sound concrete samples.

8.4.3.3. Damage Rating Index (DRI)

Before the microscopic evaluation, two consecutive specimens per the direction of the blocks and two cylinders per damage degree were initially cut axially in two, followed by subsequent mechanical polishing with grits of 30, 60, 140, 280 600 1200 and 3000. Once the surface of the polished concrete section was properly polished, a 1 x 1 cm grid was drawn on the surface of the samples before the microscopic evaluation. Distress features of 1mm in size or higher observed in the cement paste and aggregate particles were evaluated using the weighting factors proposed by Villeneuve et. al. [37] (Figure 2) to compute the DRI numbers. Ultimately, it is worth mentioning that the damage orientation of concrete specimens has been evaluated using an image analysis protocol following the procedure proposed by Zahedi et al. [16], where the observed damage features in each 1x1 cm DRI grid (Figure 2) drawn on the polished concrete specimens were highlighted through the use of a commercial software.

8.5. Results

8.5.1 ASR kinetics and development

The average expansions as a function of time (i.e., average value of four consecutive measurements per specimen per direction over time with standard deviations between 0.02% to 0.06%) of the different surfaces of the concrete blocks incorporating a reactive coarse aggregate (i.e., Springhill) and reactive sand (i.e., Texas), and displaying different reinforcement configurations are presented in Figure 7. Figure 7A also illustrates the average longitudinal expansion of cylinders (with a standard deviation of 0.02% to 0.04%). It is interesting to note that all directions of most of the concrete blocks displayed a significant amount of shrinkage at the beginning of the reaction. It took 35, 75, 105 and 75 days on average for the none-confined concrete blocks-SP, 1D-SP, 2D-SP and 2D-TX, respectively, to recover from shrinkage.

As Figure 7A displays, the expansion graphs of distinct directions of unrestrained blocks-SP are almost identical, where 0.15% expansion was reached after 212, 190, and 175 days on longitudinal side, longitudinal top, and transverse directions, respectively. Furthermore, according to Figures 7B, 7C and 7D, all restrained concrete blocks exhibited a significantly slower ASR expansion than unreinforced blocks, where 0.15% expansion was reached at 255, 212 and 190 days by 1D reinforced blocks-SP on the longitudinal side, longitudinal top, and transverse, respectively. 2D reinforced blocks-SP achieved 0.15% expansion after 340, 275, and 235 days, whereas 255, 235 and 190 days were required by 2D blocks-TX on longitudinal side, longitudinal top, and transverse side, respectively. This clearly shows that the achieved expansion levels are impacted by the direction of the reinforcement (i.e., transverse > longitudinal top > longitudinal side), as previously observed by [43]. Furthermore, comparing the attained expansion level of distinct concrete blocks at a given time, the unrestrained-SP blocks display a much higher expansion level than the restrained blocks, which demonstrates the impact of reinforcement on ASR-induced development (especially kinetics); the higher the restraint level, the slower the expansion rate and the lower the ultimate

expansion over the same period. Accordingly, averaging all directions, it was found that after 340 days of exposure, the unrestrained-SP blocks attained (on average) a higher maximum expansion of 0.27% followed by 1D-SP, 2D-TX and 2D-SP concrete blocks which achieved expansion levels of 0.23%, 0.22% and 0.18% (on average) over the same period. Otherwise, both concrete cylinders demonstrated much quicker ASR kinetics when compared to all blocks, where on average, concrete cylinders-SP and concrete cylinders-TX reached 0.15% of expansion after 70 and 55 days, respectively (Figure 7A). It is worth noting that the expansion adopted as "*representative*" of a given damage degree was the one recorded on the longitudinal side of concrete blocks (as Figure 5A -points 3 and 4); this expansion presents the lowest expansion level among all the blocks directions, since it is measured parallel to the main reinforcement and is not (or at least less) impacted by local effects [14,15].

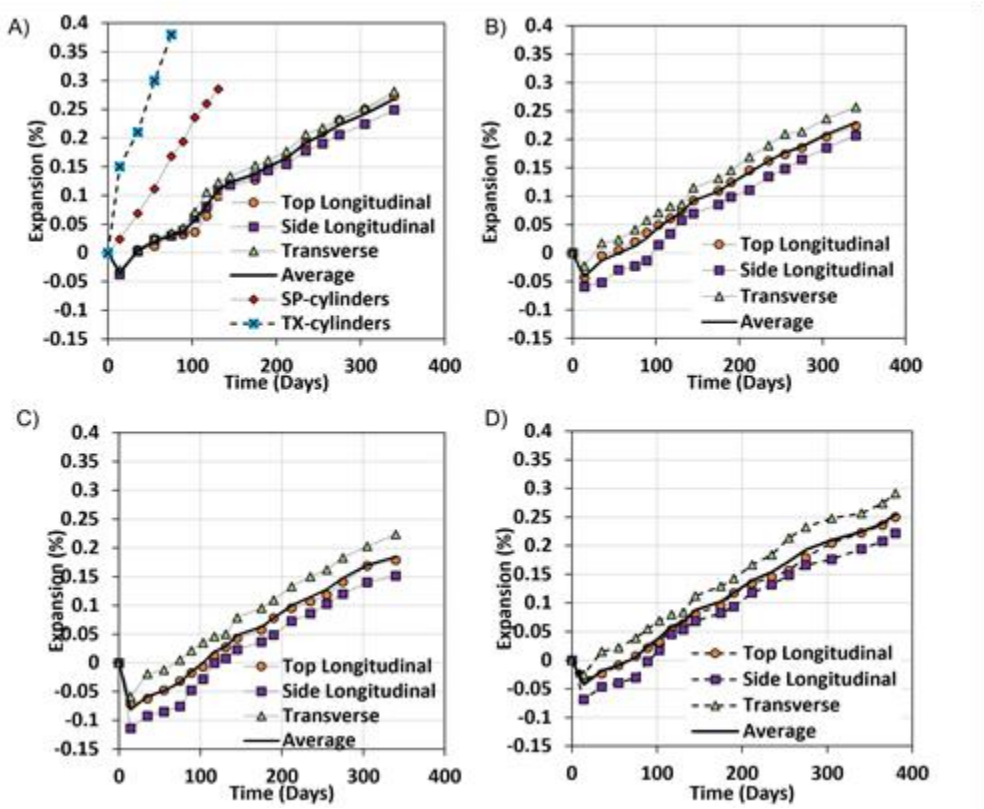

Figure 7: Expansion as a function of time for: A) unreinforced concrete, B) 1D - SP, C) 2D – SP, and D) 2D – TX, as per the distinct block's directions.

8.5.2 Stiffness Damage Test (SDT)

The results displayed in this section are the average values obtained from three core specimens from each coring direction of the ASR-affected blocks (i.e., vertical, transverse and longitudinal as per Figure 6 A, B and C, respectively) and three concrete cylinders at each expansion level tested. Analyzing the plots (Figure 8), one notices that the higher the ASR-induced expansion level, the higher the SDI and PDI indices as well

as the lower the modulus of elasticity (ME), for all concrete specimens of this study. As Figure 8A displays, there is not a considerable difference in SDI values (standard deviations presented in the plot) for unrestrained concrete-SP specimens as per distinct directions where SDI of 0.26-0.27 were gathered at 0.15% of expansion. On the other hand, results from the restrained concrete blocks were significantly influenced by the coring orientation. SDI values of 0.28, 0.28 and 0.22 from 1D blocks and 0.30, 0.23 and 0.22 from 2D-SP blocks at 0.15% expansion were obtained from the vertical, transverse and longitudinal directions, respectively. Similarly, SDI values of 0.32, 0.24 and 0.23 were obtained at 0.15% of expansion on the vertical, transverse and longitudinal directions of the 2D-TX blocks, respectively. Otherwise, concrete cylinders manufactured with SP and TX displayed an initial SDI value of 0.12 and 0.13, respectively and then it increases to 0.26 for both concrete mixtures at 0.15% of expansion.

Figure 8B presents the PDI values (standard deviations added to the plot) of concrete cylinders and various core specimens. Although distinct directions of unrestrained-SP blocks exhibited PDI values of 0.24 at 0.15% of expansion, 1D-SP blocks yielded PDI values of 0.26, 0.26 and 0.22 at moderate expansion for the vertical, transverse and longitudinal cores, respectively. Furthermore, PDI values of 0.29, 0.20 and 0.20 were obtained from 2D-SP while 0.31, 0.22 and 0.22 were gathered from 2D-TX at 0.15% of expansion for the vertical, transverse and longitudinal cores, respectively. Otherwise, both concrete mixture's control samples showed a PDI value of 0.08 and then it increases to 0.24 at 0.15% of expansion.

Figure 8C illustrates the modulus of elasticity (ME- including standard deviations) for all concrete specimens of this work. Although an initial ME of 30 and 34 GPa was obtained for the undamaged/sound samples incorporating SP and TX aggregate, respectively, a decreasing trend is noticed for all specimens; as such, all coring directions of unrestrained -SP blocks showed an ME of 19 GPa at 0.15% of expansion. This represents an ME reduction (Figure 8D-with their standard deviations) of 35% at moderate expansion of all coring directions of unrestrained-SP blocks. Otherwise, the vertical, transverse and longitudinal cores of 1D-SP blocks showed ME values of 18, 18, 21 GPa which represent an ME reduction of 39%, 39% and 29% at moderate expansion (0.15%), respectively. Moreover, MEs of 15, 21 and 21 GPa (i.e., representing an ME reduction of 50%, 30% and 30%) were gathered from 2D-SP blocks, while MEs of 14, 21, 21 GPa (i.e., showing an ME reduction of 59%, 38% and 38%) were obtained from 2D-TX at 0.15% of expansion for the vertical, transverse and longitudinal cores, respectively. Finally, ME values of 19 GPa and 20 GPa for cylinders-SP and cylinders-TX were obtained at 0.15% of expansion, respectively; this represents an ME reduction of 37% and 40% at moderate expansion for concrete cylinders made of SP and TX, respectively.

A)

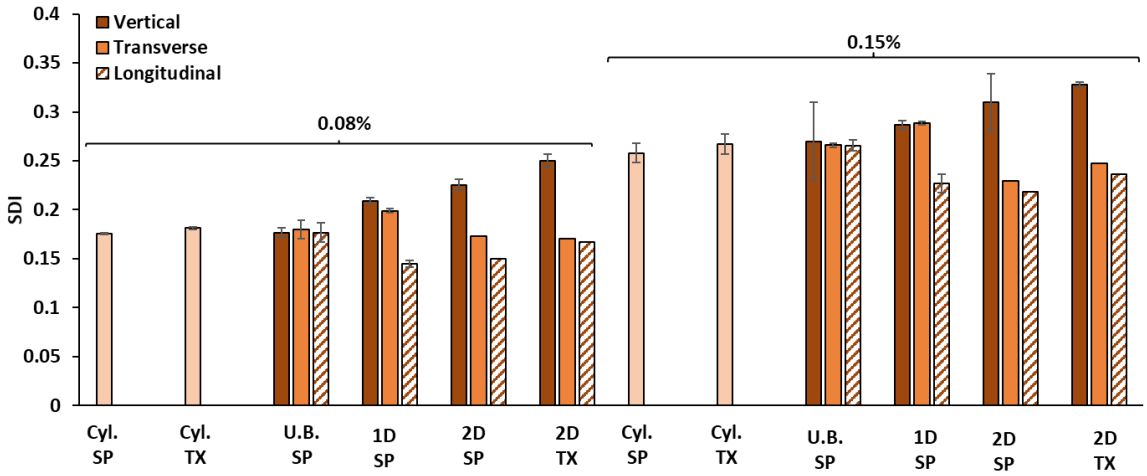
Vertical
Transverse
Longitudinal
0.08%
0.15%
SDI
0.4
0.35
0.3
0.25
0.2
0.15
0.1
0.05
0
Cyl. SP
Cyl. TX
U.B. SP
1D SP
2D SP
2D TX
Cyl. SP
Cyl. TX
U.B. SP
1D SP
2D SP
2D TX

B)

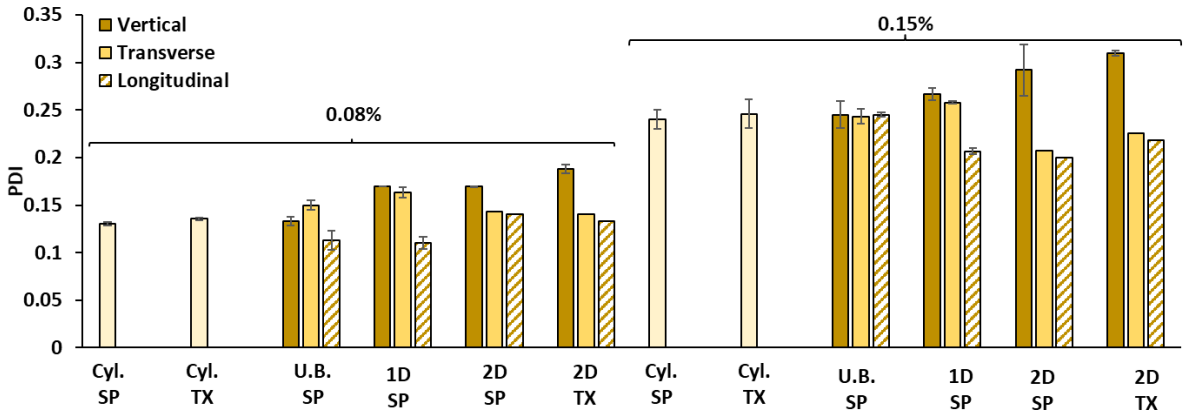
Vertical
Transverse
Longitudinal
0.08%
0.15%
PDI
0.35
0.3
0.25
0.2
0.15
0.1
0.05
0
Cyl. SP
Cyl. TX
U.B. SP
1D SP
2D SP
2D TX
Cyl. SP
Cyl. TX
U.B. SP
1D SP
2D SP
2D TX

C)

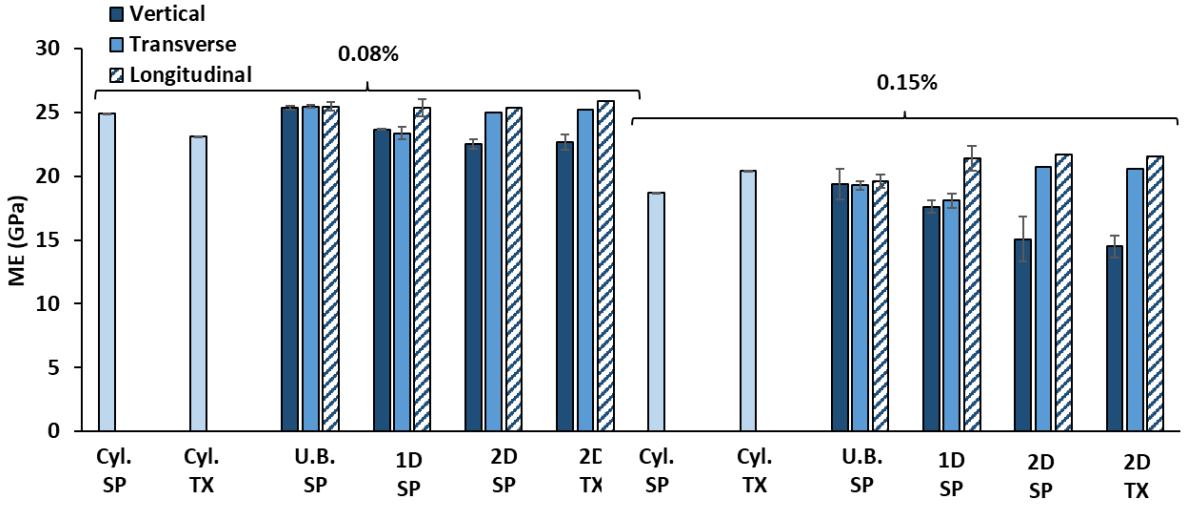
Vertical
Transverse
Longitudinal
0.08%
0.15%
ME (GPa)
30
25
20
15
10
5
0
Cyl. SP
Cyl. TX
U.B. SP
1D SP
2D SP
2D TX
Cyl. SP
Cyl. TX
U.B. SP
1D SP
2D SP
2D TX

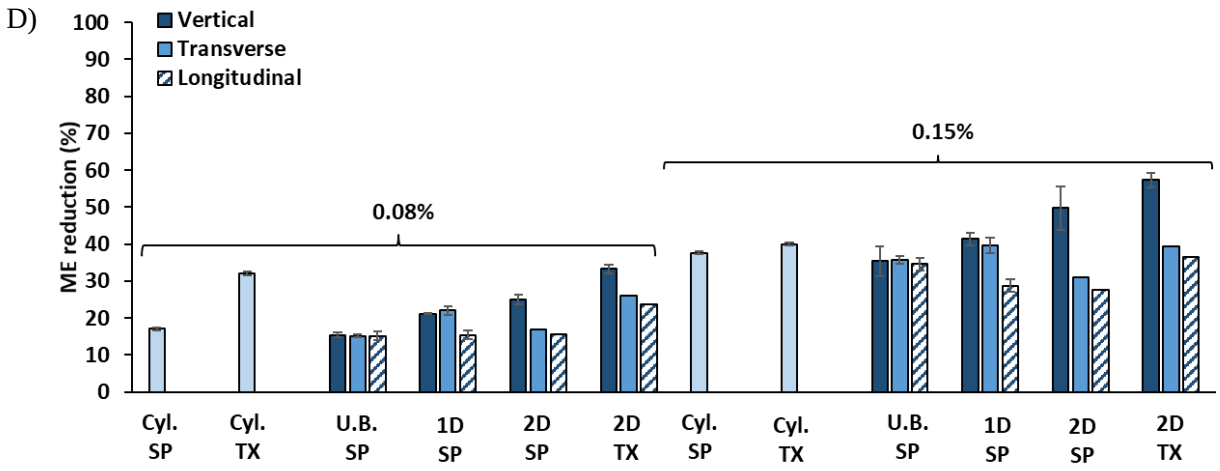

Figure 8: Stiffness damage results A)SDI; B) PDI, C) Modulus of Elasticity (GPa) and D) ME reduction (%).

8.5.3 Compressive strength

The compressive strength results (standard deviations added to the plot) as a function of ASR-induced expansion are illustrated in Figure 9. The compressive strength obtained in the control/sound samples made with SP and TX was 35 MPa and 36.5 MPa, respectively. Later, all cores extracted from unrestrained-SP blocks showed compressive strength (CS) of 28 MPa, representing a 18% reduction at 0.15% of expansion. Otherwise, the vertical, transverse and longitudinal cores of 1D-SP blocks exhibited CS values of 27, 27 and 31 MPa which represented the CS reduction of 22%, 22% and 11% at 0.15% of expansion, respectively. Similarly, CS values of 24, 31 and 31 MPa (i.e., representing a CS reduction of 30%, 14% and 14%) were obtained from 2D-SP, while 2D-TX exhibited CS values of 21, 31 and 31 MPa (i.e., presenting CS reduction of 42%, 15% and 15%) at 0.15% of expansion on the vertical, transverse and longitudinal cores, respectively. Additionally, a CS value of 28 MPa was gathered for both SP and TX cylinders which represents a CS reduction of 19% for SP-cylinders and 22% for TX-cylinders at 0.15% of expansion.

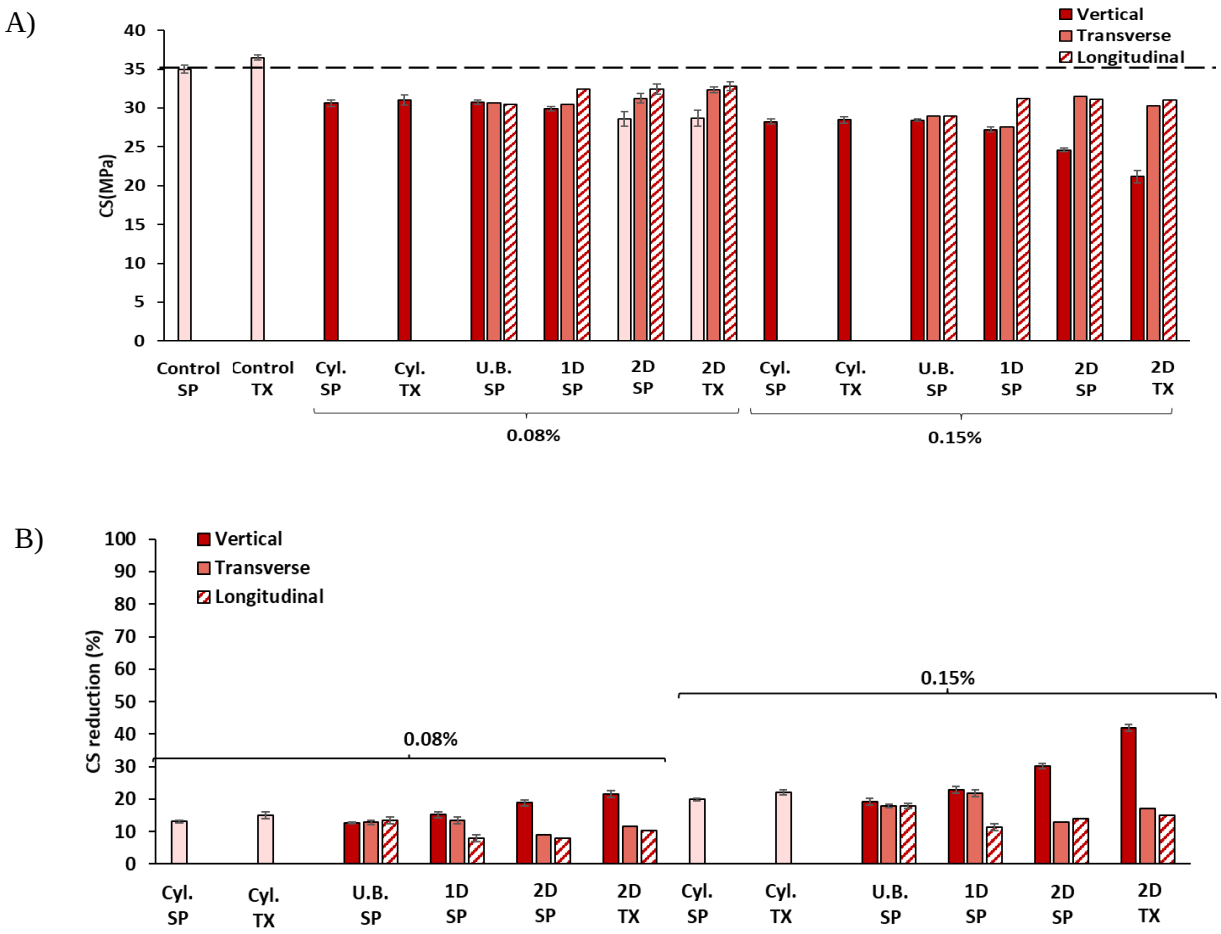

Figure 9: A) Compressive strength (CS) and B) CS reduction (%) as a function of expansion.

8.5.4 Damage Rating Index (DRI)

Figure 10 displays the DRI charts obtained from all specimens evaluated in this work. While the DRI values ranged from 570-580 were obtained for all directions of unrestrained blocks, the vertical, transverse and longitudinal directions of the 1D-SP blocks showed to have the DRI number of 646, 613 and 479 at 0.15% of expansion, respectively. Moreover, DRI numbers of 766, 485 and 479 were gathered from 2D-SP, while the 2D-TX blocks displayed DRI numbers of 802, 480 and 475 at 0.15% of expansion on the vertical, transverse and longitudinal cores, respectively. Otherwise, SP and TX cylinders showed the DRI numbers of 561and 564 at 0.15% of expansion, respectively.

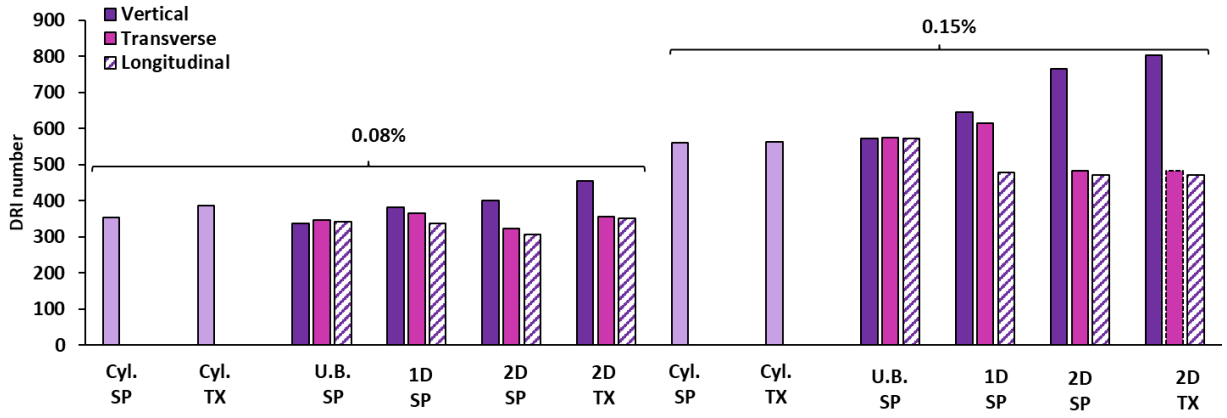

Figure 10: DRI number as a function of expansion.

8.6. Discussion

8.6.1 Understanding the impact of reinforcement on ASR-induced development

8.6.1.1. Induced expansion

As per Figure 7, ASR expansion as a function of time of the concrete cylinders and blocks displaying various restraint conditions presented considerable differences. First, it is evident that the kinetics behavior of cylinders do not properly represent the behavior of larger size members, possibly due to the influence of size on moisture transfer [46]; therefore, significantly higher (and faster) expansion levels were observed when compared to the blocks. Second, although no significant difference was observed on the achieved expansion levels from the distinct surfaces of unrestrained blocks (Figure 7A), those restrained by the steel bars demonstrated an ‘‘expansion transfer’’, where the induced expansion transferred from the restrained directions to the less/non restrained directions, leading to higher expansion levels in the less restrained directions.

As Figures 7B, 7C and 7D display, all restrained concrete blocks followed the same trend where the transverse sides achieved the highest expansion followed by the top sides and longitudinal faces, respectively. This certainly confirms the development of a higher ASR expansion in the direction with less/no restraint in the reinforced concrete blocks, indicating the influence of restraint on the constitutive anisotropy of the blocks as currently observed by a number of researchers [14,16,19,44,45]. The above results attest that the anisotropic behavior observed in the blocks is more pronounced with the increase of reinforcement, which results in higher expansion scattering amongst distinct directions. Nevertheless, comparing the distinct aggregate types (fine vs coarse), a higher expansion level was observed in members incorporating the reactive fine aggregate; this behavior was expected since past research has verified the higher potential reactivity of the TX sand when compared to the SP coarse aggregate [6,47] which could be in attributed to the aggregate size effect as per [48] and/or the mineralogy/origin of Tx fine aggregate.

8.6.1.2. Induced deterioration

Besides anisotropy in induced expansion, Barbosa et al. [21] verified that the restraint configuration can also significantly influence on the damage development caused by ASR (i.e., cracks generation and propagation) and mechanical properties degradation of affected concrete. However, the authors [21] have never systematically quantified such impact on ASR-affected restrained members. Therefore, the use of the multi-level protocol as per Sanchez et al. [6], composed of mechanical and microscopic test procedures, is essential to systematically understand and quantify the effect of reinforcement on the damage development caused by ASR in the distinct blocks as a function of induced expansion. It is worth noting that in this section, the results of this study will be discussed in two different, yet complementary ways: first, in order to evaluate the influence of distinct reinforcement configurations on the "overall deterioration" of the ASR-affected blocks, the microscopic and mechanical results gathered were initially averaged from distinct coring orientations. Second, to assess and quantify the anisotropic behavior of ASR as a function of the restraint conditions, the microscopic and mechanical results were also appraised according to the orientation of the coring.

- *Microscopic assessment*

As previously mentioned, the results of microscopic assessment (Figure 10) obtained from the distinct coring directions at each expansion level were initially averaged to have a broad picture of the effect of each restraint configuration on the concrete blocks behavior. Therefore, Figure 11A displays the "overall deterioration" of distinct concrete blocks by averaging the DRI values of 6 specimens from each block at a given expansion level (i.e., two specimens per restraint type per direction). Accordingly, the DRI number of the concrete specimens reaching 0.15% ranged from 550 to 590 for concrete mixtures containing both the reactive coarse (SP) and reactive fine aggregates (TX). The above confirms that the DRI results demonstrate a fairly similar "overall" microscopic behavior (i.e., disregarding the distinct directions appraised), where higher DRI values are observed for higher levels of deterioration caused by ASR. Notably, the "overall" results obtained through the microscopic assessment from reinforced concrete members follow the same trend as suggested by [6] when appraising unrestrained specimens as previously observed by Zahedi et al. [16]. Sanchez et al. proposed a table (Table 4) illustrating the variations of microscopic (i.e., DRI number) and mechanical (i.e., SDI as well as compressive, tensile and modulus of elasticity reductions) data as a function of ASR-induced expansion with a significance level of 5%; Table 4 was developed after evaluating 20 different concrete mixtures incorporating a wide range of concrete strengths (i.e., 25MPa, 35MPa, 45MPa) and reactive aggregate types (fine and coarse) and natures (mineralogy) [6]. The data in brief for the "overall" analysis can be found in Table 6 of the supplementary materials section. Analyzing the results obtained through the microscopic assessment performed on the

specimens retrieved from the distinct blocks and directions (Figure 10), one observes that unlike unrestrained blocks where not a considerable difference was observed among their distinct directions, all restrained concrete blocks demonstrated not only an "expansion transfer" but also a "deterioration transfer" from restrained to unrestrained directions. For instance, at the moderate expansion (0.15%), unrestrained direction of 2D-SP and 2D-TX blocks (i.e., vertical cores) exhibited a rise of 37% and 40% of DRI numbers when compared to the transverse and longitudinal cores (i.e., reinforced directions), respectively. Besides the anisotropic effects generated by the partial restrainment of ASR-induced damage development in reinforced concrete, restraint may also influence the deterioration pattern (e.g., cracks orientation) of ASR affected concrete; this phenomenon will be discussed in the next sections. The data in brief for the "anisotropic" analysis can be found in Table 7 of the supplementary materials section.

- *Mechanical properties*

Similar to the microscopic section, at first, the SDT and compressive strength outcomes (Figures 8 and 9, respectively) gathered from the three main directions at each expansion level were averaged to discuss the effects of reinforcement on the "overall" mechanical degradation of distinct concrete blocks. Thus, Figure 11B, C and D illustrate the "overall" SDI, ME and CS loss, respectively; the average SDI (Figure 11B) and ME reduction (Figure 11C) range from 0.25-0.27 and 35-44% are obtained for 0.15% expansion, respectively. It is worth mentioning that although the SDI value (i.e., number of cracks within a deteriorated concrete) of all concrete specimens are almost identical (Figure 11B), the ME loss of the specimens incorporating the reactive fine aggregate (i.e., TX) is slightly higher than the ones incorporating the reactive coarse aggregate (i.e., SP - Figure 11C); this could be due to the different deterioration mechanism (i.e., cracking pattern) of concrete specimens incorporating five versus coarse aggregates, which will be further discussed in the next section. Moreover, a range of 17-24% for CS reduction is identified for moderately damaged concrete specimens (Figure 11D). The presented mechanical results follow the same trend as per the microscopic section where higher SDI and lower ME and CS values are obtained with ASR progress. Such results clearly show that they once again follow the same tendency as proposed by [6] while assessing unrestrained concrete specimens (Table 4). The above discussion on the "overall" microscopic and mechanical deterioration obviously suggests that ASR development does not seem to considerably change the "overall" (i.e., averaged) deterioration behavior of concrete members displaying distinct restraint configurations and aggregate types. The data in brief for the "overall" analysis can be found in Table 6 of the supplementary materials section.

Otherwise, observing the mechanical test results from Figures 8 and 9, one notices that despite the unrestrained blocks, which do not show a significant variation of SDT and CS outcomes as per the distinct coring directions, the other restrained members exhibit an anisotropic ASR-induced damage development;

this “damage transfer” takes place from the restrained to the non/less restrained directions. For instance, the vertical cores of 2D-SP and 2D-TX (i.e., unrestrained direction) demonstrated an increase of almost 25% and 26% of the SDI along with a decrease of 10% and 13% of ME and 9% and 31% of CS at the moderate expansion, respectively when compared to the longitudinal and transverse cores (i.e., restrained directions). The data in brief for the “anisotropic” analysis can be found in Table 7 of the supplementary materials section.

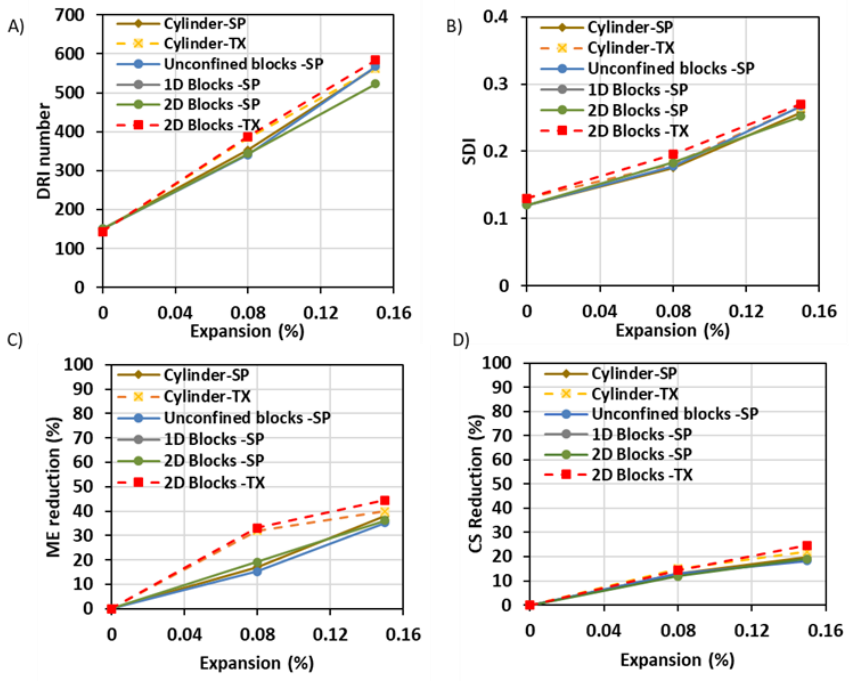

Figure 11: “Overall” results of A) DRI number, B) SDI, C) ME reduction (%) and D) CS reduction (%).

Reviewing the results obtained through the multi-level assessment (i.e., coupling of microscopic and mechanical test procedures) of affected unrestrained/restrained concrete specimens, a four-quadrant chart along with a classification table for the damage degree of the different directions of the various concrete blocks may be plotted as proposed by [6] (Figure 12 and Table 5). The chart and table display “visually” and “descriptively” the damage development of distinct directions of concrete blocks having various restraint conditions along with concrete cylinders incorporating SP and TX aggregate. As such, Figure 12 illustrates the correlation of the expansion level of concrete specimens (positive x axis) with a) SDI or PDI which addresses the extent of internal cracking in the affected concrete [6] (positive y axis), b) DRI number/1000 (negative y axis), which indicates the microscopic damage degree of affected concrete [6], and c) damage variable “δ” which represents the reduction of a given mechanical property of the deteriorated concrete [6]; in this work, the reduction of ME was selected (negative x axis). Analyzing the plots and table, one notices the anisotropic behavior of ASR-induced damage (both microscopic and

mechanical) where the damage transfer from the restrained to the non/less restrained directions has been previously described in this work and reported by Zahedi et al. [16]. Ultimately, engineers may use such charts and table (Figure 12 and Table 5) as “reference” values and these data might be used in two distinct ways: 1) by selecting data from a similar restraint configuration and coring direction or 2) by comparing the results gathered from the available cored specimens to predict the behavior of those inaccessible/ unavailable directions.

Table 4: Classification of the "overall" damage degree in concrete affected by ASR [6] *(Reproduced with permission of Elsevier)*.

Classification of ASR damage degree (%)	Reference expansion level (%) [39]	Assessment of ASR																			
		Conventional Concrete [6]				-	unconfined concrete blocks-SP				1D concrete blocks-SP				2D concrete blocks-SP				2D concrete blocks-TX			
		ME loss (%)	CS loss (%)	SDI	DRI	Expansion level from this study	ME loss (%)	CS loss (%)	SDI	DRI	ME loss (%)	CS loss (%)	SDI	DRI	ME loss (%)	CS loss (%)	SDI	DRI	ME loss (%)	CS loss (%)	SDI	DRI
Negligible	0.00–0.03	-	-	0.06–0.16	100–155																
Marginal	0.04 ± 0.01	5–37	10–15	0.11–0.25	210–400	0.08%	15	13	0.17	330-350	19	12	0.18	328-350	19	12.5	0.18	330-355	33	13	0.18	350-375
Moderate	0.11 ± 0.01	20–50	0–20	0.15–0.31	330–500	0.15%	35	18.5	0.26	565-580	36	18	0.26	540-580	36	17.5	0.25	520-580	44	24	0.26	550-590
High	0.20 ± 0.01	35–60	13–25	0.19–0.32	500–765																	
Very high	0.30 ± 0.01	40–67	20–35	0.22–0.36	600–925																	

Table 5: Classification of the ASR-induced damage as per the distinct coring directions of the concrete blocks.

Assessment of ASR		Classification of ASR damage degree (%)							
		0.08%				0.15%			
Confinement configuration	Coring direction	ME loss (%)	CS loss (%)	SDI	DRI	ME loss (%)	CS loss (%)	SDI	DRI
Unconfined concrete	Vertical	13-18	10-15	0.15-0.19	330-341	32-39	15-20	0.24-0.28	565-580
	Transverse	13-18	10-15	0.15-0.19	333-347	32-39	15-20	0.24-0.28	565-580
	Longitudinal	13-18	9-15	0.15-0.19	335-345	32-37	15-20	0.24-0.28	570-585
1D	Vertical	20-26	14-20	0.18-0.23	378-390	37-47	20-26	0.26-0.30	640-660
	Transverse	20-26	10-18	0.18-0.23	360-375	37-45	20-26	0.26-0.30	610-625
	Longitudinal	14-18	5-10	0.13-0.16	330-345	25-30	10-15	0.20-0.24	470-485
2D	Vertical	25-36	16-22	0.20-0.26	400-450	48-60	30-43	0.27-0.34	760-800
	Transverse	15-24	7-12	0.15-0.18	320-355	30-39	12-18	0.20-0.25	480-490
	Longitudinal	15-24	8-11	0.15-0.18	300-350	30-39	12-17	0.20-0.24	465-475

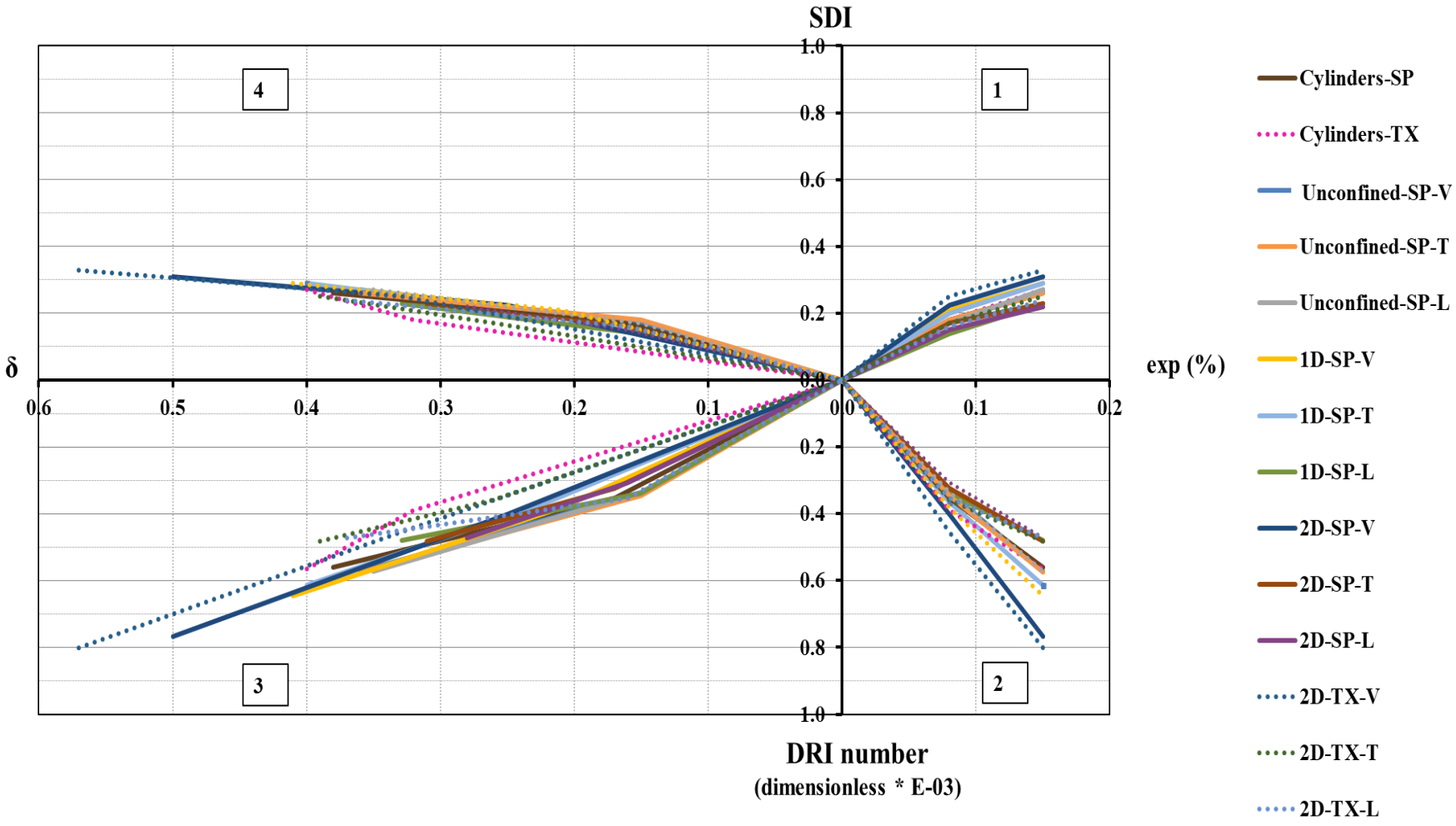

Figure 12: Global analysis charts for all concrete mixtures and coring direction appraised in this research.

8.6.2 Effect of reactive fine versus coarse aggregates on ASR-induced damage development under restraint

In this section, the effects of distinct reactive aggregate types (i.e., fine vs coarse aggregate) on ASR development (i.e., mechanical response and microscopic distress development) of restrained concrete are investigated. This section will therefore be discussed in the following subsections:

- *Microscopic assessment*

Comparing the "overall" results obtained through the microscopic assessment (i.e., Figure 11A) on the specimens incorporating distinct aggregate types (i.e., SP and TX), one observed only slight differences in the final DRI numbers. However, when a thorough microscopic assessment of the specimens obtained from distinct directions is performed, the influence of the type of reactive aggregate as well as restraint configurations is more pronounced (Figure 10). For a better understanding of the above, Figure 13 displays the detailed DRI charts of the concrete specimens obtained from distinct directions of the various unrestrained/restrained blocks. Besides the anisotropic effect of ASR on restrained concrete blocks as discussed in previous sections, the following differences have been observed between damage features of restrained (Figures 13B, C and D) and unrestrained concrete/ specimens (Figure 13A): a) concrete specimens retrieved from all restrained blocks bear slightly lower open cracks in the aggregates (i.e., red chart for SP-concrete and red and white striped chart for TX-concrete in Figures 13B, C and D) when compared to unrestrained specimens (Figure 13A); b) open cracks in the non-reactive aggregates (i.e., red and white striped chart for SP-concrete and red chart for TX-concrete in Figures 13B, C and D) of both concrete mixtures start being noticed at moderately damage restrained specimens (0.15%- Figure 14) while such a damage feature has never been observed in unrestrained specimens of this study (Figure 13A). To further quantify the latter, the "overall" development of cracking in non-reactive aggregate particles (i.e., average results from different directions) in all reinforced blocks was evaluated according to the method proposed by Villeneuve et al. [37]. Accordingly, the polished sections retrieved from the concrete blocks were analyzed by counting the number of non-reactive coarse and fine aggregate particles and the number of cracks within those individual particles. As per Figure 15, all restrained concrete blocks incorporating reactive coarse aggregates (i.e., 1D-SP and 2D-SP) present an almost identical number of cracks in the non-reactive aggregates (0.31 cracks, on average) counted over the number of non-reactive fine aggregate particles while a higher number of cracks (0.40 cracks, on average) counted over the number of non-reactive coarse aggregate was obtained for the 2D reactive sand blocks (2D-TX). Cracking of non-reactive aggregates in reinforced concrete can be attributed to the anisotropic behavior of ASR in restrained conditions [16]; c) the number of cement paste cracks (i.e., CCP-orange bar in Figure 13) in restrained specimens is slightly higher than those observed in unrestrained specimens; d) a higher number of open cracks in the aggregate and cement paste cracks with ASR products (i.e., OCAG- green chart and CCPG-

light blue chart in Figure 13, respectively) is identified in restrained concrete. Comparing the distinct concrete blocks incorporating various aggregate types, one sees that those blocks manufactured with SP aggregate particles present higher and more pronounced open cracks in the aggregates containing reaction products (Figures 16A and B illustrated), while more ASR gel was observed in the cement paste cracks in the 2D-TX (Figures 16C and D); d) a small amount of disaggregate/corroded aggregate particles (i.e., the aggregate particles presenting the signs of disintegration, DAP- dark blue chart in Figure 13) was found in 2D blocks made with reactive sand (Figures 16 E and F) while such a damage feature has never been observed in all specimens made of reactive coarse aggregate as well as those TX-unrestrained cylinders of this study; e) further microscopic analysis demonstrate that when one averages the results from distinct directions, concrete members made of reactive coarse aggregates (i.e., SP) produce longer (21% and 25% for the slightly/moderately damaged, respectively) and wider cracks (33% wider cracks in 0.15% of expansion) than those generated in reactive sand concrete specimens, while no significant difference is noticed in the crack widths at 0.08% of expansion (Figure 17); f) according to the image analysis conducted in this study (i.e., as per the method explained in section 4.3.3), ASR triggered by reactive coarse aggregate particles induces a much localized pattern of cracking (Figure 18A) whereas, the reactive sand produced cracks that are somewhat more sparsely distributed within the cement paste (Figure 18B), which is in accordance with the observation made by Sanchez et. al. [7,8] on unrestrained concrete specimens. The above differences suggest that the effect of ASR on the mechanical degradation of affected concrete is different when the mechanism is triggered by a reactive coarse (i.e., SP) or a reactive fine (i.e., TX) aggregate, and will be discussed in the next section.

A) Unrestrained concrete specimens

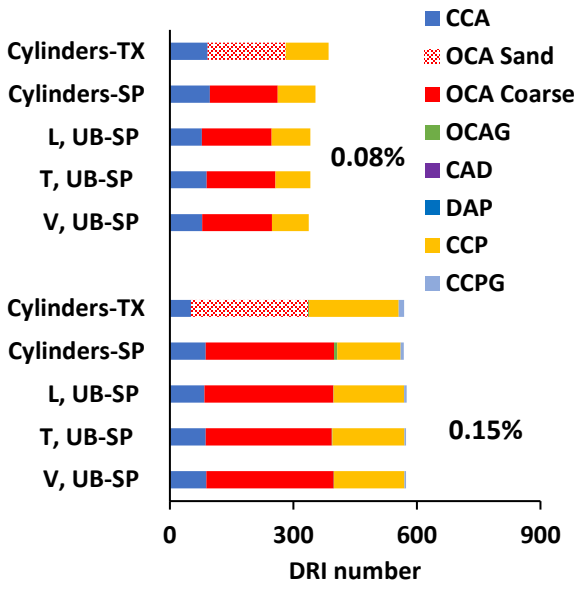

B) 1D-SP

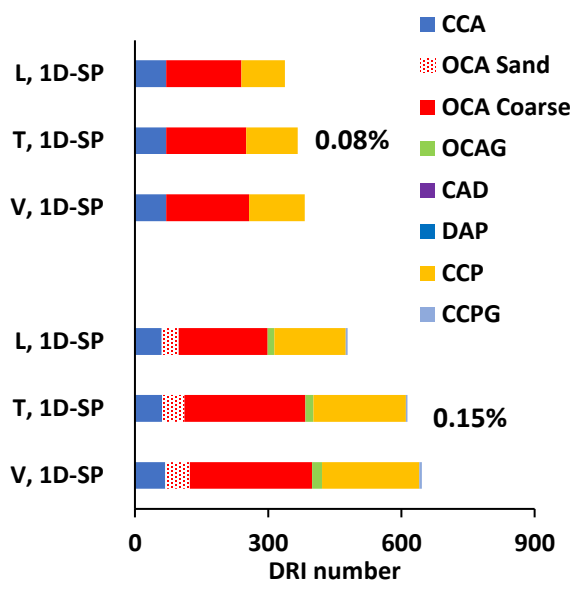

C) 2D-SP

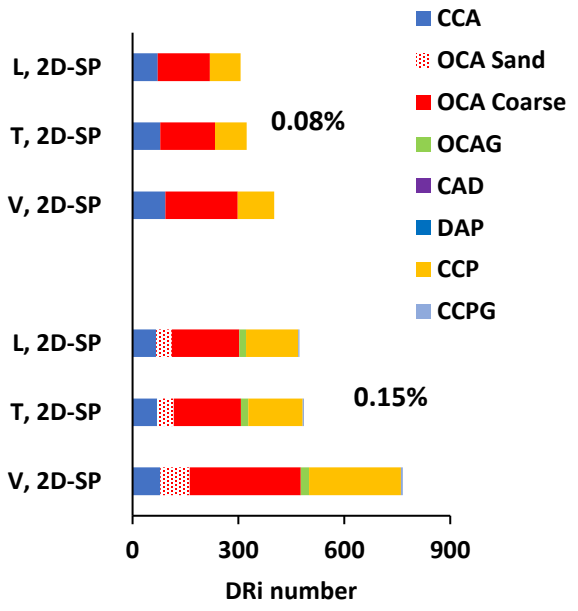

D) 2D-TX

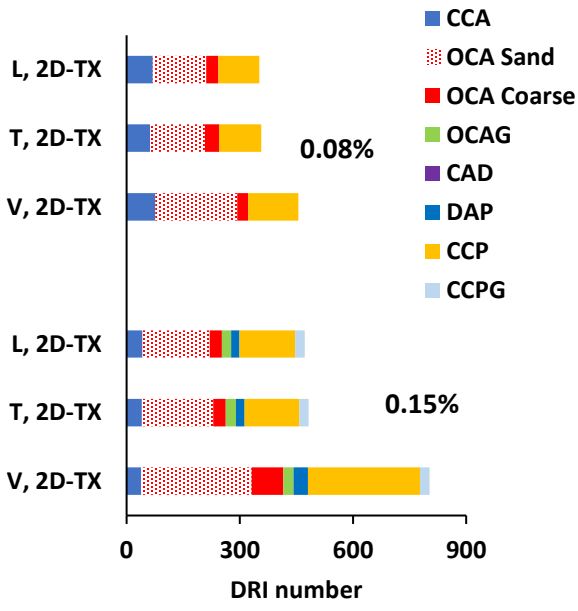

Figure 13: Damage rating index outcomes as a function of ASR-induced expansion and coring direction.

A) 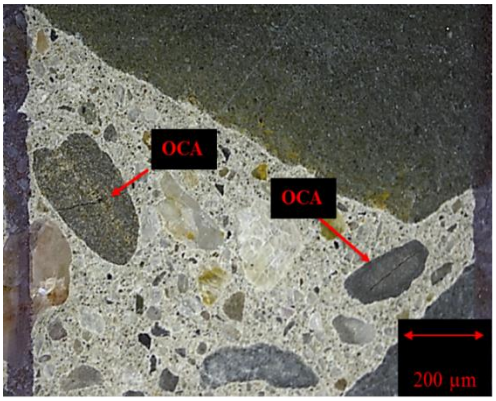

B) 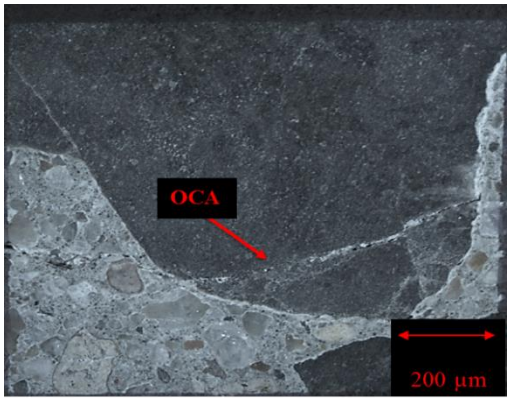

Figure 14: Open crack in non-reactive aggregate particles of the concrete members incorporating A) Springhill coarse aggregate B) Texas fine aggregate, for the highest expansion levels observed in the members.

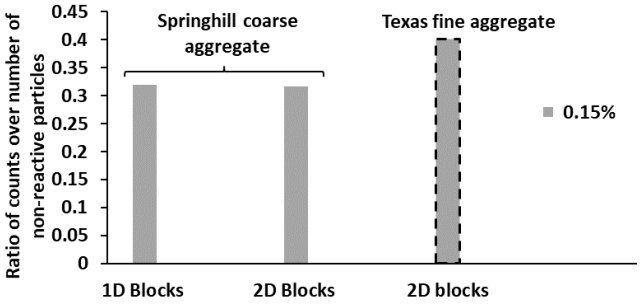

Figure 15: Crack development in non-reactive aggregate particles as a function of expansion.

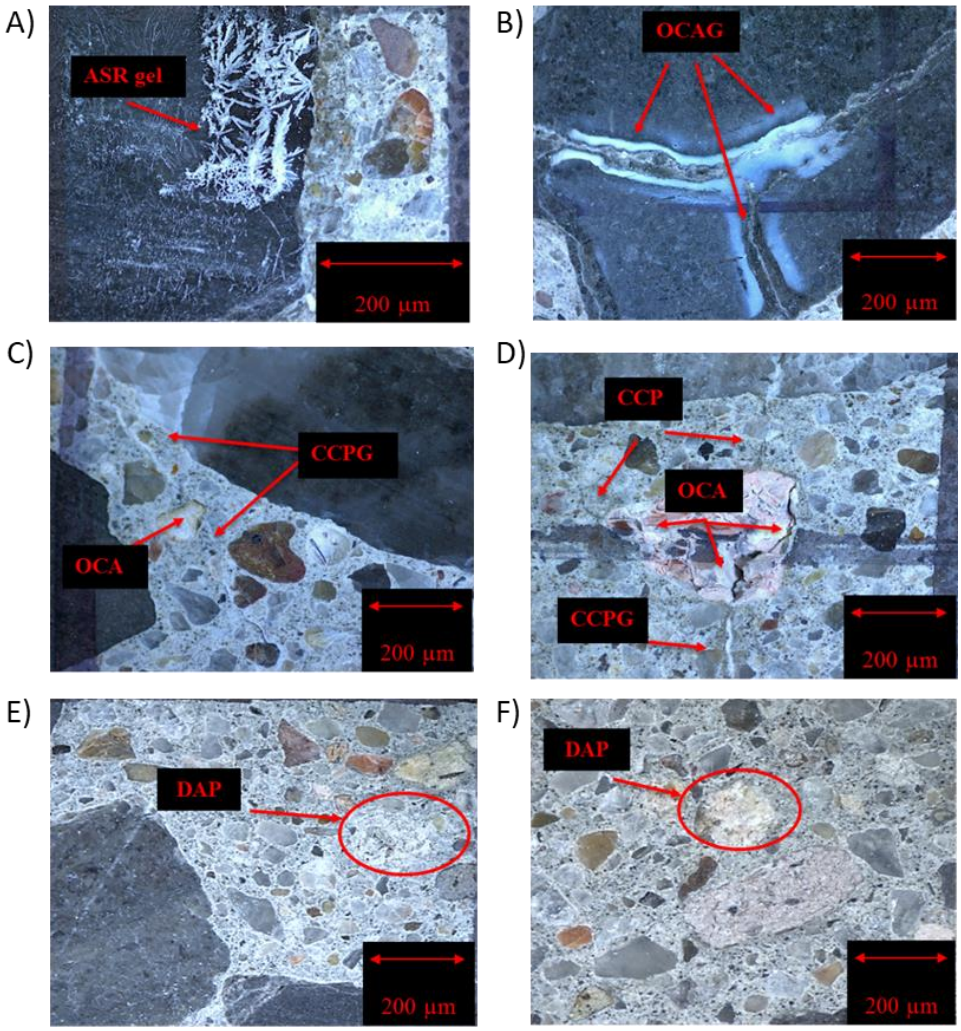

Figure 16: Cracking features in the concrete members incorporating A and B) Springhill coarse aggregate C, D, E and F) Texas fine aggregate, for the highest expansion levels observed in the concrete specimens.

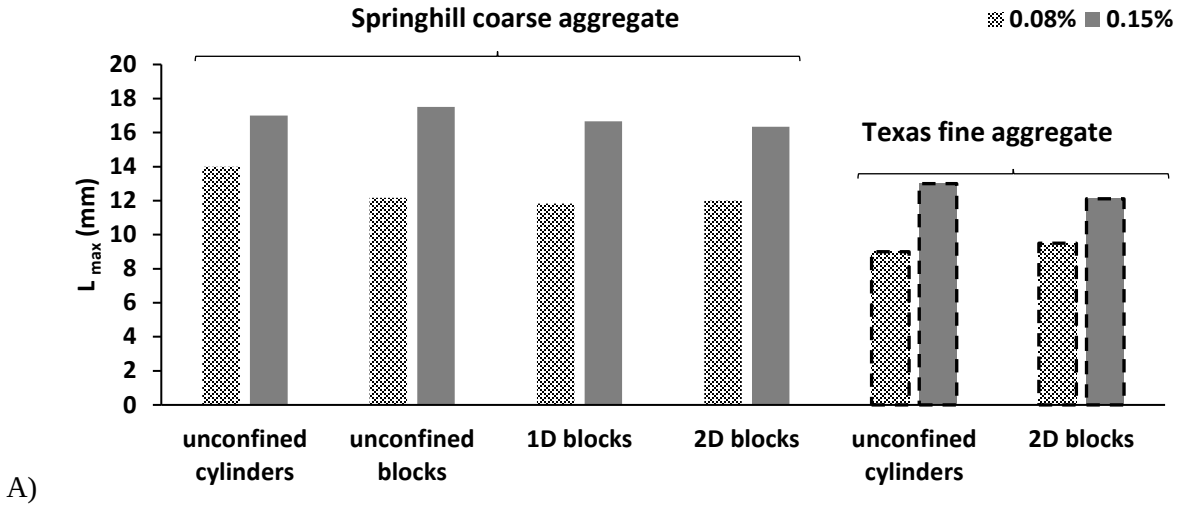

A)

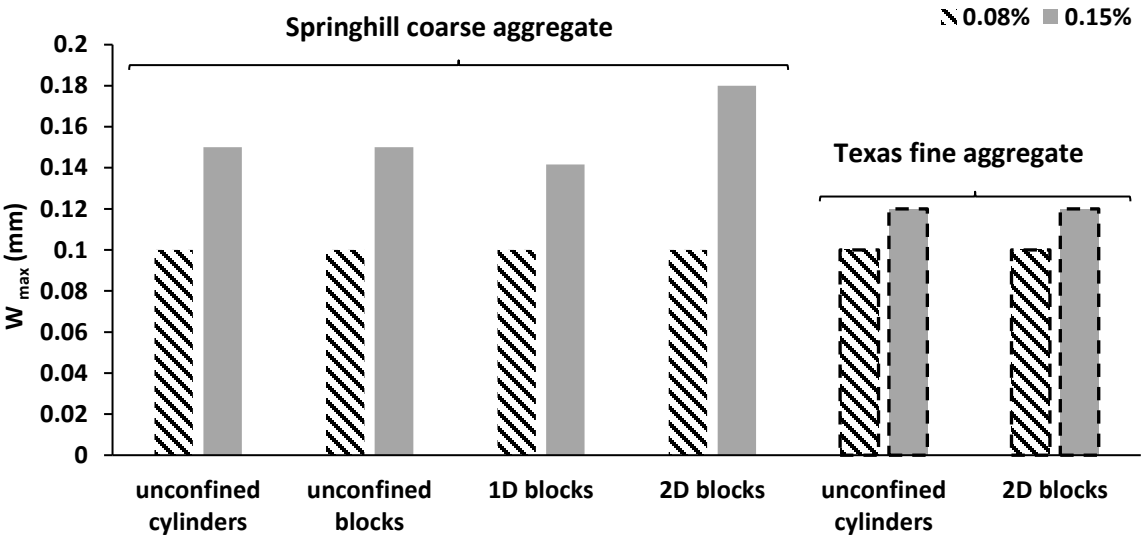

B)

Figure 17: A) Maximum crack length and B) maximum crack width for all concrete members of this study.

A) 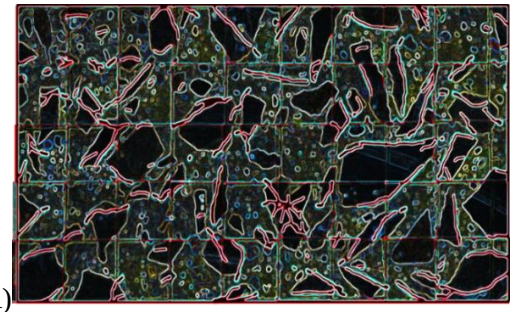 B) 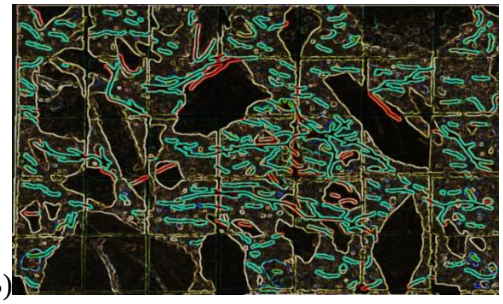

Figure 18: Polished concrete cores under image analysis: (a) concrete incorporating reactive SP coarse aggregate at the highest expansion level observed. The cracks present in the reactive coarse aggregate particles (SP) are highlighted in red; some of these cracks extend into the cement paste.; (b) concrete incorporating reactive TX sand at the highest expansion level observed; the reactive fine aggregate particles (TX) are heavily cracked (i.e., green traces), while some non reactive coarse aggregates also bear some internal cracks.

- *Mechanical properties*

Similar to the microscopic data, ASR deterioration does not seem to noticeably influence the "overall" results obtained through mechanical testing (i.e., Figures 11B, C and D) on the specimens displaying various restraint configurations and incorporating distinct aggregate types (i.e., SP and TX). However, when the mechanical properties of specimens obtained from distinct directions are assessed, the impacts of various types of reactive aggregate are more prominent (Figures 8 and 9). As such, one observes that the vertical specimens (i.e., unrestrained) extracted from the 2D-TX exhibit a 10% higher SDI and PDI at low expansion (0.08%), and a 6% higher SDI and PDI at moderate expansion (0.15%) when compared to those retrieved from 2D-SP. The influence of the reactive aggregate type was not captured in the transverse and longitudinal directions in 2D blocks through the SDI and PDI at low expansion levels; yet, an 8% higher SDI and PDI was observed at moderate expansion levels for the reactive sand (TX) when compared to those specimens extracted from the 2D blocks made of reactive coarse aggregate (SP). Moreover, the vertical, transverse and longitudinal cores from the 2D-TX show a greater ME reduction of 15%, 22% and 22% at moderate expansion, respectively, than the cores retrieved from 2D-SP blocks. Likewise, a greater reduction in CS is observed in 2D-TX such that differences of 28%, 23% and 6% at moderate expansion were obtained from the vertical, transverse and longitudinal cores, respectively. Such results could be attributed to the higher number of cracks extending into the cement paste (i.e., CCP- orange chart), affecting both the bulk cement paste and some areas of the interfacial transition zone (ITZ) in the concrete blocks made of the reactive TX sand (Figure 13). Moreover, the higher mechanical properties reductions of TX-concrete specimens compared to those SP-specimens could be attributed to the cracking pattern observed in Figure 18, where several sparsely cracks are distributed in cement paste of TX- specimens, while SP-concrete

members experienced a more localized damage pattern, displayed mainly inside the reactive aggregate particles.

8.6.3 Impact of reinforcement on the cracks orientation of ASR affected concrete members

This section aims to qualitatively describe the orientation of ASR-induced cracks in restrained concrete based on the results obtained through the use of mechanical testing (i.e., SDT) and microscopic assessment (i.e., DRI). The Non-Linearity Index (NLI- output parameter of SDT) has been proposed by Crisp et al. [31,33] as a useful parameter to appraise the cracks' orientation of ASR-affected concrete. As such, Figures 19A and 19B display a typical concave stress-strain curve (i.e., obtained from vertical and transverse specimens of 2D-SP) and convex shaped curve (i.e., obtained from longitudinal specimens of 2D-SP), respectively, while Figure 19C shows the NLI values corresponding to the various directions of concrete made of SP and TX aggregates. Analyzing the data, one verifies that the longitudinally cored specimens (convex-shaped curves) from all restrained concrete blocks exhibit an NLI< 1, presenting a cracking network parallel to the loading as per Crisp et al. [31,33]. Conversely, transverse and vertically cored specimens (concave-shaped curves) display an NLI>1 revealing a cracking network perpendicular to the loading. This clearly demonstrates that the longitudinal specimens display ASR-induced cracks that are parallel to the coring/loading direction, while the cracks are perpendicular to the coring/loading direction for vertical and transverse cores. Moreover, as per Sanchez et al. [6], besides the ability of the NLI to assess the cracks' orientation of affected specimens, the latter could also act as an interesting complementary index to show the progress of ASR. As such, for the specimens showing a concave and convex trend (NLI greater/lower than 1, respectively), this parameter was found to increase/decrease steadily with ASR progress, respectively. Comparing the NLI calculated for the specimens retrieved from distinct directions, one notices that among the specimens showing concave and convex trends, vertical and longitudinal samples cored from 2D-TX showed the highest and lowest NLI amongst all the specimens appraised in this study, respectively; these results agree with previous findings where for the same expansion level, ASR triggered by TX sand seemed to generate a higher deterioration degree to affected concrete than when triggered by SP coarse aggregate.

Finally, in order to validate the results obtained from the SDT, a simple image analysis protocol (as explained in section 4.3.3) was performed on all concrete cores extracted from the various blocks, where the distinct damage features of two hundred DRI grids were highlighted per coring direction (one hundred grids per core - two cores per direction) and later stitched together; thus, 100 by 400 mm polished concrete sections were entirely appraised in the distinct directions (Figure 20). The image analysis outcomes obtained in this work validate the results obtained through the NLI since the vast majority of ASR-induced cracks in all restrained concrete specimens are propagated parallel to the longitudinal steel bars, which is

in accordance with previous results obtained by Zahedi et al. [16] and Barbosa et. al. [21]. The above discussion indicates the importance of computing the NLI for evaluating ASR-affected restrained concrete members and thus understanding the main orientation of induced cracks.

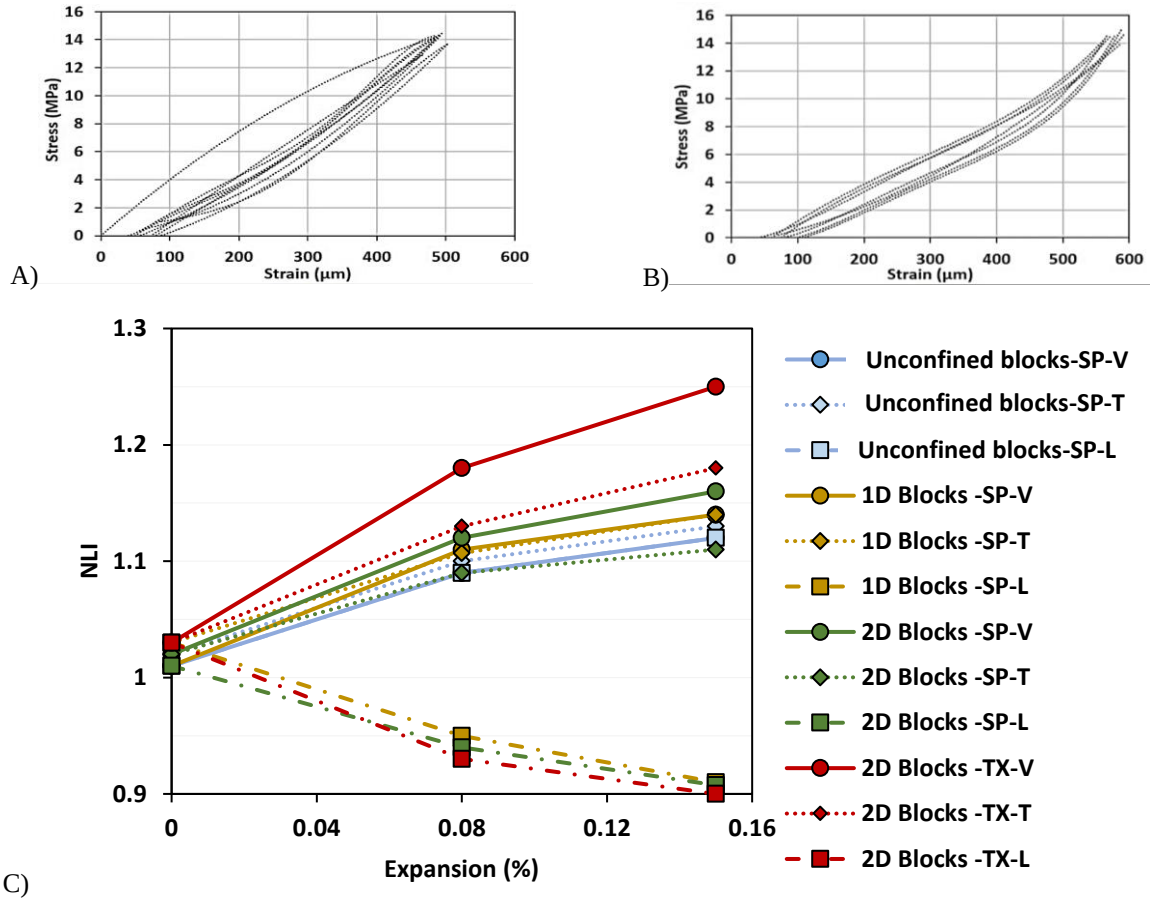

Figure 19: A) Concave SDT stress versus strain curves (vertical and transverse cores) B) Convex SDT stress versus strain curves (longitudinal cores), and C) NLI plot for both mixtures used in this study.

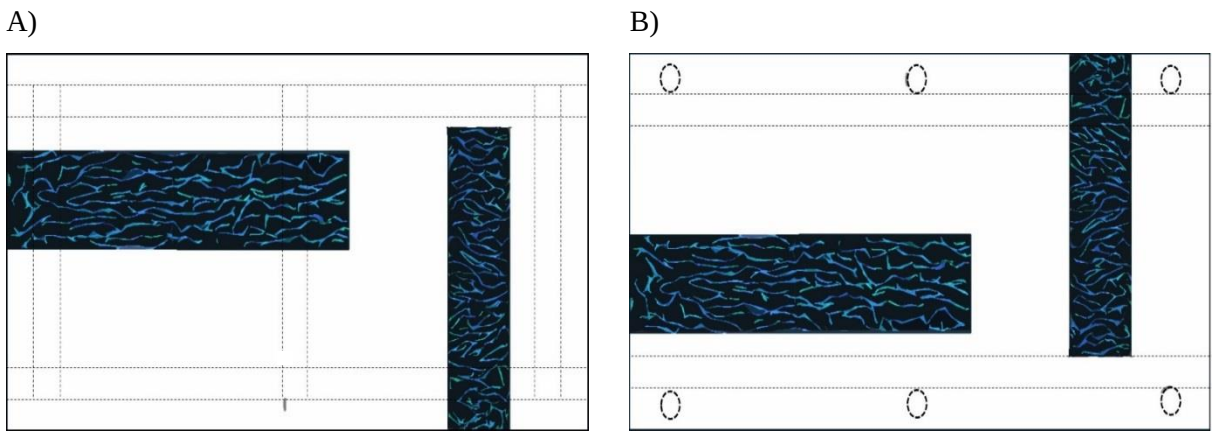

Figure 20: Results obtained from the image analysis performed on retrieved cores from the 2D deteriorated blocks incorporating SP coarse aggregate: A) Top view, and B) Longitudinal side view [16].

8.7. Conclusions

The main objective of the research program performed in this study was to investigate the effect of distinct restraint configurations (unrestrained, 1D and 2D) on ASR-induced development of concrete blocks manufactured with various aggregate types (fine and coarse) through the use of a multi-level assessment (i.e., coupling of mechanical and microscopic techniques). The main findings of this research are presented hereafter:

- Comparing ASR-induced development of the distinct concrete blocks evaluated in this work, one verifies that reinforcement contributes to the mitigation of ASR-induced expansion; the higher the restrainment degree, the lower the expansion captured over time. Furthermore, one observes an anisotropic behavior in the reinforced concrete blocks where the induced expansion transfers from restrained to less/non restrained directions. The latter clearly demonstrates the influence of the restraint configuration on the achieved expansion levels (i.e., transverse > longitudinal top > longitudinal side). Conversely, concrete cylinders display a much faster ASR development when compared to various concrete blocks, which confirms the impact of the specimen's size on ASR-induced expansion and deterioration.

- The multi-level protocol (i.e., coupling of Stiffness Damage Test- SDT and the Damage Rating Index- DRI) is a reliable and complementary approach for the condition assessment of unrestrained/restrained concrete affected by ASR. As such, the "overall" degree of damage (i.e., averaging the results obtained from the distinct directions at each damage degree) of the various concrete blocks gathered through the use of a multi-level protocol is in accordance with the ranges corresponding to the classification of damage degrees proposed by Sanchez et al. [6] for unconfined concrete samples.

- Similar to the expansion behavior, anisotropic ASR damage development was identified in all reinforced concrete blocks, where a greater damage was observed in the directions with less/no confinement when compared to the more restrained directions. Furthermore, it has been found that the higher the degree of restrainment, the lower the deterioration in the restrained direction(s), but the higher the damage in the non-restrained direction(s).

- A quantitative four-quadrant chart and a damage classification table were proposed for the distinct directions of the various ASR-affected reinforced concrete blocks; the above was based on the correlation of the following multi-level parameters: a) SDI/PDI b) DRI and c) stiffness reduction. The use of such a chart and table is very useful for engineers and should be referred to as a

"reference" point for either selecting data from a similar restraint configuration and coring direction or predicting the behavior of inaccessible directions of affected concrete members.

- Microscopic and mechanical investigations performed on the reinforced and non-reinforced concrete blocks incorporating distinct aggregate particles clearly demonstrated the different deterioration mechanisms taking place; concrete specimens made of reactive fine aggregates not only display faster ASR kinetics and higher potential for ultimate expansion than those manufactured with reactive coarse aggregates, but they also show a quite different deterioration pattern. As such, ASR-affected concrete bearing Texas sand presents more sparsely distributed cracks while a much more localized and sharp cracking pattern is observed in SP-concrete specimens. The above differences could be attributed to the mineralogy/origin as well as the aggregate particle size of TX sand as per [48].

- A thorough analysis of the samples retrieved from the various directions of the ASR-affected reinforced concrete blocks through mechanical (i.e., SDT-NLI) and microscopic (i.e., DRI- image analysis protocol) assessment confirmed a preferential orientation for ASR-induced crack propagation. Most cracks in restrained blocks were generated parallel to the longitudinal steel bars. This finding is a very important point to be considered to evaluate and understand the structural performance of ASR-affected restrained concrete members in the field.

Acknowledgments

The authors wish to thank technical officers of Materials and Structures lab (Drs. Muslim Majeed and Gamal Elnabelsya) at the University of Ottawa, as well as Ms. Nusrat Zubaida who helped with the fabrication of the concrete blocks of this study. Similarly, the authors wish to thank Advance Cutting & Coring for easing the critical steps of retrieving the core samples from the blocks. Finally, Mr. Zahedi benefits from the University of Ottawa graduate bursary for international Ph.D. students.

References

[1] B. Fournier, M. Bérubé, Alkali–Aggregate Reaction in Concrete: a Review of Basic Concepts and Engineering Implications, Can. J. Civ. Eng. 27 (2000) 167–191.
[2] V.E. Saouma, Diagnosis & prognosis of AAR affected structures : state-of-the-art report of the RILEM Technical Committee 259-ISR, Springer, Switzerland, 2021.
[3] A. Allard, S. Bilodeau, F. Pissot, B. Fournier, J. Bastien, B. Bissonnette, Expansive behavior of thick concrete slabs affected by alkali-silica reaction (ASR), Constr. Build. Mater. 171 (2018) 421–436.
[4] M.D.A. Thomas, K.J. Folliard, B. Fournier, P. Rivard, T. Drimalas, Methods for Evaluating and Treating ASR-Affected Structures: Results of Field Application and Demonstration Projects—Volume II: Details of Field Applications and Analysis, Washington, DC, 2013.
[5] M.D.A. Thomas, J. Ideker, North America (USA and Canada), in: I. Sims, Alan Poole, Alkali-Aggregate React. A World Rev., 1st ed., C, Florida, 2017.
[6] L.F.M. Sanchez, B. Fournier, M. Jolin, D. Mitchell, J. Bastien, Overall assessment of Alkali-

Aggregate Reaction (AAR) in concretes presenting different strengths and incorporating a wide range of reactive aggregate types and natures, Cem. Concr. Res. 93 (2017) 17–31.
[7] L.F.M. Sanchez, B. Fournier, M. Jolin, J. Duchesne, Reliable quantification of AAR damage through assessment of the Damage Rating Index (DRI), Cem. Concr. Res. 67 (2015) 74–92.
[8] L.F.M. Sanchez, B. Fournier, M. Jolin, M.A.B. Bedoya, J. Bastien, J. Duchesne, Use of Damage Rating Index to quantify alkali-silica reaction damage in concrete: Fine versus coarse aggregate, ACI Mater. 113 (2016) 395–407.
[9] L.F.M. Sanchez, B. Fournier, D. Mitchell, J. Bastien, Condition assessment of an ASR-affected overpass after nearly 50 years in service, Constr. Build. Mater. 236 (2020) 117554.
[10] B. Fournier, A. Bérubé, J. Folliard, M. Thomas, Report on the Diagnosis, Prognosis, and Mitigation of Alkali-Silica Reaction (ASR) in Transportation Structures, U. S. Department of Transportation, 2010.
[11] S. Multon, F. Toutlemonde, Effect of applied stresses on alkali-silica reaction-induced expansions., Cem. Concr. Res. 36 (2006) 912–920.
[12] N. Smaoui, Contribution à l'évaluation du comportement structural des ouvrages d'arts affectés de réaction alcalis-silice., Département Génie Civil, Univ. Laval, Canada. (2003).
[13] A. Zahedi, L. Sanchez, M. Noël, Effect of Confinement on AAR-induced expansion and damage, in 16th ICAAR, Int. Conference Alkali Aggreg. React. Concr. 1-3 June, Portugal, 2020.
[14] P. Morenon, S. Multon, A. Sellier, E. Grimal, F. Hamon, E. Bourdarot, Impact of stresses and restraints on ASR expansion, Constr. Build. Mater. 140 (2017) 58–74.
[15] D. Wald, M.T. Allford, O. Bayrak, T.D. Hrynyk, Development and multiaxial distribution of expansions in reinforced concrete elements affected by alkali-silica reaction, Struct. Concr. 18 (2017) 914–928.
[16] A. Zahedi, C. Trottier, L. Sanchez, M. Noël, Microscopic Assessment of ASR-Affected Concrete Under Confinement Conditions, Cem Concr Res. (2021) 106456.
[17] D.J. Deschenes, ASR/DEF-damaged bent caps: shear tests and field implications, The University of Texas at Austin, 2009.
[18] J.M. Bracci, P. Gardoni, M. Eck, D. Trejo, Performance of Lap Splices in Large-Scale Column Specimens Affected by ASR and/or DEF, Texas Transportation Institute, 2012.
[19] S. Sørgaard, O. Oseland, T. Kanstad, M.A.N. Hendriks, E. Rodum, Experimental investigation of ASR-affected concrete – The influence of uniaxial loading on the evolution of mechanical properties, expansion and damage indices, Constr. Build. Mater. 245 (2020) 118384.
[20] A. Abd-Elssamd, Z.J. Ma, Y. Le Pape, N.W. Hayes, M. Guimaraes, Effect of alkali-silica reaction expansion rate and confinement on concrete degradation, ACI Mater. J. 117 (2020) 265–277.
[21] A.R. Barbosa, S. Gustenhoff, K. Kielsgaard, L. Cao, B. Grelk, Influence of alkali-silica reaction and crack orientation on the uniaxial compressive strength of concrete cores from slab bridges, Constr. Build. Mater. 176 (2018) 440–451.
[22] E. Giannini, K. Folliard, Stiffness Damage and Mechanical Testing of Core Specimens for the Evaluation of Structures Affected by ASR, in Proc. 14th Int. Conf. Alkali–Aggregate React. Concr., Austin, 2012.
[23] N.W. Hayes, A.B. Giorla, W. Trent, D. Cong, Y. Le Pape, Z.J. Ma, Effect of alkali-silica reaction on the fracture properties of confined concrete, Constr. Build. Mater. 238 (2020).
[24] A.E.K. Jones, L.A. Clark, S. Amasaki, The suitability of cores in predicting the behavior of structural members suffering from ASR, Mag. Concr. Res. 46 (1994) 145–150.
[25] P. Li, N. Tan, X. An, K. Maekawa, Z. Jiang, Restraint effect of reinforcing bar on ASR expansion and deterioration characteristic of the bond behavior, J. Adv. Concr. Technol. 18 (2020) 192–210.
[26] E.R. Giannini, Evaluation of Concrete Structures Affected by Alkali-Silica Reaction and Delayed Ettringite Formation, PhD thesis, University of Texas at Austin, USA, 2012.
[27] T. Ahmed, E. Burley, S. Rigden, The Static and Fatigue Strength of Reinforced Concrete Beams Affected by Alkali-Silica Reaction, ACI Mater. J. 95 (1999) 376–388.
[28] S.G. Hansen, R.A. Barbosa, L.C. Hoang, Prestressing of reinforcing bars in concrete slabs due to concrete expansion induced by Alkali-Silica Reaction, in Fib Symp., Cape Town, 2016.

[29] L.F.M. Sanchez, B. Fournier, M. Jolin, J. Bastien, Evaluation of the Stiffness Damage Test (SDT) as a tool for assessing damage in concrete due to alkali-silica reaction (ASR): Input parameters and variability of the test responses, Constr. Build. Mater. 77 (2015) 20–32.
[30] L.F.M. Sanchez, B. Fournier, M. Jolin, J. Bastien, D. Mitchell, Practical use of the Stiffness Damage Test (SDT) for assessing damage in concrete infrastructure affected by alkali-silica reaction, Constr. Build. Mater. 125 (2016) 1178–1188.
[31] T.M. Crisp, J.G.M. Wood, P. Norris, Towards Quantification of Microstructural Damage in AAR Deteriorated Concrete. Int. Conf. on Recent Developments on the Fracture of Concrete and Rock, The University of Wales, Cardiff, 1989.
[32] T.M. Crisp, W. P., W.J.G. M., Development of a non-destructive test to quantity damage in deteriorated concrete, Mag. Concr. Res. 45. (1993) 247-256.
[33] T.M. Chrisp, P. Waldron, J.G.M. Wood, Development of a non-destructive test to quantify damage in deteriorated concrete, Mag. Concr. Res. 45 (1993) 247–256.
[34] Y. Zhu, A. Zahedi, L.F.M. Sanchez, B. Fournier, S. Beauchemin, Overall assessment of alkali-silica reaction affected recycled concrete aggregate mixtures derived from construction and demolition waste, Cem. Concr. Res. 142 (2021) 106350.
[35] P.A. Dunbar, P.E. Grattan-Bellew, Results of damage rating evaluation of condition of concrete from a number of structures affected by ASR, CANMET, in: ACI Int. Work. AAR Concr., Darmouth, Canada, 1995: pp. 257–266.
[36] P.E. Grattan-bellew, Laboratory Evaluation of Alkali-Silica Reaction in Concrete from Saunders Generating Station, Mater. J. 92 (1996) 126–134.
[37] V. Villeneuve, B. Fournier, Determination of the damage in concrete affected by ASR — the damage rating index (DRI), in: 14th ICAR — Int. Conf. Alkali– Aggreg. React. Concr., Austin, 2012.
[38] ASTM C1293, Standard test method for determination of length change of concrete due to alkali-silica reaction, Annu. B. ASTM Stand. (2015) 1–7.
[39] CSA A23.3:19:Design of concrete structures, 2019.
[40] CSA23.2-14C: Obtaining and testing drilled cores for compressive strength testing, 2019.
[41] ASTM C93, Standard Test Method for Compressive Strength of Cylindrical Concrete Specimens, USA, 2012.
[42] ASTM C1074-19, Standard Practice for Estimating Concrete Strength by the Maturity Method, USA, 2019.
[43] B. Fournier, P.C. Nkinamubanzi, R. Chevrier, Comparative field and laboratory investigations on the use of supplementary cementing Materials to control alkali-silica reaction in concrete, in: 12th Int. Conf. Alkali-Aggregate React., China, 2004.
[44] B.P. Gautam, D.K. Panesar, A New Method of Applying Long-Term Multiaxial Stresses in Concrete Specimens undergoing ASR, and their Triaxial Expansions, Mater. Struct. 49 (2016) 3495–3508.
[45] J. Liaudat, I. Carol, M.L. Carlos, ASR expansions in concrete under triaxial confinement, Cem. Concr. Compos. 86 (2018) 160–170.
[46] N. Smaoui, B. Fournier, B. Bissonnette, Influence of Specimen Geometry, Orientation of Casting Plane, and Mode of Concrete Consolidation on Expansion Due to ASR, Cem. Concr. Aggregates. 26 (2004) 1–13.
[47] Z. Mahomed, M. Alexander, H. Beushausen, ASR expansion due to use of reactive fine and coarse aggregates, and its effect on concrete compressive strength, Concr. Bet. Tech. J. (2019).
[48] K. Ramyar, A. Topal, Ö. Andiç, Effects of aggregate size and angularity on alkali-silica reaction, Cem. Concr. Res. 35 (2005) 2165–2169.

SUPPLEMENTARY MATERIAL

Table 6: Data in brief for the "overall" analysis.

Block Type	SDI		PDI		E (GPa)		E Reduction (%)		CS (MPa)		CS Reduction (%)	
	0.08%	0.15%	0.08%	0.15%	0.08%	0.15%	0.08%	0.15%	0.08%	0.15%	0.08%	0.15%
Cylinder -SP	0.18	0.26	0.13	0.24	25.00	19.00	17.00	36.00	31.00	28.00	12.00	21.00
Cylinder -TX	0.18	0.27	0.14	0.25	23.10	20.39	32.06	40.03	31.03	28.47	15.00	22.00
Unrestrained Blocks-SP	0.18	0.27	0.13	0.24	25.00	19.00	17.00	36.00	31.00	29.00	12.00	18.00
1D Blocks-SP	0.18	0.27	0.15	0.24	24.00	19.00	20.00	36.00	31.00	29.00	12.00	18.00
2D Blocks-SP	0.18	0.25	0.15	0.23	24.00	19.00	20.00	36.00	31.00	29.00	12.00	18.00
2D Blocks-TX	0.20	0.27	0.15	0.25	22.72	18.88	33.18	44.46	31.00	27.00	14.40	24.67

Table 7: Data in brief for the "anisotropic" analysis.

Block Number	Core orientation	SDI		PDI		E		E Reduction (%)		CS (MPa)		CS Reduction (%)		DRI	
		0.08%	0.15%	0.08%	0.15%	0.08%	0.15%	0.08%	0.15%	0.08%	0.15%	0.08%	0.15%	0.08%	0.15%
Unrestrained Blocks-SP	V	0.18	0.27	0.13	0.25	25.36	19.39	15.47	35.38	30.74	28.45	12.75	19.25	337.20	573.16
	T	0.18	0.27	0.15	0.24	25.44	19.28	15.20	35.74	30.69	28.95	12.90	17.82	345.60	575.14
	L	0.18	0.27	0.11	0.25	25.45	19.62	15.16	34.60	30.51	28.93	13.42	17.88	341.06	573.26
1D Blocks-SP	V	0.21	0.29	0.17	0.27	23.65	17.59	21.17	41.38	29.89	27.22	15.16	22.74	382.00	646.00
	T	0.20	0.29	0.16	0.26	23.37	18.09	22.09	39.70	30.48	27.58	13.48	21.71	366.00	614.00
	L	0.14	0.23	0.11	0.21	25.37	21.38	15.45	28.73	32.43	31.25	7.95	11.31	337.80	479.00
2D Blocks-SP	V	0.23	0.31	0.17	0.29	22.52	15.06	24.95	49.79	28.59	24.61	18.86	30.16	401.23	766.00
	T	0.17	0.23	0.14	0.21	24.95	20.70	16.83	31.01	31.25	31.46	11.30	10.71	323.02	483.49
	L	0.15	0.22	0.14	0.20	25.35	21.67	15.52	27.77	32.44	31.13	7.92	11.64	305.95	472.00
2D Blocks-TX	V	0.25	0.33	0.19	0.31	22.00	14.00	35.29	58.82	28.65	21.17	21.50	42.00	455.28	801.87
	T	0.17	0.25	0.14	0.23	26.00	21.00	23.53	38.24	32.30	30.30	11.50	17.00	356.74	482.69
	L	0.17	0.24	0.13	0.22	26.00	21.00	23.53	38.24	32.78	31.03	10.20	15.00	351.99	471.85

9. IMPROVING THE KNOWLEDGE OF VISUAL INSPECTION ON ASR AFFECTED CONCRETE UNDER VARIOUS RESTRAINT CONDITIONS

Andisheh Zahedi [1], Leandro Sanchez [2], Martin Noel [3]

Abstract

It is agreed that the conventional visual inspection technique is generally qualitative and therefore unable to provide accurate information on the extend of damage of Alkali-Silica Reaction (ASR) affected concrete. Therefore, improving and finding a better visual inspection technique could play an important role in the condition assessment of ASR-affected infrastructure. This work intends to assess the ASR damage development on distinct surfaces of thirty-two concrete blocks displaying various restraint configurations (none, 1D and 2D) and incorporating different aggregate types (reactive fine and coarse) through the use of distinct visual inspections and microscopic techniques. Three expansion levels were selected for analysis (0.08%, 0.15% and 0.25%) and once reached, visual inspections (qualitative, semi quantitative and quantitative) as well as the Damage Rating Index (DRI), a semi-quantitative petrographic analysis, were conducted on the surface of those blocks. Moreover, once the blocks reached the first two expansion levels, cores were extracted from three different directions (longitudinal, transverse, and vertical) and the DRI was performed on those with the aim to quantitatively compare the damage on the surface and core of the blocks. Results show that the higher the restraint, the higher the surface damage on the concrete elements. Furthermore, the DRI results obtained from the cores and surfaces of the concrete blocks demonstrate that the surface of the specimens underwent significantly higher damage than cored specimens which may increase the likelihood of further durability issues (e.g., corrosion) in reinforced concrete. Finally, the authors proposed a correlation between the measured cracking index (C.I) and expansion levels of distinct surfaces of concrete specimens as well as the qualitative ASR distress models on the surface of the concrete were defined.

Keywords: Alkali-Silica Reaction, Visual inspection, Damage Rating Index (DRI), Cracking index (CI) restrained concrete.

9.1. Introduction

One of the biggest challenges in civil engineering nowadays is to have an efficient management protocol for critical infrastructure affected by internal swelling reactions, such as alkali-silica reaction (ASR),

delayed ettringite formation (DEF), and freeze-thaw (FT) cycles [1,2]. The assessment of the cause(s) and extent of deterioration (i.e., diagnosis) along with the evaluation of the structural integrity of affected structures is often defined as condition assessment [3,4]; appraising the current and forecasting future condition (i.e., prognosis) are fundamental steps towards the optimization of management protocols and rehabilitation strategies of concrete infrastructure affected by internal swelling reactions.

Concrete infrastructure such as bridges, road networks, dams, pipelines and tunnels requires periodic condition assessment to appraise their functional conditions along with identifying deterioration signs such as cracks and defects prior to the onset of failure [5,6]. Cracks and defects in concrete can significantly impact on the durability of affected structures (i.e., higher risk of carbonation and chloride penetration leading to induced steel corrosion, freezing and thawing distress, sulfate ions penetration, etc.) [7]; the wider the cracks opening, the higher the likelihood of further deterioration [8,9]. Condition assessment of civil infrastructure, in general and in structures affected by internal swelling reactions, is primarily conducted through visual inspection [10]; it typically includes an evaluation of the type (i.e., cracking, spalling, defective joints, corrosion, etc.) and extent (i.e., number, width, length, etc.) of the existing deterioration signs present at the time of appraisal [6,11,12]; Although important, the result of visual inspection is often qualitative and thus unable to provide infrastructure owners with detailed and accurate information on the extent of deterioration of affected structures. Hence, despite the regular visual inspections of infrastructure assets, some degree of uncertainty still remains and, unfortunately, accidents associated with deficient appraisal may occur, such as the failure of the de la Concorde overpass on Autoroute 19 in Laval (Quebec, Canada) in September 2006, where 5 people died and 6 were severely injured [13–15].

Recently, researchers proposed the use of techniques that could help engineers to make better visual inspections of concrete affected by internal swelling reactions [16–18]. Amongst those, the cracking index (CI), a crack mapping process that can provide a quantitative assessment of the existing cracking extent on the surface of affected concrete members [17,18], was shown to be quite suitable to evaluate the condition of deteriorated infrastructure. However, at the best knowledge of the authors, only a few studies (e.g., [19]) aimed to compare and correlate the results of the cracking index (CI) with internal damage (i.e., measured by microscopic and/or mechanical test procedures from extracted cores) of affected members. Therefore, this work deals with the use and comparison of distinct visual inspection techniques (i.e., conventional-qualitative, measuring the crack width- semi quantitative and cracking index (CI)- quantitative), as a means of better understanding of the induced expansion (i.e., at the surface vs. steel bars), and internal deterioration (i.e., gathered through microscopic distress features) of reinforced concrete blocks affected by internal swelling reactions, particularly alkali-silica reaction (ASR).

9.2. Background

9.2.1. Alkali-silica reaction (ASR)

Alkali-silica reaction (ASR), a chemical reaction between certain mineral phases from the aggregates and the alkali hydroxides (i.e., Na^+, K^+, OH^-) from the concrete pore solution is one of the main deleterious processes affecting the durability of concrete infrastructure worldwide [16,17,20]. ASR produces a secondary reaction product (i.e., *alkali-silica gel*) that swells upon moisture uptake, leading to expansion and cracking of the affected material [16,17,20]. It has been found that ASR-induced expansion causes cracks within the aggregate particles which propagate to the cement paste as the expansion progresses [21]. Moreover, according to Courtier [22], ASR-induced expansion is less developed at the surface of affected concrete members when compared to their core due to alkali leaching, which creates a gradient; this expansion gradient generates a higher number of cracks at the surface of the affected elements due to secondary effects such as exposure to weathering, shrinkage induced by drying wetting cycles along with a lower quality material normally presented by the concrete cover (i.e., bearing pore paste and porosity than the bulk volume of the member). Such surface cracks can be classified in three distinct zones within a particular concrete member (Figure 1). The first and central zone of the member bears a roughly random cracking pattern which is associated with the weak local restraint in this area. Moving toward the top part of the concrete element, a zone close to the longitudinal rebars, most of the cracks are generally propagated parallel to the main steel bars. Finally, most of the ASR-induced cracks in the space between the main rebar and the top surface of the concrete member are more likely to propagate in a direction normal to the surface, which could be attribute to the lack of restraint on that area [22]. Afterwards, with the progress of ASR, the number as well as the length and width of those previously formed cracks on the surface of concrete elements increase and thus create a mixture of radial and circumferential cracks [22,23].

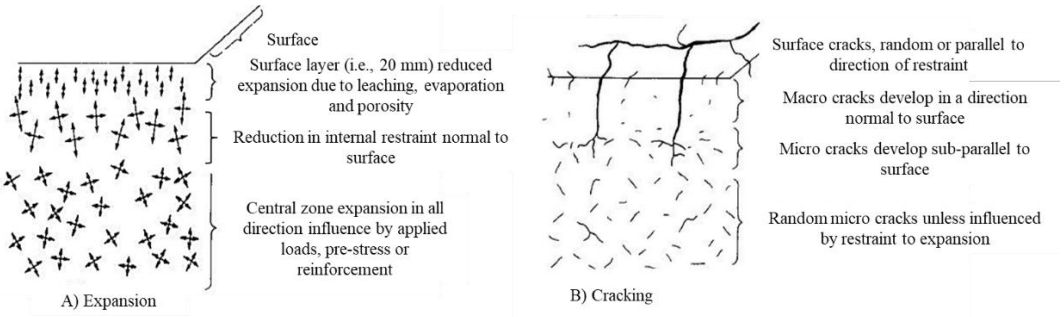

Figure 1: A) Development of expansion and B) cracking linked to ASR [22] *(Reproduced with permission of Elsevier)*.

The vast majority of past works on ASR have been conducted using concrete specimens under unrestrained (i.e., free expansion) conditions (e.g., [24,25]); very few works dealt with restrained concrete specimens. Most of them have demonstrated that reinforcement could partially mitigate ASR-induced expansion in

affected concrete members [2,3,26–28]. As such, Smaoui [26] compared the expansion level attained by ASR-affected concrete beams (810 x 228 x 228 mm) under unrestrained conditions with those having a reinforcement ratio of 1.53%, reporting a reduction of almost 60% in the direction of confinement in the reinforced beams. Moreover, unlike unrestrained members, such an expansion reduction in the direction of confinement led to anisotropy of induced expansion and deterioration [3,27,29]; ASR-induced expansion is reduced in the restrained directions while less/non restrained directions tend to display an increase in expansion; this phenomenon is called expansion transfer [23,27,29–31]. In this regard, Allard et. al. [23] observed that specimens with rectangular cross-sections (i.e., thick slabs with longitudinal reinforcement asymmetrically distributed about the centroidal axis) deformed into trapezoidal sections after moderate to high (i.e., 0.20%, on average) ASR-induced expansions.

It is well accepted that the importance (i.e., length and width) of ASR-induced cracks on the surface of unrestrained/restrained members could play a critical role in the performance and functionality of affected infrastructure [32]. In general, conventional visual inspection techniques are rather qualitative and thus unable to record the importance of existing surface cracks in ASR-affected concrete; therefore, engineers and researchers have tried over the past years to implement more quantitative assessment while conducting visual inspections. Karthik et. al. [33] proposed a correlation between the expansion measured on the surface of confined concrete members and the crack widths measured through visual inspection as follows:

$$\varepsilon_{CW} = \gamma \left(\frac{\sum W_{cr}}{X_{gauge}} \right) \quad (1)$$

in which $\sum W_{cr}$ is the sum of all crack widths measured across a specific gauge length X_{gauge} , and γ is a correction factor, which was calibrated as $\gamma = 2$ based on the results obtained. Although very interesting, this equation could not be generalized for all ASR-affected members since the impact of different reactive aggregate types (i.e., fine vs coarse), member's geometry and restraint configurations on ASR-induced cracking development and cracking pattern have never been thoroughly studied. Therefore, there is still a need for a systematic investigation of the impact of ASR-induced visual integrity (i.e., surface deterioration) through the use of various visual inspection techniques (conventional, semi quantitative- measuring the crack width and quantitative- cracking index) and correlate it with the internal damage (e.g., appraised through the microscopic assessment-DRI) of concrete elements displaying distinct reinforcement configurations, aggregate types, and presenting distinct damage degrees (i.e., induced expansion levels).

9.2.2. Diagnostic assessment tools

9.2.2.1. Surface assessment: cracking index (CI)

Initially, Fasseu and Michel [34] proposed the cracking index (CI) and later Fournier et al. [17,18] adopted the latter as an alternative to traditional qualitative visual inspection [17,18]. The cracking index (CI), a quantitative visual inspection technique, is a crack mapping process that averages crack widths and frequencies along the vertical and horizontal directions displayed by a grid drawn on the surface of the evaluated concrete member having ideally the dimensions of 0.5 x 0.5 m [17,18]; yet as per the authors [17,18], a smaller length (e.g., 0.20x0.20 m) can also be adopted for smaller concrete members. Therefore, a 0.5x0.5m reference square frame is drawn (i.e., as a base length - Figure 2) on the surface of the concrete elements [17,18], then each axis of those square frames are divided into ten intervals. Later, the width of the cracks greater than 0.05 mm which intersect each segment is measured with the aid of a comparator and a cracking index is calculated by summing the measured crack width per length unit as follows

$$CI = \frac{\sum Crack\ opening}{Base\ length} \quad (2)$$

in which $\sum crack\ opening$ = the sum of all crack widths measured across the base length (i.e., generally 0.5 m). Such method gives a quantitative assessment of the extent of cracking in the affected members [17,18]; as per Fournier et. al. [17], a concrete member with CI > 0.5 mm/m (and/or cracks of width > 0.15 mm) require more detailed investigations to identify the extent of cracking.

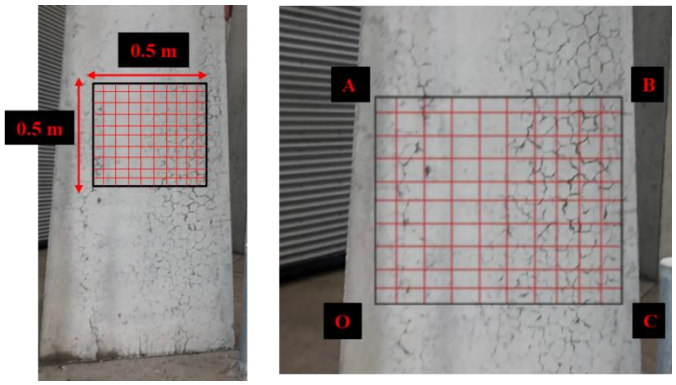

Figure 2: A) Cracking Index (CI) grid on damaged concrete.

9.2.2.2. Internal deterioration appraisals: damage rating index (DRI)

The damage rating index (DRI), a semi-quantitative microscopic tool used to evaluate damage in concrete, was proposed by Grattan-Bellew and colleagues [34,35] for the first time in 1992. Petrographic features present in 1x1 cm squares drawn on the surface of polished concrete sections are counted using a stereomicroscope at 15-16x magnification. The petrographic features are then multiplied by weighting factors whose purpose is to balance their relative importance [36]. At the end of the analysis, a DRI number is computed; the higher the DRI number, the higher the induced deterioration of the affected concrete [4]. Ideally, a surface of at least 200 cm² should be assessed; however, for comparative purposes, the final DRI

number is normalized to a 100 cm² area. The distress features included in the DRI evaluation are listed in Figure 3A along with their corresponding weighting factors; some of the distress features can be found and identified in Figure 3B.

A)

Petrographic features	Weighting factors
Closed cracks in aggregates (CCA)	0.25
Opened cracks in aggregates (OCA)	2
Opened crack with reaction product in aggregate (OCAG)	2
Coarse aggregate de-bonded (CAD)	3
Disaggregate/corroded aggregate particle (DAP)	2
Cracks in cement paste (CCP)	3
Cracks with reaction product in cement paste (CCPG)	3

B)

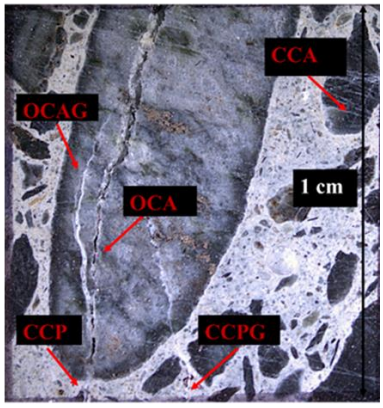

Figure 3: Damage Rating Index: A) Current weighting factors as per [36] and B) Micrograph illustrating a 1cm² section where some of the petrographic features listed in A can be observed and identified *(Reproduced with permission of Elsevier)*.

9.3. Scope of work

As previously stated, there is still a need to find tools to thoroughly quantify surface deterioration of ASR-affected unrestrained/restrained concrete and be able to associate it to a damage degree, particularly induced expansion. Moreover, a better understanding and correlation between ASR-induced surface and internal deterioration of affected concrete is still required; therefore, thirty-two concrete blocks incorporating reactive coarse and fine aggregates (Springhill coarse and Texas sand, respectively) and displaying distinct reinforcement configurations (i.e., none, 1D and 2D) were fabricated in the laboratory and monitored (surface and steel bars expansion) over time. Initially, at various induced expansion levels (i.e., 0.08%, 0.15% and 0.25%), numerous surface deterioration measurements (i.e., various visual inspection techniques and microscopic assessment) were conducted on the external surfaces of affected concrete blocks. Later, the blocks were cored in three distinct directions (i.e., longitudinal, transverse, and vertical) at the low and moderate (i.e., 0.08% and 0.15%, respectively) expansion levels and microscopic analyses were conducted on those specimens, with the aim to compare surface vs. internal ASR-induced deterioration. Finally, an empirical model correlating the crack size (i.e., width and length) obtained through quantitative visual inspection (CI) and ASR-induced damage degree (i.e., expansion attained to date) is proposed.

9.4. Methodology

9.4.1 Materials and mixture proportions

Thirty-two blocks of 450 × 450 × 675 mm (Figure 4) were manufactured using a concrete mixture with a design compressive strength of 35 MPa in this study. A highly reactive coarse (i.e., Springhill-SP) and sand aggregate (i.e., Texas-TX) combined with non-reactive aggregate particles (Ottawa natural sand-OT and Ottawa limestone coarse aggregate-LS, respectively) were selected for concrete manufacturing. Table 1 provides information on the different aggregates used in this study, including the lithological composition of the aggregates. A conventional (CSA Type GU, ASTM type I) high-alkali (0.88% Na_2O_{eq}) Portland cement was used for both concrete mixtures. Also, the total alkali content of all mixtures was raised to 1.25% Na_2O_{eq}, by cement mass, for accelerating ASR development. The mixture proportions selected for this study are based on the Concrete Prism Test (CPT) standard mixture proportions as per ASTM C 1293 [37] and are presented in Table 2.

Table 1: Aggregate properties selected for this study.

Aggregate				Rock type	Specific gravity (g/cm^3)	Absorption (%)	AMBT [a] 14 days expansion(%)
Type	Reactivity	Location	Name				
Coarse	Reactive	New Brunswick	SP	Greywacke	2.72	0.60	0.69
	Non-reactive	Ottawa	LS	Limeston derived from quarries	2.68	0.53	0.05
Fine	Reactive	Texas (USA)	TX	Polymictic sand	2.60	0.55	0.76
	Non-reactive	Ottawa	OT	Natural derived from granite	2.65	1.18	0.07

a) Typical expansion cf. ASTM C1260.

Table 2: Concrete mix design.

Materials	Mix proportions (kg/m^3)	
	OT+SP	TX+LS
Cement	420	420
Fine aggregate	681	732
Coarse aggregate	1044	1072
Water	176	176

9.4.2 Fabrication of concrete blocks

For further investigation on the effect of restraint on ASR-induced development, three different restraint conditions were selected in this research as: 1) unrestrained concrete blocks, 2) 1D confined blocks and, 3) 2D confined blocks (Figures 4 and 5). A total of 8 blocks from each distinct restraint configuration incorporating SP aggregate (i.e., twenty-four concrete blocks) and 8 blocks of 2D incorporating TX aggregate were fabricated in the laboratory. For the restrained blocks, a reinforcement ratio of 2% was selected which represents a moderately high level of internal restraint in a reinforced concrete element. For context, several standards and design codes specify a minimum reinforcement ratio in slabs of 0.2% and a maximum practical limit in columns of 4% (e.g. CSA A23.3 [38], CSA S6 [39]). Relatively large steel reinforcing bars with a nominal diameter of 35 mm (35M) were selected to reinforce the restrained blocks

in order to achieve the desired reinforcement ratio while ensuring sufficient space between bars to allow for concrete core extraction. It is worth noting that, in the case of 2D confined blocks, transverse and longitudinal steel reinforcing bars were professionally welded together to facilitate the construction (Figure 5B). Moreover, in the case of restrained concrete, the concrete cover, spacing between the top and bottom steel rebars, as well as spacing between transverse steel reinforcing bars (in the case of 2D concrete blocks) were 50 mm, 280 mm and 230 mm, respectively (Figure 4C, 5B, and 5C). All concrete blocks were demoulded after 24 hours, and moist cured (i.e., ambient temperature) for 24 hours. Then, four holes of 10 mm in diameter by 55 mm long were drilled in three main sides of the blocks: a) top (Figure 6A - points 1 and 2), b) longitudinal (Figure 6A - points 3 and 4) and c) transverse (Figure 6A - points 5 and 6). Stainless steel gauge studs (i.e., demec gauges) were then fixed in place with a fast-setting cement slurry for longitudinal expansion measurements. The studs consisted of 55 mm-long sections cut from a stainless steel threaded rod (10 mm in diameter) with a small indentation on the end surface (Figure 6B). After two days from casting (i.e., 48 hours), the initial length readings (i.e., zero-length readings) were taken (Figure 6A). All blocks were subsequently stored in an environmental chamber enabling ASR development (38ºC and 100% RH). All blocks were monitored regularly for length changes with the aid of a micrometer (Figure 5C) until they reached low (i.e., 0.08% ± 0.01%), moderate (i.e., 0.15% ± 0.01%) and high (i.e., 0.25%± 0.01%) expansion levels. As per ASTM C 1293 [51] all concrete specimens were placed in 23°C conditions for 16 ± 4 hours prior to periodic expansion measurements.

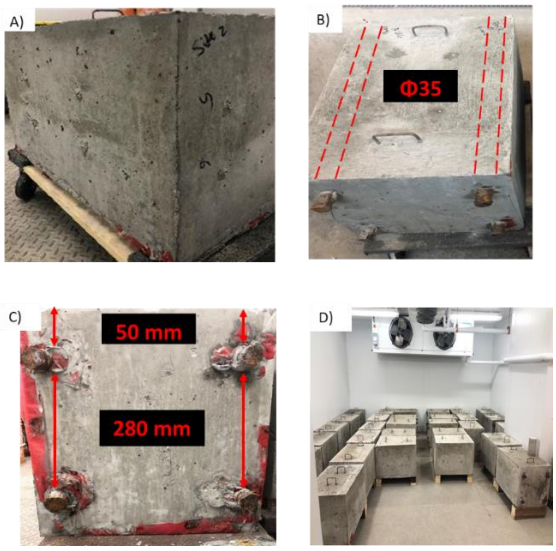

Figure 4: Concrete blocks presenting: A) unrestrained concrete block, B) 1D confined concrete block, C) 2D confined concrete block and, D) environmental chamber with 38ºC and 100% RH.

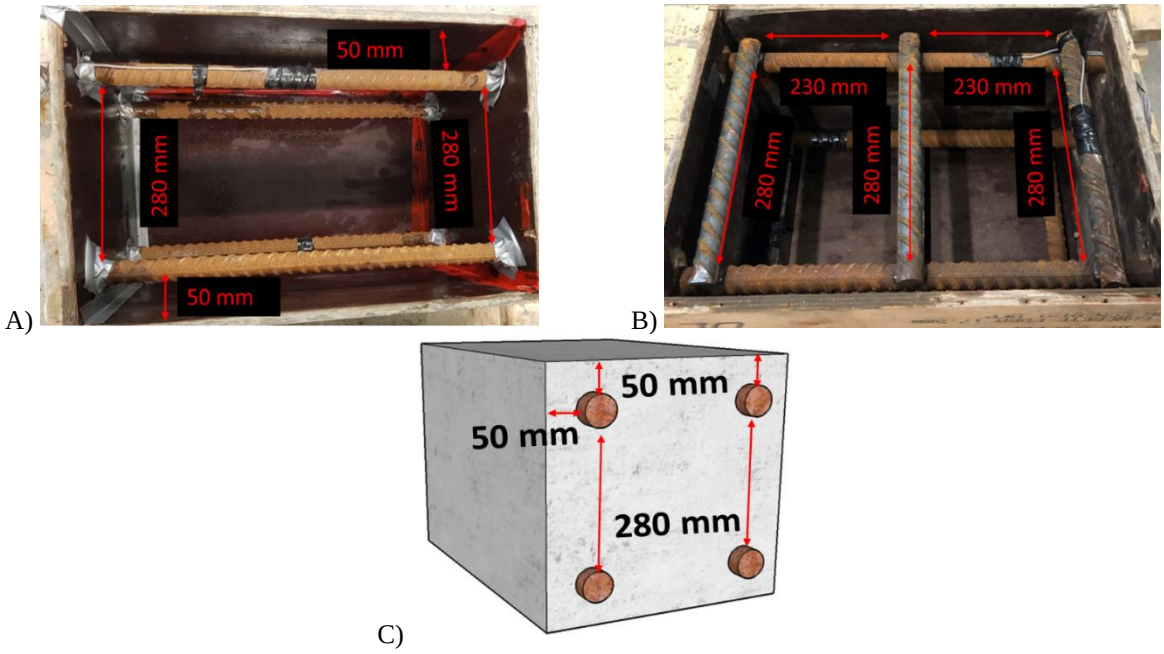

Figure 5: Restraint orientations A) 1D confinement B) 2D confinement and C) schematic of restrained blocks with 50 mm concrete cover and 280 mm distance between top and bottom steel bars.

Figure 6: A) Gauge studs orientation for blocks, B) Stainless- steel studs and C) expansion measurements on the distinct direction of concrete blocks with a micrometer.

Upon reaching the selected expansion levels (i.e., 0.08%, 0.15% and 0.25%), the concrete blocks were removed from the environmental chamber and then their surface deterioration was determined through various visual inspection techniques conducted on their distinct surfaces. Afterward, three blocks from each distinct restraint configuration and aggregate type presenting low and moderate (i.e., 0.08% and 0.15%) expansion levels were cored to produce seven cores of 100 by 450 mm in the vertical (Figure 7 A and D) and the transverse (Figure 7 B and D) directions and four of 100 by 675 mm cylinders in the longitudinal (Figure 7 C and E) direction for further analysis. Later, all concrete cores were sawed cut into specimens

of 200 mm length and then wrapped in plastic film and stored at 12°C until testing (because of testing capacity issues).

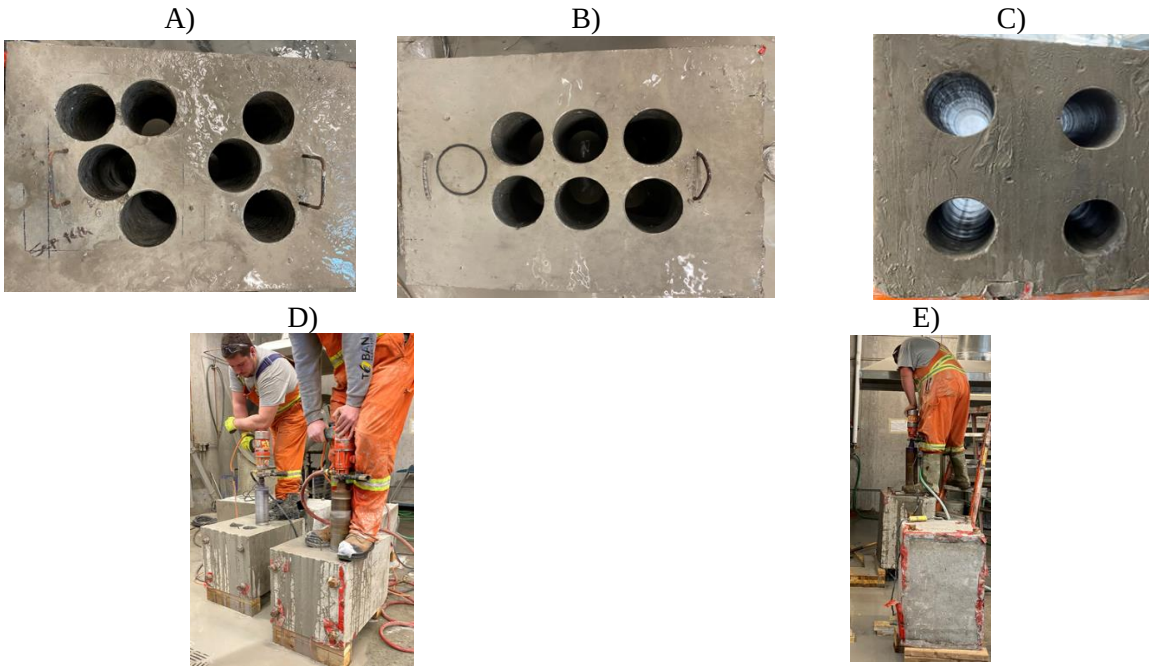

Figure 7: Concrete blocks cored in the direction of A) Vertical, B) Transverse, C) Longitudinal, D) process of coring extraction in vertical and transverse and E) Longitudinally direction.

In order to monitor the actual behaviour (i.e., induced expansion) of steel bars and compare the likely differences in ASR-induced expansion on them when compared to the values gathered at the surface of the blocks using gauge studs (i.e., demec gauges), 10 mm electrical strain gauges were installed on the reinforcing bars for all sets of restrained concrete and coated with M-Coat W-1 Wax. The locations of the strain gauges in concrete blocks are presented in Figure 8. Two strain gauges were installed in 1D blocks (i.e., one on a top-layer longitudinal bar and one at the bottom layer, Figure 8A) and four strain gauges (i.e. two on top-layer longitudinal and transverse bars and two at the bottom layer) were installed for all 2D blocks (Figure 8B).

A) B)

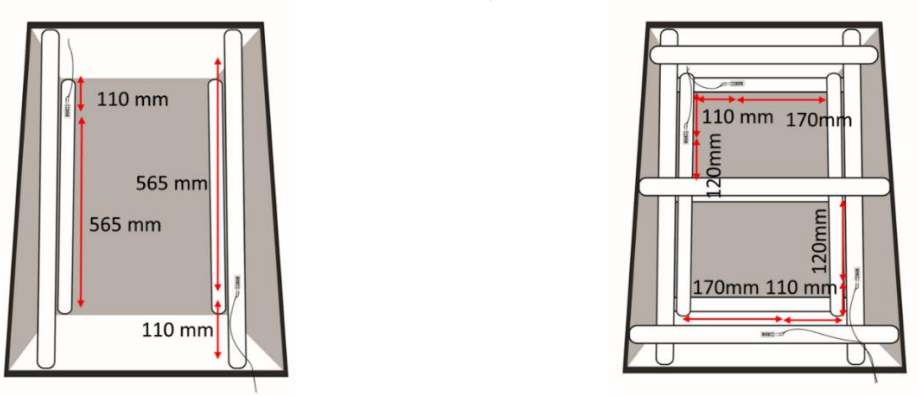

Figure 8: Location of the installed strain gauges in A) 1D and B) 2D blocks.

9.4.3 Experimental program

9.4.3.1. Visual Inspection and Imaging-based detection

A detailed visual inspection was performed on the three main surfaces (i.e., side longitudinal, top longitudinal, and transverse) of each concrete block of this study. During the visual inspection, qualitative, semi-quantitative (i.e., measurements of cracks openings) and quantitative assessments (i.e., cracking index) of the damage were conducted. It is worth noting that, due to the size restriction of the concrete blocks, a base length of 400 mm (i.e., a grid of 0.4 x 0.4 m) has been used in this study for conducting cracking index on the distinct surfaces of each concrete specimen (Figure 9A).

In addition to the various conducted visual inspection techniques, image-based detection was also performed on three main sides of each block with the aim to investigate ASR-induced development (i.e., crack generation and propagation) on the distinct surfaces of the concrete members. Initially, high-resolution images were collected from the three main surfaces (i.e., side longitudinal, top longitudinal, and transverse) of each block prior to the storage at 38oC and 100% RH (i.e., undamaged/sound condition). Then, every 30 days, the generated cracks on the distinct surfaces of each block were highlighted with a permanent marker pen and once again captured using a high-resolution camera; such procedure was repeated up to 500 days of exposure (i.e., every 30 days). Comparing the various captured images from the distinct surfaces of the concrete blocks may help to better understand the process of ASR-induced crack generation and propagation of the distinct concrete blocks manufactured in this research.

9.4.3.2. Damage Rating Index

After conducting the distinct visual inspection techniques on the various surfaces of each concrete block, the DRI was initially performed using a stereomicroscope at 16x magnification on the three main surfaces of each block (i.e., side longitudinal, top longitudinal, and transverse) at distinct expansion levels (i.e., 0.08%, 0.15% and 0.25%). Accordingly, a 200 cm2 area on three main sides of each concrete block having reached the targeted expansion levels was first ground and then polished with the mechanical hand polisher

followed with grits of 30 (coarse), 60, 140, 280, 600, 1200 and 3000 (very fine) as per Figure 9B. Once the surface of the polished section was considered suitable for analysis, a 1 by 1 cm grid was drawn on the polished surface of the specimens prior to evaluation. The distress features were then evaluated as per Villeneuve and Fournier [37]. Similarly, the DRI assessment was conducted on core specimens retrieved from the blocks; thus, two consecutive core specimens per direction of the blocks (i.e., a total of 6 core specimens per restraint level per expansion level) were cut in half longitudinally using a diamond bladed masonry saw and then polished followed the same procedure as the surface of concrete blocks (i.e., Figure 9C) and finally DRI assessment conducted on the prepared cored specimens. Such microscopic assessment on the distinct surfaces of each concrete block as well as the cored specimens was conducted with the aim of quantifying and comparing the damage development on the surface and core of the concrete blocks as a function of induced expansion.

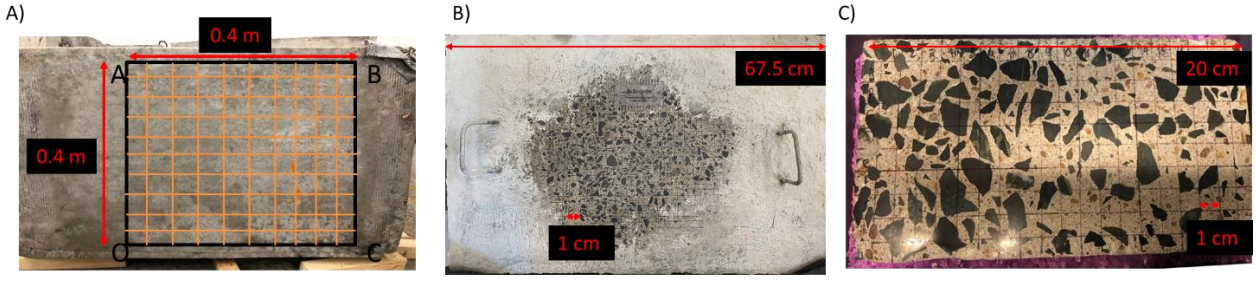

Figure 9: Cracking Index (CI) grid on the surface of concrete block (0.4 x 0.4 m) and the polished section of B) Top surface (450×675 mm) of 2D block and C) 100×200 mm core specimens.

9.5. Results

9.5.1 ASR kinetics and development

Figure 10 presents the average induced expansions (i.e., average value of four consecutive measurements per specimen at two different points per direction with standard deviations ranging from 0.02% to 0.06%) as a function of time for the various directions of the ASR-affected concrete blocks incorporating the reactive coarse (i.e., Springhill-SP) and reactive sand (i.e., Texas-TX) aggregates displaying different reinforcement configurations. Analyzing the plots, one notices that all concrete blocks presented an important amount of shrinkage (i.e., all directions) at the beginning of ASR-induced development. As such, it took 35, 75, 105 and 75 days on average for the unrestrained concrete blocks-SP, 1D-SP, 2D-SP and 2D-TX, respectively, to recover from shrinkage. Interestingly, the trends of induced expansions from the various directions as a function of time for all blocks are fairly similar, yet different expansion levels were achieved for each of the distinct directions (i.e., top longitudinal, side longitudinal, and transverse- Figure 6A) as per the restraint configurations.

Generally, the expansion curves of the distinct directions of unrestrained blocks-SP are almost identical regardless of the direction, where a 0.25% expansion (for instance) was achieved at 305, 315, and 340 days in the transverse, longitudinal top, and longitudinal side directions, respectively (Figure 10A). Otherwise, as Figure 10B, 10C and 10D illustrate, all restrained concrete blocks exhibited a much slower ASR-induced expansion development than unrestrained blocks, where a 0.25% expansion was achieved after 340, 360, and 400 days by 1D-SP blocks (Figure 10B), while 370, 460, and 500 days were required for the 2D-SP blocks in the transverse, longitudinal top, and longitudinal side, respectively (Figure 10C). Moreover, the 2D-TX restrained blocks presented faster ASR kinetics than the 2D-SP blocks, reaching 0.25% within 340, 380, and 430 days in the transverse, longitudinal top, and longitudinal side, respectively (Figure 10D). It is worth noting that for the sake of further analysis, the expansions adopted as *"representative"* of a given damage degree were the measurements gathered from the longitudinal side of the blocks (as Figure 6A-points 3 and 4) since they represent the lowest expansion levels among all the surfaces measured (being parallel to the main reinforcement) and are not (or at least less) affected by local effects such as the top drying/wetting cycles [27,40].

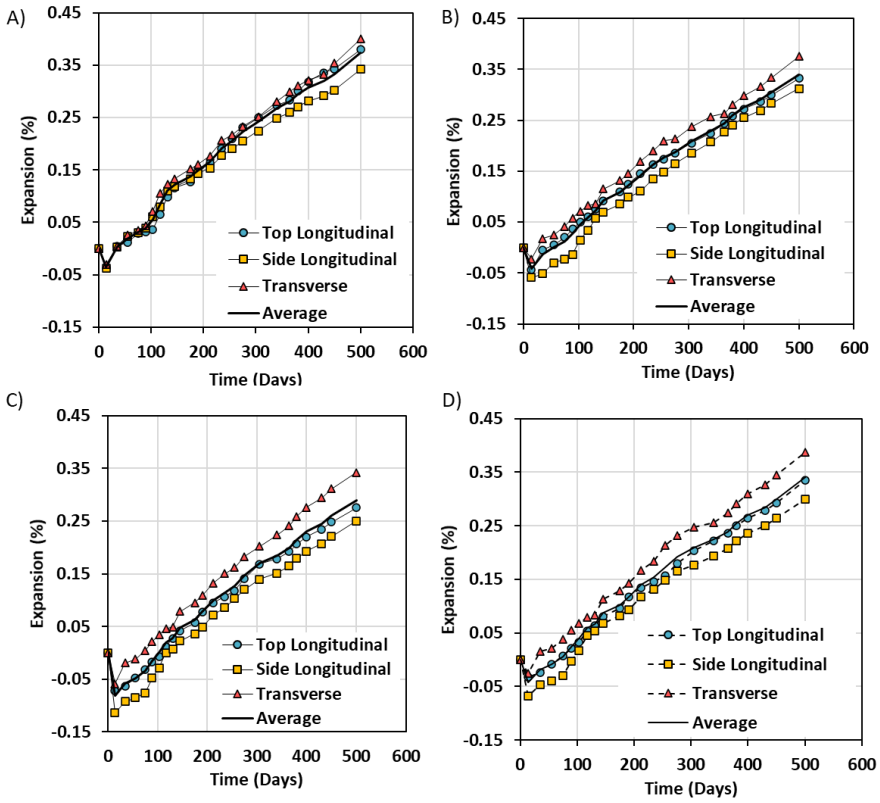

Figure 10: ASR kinetics (expansion vs. time) for A) unconfinement blocks-SP B)1D blocks-SP C) 2D blocks-SP D) 2D blocks-TX displaying distinct surfaces of the blocks.

9.5.2 Reinforcing steel expansion

Figure 11 displays the average recorded induced expansions in the internal steel reinforcing bars (i.e., average value per specimen per direction over time with standard deviations ranging from 0.01% to 0.03%) obtained through strain gauges as a function of time for the distinct steel bars of the ASR-affected concrete blocks. Analyzing the plots, it is observed that all steel bars follow the same expansion trend regardless of their location (i.e., top vs bottom, longitudinal vs transverse - Figure 10), where at the beginning the bars display an important amount of shrinkage (i.e., all directions) and later they follow a fairly linear upward expansion trend. A 0.10% of expansion, for instance, was reached after 255 and 305 days by the top and bottom longitudinal steel bars of the 1D-SP concrete block, respectively (Figure 11A). Moreover, as Figures 11B and 11C display, both 2D blocks present a slightly slower ASR-induced expansion development in the steel reinforcing bars than 1D-SP, where a 0.10% expansion was achieved after 335, 400, 305 and 340 by the top and bottom longitudinal bars as well as the top and bottom transverse steel bars of 2D-SP blocks, respectively. Otherwise, a 0.10% expansion was achieved after 275, 350, 255 and 275 days by the top and bottom longitudinal steel bars as well as by the top and bottom transverse steel bars of 2D-TX blocks, respectively.

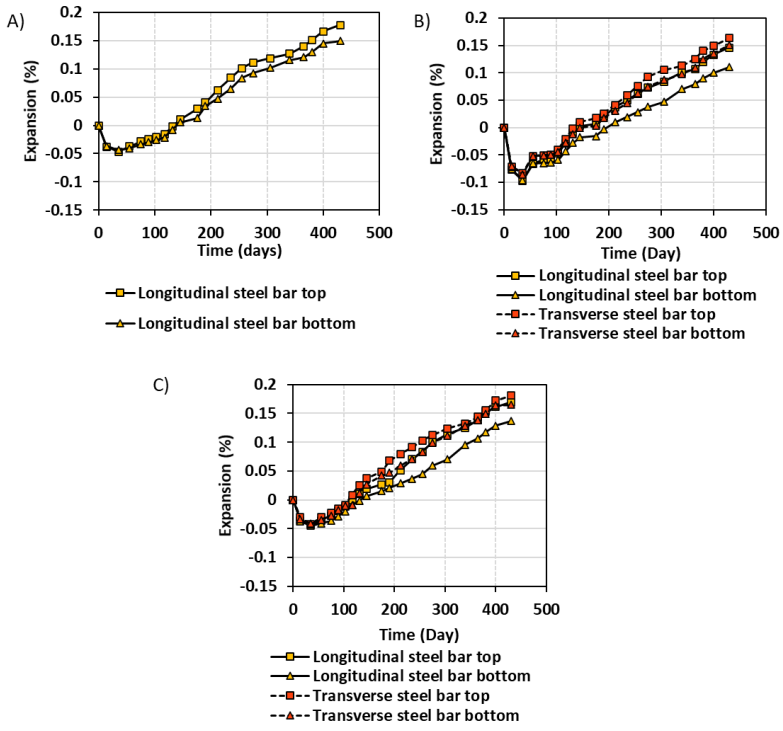

Figure 11: Average expansion (strain) of steel bars in A) 1D-SP, B) 2D-SP, C) 2D-TX in distinct directions.

9.5.3 Visual Inspection

Table 3 summarizes the overall range of the crack openings of the various sets of concrete blocks. Furthermore, Figure 12 illustrates the ‘‘average maximum” crack opening values (i.e., average of the 4

widest cracks found in each set of blocks) measured on the distinct surfaces of each concrete block during the visual inspection. As Table 3 and Figure 12 show, the results of the visual inspection were quite similar among the distinct surfaces for the unrestrained-SP blocks, where the cracks' width ranged from 0.10-1.25 mm were obtained at 0.25% of induced expansion. Moreover, in the case of 1D-SP blocks, the transverse and top surfaces demonstrated a higher range of crack opening (i.e., 0.4-2.5 mm and 0.4-2 mm, respectively), while longitudinal surfaces showed a crack range of 0.1-0.7 mm at 0.25% expansion (i.e., crack opening of 1D blocks: transverse > top > longitudinal). Moreover, both 2D blocks followed a similar trend where the transverse and longitudinal surfaces displayed significantly wider cracks when compared to the top surface. As such, transverse and longitudinal surfaces of 2D-SP presented crack widths ranging from 0.5 to 3 mm while a range of 0.1-0.8 mm was observed on the top surface at 0.25% expansion. Likewise, a range of 0.8-4.5 mm and 0.8-3.5 mm was measured on the transverse and longitudinal surfaces of 2D-TX respectively, whereas the top surface showed a range of 0.1-1 mm at 0.25% expansion (i.e., crack opening of 2D blocks: transverse > longitudinal > top).

Table 3: Visual inspection results from distinct blocks.

Group	Direction/Expansion	Range of crack opening (mm)		
		0.08%	0.15%	0.25%
Unconfined concrete-SP	Longitudinal	0.1	0.1	0.1-1
	Transverse	0.1	0.1	0.1-1.25
	Top	0.1	0.1-0.15	0.1-1
1D Concrete-SP	Longitudinal	0.1	0.1	0.1-0.7
	Transverse	0.1-0.2	0.1-0.45	0.4-2.5
	Top	0.1-0.15	0.1-0.3	0.45-2
2D Concrete-SP	Longitudinal	0.1-0.15	0.1-0.25	0.5-3
	Transverse	0.1-0.35	0.1-0.6	0.5-3
	Top	0.1	0.1-0.15	0.1-0.8
2D Concrete-TX	Longitudinal	0.1-0.35	0.4-3	0.8-3.5
	Transverse	0.1-0.65	0.4-4	0.8-4.5
	Top	0.1	0.1-0.08	0.1-1

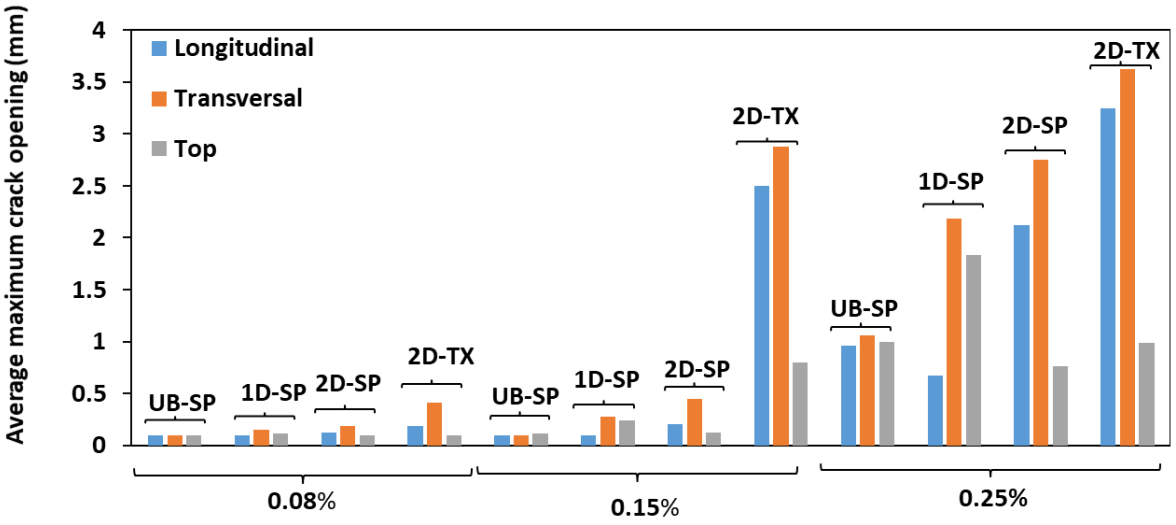

Figure 12: Average maximum crack opening (mm) of distinct surfaces of each set of blocks.

9.5.3.1. Cracking Index (CI)

The Cracking Index (CI) was measured following the drawing of a 400x400 mm square on the three main sides of all concrete blocks (Figure 9); the cracks crossing the vertical and horizontal gridlines were counted and their widths measured (using a magnifying glass and a crack-indicator card). The CI values were then computed using Eq. (2) for the distinct surfaces of each set of concrete blocks. The CI values in mm/m are illustrated in Figure 13. Evaluating the data, it is observed that the higher the ASR-induced expansion level, the higher the CI calculated for all concrete blocks studied. The CI values follow a similar trend as observed in the maximum crack opening measured on the distinct surfaces of the blocks (Figure 12). As such, not a significant difference in CI value of unrestrained concrete-SP specimens was observed on distinct surfaces of the blocks; a CI value of 4.88 mm/m was obtained at 0.25% expansion for all three distinct surfaces. Furthermore, in the case of 1D-SP blocks, transverse and top surfaces displayed a slightly higher CI (6.2 mm/m and 5.8 mm/m, respectively), while the longitudinal surface showed a CI of 5.5 mm/m at 0.25% expansion (i.e., 1D blocks, CI transverse > CI top > CI longitudinal). Otherwise, both 2D blocks followed a similar trend where transverse and longitudinal surfaces presented considerably higher CI values when compared to the top surface. Hence, transverse, longitudinal, and top surfaces of 2D-SP showed a CI of 6.9 mm/m, 6.5 mm/m, and 5.4 mm/m, respectively at 0.25% expansion. Likewise, a CI of 10.5 mm/m and 8.8 mm/m was measured for the transverse and longitudinal surfaces of 2D-TX, respectively, while the top surface showed a CI of 5.7 mm/m at 0.25% expansion (i.e., 2D blocks, CI transverse > CI longitudinal > CI top).

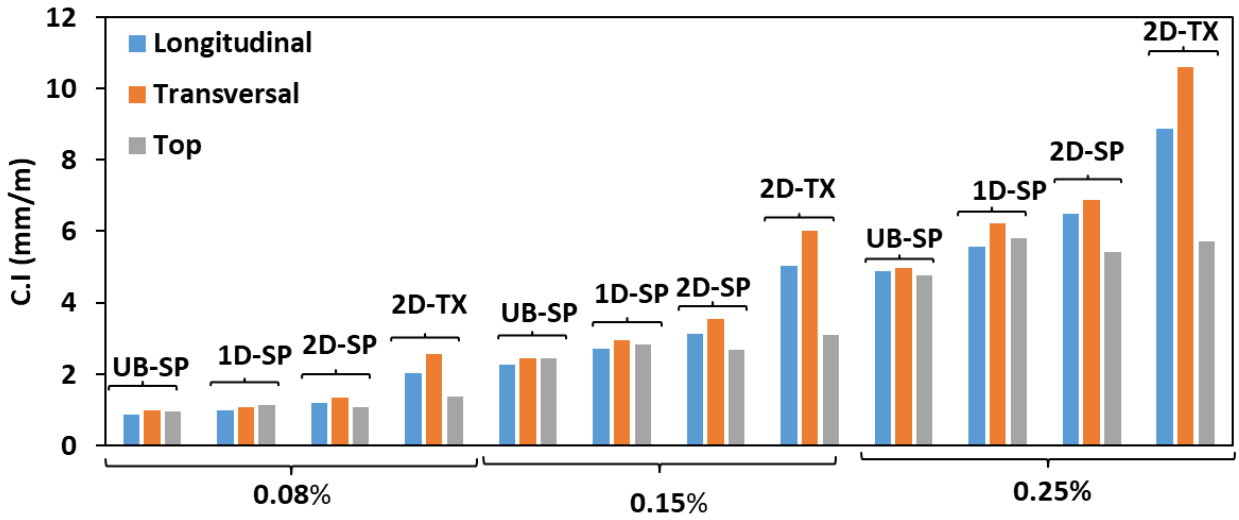

Figure 13: Cracking Index (mm/m) of distinct surfaces of each set of concrete blocks.

9.5.4 Quantitative assessment of damage through DRI

9.5.4.1 Internal damage (cored specimens)

Figure 14 represents the DRI charts obtained from the cores extracted from the distinct directions of all concrete blocks in order to assess their internal damage degrees and features at both low (i.e., 0.08%) and moderate (i.e., 0.15%) expansion levels. Evaluating the graphs, one notices that similar to the previous sections, not a significant difference was observed on the distinct directions of unrestrained-SP blocks where DRI numbers of 342, 341, and 337 were obtained at low expansion and DRI numbers of 578, 575, and 573 were gathered at 0.15% expansion for the vertical, transverse, and longitudinal cores, respectively. On the other hand, all reinforced concrete blocks demonstrated heterogeneity (i.e., anisotropic effect) in their damage development amongst distinct coring directions. As such, vertical and transverse specimens of 1D-SP presented the highest DRI numbers (382 and 366 at low expansion, and 646 and 613 at moderate expansion, respectively), while the specimens extracted longitudinally displayed DRI numbers of 337 and 479 at 0.08% and 0.15% expansion, respectively. Similarly, vertical, transverse, and longitudinal cores of 2D-SP blocks displayed DRI numbers of 401, 310, and 305 at low expansion, and 766, 485, and 479 at moderate expansion, respectively. Moreover, 2D-TX blocks yielded DRI numbers of 455, 356, and 352 at 0.08% expansion and 802, 480, and 475 at 0.15% expansion on the vertical, transverse, and longitudinal cores, respectively.

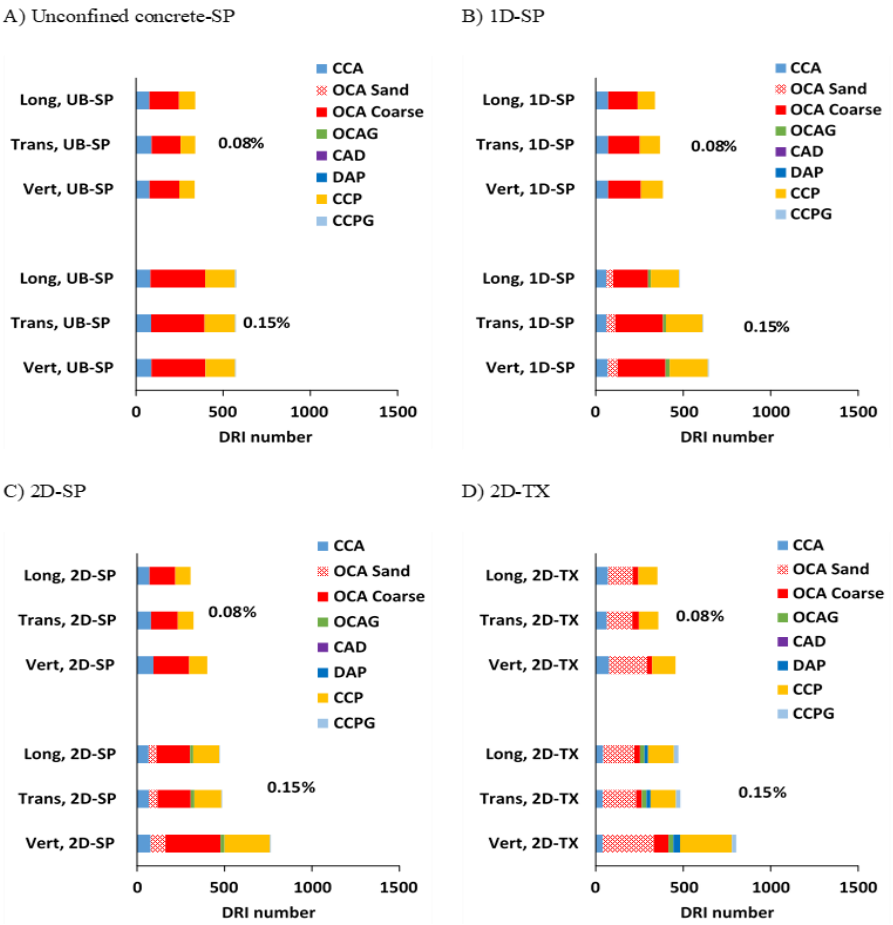

Figure 14: DRI charts for the cored samples analysis from distinct directions of A) Unrestrained blocks-SP, B)1D blocks-SP, C)2D blocks-SP and D)2D blocks-TX.

9.5.4.2. External damage (surface of ASR affected blocks)

Figure 15 illustrates and compares the DRI results obtained on the distinct surfaces of all concrete blocks at various expansion levels (i.e., 0.08%, 0.15%, and 0.25%) of this study. In general, DRI values obtained from the various surfaces of the concrete specimens followed the same trend as the ones gathered from the cored specimens, where the DRI numbers of all specimens increased with the advancement of ASR. There is no significant variation of DRI values among the distinct surfaces of unrestrained concrete-SP for all expansion levels of this study (i.e., 0.08%, 0.15%, and 0.25% of expansion). Otherwise, all reinforced concrete blocks displayed quite different values along each of the blocks' surfaces; DRI numbers of 382, 430, and 420 at 0.08% expansion, 661, 779, and 747 at 0.15% expansion, and 1015, 1150, and 1090 at 0.25% expansion were obtained from the longitudinal, transverse, and top surfaces of the 1D-SP blocks, respectively. Moreover, transverse and longitudinal surfaces of both 2D concrete blocks showed slightly higher DRI numbers when compared to the ones obtained from the top surface. Hence, DRI numbers of 409, 430, and 387 at 0.08% expansion, 754, 792, and 644 at 0.15% expansion and 1102, 1162, and 1012 at

0.25% were gathered from the longitudinal, transverse, and top surfaces of the 2D-SP blocks, respectively. Likewise, the longitudinal, transverse, and top surfaces of the 2D-TX blocks displayed DRI numbers of 457, 493, and 421 at low expansion (i.e., 0.08%), 855, 892, and 720 at moderate expansion (i.e., 0.15%), and 1155, 1255, and 1060 at high expansion (i.e., 0.25%), respectively.

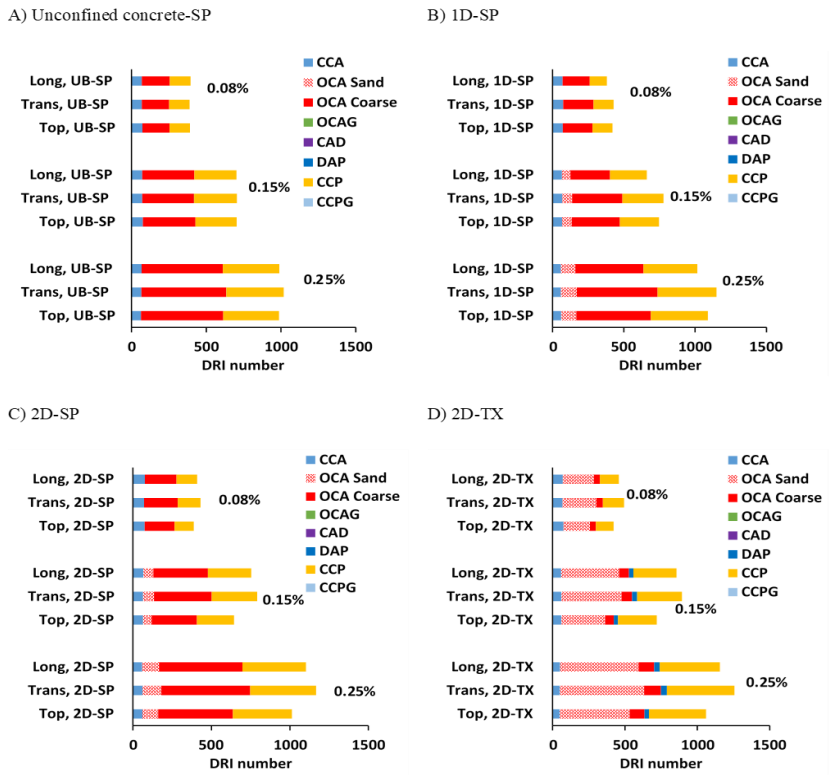

Figure 15: DRI charts for the surface analysis of A) Unrestrained Blocks-SP, B) 1D Blocks-SP, C) 2D Blocks-SP and D) 2D Blocks-TX.

9.6. Discussion

9.6.1 Effects of restraint configuration on ASR-induced expansion

- *Surface strain (demec point)*

Analyzing the expansion levels achieved by the distinct surfaces of the concrete blocks of this study, one notices that while the trend of expansion for the distinct surfaces of unrestrained-SP blocks are almost identical (Figure 10A), the reinforced/confined blocks demonstrated a clear ‘‘expansion transfer’’, where the induced expansion transfers from the restrained directions to the directions with less or no restraint (anisotropic effect), resulting in higher expansion levels in the less restrained directions specimens as previously observed in the literature [3,27]. This, therefore, confirms that the relative expansion levels achieved by the distinct surfaces of all concrete blocks are affected by the restraint direction (i.e., transverse > longitudinal top > longitudinal side) along with the reinforcement configuration and geometric features as per Fournier et. al. [41].

Comparing the achieved expansion levels of the distinct concrete blocks over time, it is observed that the unrestrained-SP blocks yielded a faster/higher expansion kinetics and ultimate expansion than the restrained blocks. The above clearly demonstrates the effect of restraint on mitigating ASR-induced development (especially kinetics) as per [2,3,42]; the higher the restraint level, the slower/ lower the expansion kinetics and expansion level achieved over the same period of time. As such, averaging all directions, it was observed that unrestrained-SP blocks required 310 days followed by the 1D-SP, 2D-TX, and 2D-SP concrete blocks at 370, 380, and 440 days, respectively, to reach 0.25% expansion. This clearly confirms the higher reactivity potential of TX-fine aggregate compared to SP-coarse aggregate as previously reported by [4].

Another interesting point of the expansion measurements of the reinforced concrete blocks is that the expansion levels measured using the external gauge studs (i.e., demec points) installed at the upper part of the longitudinal and transverse sides (i.e., 0.15 m from the top surface- Figure 8 Points 3 and 5) are slightly higher than those obtained from the lower part (i.e., 0.3 m from the top surface- Figure 8 Points 4 and 6) as per Figure 16. As an example, the top and bottom portions of the longitudinal surface, as well as top and bottom portions of transverse surface of 2D-SP blocks, reached 0.26%, 0.23%, 0.36% and 0.32% of expansion after 500 days, respectively. Such an observation could be attribute to the anisotropic behaviour of affected restrained blocks as per Allard et al. [23], which results in deformation of the blocks with a rectangular cross-section into trapezoidal sections after a high (i.e., 0.25%) ASR-induced expansion (Figure 17).

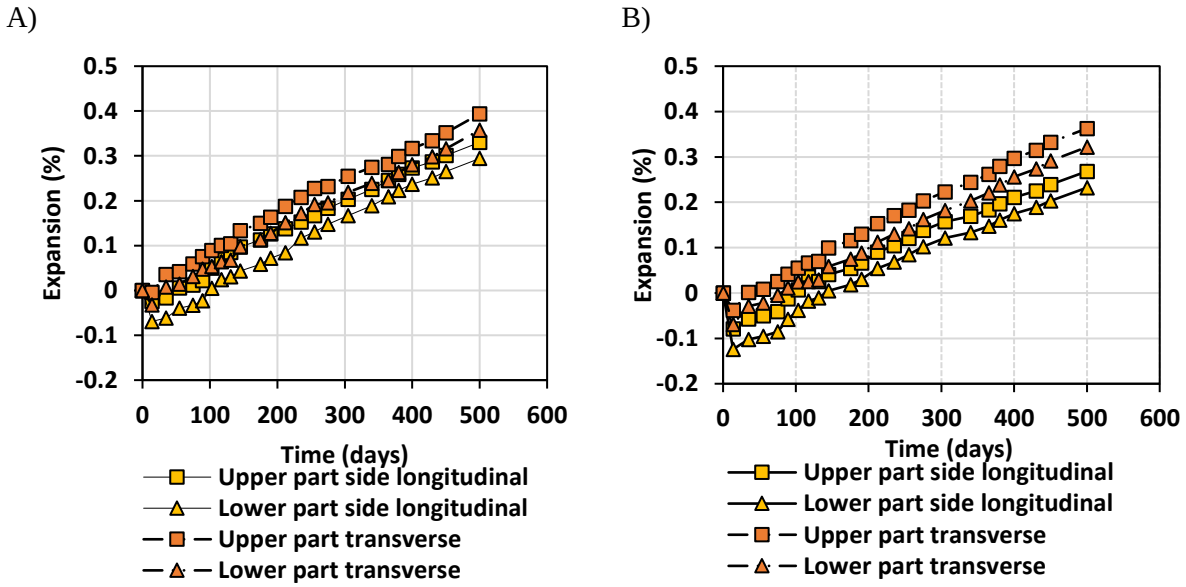

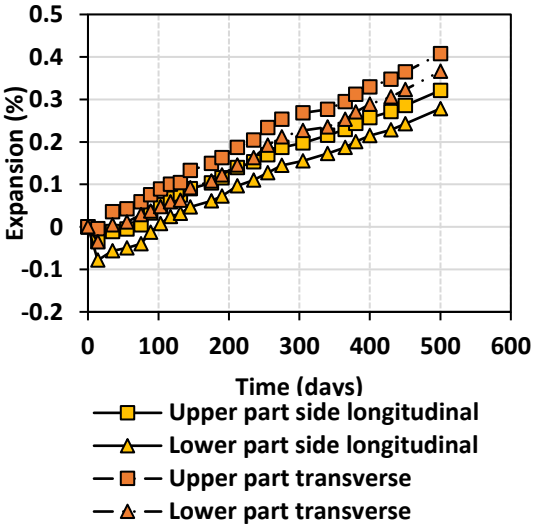

C)

Figure 16: The expansion measurement on various points of longitudinal and transverse surfaces of A) 1D-SP, B) 2D-SP, C) 2D-TX.

A)

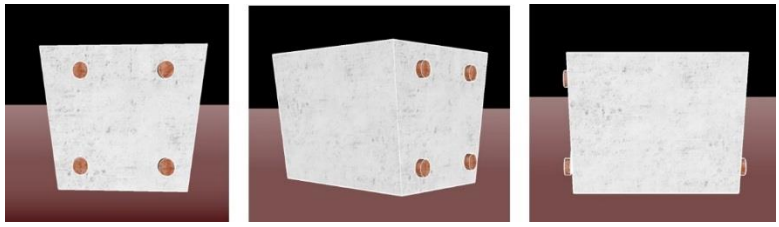

B)

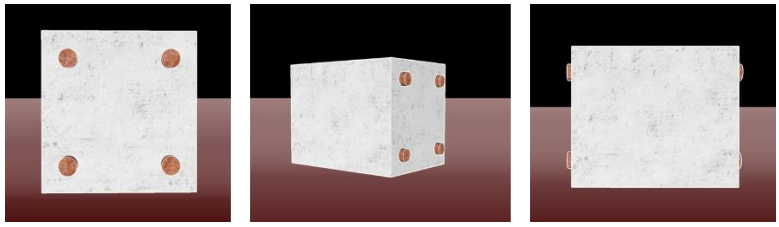

Figure 17: A) Damaged ASR affected concrete block B) Undamaged concrete block.

- *Surface strain (demec point) vs reinforcing bars strain gauges*

As previously mentioned, the strain gauges were coated with wax during the installation process prior to concrete pouring with the aim of extending their service life due to concerns about their long-term durability/reliability in harsh storage conditions. Depending on the restraint configuration, the strain gauges were able to record moderate expansions (i.e., 0.11%-0.18%- Figure 11) of the steel bars. Comparing the latter with the induced expansion obtained through the demec points (i.e., surface strain/expansion- Figure 10), one may notice that the achieved expansion levels measured using demec points are higher than those obtained via strain gauges. The above observation could be due to the presence of cracks that formed around the steel bars, which in turn create local variations in strain and thus may not present reliable expansion/strain measurements of the reinforcing bars as previously discussed by Karthik et al. [33].

Another likely source of the difference between these methods could also be the lack of adequate bond between the concrete and steel bars, especially given the large bar diameter, the proximity to the bar ends (i.e., within the bar development length), and the presence of cracks that further promote debonding. Moreover, the development of creep in the strain gauge adhesive system could result in the observation of different expansion measurements among demec point and steel bar strain gauges over extended periods of time. It is important to notice that the demec points were able to capture the expansion levels obtained at the "core" of the concrete blocks since they have a nominal length of 55mm (Figure 6B) while the block's cover is only 50 mm. Furthermore, most strain gauges stopped recording induced expansions after 430 days of exposure, which could be due to the harsh exposure conditions (i.e., humid and alkaline) of storage.

Finally, comparing the expansion level (i.e., strain) obtained by distinct steel bars of all 2D concrete blocks (Figure 11), one sees that on average transverse steel bars achieved slightly higher expansion levels than those obtained from longitudinal bars. This follows the same trend as per Figure 10, where the top surfaces of the concrete blocks reach slightly higher expansion levels than the ones obtained on the longitudinal surfaces of the blocks (i.e., longitudinal top > longitudinal side). Such observation could clearly be due to an anisotropic ASR damage development in confined concrete as previously reported by [27,44].

9.6.2 DRI measurements (block surface and cored specimens) vs cracking index

As previously stated, DRI was conducted on both surfaces of the deteriorated blocks (external DRI) as well as on the cores retrieved from distinct directions of the affected blocks with the aim to quantitatively compare the internal and external damage (i.e., obtained through the external DRI and C.I) of ASR-affected elements. Evaluating the DRI charts of all concrete blocks of this study (cored specimens vs. surface of the blocks, Figures 14 and 15, respectively), one notices that all specimens demonstrate a general increase in the number of open cracks in the aggregates without and with gel (i.e., OCA and OCAG, respectively) and cracks in the cement paste without and with gel (i.e., CCP and CCPG, respectively) with increasing ASR development (i.e., expansion level). This resulted in an overall increase in the DRI number for all concrete specimens. Moreover, comparing those figures, one observes that the vast majority of surface and cored specimens have almost identical damage features with the exception of ASR gel which has been observed in cored specimens only; the latter might either be leached out during the exposure condition or washed out during the surface preparation. Otherwise, comparing the results obtained from the cored specimens and block's surfaces, one sees that the surfaces of all concrete blocks tend to have significantly higher DRI numbers. As such, the 2D-SP and 2D-TX concrete block's longitudinal surface present 26% and 34% higher DRI values, respectively, when compared to the cores obtained from the longitudinal direction of those blocks at 0.15% of expansion. Such scattering is more pronounced for restrained concrete blocks which is

attributed to the development of expansion and deterioration gradient between the blocks' surface and core as reported by Forster et. al. [44] previously.

Another interesting point to note is that, although the DRI values obtained from both surfaces and cored specimens of unrestrained-SP concrete showed limited variation along distinct directions for the given expansion levels, an anisotropic damage development is identified for all restrained blocks (i.e., both surface and core samples) of this study. Accordingly, greater DRI values on the cored specimens were detected in less/no restraint directions (i.e., vertical and transverse direction for 1D-SP and vertical direction for both 2D blocks) than in restrained directions (Figure 14) as previously observed by Zahedi et al. [3]. On the other hand, DRI values obtained from the surface of the restrained blocks (Figure 15) do not follow a similar trend as the ones gathered from the cored specimens. For instance, while the vertical cores of both 2D concrete blocks demonstrated higher DRI value followed by the transverse and longitudinal cores which showed to have almost identical DRI values (i.e., internal DRI number of 2D blocks: vertical > transverse ≈ longitudinal), the transverse surface of those concrete blocks exhibited the highest DRI number followed by the longitudinal and top surface (i.e., external DRI number of 2D blocks: transverse > longitudinal > top). Analyzing the results obtained from the distinct surfaces of restrained blocks, one realizes that the latter follows the same trend as the calculated CI (Figure 13) and other visual inspection results (Figure 12 and Table 3). The above result could be clearly observed in Figure 18 where it attests that the results gathered from the external DRI are more in accordance with the calculated CI (R^2 is 0.89) rather than the one obtained from the cored specimens (R^2 is 0.21).

Observation of different trends between internal damage and those gathered from the external surfaces of restrained concrete blocks (i.e., significantly higher DRI number) could be due to the presence of higher tensile stresses generated at distinct surfaces of those blocks. Also, considering that the DRI values obtained from the cored specimens have previously been shown to have a good correlation with the amount of ASR-induced expansion in unrestrained [4] and restrained concrete specimens [3]. Therefore, the above discussion clearly demonstrates that the visual integrity (i.e., surface damage) of affected concrete exhibits a significantly higher amount of deterioration when compared to the data gathered from the cored specimens and thus does not accurately represent the actual damage degree of distressed element. Hence, the above, highlights the need for a guideline to correlate external to the internal damage of deteriorated concrete for the practitioners in charge of condition assessment of concrete infrastructure.

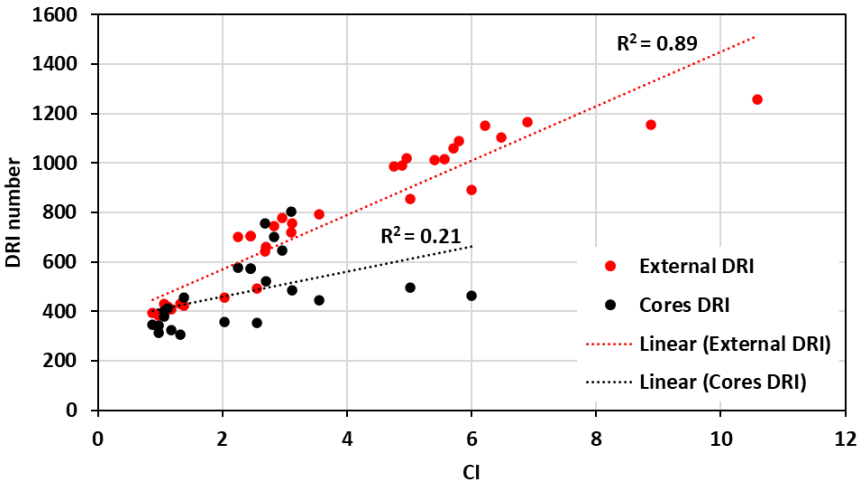

Figure 18: Correlation between the DRI number (obtained on the surface of concrete as well as those gathered from the cored specimens) and CI.

9.6.3 Empirical model to estimate induced expansion in ASR-affected concrete

Previous sections discussed the likely differences between the surface damage and internal deterioration of ASR-affected unrestrained and restrained concrete blocks; with this previous understanding, the current section aims to determine a correlation between visual inspection (i.e., CI) and the actual damage degree presented in affected concrete members. The above correlation could play an important role in condition assessment and to develop better management protocols and to optimize rehabilitation strategies of ASR-deteriorated concrete infrastructure. Therefore, with the aid of the data obtained through the semi-quantitative and qualitative (CI) visual inspection carried out on the distinct surfaces of concrete blocks at the given expansion levels, the inferred expansion (ε) can be defined as follows:

$$\varepsilon\ (\%) = CI/n \qquad (3)$$

where CI is given by Eq. (2) and n is the number of the cracks found in the base length which the CI measurement has been conducted (i.e., in this study 400mm X 400mm).

To validate the proposed normalized CI value, a database obtained on the various surfaces of distinct concrete blocks in the given expansion level of this study is presented in Table 4 and Figure 19. Accordingly, the latter initially compares the calculated CI and the expansion level measured through the use of demec points; this clearly shows that although there is a trend between the aforementioned data, the CI does not show the full picture as evidenced by the wide vertical dispersion of the data (i.e., R^2 is 0.76). Conversely, as per Figure 19B, a clear trend has been found between the actual and calculated damage degree (i.e., via proposed normalized CI- Eq. 3) of distinct concrete blocks (i.e., R^2 is 0.99) of this study. The proposed normalized CI value could give valuable information on the expansion levels of affected

concrete members, regardless of aggregate type and restraint configurations, and thus provides engineers in charge of ASR-affected infrastructure with an idea about the current state of ASR development. Although the results presented in this work can serve as a reference in the process of correlating the cracking index and the actual degree of damage in restrained/unrestrained concrete affected by ASR in the field, the validation of such analysis using field elements could be a topic of interest for future works.

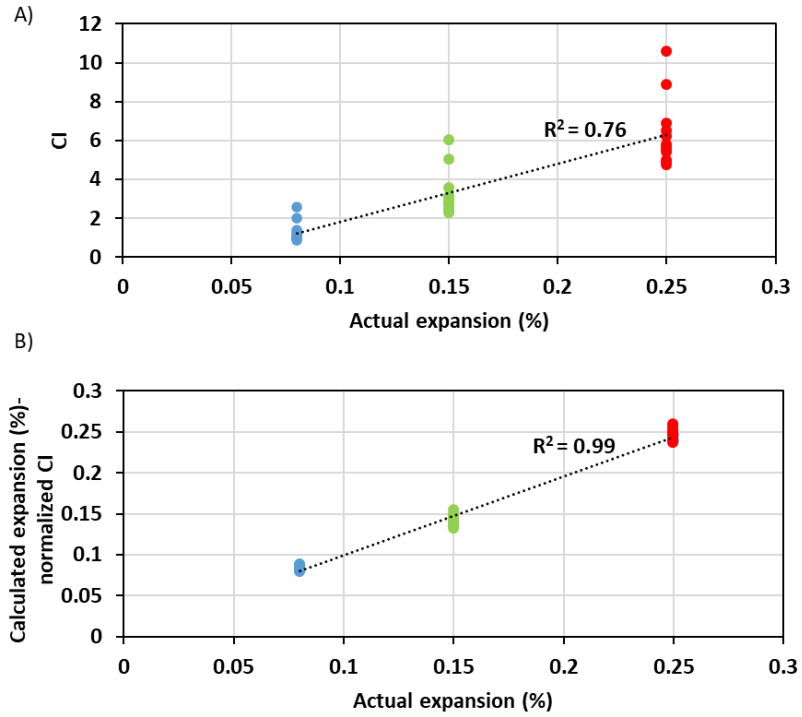

Figure 19: A) Correlation of cracking index (CI) and the actual expansion measured through the demec points and B) Correlation of the actual and calculated expansion level through the proposed normalized CI (i.e., Eq. 3).

Table 4: Measured expansion and expansion prediction through C.I. and crack length.

Presented expansion (%)	Group	Direction	Total number of cracks	C.I. (mm/m)	Calculated expansion (%)
0.08	UB-SP	Longitudinal	10	0.88	0.088
		Transverse	12	0.98	0.081
		Top	12	0.96	0.081
	1D- SP	Longitudinal	12	0.97	0.080
		Transverse	13	1.06	0.081
		Top	14	1.12	0.08
	2D -SP	Longitudinal	14	1.18	0.084
		Transverse	15	1.33	0.088
		Top	12	1.06	0.088
	2D-TX	Longitudinal	24	2.03	0.084
		Transverse	29	2.56	0.088
		Top	17	1.375	0.080
0.15	UB-SP	Longitudinal	17	2.25	0.132
		Transverse	18	2.45	0.136
		Top	18	2.45	0.136
	1D- SP	Longitudinal	19	2.7	0.142
		Transverse	20	2.96	0.148
		Top	19	2.83	0.148
	2D -SP	Longitudinal	22	3.125	0.142
		Transverse	25	3.55	0.142
		Top	19	2.68	0.141
	2D-TX	Longitudinal	35	5.02	0.143
		Transverse	42	6	0.142
		Top	20	3.1	0.155
0.25	UB-SP	Longitudinal	19	4.88	0.256
		Transverse	21	4.96	0.236
		Top	20	4.76	0.238
	1D- SP	Longitudinal	23	5.56	0.241
		Transverse	24	6.22	0.259
		Top	23	5.8	0.252
	2D -SP	Longitudinal	26	6.48	0.249
		Transverse	28	6.89	0.246
		Top	22	5.41	0.245
	2D-TX	Longitudinal	37	8.88	0.240
		Transverse	44	10.59	0.240
		Top	23	5.71	0.248

9.6.4 Models of surface damage generation due to AAR

Analyzing the results gathered from various visual inspection techniques conducted on distinct concrete blocks of this study (Figures 12 and 13 as well as Table 3) clearly demonstrates that the higher the restraint in the concrete, the higher likelihood of damage on the surface of those elements. Therefore, the image-based detection technique has been conducted on various surfaces of each concrete block, as per the method previously described in section 4.3.1. Accordingly, all induced cracks were recorded through the use of visual inspection and image-based detection that are captured every 30 days up to 500 days of exposure. Ultimately, comparing the images captured during the exposure time of each concrete block (e.g., Figure 20), the ASR-induced crack development models found on three main surfaces of the blocks displaying various restraint configurations are proposed (Figures 21, 22 and 23).

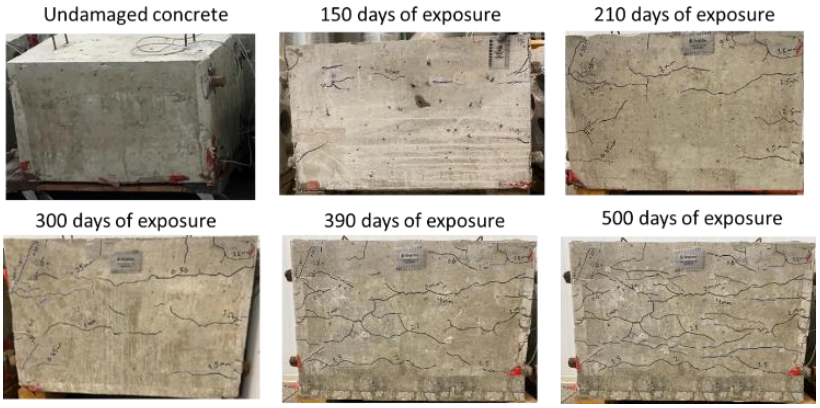

Figure 20: Visual inspection and image-based detection of longitudinal side of 2D-SP during the time.

- *Unrestrained concrete blocks*

Based on the analysis of the images captured during the image base detection procedure as well as the visual inspection data presented before (i.e., quantitative and semi quantitative visual inspection, CI as well as the external DRI), the following damage model of ASR development against expansion on the surface of unrestrained concrete incorporating reactive coarse aggregate (SP) is proposed and illustrated in Figures 21. Evaluating the figures, one notices that at the low expansion level (0.08%), most of the generated cracks were observed mostly near the corners of the distinct surfaces of the blocks, with some random cracks appeared in the middle of each surface. ASR-induced cracks with a random nature following a polygonal pattern, known as "map-cracking", started to appear on the distinct surfaces of the unrestrained-SP blocks at 40-85 days of exposure: about 65 days on average. These randomly oriented cracks further provided a pathway for ingress of moisture into the concrete blocks which in turn promoted the progress of ASR [16,29,44,46]. At the moderate expansion level (0.15%), the formation of new cracks was also followed by the widening and lengthening of the existing cracks. Such phenomenon could be attested by evaluating the surface damage features quantifications (counts and percentage- Figure 24A and B, respectively). Accordingly, the proportion of the cracks range 0.05-0.25mm was found to decrease with increasing expansion (i.e., 0.15% and 0.25%) and instead the proportion of the wider cracks (i.e., greater than 0.25mm) is increasing; this suggests that some of the former cracks are widened by the progress of ASR. Also comparing the number of cracks observed at low expansion level of unrestrained blocks with those found at moderate expansion, one sees that the number of newly generated cracks dropped by 52%. At the high expansion level (0.25%), on one hand, the number of newly generated cracks reduced by 73% when compared to the moderated damage blocks. On the other hand, the crack widening procedure has been continued where the number of cracks with size greater than 1mm was increased from 2 to 8 and 12 at 0.08%, 0.15% and 0.25% of expansion, respectively. The above discussion clearly attested that the development of the ASR-induced crack on the surface of affected concrete follows the minimum energy

law where the expanding system prefers to propagate those previously generated cracks rather than creating new ones [47].

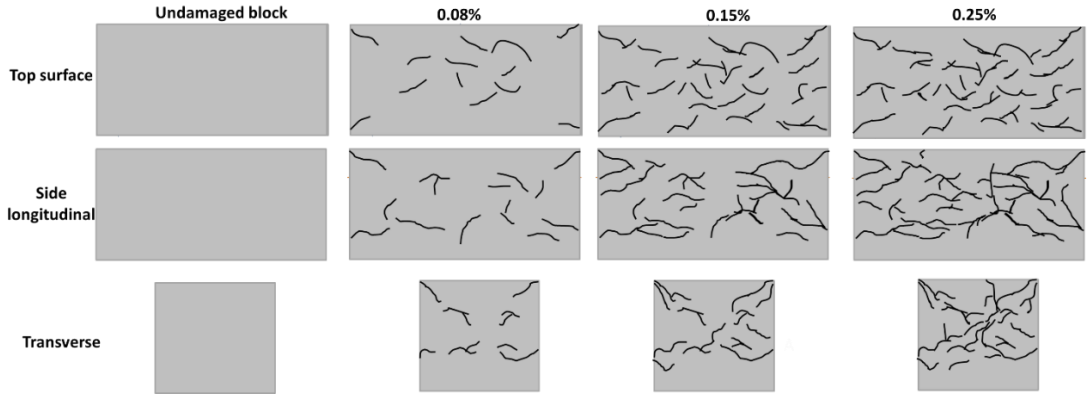

Figure 21: Qualitative ASR damage model of unrestrained block vs. levels of expansion between 0.08 and 0.25%.

- *1D concrete blocks*

Similar to the unrestrained concrete, the damage model for 1D concrete blocks has been developed as per Figure 22. At the low expansion level (0.08%), most of the damage features observed on the top and longitudinal surfaces of the 1D blocks were generated at the edge of those surfaces and aligned along the main reinforcement bars. Otherwise, more randomly oriented cracks were noticed on the transverse side of 1D-SP blocks which could be attributed to the lack of restraint across those surfaces. ASR-induced cracks started to appear on the surface of 1D-SP concrete blocks between 70-100 days of exposure: about 85 days on average. Similar to unrestrained-SP blocks, new cracks continued to be generated as the alkali reaction progressed, but the number of "new" cracks decreased with the increase in length and width of the cracks already formed; as such the number of new cracks at moderate expansion was reduced by 49% (Figure 24). Both newly generated and previously formed cracks were likely propagated parallel to the main reinforcement bars at the top and longitudinal surface, while more randomly oriented cracks keep propagating in the transverse surface of 1D block at moderate expansion. Following the same trend, the number of newly generated cracks reduces where the length and width of the previously formed cracks increase. For instance, the number of cracks greater than 1mm at the moderate and high expansion levels of 1D blocks is 63% and 78% higher when compared to the low expansion level, respectively.

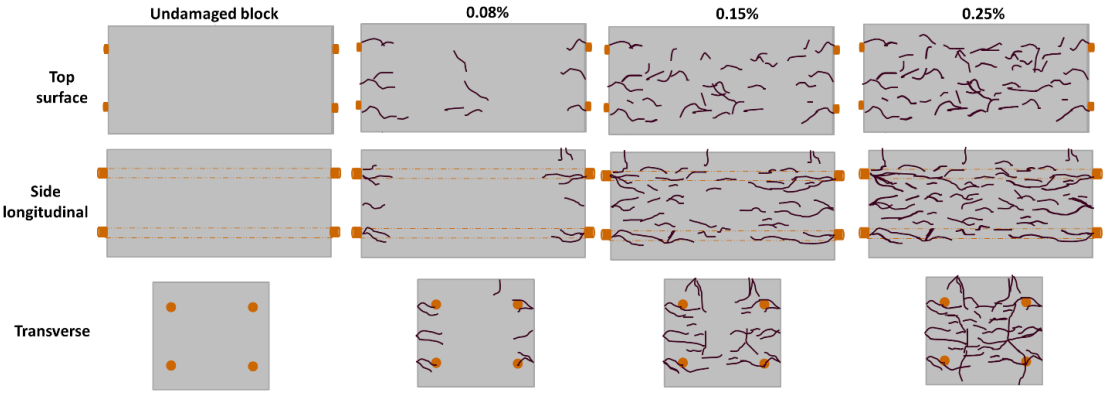

Figure 22: Qualitative ASR damage model of 1D block vs. levels of expansion between 0.08 and 0.25%.

- *2D concrete blocks*

At the beginning of the ASR-induced development (0.08%), most of the cracks generated at top and longitudinal surface were parallel to the direction of the existing rebars; i.e., while most of the cracks generated on the side longitudinal surface are parallel to the longitudinal bars, the majority of the distress features observed on top surface were propagated parallel to the transverse steel bars. On the other hand, similar to 1D-SP blocks, more randomly oriented cracks were identified on the transverse side of 2D blocks which again, could be attributed to the lack of restraint across those surfaces. The ASR-induced cracks started to appear on the surfaces of 2D-SP and 2D-TX between 95-125 and 75-110 days of exposure: about 115 and 90 days on average, respectively. Afterward, at 0.15% of expansion, those previously formed cracks in the early stages of the reaction follow the minimum energy law (i.e., increase in length and width of the cracks instead of creating new ones). As such, the number of newly generated cracks at the moderate expansion reduced by 50% and 41% for 2D-SP and 2D-TX, respectively, when compared to the low expansion. Afterward, at 0.25% of expansion, the propagation of those previously cracks continues where for instance the number of the cracks greater than 1 mm is 54% and 57% higher at moderated expansion level (0.15%) as well as 74% and 78% higher at high expansion level (0.25%) when compared to the low expansion level (0.08%) of 2D-SP and 2D-TX, respectively. Nevertheless, although the orientation of damage in both 2D concrete are almost identical, comparing the damage features observed in 2D-SP and 2D-TX, one sees that restrained blocks incorporating Texas fine aggregate experience a significantly higher amount of damage; for instance, the total number of cracks on the surface of 2D-SP and 2D-TX is 175 and 225 at high expansion level (0.25%), respectively. The above results are in accordance with those gathered from the distinct visual inspection techniques (Figures 12 and 13) and external DRI (Figure 15). This therefore clearly suggested the different deterioration mechanisms taking place in concrete blocks incorporating reactive fine (i.e., TX) and coarse (i.e., SP) aggregates.

Finally, comparing the proposed damage models of distinct concrete blocks, one sees that various restraint configurations not only change the propagation (i.e., orientation) of the damage, but also it could impact the number and severity of the visual damage. As such, the higher the restraint, the higher the number of cracks on the surface of concrete blocks. The above results are in accordance with the previous findings of this study where higher CI values (Figure 13 and other visual inspection results-Figure 12) were obtained from distinct surfaces of 2D block, followed by 1D blocks and unrestrained concrete. Such phenomenon could be described by the fact that the restraint cage generally tries to decrease/mitigate the damage in ASR affected concrete, thus the damage transfer could take place and transfer that deterioration from the steel cage to the concrete cover and surface of affected elements as per [22,23].

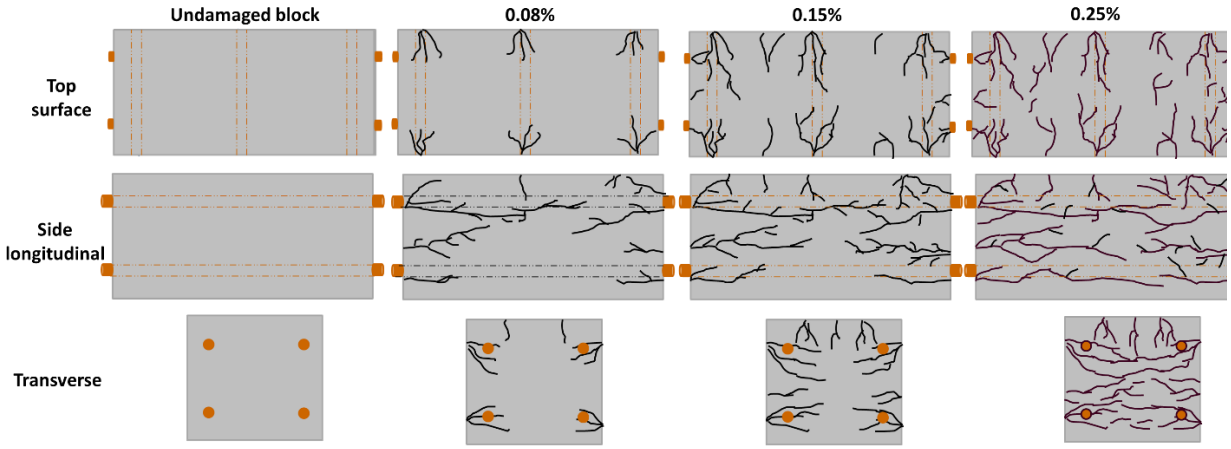

Figure 23: Qualitative ASR damage model of 2D block vs. levels of expansion between 0.08 and 0.25%..

A)

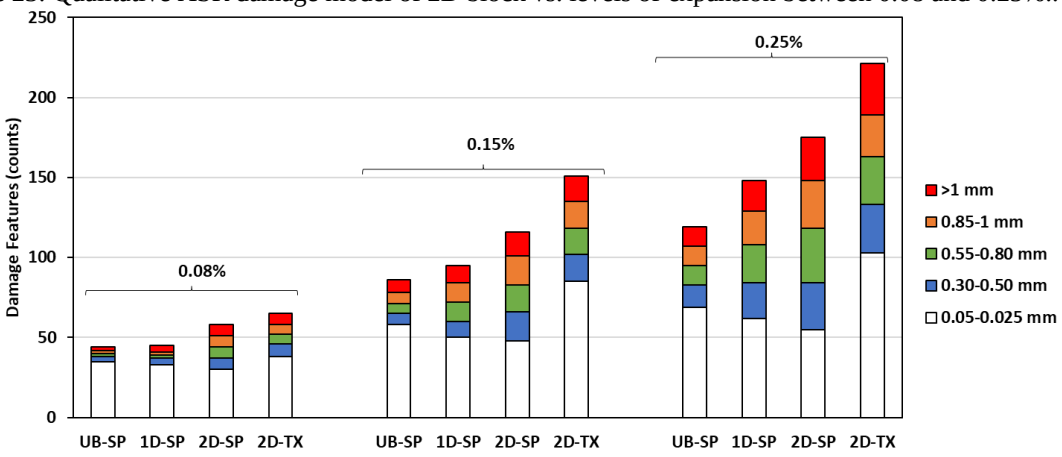

B)

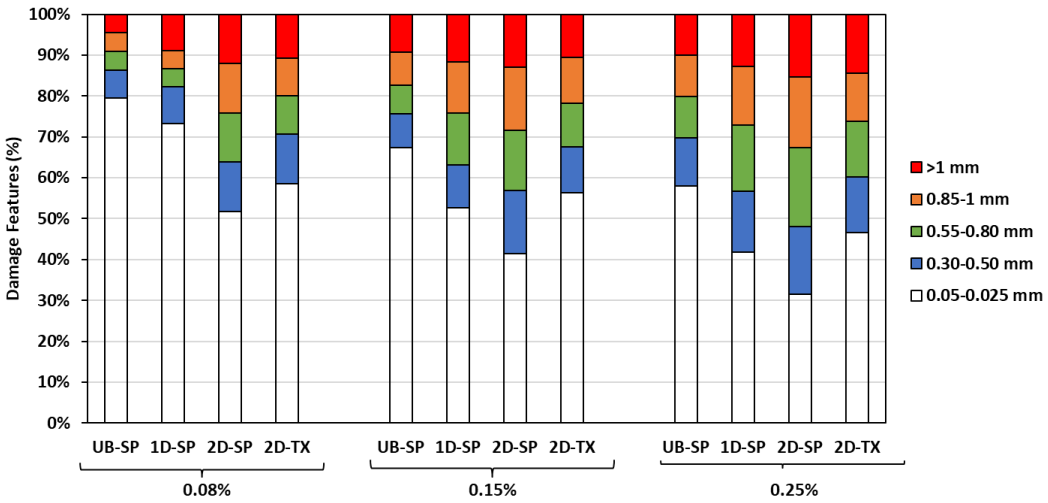

Figure 24: The generated damage Features on the surface of various concrete blocks of this study in A) counts and B) percentage (%).

9.7. Conclusion

Based on the results obtained through the evaluation of ASR-induced expansion, visual inspection, and microscopic assessment on the surfaces and extracted cores from reinforced concrete blocks, it is confirmed that the restraint configuration does affect the development of ASR in terms of expansion and the development of the physical and microscopic distress features. The following conclusions may be drawn from the findings of this research:

- Comparing ASR-induced development of the distinct concrete blocks appraised in this work, one attests that the restraint helps to the mitigation ASR-induced expansion; the higher the restraint, the lower the expansion attained over time. Moreover, comparing the achieved expansion by distinct surfaces of restrained blocks, one verifies the anisotropic behavior on the latter where the induced expansion transfers from restrained to less/non restrained directions. The latter shows clearly the influence of restraint direction on the achieved expansion levels (i.e., transverse > longitudinal top > longitudinal side). At the end of exposure, all restrained concrete blocks with a rectangular cross-section deformed into trapezoidal sections after a high (i.e., 0.25%) ASR-induced expansion.

- The results obtained using the strain gauges affixed to the steel bars demonstrated significant differences compared to those obtained using the DEMEC points. This could be due to localized strain variations, lack of an adequate bond between the concrete and steel bars, and development of creep in the strain gauge adhesive system.

- The results of distinct visual inspection techniques (qualitative, semi quantitative and CI) demonstrated that the higher the concrete blocks are restrained, the higher likelihood of damage on

the surface of those elements, this would possibly increase the likelihood of reinforcement corrosion in the long term.

- Comparing the results obtained through the petrographic analysis of cored specimens and block surfaces, it seems quite clear that not only surface specimens presented significantly higher damage than cored samples but also, they do not follow the same trend; the results of external DRI were in accordance with those gathered through the cracking index and other visual inspection techniques.

- Although compared to the conventional visual inspection method, the cracking index has shown to be quite effective to assess the visual integrity on the surface of affected concrete, it is still hard to correlate those results with the internal deterioration of those members. Thus, this study proposed a normalized CI value which correlates strongly with the measured expansion level, which can allow engineers to estimate damage degree based only on a visual inspection of the concrete surface.

- Analysis of the pictures captured through the use of image-based detection techniques helps to better understand the procedure of ASR-induced damage development on the surfaces of concrete blocks where the latter follow the minimum energy law. As such, a significant number of new cracks will generate on the surface of concrete elements at the beginning of the chemical reaction, later it is easier for the expanding system to propagate (widening and lengthening) those initially formed cracks rather than creating new ones. Thus, the rate of crack generation on the surface of concrete elements will start to slow down.

- Models for the development of ASR damage on the surface of affected elements as a function of expansion in concrete displaying distinct restraint configurations were proposed. While the distinct surfaces of unrestrained concrete blocks tend to propagate ASR-induced cracks with a random nature following a polygonal pattern, known as “map-cracking”, most of the damages observed on the top and longitudinal surface of 1D were propagated along the longitudinal rebars. Conversely, the vast majority of the ASR-induced cracks on the transverse surfaces were randomly oriented which could be attributed to the lack of restraint across those surfaces. Moreover, while the ASR cracks on the top surface of 2D blocks were aligned along the transverse rebars, most of the damage on the longitudinal surface was developed parallel to the longitudinal steel bars. Also, the transverse surfaces of 2D blocks follow the same trend as the 1D blocks where more randomly oriented cracks were propagated. Moreover, comparing the various damage models proposed in this work, one sees that the higher the restraint, the higher the number of cracks generated on the surface of affected concrete; Such observation can be due to the mitigation nature of steel bars where the latter intended

to decrease/mitigate the damage on the case but rather transfer those damage to the concrete cover and surface of affected elements.

- The results of visual inspection and the expansion measurement conducted on concrete blocks incorporating distinct aggregate particles clearly demonstrated the different deterioration mechanisms taking place; concrete specimens made of reactive fine aggregates not only display faster ASR kinetics and higher potential for ultimate expansion than those manufactured with reactive coarse aggregates, but they also show a quite different deterioration pattern.

Acknowledgments

The authors would like to thank Drs. Gamal Elnabelsya and Muslim Majeed, technical officers of Materials and Structures Laboratory in the Department of Civil Engineering at the University of Ottawa, who helped with the manufacturing and testing of the test specimens used in this project. Likewise, the authors would like to thank Mr. Matthew McDonald and his team from Advance Cutting & Coring Ltd. for facilitating the crucial process of drilling and extracting core specimens from the studied concrete blocks. Lastly, Mr. Zahedi benefits from the prestigious University of Ottawa admission scholarship for international PhD students.

References

[1] P. Chang, A. Flatau, S. Liu, Review paper: health monitoring of civil infrastructure, Struct., Heal. Monit. 2 (2003) 257–267.
[2] A. Zahedi, L. Sanchez, M. Noël, Effect of Confinement on AAR-induced expansion and damage, in: 16th ICAAR, Int. Conferance Alkali Aggreg. React. Concr. 1-3 June, Lisboa, Portugal, 2020.
[3] A. Zahedi, C. Trottier, L. Sanchez, M. Noël, Microscopic Assessment of ASR-Affected Concrete Under Confinement Conditions, Cem Concr Res. (2021) 106456. https://doi.org/https://doi.org/10.1016/j.cemconres.2021.106456.
[4] L.F.M. Sanchez, B. Fournier, M. Jolin, D. Mitchell, J. Bastien, Overall assessment of Alkali-Aggregate Reaction (AAR) in concretes presenting different strengths and incorporating a wide range of reactive aggregate types and natures, Cem. Concr. Res. 93 (2017) 17–31. https://doi.org/http://dx.doi.org/10.1016/j.cemconres.2016.12.001.
[5] S. Agnisarman, S. Lopes, K. Chalil, K. Piratla, Automation in Construction A survey of automation-enabled human-in-the-loop systems for infrastructure visual inspection, Autom. Constr. 97 (2019) 52–76. https://doi.org/10.1016/j.autcon.2018.10.019.
[6] L. David, M. Gregory, Review of robotic infrastructure inspection systems, J. Infrastruct. Syst. 23 (2017) 1–12.
[7] B. Kim, Image - based concrete crack assessment using mask and region - based convolutional neural network, (2019) 1–15. https://doi.org/10.1002/stc.2381.
[8] R. H, J. M., Permeability and diffusivity of high performance concrete with and without cracks., in: 32 Adv. Concr. Struct. Proc. Int. Conf. ICACS, China, 2003: pp. 32–43.
[9] M.C. Torrijos, G. Giaccio, R. Zerbino, Mechanical and transport properties of 10 years old concretes prepared with different coarse aggregates, 44 (2013) 706–715.
[10] H. Kim, E. Ahn, M. Shin, S. Sim, Crack and Noncrack Classification from Concrete Surface Images Using Machine Learning, Struct. Heal. Monit. 18 (2019) 725–738.

https://doi.org/10.1177/1475921718768747.
[11] V. Gattulli, L. Chiaramonte, Condition Assessment by Visual Inspection for a Bridge Management System, 20 (2005) 95–107.
[12] S. Kabir, ARTICLE IN PRESS NDT & E International Imaging-based detection of AAR induced map-crack damage in concrete structure, 43 (2010) 461–469. https://doi.org/10.1016/j.ndteint.2010.04.007.
[13] C. Koch, K. Georgieva, V. Kasireddy, B. Akinci, P. Fieguth, Advanced Engineering Informatics A review on computer vision based defect detection and condition assessment of concrete and asphalt civil infrastructure, Adv. Eng. Informatics. 29 (2015) 196–210. https://doi.org/10.1016/j.aei.2015.01.008.
[14] J. Golden, E. Gomes, A. Roy, Y.T. Su, Analysis of a Historical Failure, report no. 1: University of California, Berkeley, 2018. https://doi.org/10.13140/RG.2.2.17401.01129.
[15] J.G.M. Wood, Implications of the collapse of the de la Concorde overpass, in: 4th Int. Conf. 'Forensic Eng., 2008: pp. 16–18.
[16] B. Fournier, M. Bérubé, Alkali–Aggregate Reaction in Concrete: a Review of Basic Concepts and Engineering Implications, Can. J. Civ. Eng. 27 (2000) 167–191. https://doi.org/10.1139/l99-072.
[17] B. Fournier, A. Bérubé, J. Folliard, M. Thomas, Report on the Diagnosis, Prognosis, and Mitigation of Alkali-Silica Reaction (ASR) in Transportation Structures, Report No. FHWA-HIF-09-004, Federal Highway Administration, U. S. Department of Transportation, Washington, DC, 2010.
[18] B. Fournier, M.A. Berube, K.J. Folliard, M. Thomas, Report on the Diagnosis, Prognosis, and Mitigation of Alkali-Silica Rection (ASR) in Transportation Structures, Austin, 2010.
[19] L.F.M. Sanchez, B. Fournier, D. Mitchell, J. Bastien, Condition assessment of an ASR-affected overpass after nearly 50 years in service, Constr. Build. Mater. 236 (2020) 117554. https://doi.org/10.1016/j.conbuildmat.2019.117554.
[20] N. Smaoui, B. Fournier, M. Bérubé, B. Bissonnette, B. Durand, Evaluation of the expansion attained to date by concrete affected by alkali silica reaction. Part II: Application to nonreinforced concrete specimens exposed outside, Can. J. Civ. Eng. 31 (2004) 997–1011. https://doi.org/10.1139/l04-074.
[21] A. Leemann, T. Katayama, I. Fernandes, M.A. Broekmans, Types of alkali-aggregate reactions and the products formed,", Institut. Civ. Eng. - Constr. Mat. 169 (2016) 128.
[22] R.H. Courtier, The Assessment of ASR-Affected Structures, 12 (1990) 191–201.
[23] A. Allard, S. Bilodeau, F. Pissot, B. Fournier, J. Bastien, B. Bissonnette, Expansive behavior of thick concrete slabs affected by alkali-silica reaction (ASR), Constr. Build. Mater. 171 (2018) 421–436. https://doi.org/10.1016/j.conbuildmat.2018.03.159.
[24] N. Smaoui, M.A. Bérubé, B. Fournier, B. Bissonnette, B. Durand, Evaluation of the expansion attained to date by concrete affected by alkali-silica reaction. Part I: Experimental study, Can. J. Civ. Eng. (2004). https://doi.org/10.1139/L04-051.
[25] R. Esposito, C. Anaç, M.A.N. Hendriks, Influence of the Alkali-Silica Reaction on the Mechanical Degradation of Concrete, J. Mater. Civ. Eng. 28 (2016). https://doi.org/10.1061/(ASCE)MT.1943-5533.0001486.
[26] N. Smaoui, Contribution à l'évaluation du comportement structural des ouvrages d'arts affectés de réaction alcalis-silice., Département Génie Civil, Univ. Laval, Quebec, Canada. (2003).
[27] P. Morenon, S. Multon, A. Sellier, E. Grimal, F. Hamon, E. Bourdarot, Impact of stresses and restraints on ASR expansion, Constr. Build. Mater. 140 (2017) 58–74. https://doi.org/10.1016/j.conbuildmat.2017.02.067.
[28] A. Zahedi, N. Zubaida, L. Sanchez, P. Rivard, Effect of external confinement on Alkali-Silica Reaction (ASR)-induced expansion and damage, in: 16th ICAAR, Int. Conferance Alkali Aggreg. React. Concr. 1-3 June, Lisboa, Portugal, 2020.
[29] S. Multon, J.-F. Seignol, F. Toutlemonde, Structural behavior of concrete beams affected by alkali-silica reaction, ACI Mater. J. 102 (2005) 67–76.
[30] S. Multon, F. Toutlemonde, Effect of applied stresses on alkali-silica reaction-induced expansions., Cem. Concr. Res. 36 (2006) 912–920.
[31] M. Noël, L. Sanchez, R. Martin, B. Fournier, J. Bastien, Structural Implications of Internal Swelling Reactions in Concrete : a Review, in: 15th Int. Conf. Alkali-Aggregate React., Sao Paulo, Brazil, 2016.

[32] M.D.A. Thomas, B. Fournier, K.J. Folliard, Y.. Resendez, ALKALI SILICA REACTIVITY SURVEYING AND TRACKING GUIDELINES, 2012.
[33] M.M. Karthik, J.B. Mander, S. Hurlebaus, Deterioration data of a large-scale reinforced concrete specimen with severe ASR / DEF deterioration, Constr. Build. Mater. 124 (2016) 20–30. https://doi.org/10.1016/j.conbuildmat.2016.07.072.
[34] P.A. Dunbar, P.E. Grattan-Bellew, Results of damage rating evaluation of condition of concrete from a number of structures affected by ASR, CANMET, in: ACI Int. Work. Alkali–Aggregate React. Concr., Darmouth, Canada, 1995: pp. 257–266.
[35] P.E. Grattan-Bellew, A. Danay, Comparison of Laboratory and Field Evaluation of AAR in Large Dams, in: Int. Conf. Concr. AAR Hydroelectr. Plants Dams, Canadian Electrical Association in association with Canadian National Committee of the International Commission on Large Dams, Fredericton, New Brunswick, Canada, 1992: p. 23.
[36] V. Villeneuve, B. Fournier, Determination of the damage in concrete affected by ASR — the damage rating index (DRI), in: 14th ICAR — Int. Conf. Alkali– Aggreg. React. Concr., Austin (Texas), 2012.
[37] ASTM C1293, Standard test method for determination of length change of concrete due to alkali-silica reaction, Annu. B. ASTM Stand. (2015) 1–7. https://doi.org/10.1520/C1293-08B.2.
[38] Standard Counsil of Canada, CSA A23.3:19:Design of concrete structures, 2019.
[39] Standard Counsil of Canada, CSA S6:19: Canadian Highway Bridge Design Code, 2019.
[40] D. Wald, M.T. Allford, O. Bayrak, T.D. Hrynyk, Development and multiaxial distribution of expansions in reinforced concrete elements affected by alkali – silica reaction, Struct. Concr. 18 (2017) 914–928. https://doi.org/10.1002/suco.201600220.
[41] B. Fournier, P.C. Nkinamubanzi, R. Chevrier, Comparative field and laboratory investigations on the use of supplementary cementing Materials to control alkali-silica reaction in concrete, in: 12th Int. Conf. Alkali-Aggregate React., Beijing, China, 2004.
[42] B.P. Gautam, D.K. Panesar, "A New Method of Applying Long-Term Multiaxial Stresses in Concrete Specimens undergoing ASR, and their Triaxial Expansions," Mater. Struct. 49 (2016) 3495–3508.
[43] S. Sørgaard, O. Oseland, T. Kanstad, M.A.N. Hendriks, E. Rodum, Experimental investigation of ASR-affected concrete – The influence of uniaxial loading on the evolution of mechanical properties, expansion and damage indices, Constr. Build. Mater. 245 (2020) 118384–118398. https://doi.org/10.1016/j.conbuildmat.2020.118384.
[44] S.W. Forster, R.L. Boone, M.S. Hammer, J.F. Lamond, D.S. Lane, R.E. Miller, S.E. Parker, A. Pergalsky, J.S. Pierce, M.Q. Robert, J.W. Schmitt, R.E. Tobin, State-of-the-Art Report on Alkali-Aggregate Reactivity Reported by ACI Committee 221, 98 (1998) 1–31.
[45] L.F.M. Sanchez, B. Fournier, M. Jolin, M.A.B. Bedoya, J. Bastien, J. Duchesne, Use of Damage Rating Index to quantify alkali-silica reaction damage in concrete: Fine versus coarse aggregate, ACI Mater. J. 113 (2016) 395–407. https://doi.org/10.14359/51688983.
[46] S. Fan, J.M. Hanson, Effect of alkali silica reaction expansion and cracking on structural behavior of reinforced concrete beams, ACI Struct. J. 95 (1998) 498–505.
[47] L.F.M. Sanchez, B. Fournier, M. Jolin, J. Duchesne, Reliable quantification of AAR damage through assessment of the Damage Rating Index (DRI), Cem. Concr. Res. 67 (2015) 74–92. https://doi.org/10.1016/j.cemconres.2014.08.002.

10. INFLUENCE OF THE RESTRAINT CONFIGURATION ON ALKALI-SILICA REACTION (ASR) REACTION PRODUCT'S FEATURES

Andisheh Zahedi [1], Leandro Sanchez [2], Martin Noël [3]

Abstract

A number of studies have been conducted to characterize the different properties of either natural or synthetic ASR reaction products in concrete. Yet, the effect of distinct restraint configurations on ASR gel features obtained from aggregate particles, ITZ, and cement paste of concrete has not been fully investigated. Therefore, this study aims to characterize the impact of restraint on reaction product through chemical (i.e., SEM/EDS) and physical (i.e., micro-indentation). Nine concrete blocks incorporating a highly reactive coarse aggregate and various restraint configurations (none, 1D, and 2D) were produced in the laboratory, stored in an environmental chamber at 38°C and 100% RH and continuously monitored over time. Once they reached a moderated expansion level (i.e., 0.15%), cores were retrieved from the three main directions (i.e., vertical, transverse, and longitudinal), ASR reaction products were located, and the aforementioned tests were conducted on the specimens. Results show that the chemical composition and mechanical properties of ASR reaction product obtained from distinct locations of restrained blocks demonstrate an important anisotropic behavior as per the direction and restraint configuration.

Keywords: Alkali-Silica Reaction product, Chemical composition, mechanical properties, Restraint.

10.1 Introduction

Alkali-Silica Reaction (ASR), a physicochemical reaction between the metastable SiO2 found in the aggregates and alkaline pore solution of the concrete which is followed by the formation of ASR gel, is one of the most deleterious damage mechanisms affecting the durability and serviceability of vital infrastructure worldwide [1–3]. Recently, Leemann et al. [4] suggested that ASR product is initially developed in pre-existing pores of the aggregate particles adjacent to the cement paste and later they move into the interior part of aggregate particles as the reaction continues. This intrusion is accompanied by stress generation, eventually leading to the expansion and cracking of the affected material. Therefore, a better understanding of various factors affecting the deterioration potential of ASR product (i.e., chemical composition, mechanical properties, and viscosity) is crucial to develop computer models for predicting the actual service-life of ASR-affected infrastructures [5]. Recently, several studies have investigated the chemical composition (e.g., [6–8]), microstructure characterization (e.g., [9–11]), mechanical properties (e.g., [12–14]), and viscosity (e.g., [15,16]) of either natural or synthetic ASR gel retrieved from unrestrained concrete specimens which may not reflect the real scenario of the formation of ASR secondary products in reinforced

concrete members in the field. However, only few research studies (e.g., [17–19]) have worked to understand the effect of confinement on ASR reaction product and they have all agreed that the confinement reduces the reactivity of the reactive aggregate and, hence, the gel formation. Yet, to the best of the authors' knowledge, there is still a lack of information on the impact of distinct confinement configurations on the chemical composition, mechanical properties, and viscosity of ASR reaction product in reinforced concrete. Therefore, this study aims to characterize the chemical composition and mechanical properties of ASR product extracted from the concrete blocks displaying distinct reinforcement configurations (i.e., none, 1D, and 2D).

10.2 Background

10.2.1 Mechanism of ASR

It is well accepted that the reactive aggregate that triggered ASR chemical reaction could simply be represented by their metastable silica components (SiO2) [3,20–22]. As per Varsheneya and Mauro [23], the interior part of those metastable silica components is mainly composed of a network of tetrahedral SiO2 with one silicon atom surrounded by four oxygen atoms which are connected by the oxygen vertices to form siloxane (≡Si–O–Si≡) bonds ("≡" indicates that each Si atom is connected to 3 other oxygen atoms). The exterior part of the abovementioned network ends with either Si+ or O- ions which could cause the siliceous material to be unstable [24,25]. Thus, hydrolysis can take place on the surface of such unstable material when it is exposed to water as per reaction 1 [25]. Later, the siloxane bonds are progressively attacked by the hydroxyl ions (OH-) in an alkaline environment of pore solution to dissolve silica and form Si(OH)4 following reaction 2 [3,24,25]:

$$(\equiv Si^{+}, \equiv Si - O^{-})_S + H_2O \leftrightarrow 2(\equiv Si - OH)_S \qquad \text{Reaction 1}$$

$$(\equiv Si - OH)_S + 3(OH^{-})_{aq} \leftrightarrow (Si(OH)_4)_{aq} \qquad \text{Reaction 2}$$

Hereafter, the alkali ions from the cement paste could replace hydrogen in $Si(OH)_4$ as per reaction 3 which is typically known as ion exchange, where A stands for alkalis (i.e., Na and K):

$$(Si(OH)_4)_{aq} + A^{+} \leftrightarrow ((OH)_3 \equiv \mathrm{Si} - O^{-} - A^{+})_{aq} + {H^{+}}_{aq} \qquad \text{Reaction 3}$$

Subsequently, the products of reaction 3 join together and undergo the condensation process as per reaction 4 and form nano-colloidal silica sol. This step is a very time-consuming process at high pH, since one of those reactants needs to donate one OH-, which is a huge barrier due to the high concentration of hydroxyl ions in the aqueous solution.

$$2\ ((OH)_3 \equiv \mathrm{Si} - O^- - A^+)_{aq} \leftrightarrow\ 2\ ((OH)_3 \equiv \mathrm{Si} - O^- - A^+)_{sol} + H_2O \qquad \text{Reaction 4}$$

Lastly, the silica gel with a three-dimensional network could be formed through the polymerization process; however, the presence of alkali ions would reduce the kinetics of condensation and polymerization. Conversely, the presence of calcium could significantly increase the kinetics of the condensation and polymerization of the silica species [26]; calcium from the pore solution could replace alkalis incorporated in silica gel which recycle the alkali ions back into the concrete pore solution and thus maintain a high pH in the latter [27], as per reaction 5. According to Rajabipour et al. [3], the final product of reaction 5 could be alternatively written as H6CaSi2O8 or CS2H3 in cement chemistry notation.

$$2\ ((OH)_3 \equiv \mathrm{Si} - O^-)_{aq} +\ Ca^{2+} \leftrightarrow\ ((OH)_3 \equiv \mathrm{Si} - O - \mathrm{Ca} - \mathrm{O} - \mathrm{Si} \equiv (OH)_3)_{sol} \qquad \text{Reaction 5}$$

Unlike the several studies conducted on the effect of calcium on ASR reaction product, there is still no agreement amongst researchers on the exact role of calcium in suppressing or escalating ASR deterioration [28]. On one hand, several authors suggested the essentiality of calcium for the formation of the ASR gel; the presence of calcium is necessary for the alkali silicate species condensation which leads to gelation [29,30]. On the other hand, a few works observed the mitigating nature of calcium where a calcium-rich gel could be considered as a non-swelling gel [28,31,32]. This clearly suggests that the mere presence of ASR reaction product does not always result in concrete deterioration; according to Kawamura and Iwahori [19], the different chemical compositions of ASR product can play an important role for the latter to be considered deleterious or innocuous.

10.2.2 Characteristics of ASR gel

ASR gel has a general composition of $(SiO_2)\cdot(Na_2O)_n\cdot(K_2O)_k\cdot(CaO)_c\cdot(H_2O)_x$, known as alkali–calcium–silicate–hydrate [5,7,9,13,16]. Although ASR gel consists of various chemical elements, the most important compositional parameters of an ASR gel are the atomic ratios of Ca/Si, K/Si, Na/Si and (Na + K)/Si, as per several authors (e.g., [9,10,33]). After reviewing the current literature on the composition of ASR gel obtained from concrete/mortar specimens made in the laboratory (e.g., [10,12,34,35]) as well as those retrieved from real structures (e.g., [34,36–40]), the authors concluded that the chemical composition of ASR gel in most of the studies comprises of the following ratios: $0 < Na/Si < 0.55$, $0 < K/Si < 0.45$, $0 < Ca/Si < 1.2$, , $0.1 < (Na + K)/Si < 1.2$. Such a wide range of chemical compositions of ASR gel could clearly confirm that those ASR products with only certain compositions can be considered deleterious while other compositions might be innocuous. A deleterious gel is the one that has a high hydrophilic potential as well as high free and restrained swelling capacity [5,15,16]. The free swelling capacity of ASR gel is the

ability of the latter to swell when there is no resistance against its expansion, while the restrained swelling capacity is a measure of how much confining pressure the gel could withstand prior to flowing into adjacent capillary pores and microcracks of the surrounding paste [5,15,16]. As per Gholizadeh et al. [5,9,16], those hydrophilic and expansive ASR gels which also have a high viscosity could be considered as the most deleterious ASR products [5,9,16]. Prezzi et al. [41] described the role of monovalent (i.e., Na+ and K+) and divalent (i.e., Ca 2+ and Mg2+) cations on the swelling behaviour of ASR gel through the use of electric double-layer theory. The authors [41] suggested that relatively high swelling pressures in ASR gel can be observed after a diffuse layer containing monovalent cations offsets the negative charges on silica particles. Otherwise, Kawamura et al. [19] and Gholizadeh et al. [16] observed that a diluted ASR gel containing a high amount of alkali could expand freely, yet they might not be able to impose deleterious pressure to its surrounding environment because of slightly low viscosity which makes them flow easily and relieve their stress.

Viscosity is the most important rheological property of ASR gel [16]; viscosity is generally known as the internal resistance of a fluid to flow [42]. Previously, several computer models have been developed for simulating the kinetics and mechanisms of ASR expansion [43–46]. Most of those assumed that ASR gel is a Newtonian fluid that could flow immediately upon formation into the bulk cement paste in the close vicinity of the aggregate particles. However, as per Gholizadeh et al. [16], ASR gel is deemed to display a non-Newtonian yield stress behavior where the latter showed an elastic behavior until the stress exceeds a certain limit. A direct way to measure the yield stress and thus the viscosity of ASR gel obtained from real concrete structures as well as laboratory specimens has not yet been found, therefore, researchers have tended to use synthesized ASR products which have been proved to have an identical molecular and nanoscale structure as the ones retrieved from in-service concrete [6]. The studies on the synthesized gels with various chemical compositions once again attested that monovalent and divalent cations are playing a crucial role in the various rheological properties of those gels [5,9,25]. As such, Rajabipour et al. [3] suggested that higher amounts of calcium in ASR gels may increase the viscosity and yield strength of those gels.

The above information clearly confirms the effects of chemical composition and their molar ratio (primarily Ca/Si and Na or K/Si) on the rheological (e.g., yield stress) and swelling properties of ASR gels. Gholizadeh et al. [16] proposed that the gel having intermediate calcium and high sodium contents could represent an ASR gel with the highest swelling capacity. Likewise, such chemical composition and molar ratios could significantly change the mechanical properties of ASR gel [14,15]. As such, those gels with lower calcium and higher alkali content (i.e., generally found in the center of aggregate particles with a crystalline structure [7,10,13,14,24]), showed to have a significantly lower modulus of elasticity and hardness compared to those

having higher calcium and lower alkali content (i.e., can be found either at the edge of the aggregate particles or cement paste with amorphous structure) [13,14]. Leemann et al. [13] observed that the modulus of elasticity and Vickers hardness of crystalline ASR gel range from 9-11 GPa and 13-18, respectively, while those properties increase significantly for the amorphous product to maximum values of 45 GPa and 270, respectively. Moreover, after reviewing the available literature investigating the modulus of elasticity of ASR gel [12–14,40,47,48], the authors observed a large variation among distinct works; while a range of 5-40 GPa was reported by Wu et al. [12] and Hu et al. [14], Zhang et al. [40] found that the modulus of elasticity of ASR gel is around 65 GPa. Such a huge variation in the modulus of elasticity of ASR gel could be attributed to the complex nanostructures of the latter (e.g., pores, defects, and cracks) or even the different testing procedures that they have used.

Although the above information is very interesting and indeed reveals the importance of ASR gel characterization, there is still a lack of research works to systematically characterize the chemical composition and mechanical properties of those ASR products retrieved from the concrete elements displaying distinct reinforcement configurations. Considering that the ASR features (i.e., chemical composition, mechanical properties and viscosity) might be impacted by restraint configurations, thus this study aims to deal with that.

10.3 Scope of Work

As previously mentioned, there is a need for a systematic study on the impact of restraint on ASR gel features in order to have a deeper understanding of the real mechanism of ASR in the field as well as the likely different processes of secondary products formation that may change the ASR deterioration process in reinforced concrete. Thus, concrete blocks having various reinforcement configurations (i.e., none, 1D, and 2D) were manufactured with a highly reactive coarse aggregate in the laboratory, stored in conditions accelerating ASR-induced development (i.e., 38 °C and 100% R.H.) and monitored over time. They were cored in three perpendicular directions (i.e., longitudinal, transverse, and vertical) at moderate expansion level (i.e., 0.15%) and then the chemical composition and mechanical properties of the ASR gel retrieved from those core specimens were determined. Ultimately, comparisons on the chemical composition and mechanical properties of ASR gel in various directions of each concrete block were conducted.

10.4 Materials and methods

10.4.1 Materials and mixture proportions

Nine concrete blocks incorporating a highly reactive coarse aggregate (i.e., Springhill – Sp- ranges of 5 to 20 mm) combined with a non-reactive fine aggregate (Ottawa natural sand – Ot) with dimensions of 450×450×675 mm (Figure 1) and design strength of 35 MPa were cast in the laboratory. The mineralogical composition of both aggregates can be found in Table 1. A conventional Portland cement (CSA Type GU, ASTM type 1) with a high alkali content (0.88% Na2Oeq) was used in the concrete mixture (cement composition is given in Table 2). Moreover, in order to accelerate ASR-induced expansion, the total alkali content of the pore solution was increased to 1.25% Na2Oeq by cement mass, with the aid of reagent grade sodium hydroxide pellets. The Concrete Prism Test (CPT) standard mixture proportion (ASTM C 1293 [49]) was used to proportion all concrete blocks of this study (Table 3).

Table 1: Aggregate properties selected for this study.

Aggregate				Rock type	Specific gravity (g/cm^3)	Absorption (%)	AMBT [a] 14 days expansion (%)
Type	Reactivity	Location	Name				
Coarse	Reactive	New Brunswick	Sp	Crushed greywacke	2.72	0.602	0.69
Fine	Non-reactive	Ottawa	Ot	Natural, derived granite	2.65	1.18	0.07

a) Typical expansion of ASTM C 1260.

Table 2: Cement composition in mass-%.

	SiO_2	Al_2O_3	Fe_2O_3	CaO	SO_3	MgO	K_2O	Na_2O	LOI	Na_2O_{eq}
CSA-GU	18.7	4.7	3.8	60.3	4.0	2.4	0.88	0.30	2.133	0.88

Table 3: Concrete mix design.

Materials	Quantities in the mix (kg/m^3)
Cement	420
Fine aggregate (Ot)	681
Coarse aggregate (Sp)	1044
Water	176

10.4.2 Manufacture of concrete blocks and cylinders

The following restraint conditions/configurations were selected for this work in order to evaluate the impact of restraint on the characterization of ASR gel: 1) unrestrained blocks, 2) 1D confined blocks, and 3) 2D confined blocks (Figure 1). The internal steel reinforcing bars at a reinforcement ratio of 2% was introduced to 1D (i.e., longitudinal direction) and 2D (i.e., the longitudinal and transverse directions) concrete blocks. 35M steel bars were used in this study to achieve a sufficiently large bar spacing to allow for core extraction (Figure 1B). It is worth noting that the spacing between top and bottom rebars and the concrete cover was 280 mm and 50 mm, respectively (Figure 1C). Moreover, to eliminate curvatures caused by non-uniform expansion, the steel bars were evenly distributed between the top and bottom sections of each block.

All concrete blocks were demoulded after a day, and then moist cured (i.e., 20°C) for another day. Later, four holes of 10 mm diameter by 55 mm long, were drilled in three sides of each concrete block (i.e., Figure 1E- top: point 1and 2, longitudinal: point 3 and 4 and transverse: point 5 and 6). Then stainless-steel gauge studs were glued in place with a fast-setting cement slurry for longitudinal expansion measurements.

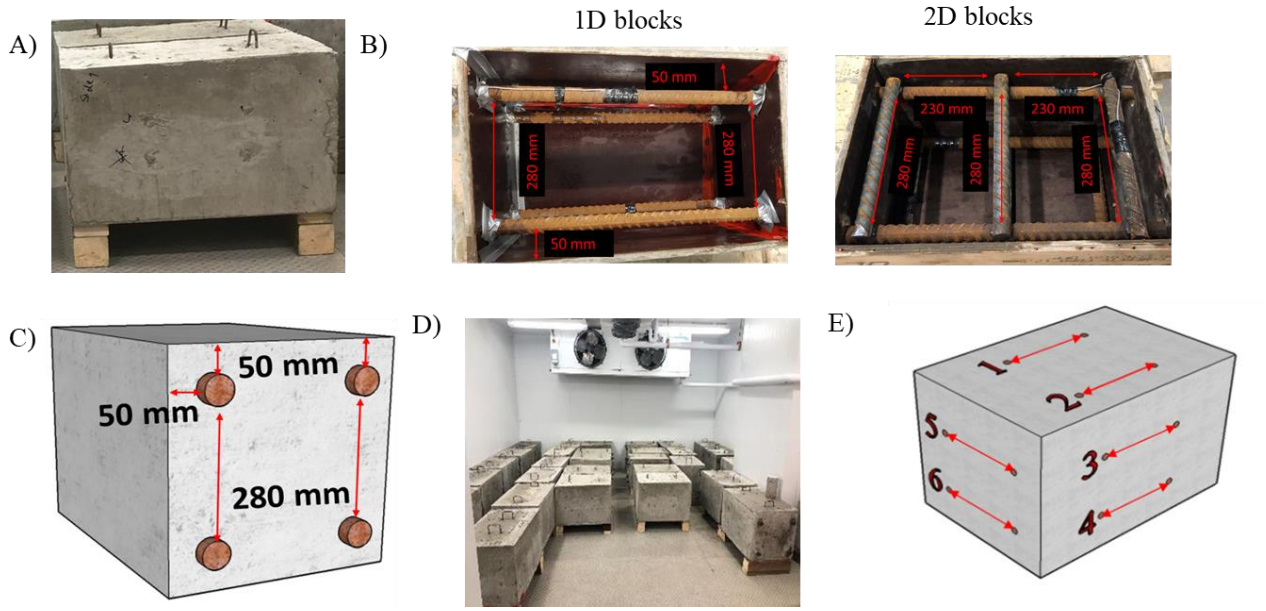

Figure 1: A) unrestrained blocks, B) restraint orientations of 1D and 2D blocks C) schematic of restrained blocks, D) environmental chamber at 38ºC and 100% RH and E) gauge studs orientation for blocks.

48 hours after casting, the initial expansion measurement (i.e., zero reading) was conducted on each side of all concrete blocks (Figure 1E- top longitudinal, side longitudinal, and transverse) and then they were placed in an environmental chamber to accelerate ASR-induced expansion (i.e., 38oC and 100% RH- Figure 1D). Meanwhile, all blocks were monitored for length changes regularly and placed at room temperature for 16 ± 4 hours prior to periodic expansion measurements. Once the blocks reached the expansion level selected for further analysis (i.e., 0.15 ± 0.01%), they were removed from the environmental chamber and cored from three main directions of each concrete block (Figure 2). It is worth noting that the expansion level used as "representative" of the desired expansion level of this study (i.e., 0.15 ± 0.01%) was measured on the longitudinal side for all concrete blocks (as Figure 1E -longitudinal measurements- points 3 and 4). Upon the core extraction, they were wrapped in several layers of plastic sheet and stored in a temperature-controlled room (12°C) as per Sanchez et al. [50] to suppress further ASR expansion since not all specimens could be analyzed at the same time due to testing capacity issues.

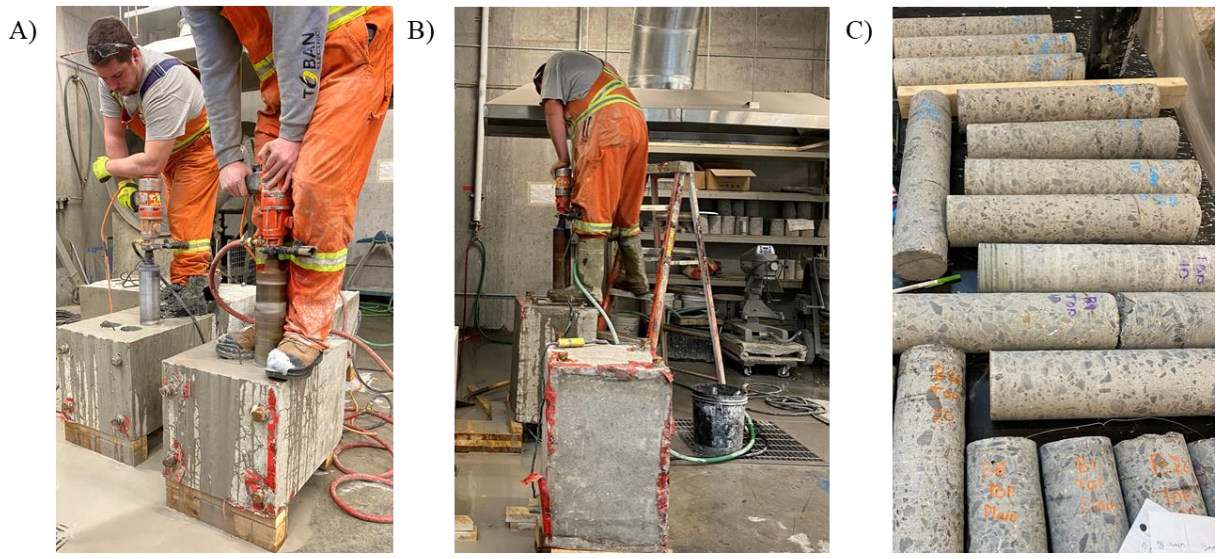

Figure 2: Coring process of distinct concrete blocks from A) vertical and transverse direction, B) longitudinal direction and D) 100 × 450 mm cored obtained from vertical and transverse directions.

10.4.3 Experimental procedures

Two concrete cores per coring direction of each concrete block were initially cut longitudinally into 10 mm-thick slabs with the aid of a diamond bladed masonry saw followed by subsequent mechanical polishing using liquid paraffin oil with grits of 30 (coarse), 60, 140, 280, 600, 1200 and 3000 (very fine). The slabs were then evaluated through a stereomicroscope to find some cracks filled with ASR gel (Figure 3), and further cutting was performed to produce a proper size sample for further testing. It is worth mentioning that as previously observed by Zahedi et al. [1], all cored specimens of this work present some large cracks containing ASR gel formed in aggregate particles and propagate into ITZ and cement paste. Later, the specimens which deemed properly cut were finely polished (i.e., up to 0.25µm) based on the procedure proposed by Leemann et al. [13] and Zhang et al. [40] as shown in Table 4. Finally, the finely polished specimens were protected in air-tight plastic bags and subjected to the following testing procedures within 24 h after the completion of the polishing operations:

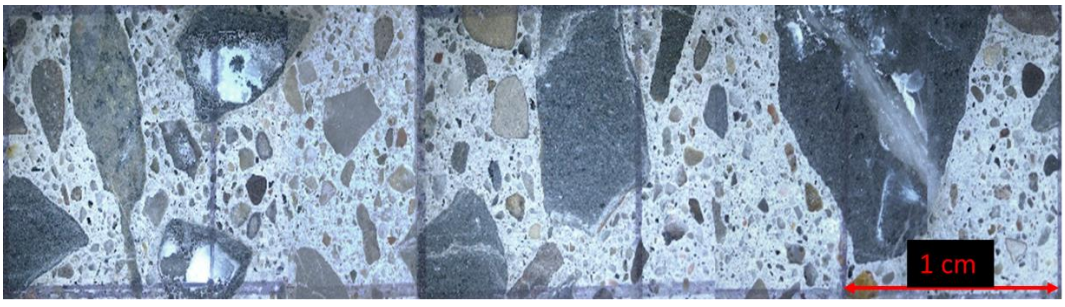

Figure 3: Photos taken from the polished concrete section from the 2D concrete blocks showing numerous aggregate particles with cracks filled with alkali-silica reaction under a stereomicroscope.

Table 4: Polishing procedure used in this study [13-40].

Sandpaper	Microns (µm)	Methods	Durations (mins)
SiC sandpaper 400-400	22	with liquid paraffin oil	10
SiC sandpaper 400-800	12	with liquid paraffin oil	10
SiC sandpaper 400-1200	6.5	with liquid paraffin oil	15
Oil based Diamond suspension	6	Acetone flush, air gun dry	40
Oil based Diamond suspension	1	Acetone flush, air gun dry	30
Diamond paste	0.25	Acetone flush, air gun dry	60

10.4.3.1 SEM/ EDS analysis

Backscattered electrons (BEC) imaging was performed on two specimens containing ASR-filled cracks propagating from within aggregate particles to the cement paste per coring direction of each concrete block (e.g., Figure 4) using scanning electron microscopy (SEM- JEOL 6610LV) with operating parameters set at 15 kV and a beam current of 200–220 mA. Energy-dispersive X-ray spectroscopy (EDX) was also used to analyze the chemical composition of the reaction product (i.e., ASR gel). It is worth mentioning that the concrete specimens were placed in 50o C for one day (24 hours) and then a thin layer of Au-Pd was used to coat them.

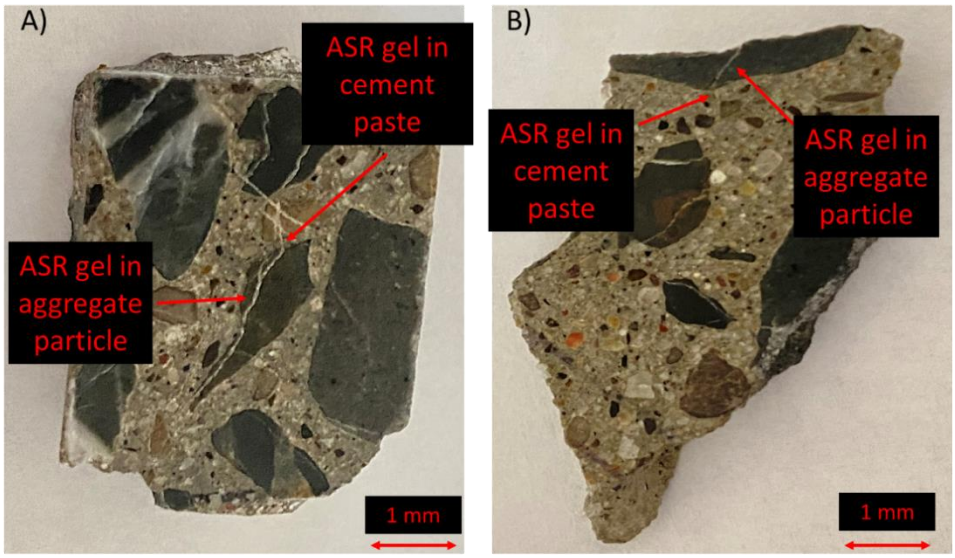

Figure 4: Polished specimens obtained from A) vertical -2D blocks and B) longitudinal-2D blocks.

10.4.3.2 Micro indentation

Indentation measurements were performed on similar specimens as per SEM analysis (i.e., two samples with ASR gel formed in aggregate particles and propagating into the cement paste per coring direction of each concrete block - Figure 4) with a Vickers micro-hardness tester (Struers Duramin-1 micro-hardness). The latter has an indenter with a square-based pyramid shape with an angle of 136 (Figure 5A) [51]. The

Vickers hardness value, HV, is generally calculated using the indenter load L and the actual surface area of the impression Ac [51] as shown in Figure 5B. The load used in this study is either 12.5mN, 25mN (only for cracks in aggregate particles), or 50 mN (for cracks in aggregate particles and cement paste) similar to the one proposed by Leemann et al. [13]. As the authors [13] suggested, the increase of linear loading takes 20 s and then the maximum load is kept constant for 5 s and later linear unloading takes 20 s (Figure 5C). After conducting the indentation procedure, the diagonal width (i.e., d- Figure 5A) is measured under a microscope at 400X which helps to find the hardness of the material. It is worth noting that the indentation procedure was carried out on aggregate particles and cement paste as per the distance shown in Figure 6.

It is worth noting that the above testing procedures have been performed in two different, yet related ways. First, the results obtained from SEM and micro indentation were averaged from the three coring orientations to evaluate the impact of the reinforcement on the "overall deterioration" of ASR-affected blocks (i.e., Results section). Second, the result of SEM and micro indentation were appraised as per the coring direction to assess and quantify ASR anisotropic behaviour as a function of the restraint effect (i.e., Discussion section).

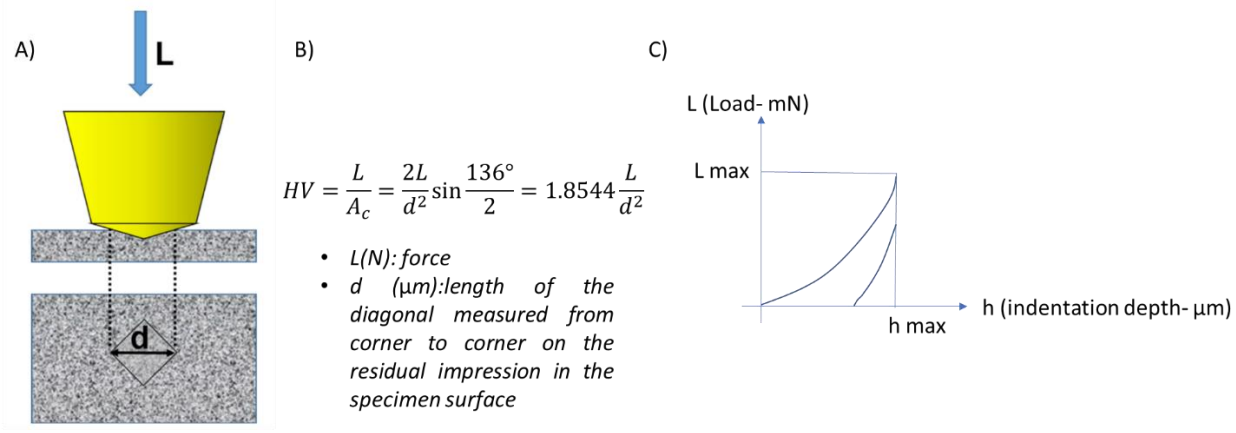

Figure 5: A) Schematic of Vickers hardness [51], B) Vickers hardness calculation [51] and C) typical load-indentation depth (P-h) curve.

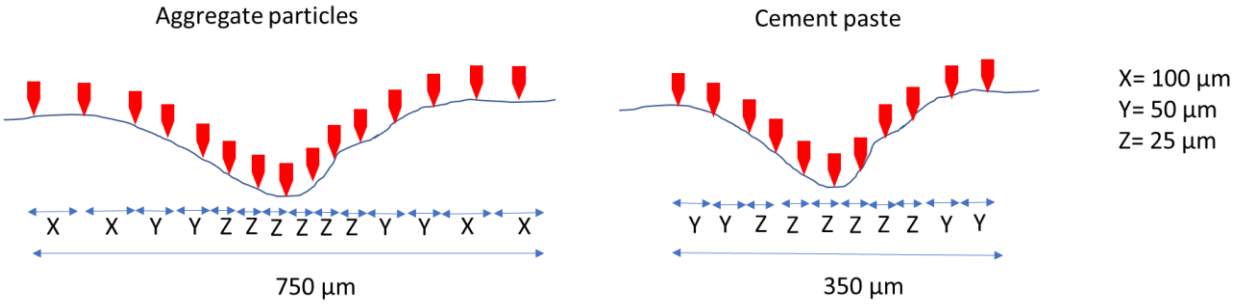

Figure 6: Indentation distance profile across a crack in aggregate particles and cement paste.

10.5 Results

10.5.1 Morphology and chemical composition

Figure 7 illustrates the typical micro-texture of the ASR gel presented within the reactive aggregate particles displayed in Figure 4. Despite the small volumes of ASR gel present in the specimens extracted from all concrete blocks at the selected expansion level of this study (i.e., 0.15%), which may limit the possibilities to analyze the products, both crystalline and amorphous reaction products could be identified in all concrete specimens (regardless of the restraint condition) of this study. As previously suggested by several authors [7,10,13,14,24] the ASR granular product (i.e., amorphous) progressively transform to the rosette-like product (i.e., crystalline) over time; similarly, as Figure 7 illustrates, the amorphous ASR product was trying to transform to crystalline (i.e., the appeared small lines on the amorphous product could be a good sign for the above discussion). The latter could result in the observation of different chemical compositions of ASR product in various locations of concrete specimens. As such, Figure 8A illustrates the ternary plots of chemical compositions of ASR gels formed within reactive aggregate particles, ITZ and cement paste. Evaluating the plot, one notices that unlike the ASR gel found in aggregate particles which contains high silica, sodium and potassium, those obtained from ITZ and cement paste have significantly higher calcium content. It is worth mentioning that the evaluation of the chemical composition of ASR product in aggregate particles has been conducted mainly on the spectra obtained at a distance to the interface with the cement paste >100 μm similar to the procedure proposed by Leemann et al. [10] in order to evaluate mainly the crystalline reaction product formed in the aggregate particle. Moreover, in order to evaluate the impact of restraint on the "overall" chemical composition of ASR gel, Figure 8B illustrates the average chemical composition of ASR gel obtained from aggregate particles, ITZ and cement paste of various directions (i.e., longitudinal, vertical and transverse) of concrete blocks. Comparing the "overall" chemical composition of ASR gel obtained from the abovementioned locations of concrete blocks displaying various restraint conditions, one sees that the latter is almost identical for all concrete of this study. For instance, the "overall" Ca/Si ratio of ASR gel obtained from aggregate particles, ITZ and cement of various concrete blocks falls in the range of 0.23 to 0.26, 0.32 to 0.35 and 0.35 to 0.38, respectively.

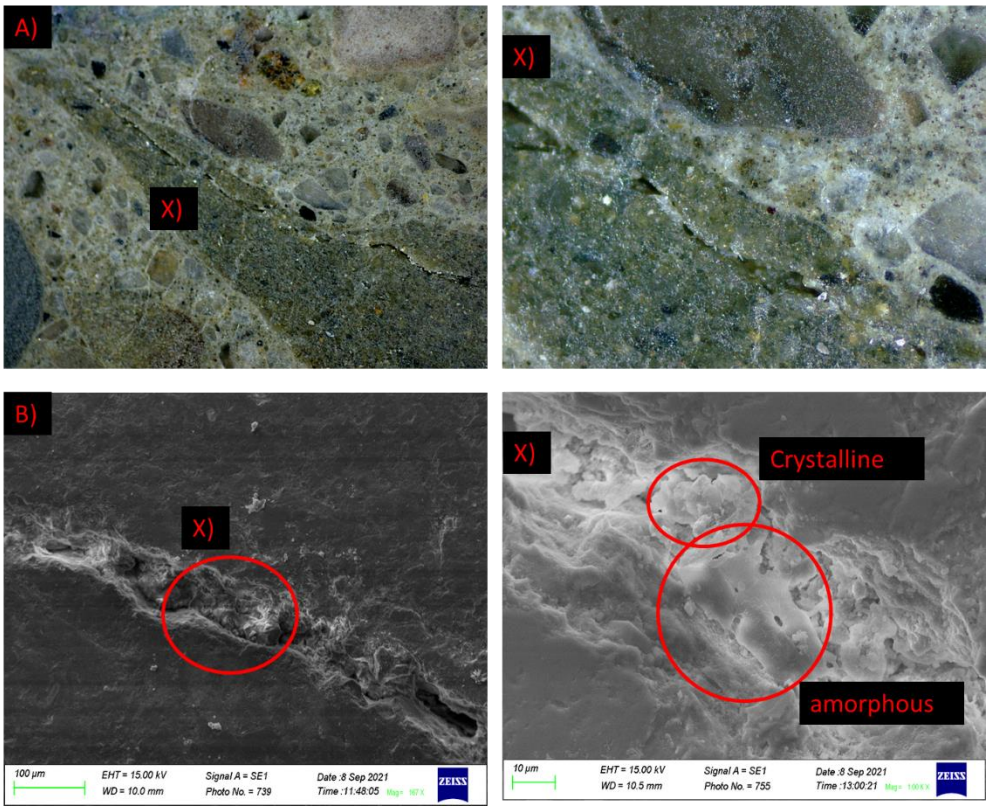

Figure 7: A) picture of the reaction products in aggregate of vertical direction of 2D concrete blocks obtained through stereomicrsocpe, B) SEM image of the latter (X: magnified section).

A)

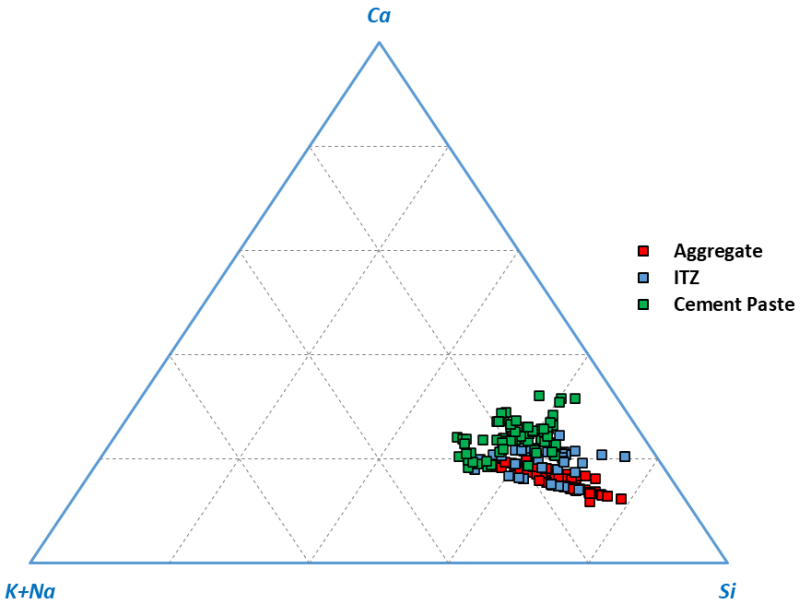

B)

Source	Specimens	O	Na	Mg	AL	Si	S	K	Ca	Fe	Ca/Si	Na/Si	(Na+K)/Si	K/Na	Number of points
		[atom-%]									[-]				
Aggregate	Unconfined	43.15	2.62	0.35	0.6	36.57	0.1	6.91	9.69	0	0.265	0.071	0.260	2.639	342
	1D	43.47	2.64	0.35	0.6	36.17	0.1	7.18	9.47	0	0.261	0.073	0.271	2.715	357
	2D	41.60	2.88	0.35	0.6	39.03	0.1	6.43	8.99	0	0.230	0.073	0.238	2.232	354
ITZ	Unconfined	45.23	3.53	0.41	0.6	34.63	0.41	3.84	11.21	0.13	0.323	0.101	0.212	1.088	81
	1D	45.23	3.57	0.41	0.6	33.88	0.41	3.89	11.88	0.11	0.350	0.105	0.220	1.091	77
	2D	44.08	4.01	0.41	0.6	35.31	0.41	3.63	11.41	0.103	0.323	0.113	0.216	0.905	81
Cement paste	Unconfined	45.09	3.40	0.4	0.6	32.70	0.6	4.45	12.54	0.2	0.383	0.104	0.240	1.309	136
	1D	45.36	3.47	0.4	0.6	32.41	0.6	4.51	12.45	0.19	0.384	0.107	0.246	1.300	160
	2D	44.26	3.75	0.4	0.6	33.84	0.593	4.26	12.08	0.18	0.357	0.110	0.237	1.136	148

Figure 8: A) Ternary phase diagram for ASR gels and B) average of the chemical composition of ASR gel formed in distinct locations of various concrete blocks of this study.

The above numbers (Figure 8A and B) clearly show the variations in the composition of ASR products formed in the various locations of concrete specimens; these differences are easily visible in ratio-plots illustrated in Figure 9. While Figure 9 A displays the (Na + K)/Si ratio of all evaluated ASR products formed in aggregate particles, ITZ and cement paste of concrete blocks as a function of their Ca/Si-ratio, Figure 9B exhibits the "overall" of the (Na + K)/Si ratio as a function of Ca/Si for different locations of each concrete block of this study. Analyzing both graphs, one sees the following points: a) the (Na + K)/Si ratio obtained from ASR gels formed in aggregate particles falls in the range of 0.15-0.40 which is similar to what Leemann et al. [10] observed on ASR products obtained from aggregate particles of distinct concrete specimens; b) ASR gel in cement paste showed to have the highest Ca/Si ratio (ranges of 0.30-0.56), followed by ITZ (ranges of 0.20-0.42) and aggregate particles (ranges of 0.14-0.35). The above observation could be due to the calcium uptake of ASR gel when moving from aggregate particles to cement paste; c) in spite of the "overall" (Na + K)/Si and Ca/Si ratio of various specimens obtained from unrestrained blocks which showed to have a small standard deviation, those retrieved from reinforced blocks demonstrate a large standard deviation which could be due to anisotropic effects of restraint on ASR affected concrete as previously observed by Zahedi et al. [1] and will be discussed in next sections.

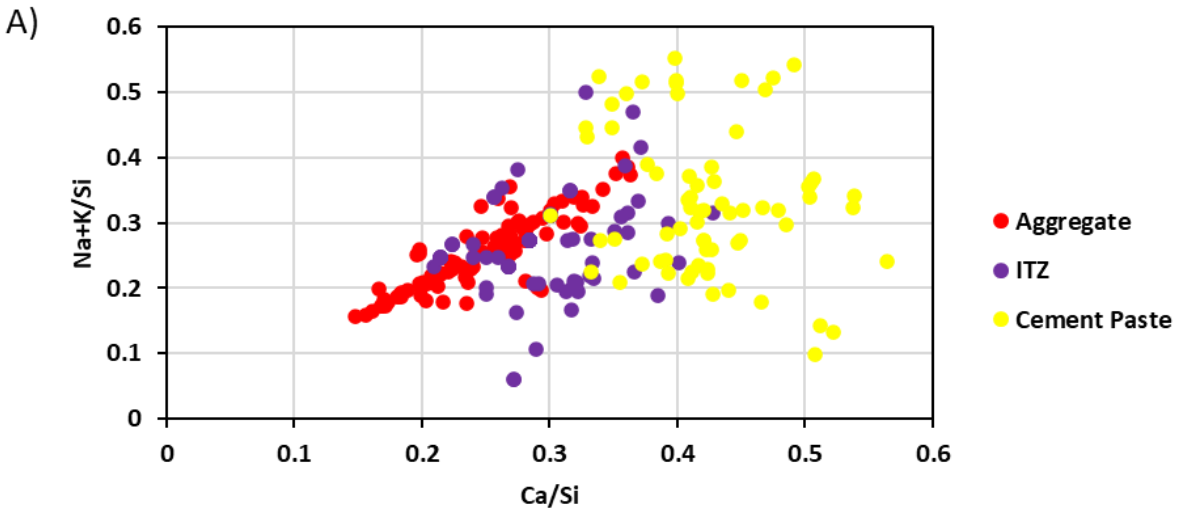

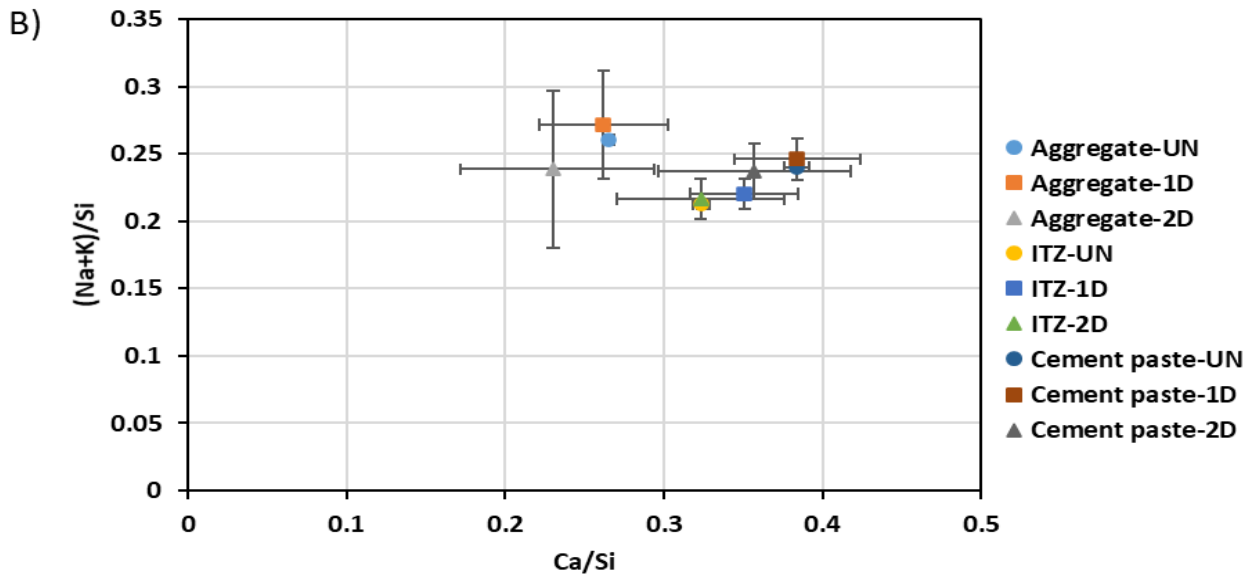

Figure 9: A) (Na + K)/Si-ratio of ASR products formed in distinct locations of concrete blocks as a function of their Ca/Si-ratio and B) Mean values ("Overall") of (Na + K)/Si-ratio of distinct concrete blocks as a function of their Ca/Si-ratio with standard deviations.

10.5.2 Micro-indentation

Figure 10 illustrates the "overall" diagonal Vickers hardness profile (average of all hardness obtained from various directions of each concrete block- longitudinal, vertical, and transverse) across a crack on aggregate particles and cement paste, derived from indentation measurements performed with the proposed loads of this study (aggregate particles: 12.5mN, 25mN, and 50 mN and cement paste: 50 mN). It is worth mentioning that due to the limited availability of ASR gel in ITZ of various concrete elements of this study, the micro-indentation test has not been conducted on those locations. Evaluating the plots one observes the following points: a) all analyzed cracks in the aggregate particles were found to have an identical behavior for each of the distinct load magnitudes used in this study; b) ASR gel found in the aggregate particles (i.e., center of each crack- around 350 µm from the initial point) of all concrete blocks (disregarding the restraint condition as well as the amount of loading) showed to have an almost identical Vickers hardness (i.e., range of 25-40); c) similar to the "overall" hardness obtained from various aggregate particles of this study, the cement paste of distinct concrete blocks showed to have an identical behaviour; and d) the ASR gel found in the cement paste (i.e., at the center of the cracks- around 170 µm from the initial point) showed to have significantly higher "overall" hardness compared to those obtained from distinct aggregate particles of this study; ASR gel at the center of the cracks observed at aggregate particles and cement paste showed to have a range of 30-40 and 210-230 at 50 mN, respectively.

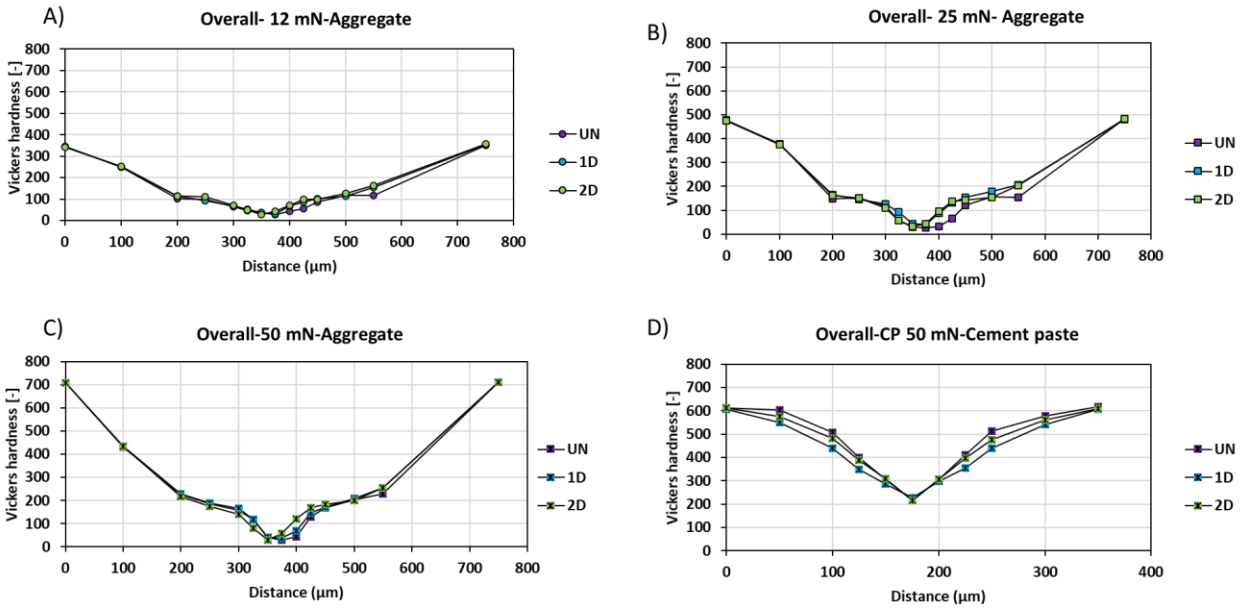

Figure 10: "Overall" Vickers hardness Profile across a crack of distinct concrete blocks, derived from A) aggregate particle with the loading of 12mN, B) aggregate particle with the loading of 25mN and C) aggregate particle with the loading of 50mN and D) cement paste with the loading of 50 mN.

10.6 Discussion

10.6.1 Effect of restraint on the chemical composition of ASR gel

The SEM and EDS analysis (i.e., overall results, disregarding the direction of the core) carried out during this study help to better understand the chemical composition of ASR gel in restrained concrete. The analysis of the distinct chemical elements of ASR gel formed in various concrete blocks clearly shows that the restraint does not seems to considerably change it as a function of the restraint configuration. However, if one analyzes the most important compositional parameters of ASR gel (i.e., Ca/Si, (Na+K)/Si, Na/Si, Na/K), it could easily see that despite the ones obtained from unrestrained concrete which does not show a huge data range, those gathered from restrained concrete showed to have a large standard deviation (e.g., Figure 9B). As such, evaluating the graph (Figure 9B), a large standard deviation has been observed on both molar ratios of Ca/Si, (Na+K)/Si obtained from distinct locations (i.e., aggregate particles, ITZ and cement paste) of restrained concrete specimens which as previously mentioned could be attributed to the anisotropic ASR-induced damage development of restrained concrete [1,52,53]. Thus, investigation of ASR anisotropy is required to fully understand the impact of restraint on the chemical composition of ASR gel obtained from distinct directions (i.e., longitudinal, vertical, and transverse) of each concrete block. Therefore, Tables 5A, B, and C display the chemical composition of reaction products developed in aggregate particles, ITZ, and cement paste of various directions of distinct concrete blocks, respectively. To better describe the results displayed in Table 5, a thorough evaluation of the chemical composition of

ASR products obtained from aggregate particles, ITZ, and cement paste of various concrete blocks as a function of coring directions will be conducted in the following subsections:

- *ASR gel obtained from aggregate particles*

As per Table 5A, a minimal difference has been observed on the chemical composition of ASR products obtained from aggregate particles of distinct directions of unrestrained blocks; e.g., Ca/Si ratio of 0.261, 0.265, and 0.265 as well as (Na+K)/Si ratio of 0.265, 0.256, and 0.261 were obtained from vertical, transverse, and longitudinal directions of unrestrained concrete, respectively. Conversely, the restrained concrete blocks demonstrate quite different behavior corresponding to different coring orientations. As such, on the one hand, ASR gel found in the aggregate particles of the vertical and transverse specimens (i.e., unrestrained directions) of 1D concrete have higher K (i.e., 7.66 and 7.89, respectively) and Ca (i.e., 10.11 and 9.98, respectively) when compared to the longitudinal cores (restrained direction- K: 6.01 and Ca: 8.32). On the other hand, those specimens obtained from the restrained direction of 1D blocks have slightly higher Na (i.e., 2.74) and Si (i.e., 40.09) when compared to those obtained from unrestrained directions (i.e., vertical and transverse specimens- Na: 2.58 and 2.62 and Si: 33.96 and 34.46, respectively). Likewise, the ASR gel found in the aggregate particles of the unrestrained direction of 2D concrete (i.e., vertical cores) has almost 30% and 25% higher potassium and calcium as well as almost 5% and 20% lower sodium and silica, respectively, when compared to those obtained from restrained directions (i.e., longitudinal and transverse cores). For a better understanding of the above, Figure 11 illustrates the (Na+K)/Si and Ca/Si ratio-plot obtained from the ASR gel retrieved from aggregate particles of distinct directions of concrete blocks of this study. Evaluating the plot, one sees that the ASR gel obtained from aggregate particles of unrestrained direction/s of reinforced concrete has significantly higher (Na+K)/Si and Ca/Si when compared to the restrained directions of those blocks. One more interesting point that can be found after analyzing Figure 11 is, although both unrestrained concrete blocks and unrestrained directions of reinforced blocks are unrestrained specimens, the ASR gel found in those directions are behaving completely differently; the latter showed to have higher (Na+K)/Si and Ca/Si.

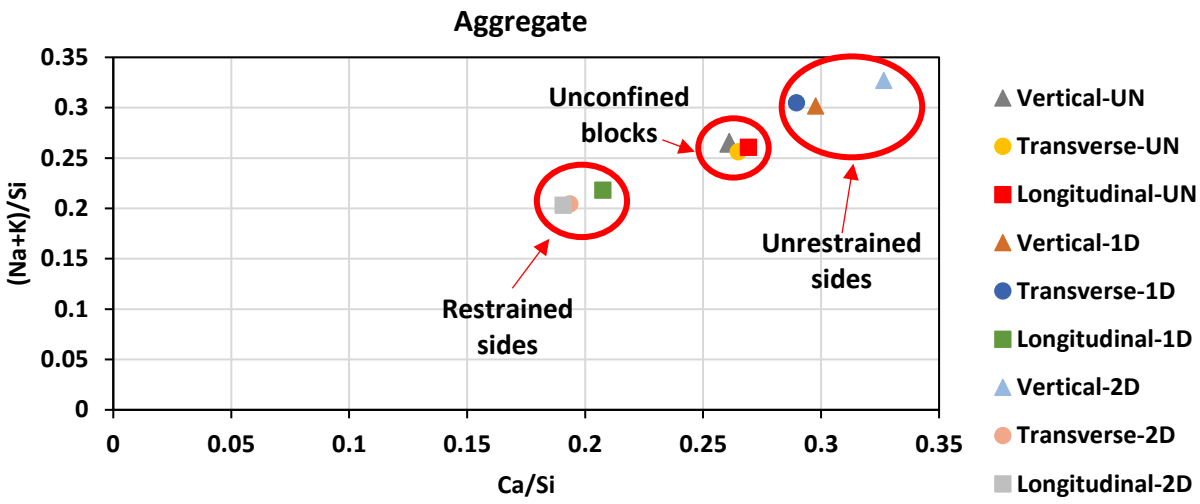

Figure 11: (Na + K)/Si-ratio of ASR products formed in aggregate particles of distinct directions of various concrete blocks of this study as a function of their Ca/Si-ratio.

Moreover, Gholizadeh et al. [9] previously suggested the impact of Na/Si and Ca/Si on the free swelling of the gel as follows: a) the higher Na/Si of ASR gel, the higher free swelling potential of those ASR products and; b) while the Ca/Si lower than 0.23 or higher than 0.37 diminish the free swelling of those gel, the latter with 0.23< Ca/Si< 0.37 has the highest free swelling potential. Therefore, Figures 12A and B illustrate the Na/Si and Ca/Si ratio of 12 arbitrary EDS analyzed points of ASR product found in aggregate particles of various concrete specimens obtained from distinct directions of concrete blocks of this study. Evaluating the graphs, one sees the following important points: a) the Na/Si ratio of ASR gel gathered from restrained directions of reinforced blocks of this study (i.e., longitudinal core of 1D blocks as well as longitudinal and transverse cores of 2D blocks) have a slightly lower value compared to the other samples; b) conversely, the specimens obtained from unrestrained directions of reinforced block (i.e., vertical and transverse cores of 1D blocks as well as vertical core of 2D blocks) showed to have the highest Na/Si ratio; c) while, the ASR gel obtained from the restrained directions of reinforced blocks of this study showed to have the Ca/Si < 0.23, the other specimens have the 0.23< Ca/Si< 0.37. The above discussion could directly be in attributed to anisotropic ASR-induced development caused by restraint in reinforced concrete. Accordingly, Figure 13 displays the induced expansion curves of distinct surfaces of various blocks of this study. Unlike the unrestrained blocks, which exhibited a negligible difference in the expansion level attained by their various surfaces (Figure 13A), the restrained concrete blocks displayed an anisotropic behavior. As Figures 13B and C show, the expansion measurements on distinct surfaces of the restrained blocks showed the transfer of induced expansion from restrained directions to directions with less or no restraint resulting in higher expansion levels. For example, while the longitudinal and transverse directions of 2D blocks (i.e., restrained

directions) reached 0.15% and 0.17% of expansion after 340 days, the vertical surface attained 0.22% at the same time period.

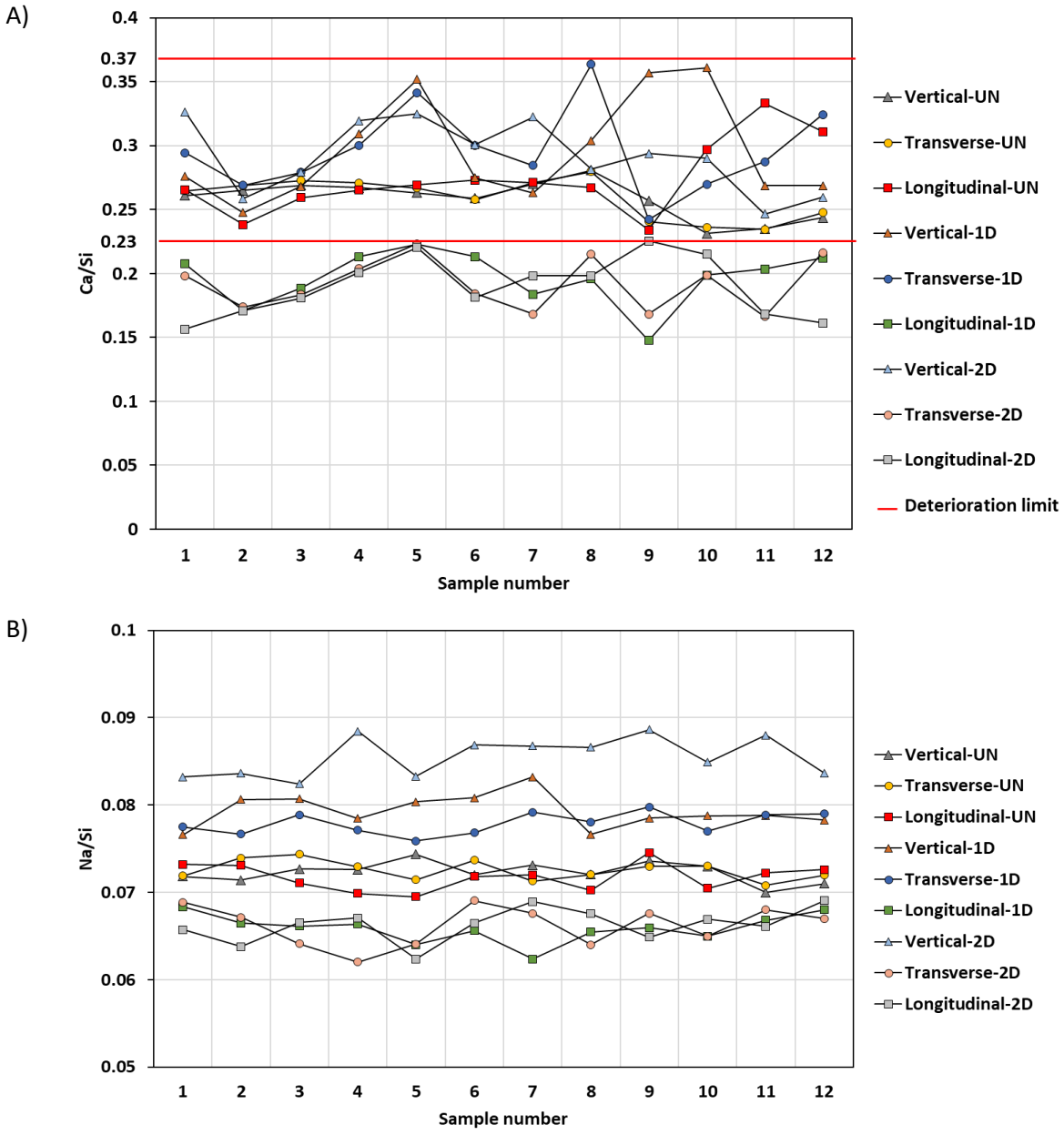

Figure 12: A) comparison of Na/Si ratio of ASR gel formed in aggregate particles of distinct directions of various concrete blocks and B) comparison of Ca/Si ratio of ASR gel formed in aggregate particles of distinct directions of various concrete blocks.

A) B)

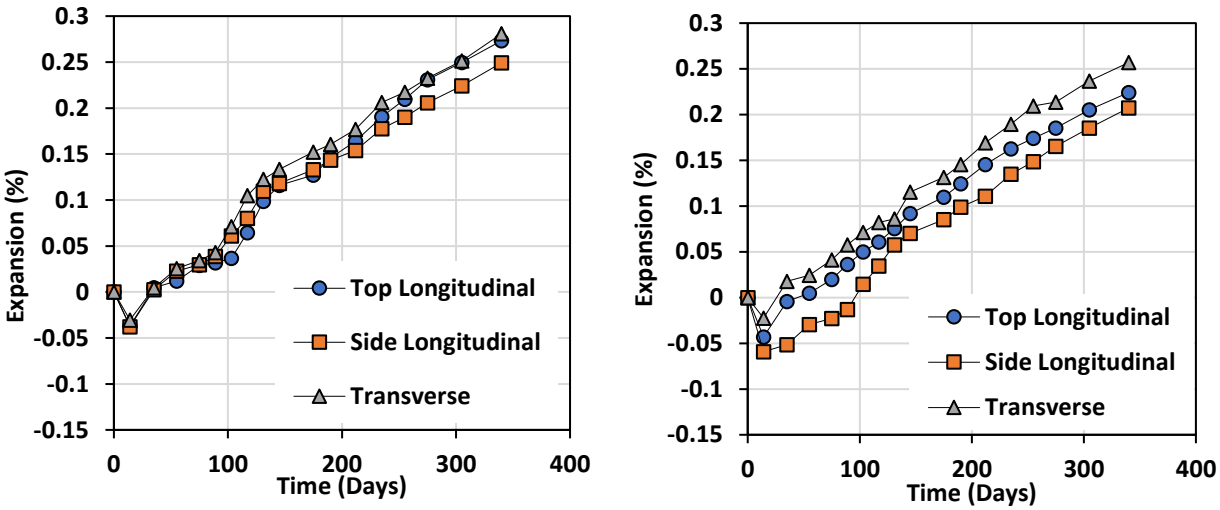

C)

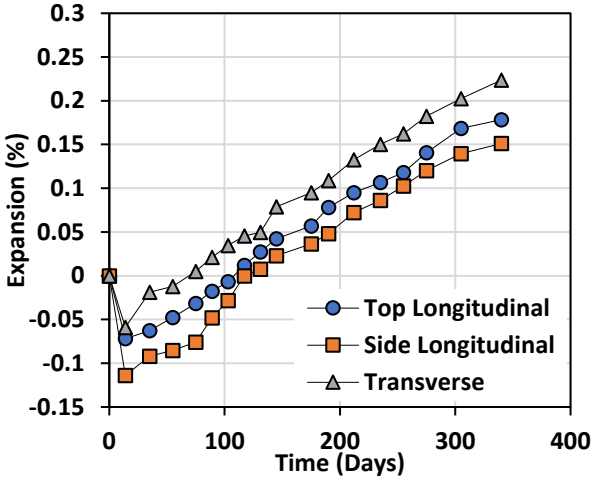

Figure 13: ASR kinetics (expansion vs. time) for: A) unrestrained concrete specimens, B) 1D concrete blocks and, C) 2D concrete blocks incorporating distinct surfaces of the blocks.

- *ASR gel obtained from ITZ and cement paste*

Similar to the chemical composition of ASR gel obtained from aggregate particles, those gathered from ITZ and cement paste of distinct directions of unrestrained concrete blocks did not show a significant difference (Table 5B and C). On the other hand, the chemical composition of ASR products formed in the ITZ and cement paste of distinct directions of restrained blocks behave quite differently; similar to the chemical composition obtained from ASR gels in aggregate particles, those ASR products retrieved from the unrestrained directions of restrained blocks had slightly higher K and Ca and lower Na and Si when compared to the restrained directions of those blocks. Therefore, the (Na+K)/Si, Ca/Si ratio-plot of ASR

gel obtained from ITZ and cement paste (Figure 14A and B, respectively) could highlight the abovementioned differences. Analyzing the graphs, one notices that the ASR gel gathered from the unrestrained direction/s of restrained concrete has considerably higher (Na+K)/Si and Ca/Si when compared to the unrestrained directions of those blocks. Such observation could once again be attributed to the anisotropic behavior of ASR-affected reinforced blocks. In the next section, the effect of restraint on the correlation of distinct chemical elements of ASR gel will be discussed.

A)

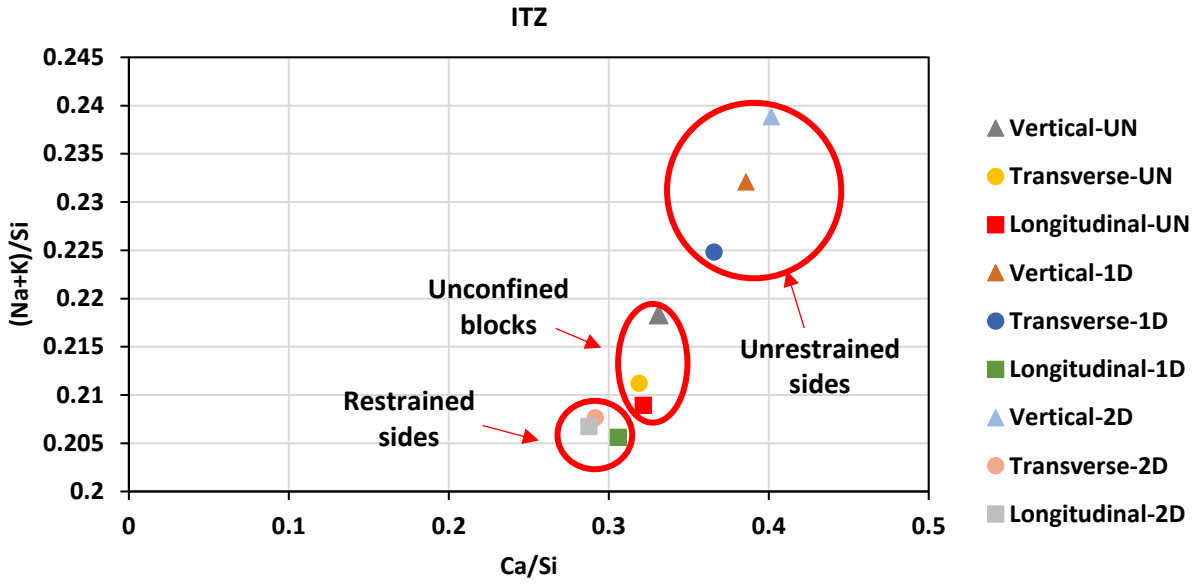

B)

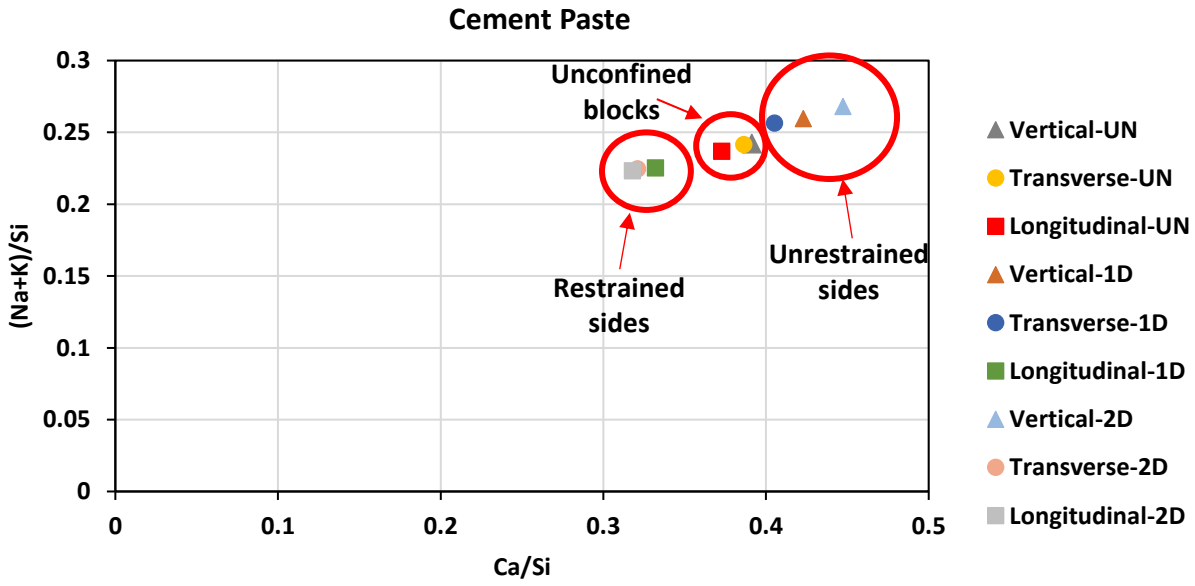

Figure 14:A) (Na + K)/Si-ratio of ASR products formed in ITZ of distinct directions of various concrete blocks of this study as a function of their Ca/Si-ratio and B) (Na + K)/Si-ratio of ASR products formed in cement paste of distinct directions of various concrete blocks of this study as a function of their Ca/Si-ratio.

Table 5: chemical composition of ASR gel formed obtained from A) aggregate particles, B) ITZ and C) cement paste of distinct directions of various concrete blocks of this study.

A)

Specimens	O	Na	Mg	AL	Si	S	K	Ca	Fe	Ca/Si	Na/Si	(Na+K)/Si	K/Na	Number of points	Compressive strength (MPa)
	[atom-%]									[-]					
Vertical-UN	43.7	2.6	0.35	0.6	36.2	0.1	7	9.45	0	0.261	0.072	0.265	2.692	107	11.251
Transverse-UN	42.9	2.64	0.35	0.6	36.85	0.1	6.8	9.76	0	0.265	0.072	0.256	2.576	111	11.449
Longitudinal-UN	42.86	2.62	0.35	0.6	36.66	0.1	6.94	9.87	0	0.269	0.071	0.261	2.649	124	11.468
Vertical-1D	44.64	2.58	0.35	0.6	33.96	0.1	7.66	10.11	0	0.298	0.076	0.302	2.969	131	11.446
Transverse-1D	44	2.62	0.35	0.6	34.46	0.1	7.89	9.98	0	0.290	0.076	0.305	3.011	102	11.266
Longitudinal-1D	41.79	2.74	0.35	0.6	40.09	0.1	6.01	8.32	0	0.208	0.068	0.218	2.193	124	10.756
Vertical-2D	43.9	2.78	0.35	0.6	33.29	0.1	8.11	10.87	0	0.327	0.084	0.327	2.917	104	11.570
Transverse-2D	40.52	2.91	0.35	0.6	41.8	0.1	5.63	8.09	0	0.194	0.070	0.204	1.935	122	10.646
Longitudinal-2D	40.4	2.96	0.35	0.6	42.01	0.1	5.57	8.01	0	0.191	0.070	0.203	1.882	128	10.599

B)

Specimens	O	Na	Mg	AL	Si	S	K	Ca	Fe	Ca/Si	Na/Si	(Na+K)/Si	K/Na	Number of points	Compressive strength (MPa)
	[atom-%]									[-]					
Vertical-UN	45.2	3.56	0.43	0.6	34.3	0.49	3.93	11.36	0.13	0.331	0.104	0.218	1.104	32	12.668
Transverse-UN	45.4	3.5	0.4	0.6	34.7	0.37	3.83	11.07	0.13	0.319	0.101	0.211	1.094	25	12.680
Longitudinal-UN	45.1	3.53	0.4	0.6	34.89	0.37	3.76	11.22	0.13	0.322	0.101	0.209	1.065	24	12.721
Vertical-1D	46.05	3.3	0.4	0.6	32.4	0.41	4.22	12.5	0.12	0.386	0.102	0.232	1.279	22	12.650
Transverse-1D	45.98	3.4	0.45	0.6	32.96	0.43	4.01	12.06	0.11	0.366	0.103	0.225	1.179	31	12.709
Longitudinal-1D	43.66	4.01	0.4	0.6	36.28	0.4	3.45	11.1	0.1	0.306	0.111	0.206	0.860	24	12.633
Vertical-2D	46.08	3.33	0.45	0.6	31.9	0.43	4.29	12.81	0.11	0.402	0.104	0.239	1.288	27	12.540
Transverse-2D	43.12	4.33	0.4	0.6	36.94	0.4	3.34	10.77	0.1	0.292	0.117	0.208	0.771	28	12.485
Longitudinal-2D	43.06	4.39	0.4	0.6	37.1	0.4	3.28	10.67	0.1	0.288	0.118	0.207	0.747	26	12.459

C)

Specimens	O	Na	Mg	AL	Si	S	K	Ca	Fe	Ca/Si	Na/Si	(Na+K)/Si	K/Na	Number of points	Compressive strength (MPa)
	[atom-%]									[-]					
Vertical-UN	45.6	3.4	0.4	0.6	32.2	0.6	4.4	12.6	0.2	0.391	0.106	0.242	1.294	45	12.538
Transverse-UN	44.69	3.38	0.4	0.6	32.87	0.6	4.56	12.7	0.2	0.386	0.103	0.242	1.349	44	12.573
Longitudinal-UN	45	3.43	0.4	0.6	33.05	0.6	4.4	12.32	0.2	0.373	0.104	0.237	1.283	47	12.609
Vertical-1D	46.59	3.12	0.4	0.6	30.66	0.62	4.84	12.97	0.2	0.423	0.102	0.260	1.551	51	12.346
Transverse-1D	46.32	3.33	0.4	0.6	31.22	0.6	4.68	12.65	0.2	0.405	0.107	0.257	1.405	52	12.395
Longitudinal-1D	43.17	3.96	0.4	0.6	35.36	0.58	4.01	11.74	0.18	0.332	0.112	0.225	1.013	57	12.572
Vertical-2D	46.87	3.01	0.4	0.6	29.91	0.62	5.01	13.38	0.2	0.447	0.101	0.268	1.664	42	12.153
Transverse-2D	43.01	4.11	0.4	0.6	35.73	0.58	3.92	11.47	0.18	0.321	0.115	0.225	0.954	44	12.511
Longitudinal-2D	42.91	4.15	0.4	0.6	35.9	0.58	3.87	11.41	0.18	0.318	0.116	0.223	0.933	62	12.504

10.6.1.1 Effect of restraint on the correlation of distinct chemical elements of ASR gel

The importance of anisotropic effects generated by the restrained members has been thoroughly discussed where generally ASR gel obtained from restrained directions of reinforced blocks has a higher Na and Si as well as a lower K and Ca ion concentration (Table 5). In this section the role of each element on ASR-induced anisotropy will be discussed separately in the following sections:

- *Role of Na and Si*

Observation of higher sodium and silicate in the restrained directions of reinforced concrete blocks could probably be due to the fact that those gels are restrained and cannot easily leave the reaction site as previously observed by Ostertag et al. [17]. According to the authors [17], ASR gels obtained from the mortar bars restrained by steel microfibers have significantly higher sodium and silicate when compared to

unrestrained mortar bars. Moreover, because of the higher Si concentration in restrained directions of reinforced concrete blocks, the dissolution of the reactive aggregate of those directions is retarded, which could reduce the reactivity of the aggregate particles, and thus the gel formation. This could clearly result in an observation of lower ASR kinetics in restrained directions of reinforced blocks as shown in Figure 13.

- *Role of Ca*

As previously mentioned, the silica gel generally contains silica alkali chains ($\mathrm{Si}-O^{-}-Na^{+}$) which is normally unstable in the absence of calcium. Therefore, the presence of calcium could start to be exchanged with alkalis and form calcium silicate chains ($\ldots\mathrm{Si}-O^{-}Ca^{2+-}\mathrm{O}-\mathrm{Si}\ldots$) [9,25]. Such ion-exchange reaction is known as "alkali-recycling" as per Thomas [27] which could result in a slight increase in the osmotic pressure of the gels' pore solution and thus increase the gel's tendency to absorb water and swell [3,9]. Considering the above discussion and evaluating the results gathered in this study (Table 5), one sees that the calcium concentration of all specimens obtained from unrestrained directions of reinforced blocks has a quite higher value when compared to those gathered from restrained directions. This clearly attests that restraint could significantly reduce the swelling capacity of ASR gel and thus the expansion (Figure 13) in restrained directions while transferring it to unrestrained directions.

- *Role of K*

As per Gholizadeh [25] and Dove [54], the impact of potassium and sodium as two alkali elements of ASR gel is not similar which could be due to their different atomic sizes and field strengths. Although recently several research studies have been performed on the role of sodium in ASR gel [5,9,29], very few studies have been conducted to understand the exact role of potassium on the bonding of cations or water to silica gel. Considering that no experimental results have been reported on the latter an also similarity of clay mineral's behavior to silica gels. Therefore, Lal and Shukla [55] investigated the swelling capacity of two different clay minerals with various cations and reported that the swelling sensitivity of clay minerals is found to follow the Hoffmeister series Ca > K > Na [56]. Similarly, Leemann et al. [57] reported a higher rate of dissolution for potassium hydroxide than for sodium hydroxide. The above clearly suggests the importance of potassium concentration on the swelling potential of ASR gel. Therefore, comparing the results obtained in this study (Table 5), one sees that the potassium concentration of ASR gel follows a similar trend as calcium content; the potassium concentration of all specimens gathered from unrestrained directions of reinforced blocks has a quite higher value when compared to those gathered from restrained directions.

The above discussions clearly attest the fact that the chemical composition of ASR gel is completely different in various directions of reinforced concrete blocks and thus highlight the importance of investigating anisotropic effects in ASR-affected structures. Therefore, in order to have a better picture of the effect of distinct restraint conditions on the correlation of distinct chemical compositions of ASR gel, a number of easy-to-use contour plots were developed as per Figure 15. Part A of the latter shows the variations of K/Si of ASR gel sourced from aggregate particles of unrestrained concrete blocks as a function of different pairs of the composition variables (i.e., Na/Si and Ca/Si). Similar contour plots were plotted in Figures 15B and C for the same chemical composition correlation obtained from the ASR gel retrieved from aggregate particles of unrestrained and restrained directions of reinforced blocks, respectively. It is worth noting that the same contour plots have been developed for the chemical compositions of ASR gel obtained from aggregate particles of 1D blocks (for unrestrained direction- transverse and vertical cores as well as restrained direction-longitudinal cores, Figure 17A and B, respectively), 2D blocks (for unrestrained direction- vertical cores and restrained directions-longitudinal and transverse cores, Figure 18A and B, respectively) and cement paste (for unrestrained blocks, unrestrained and restrained directions of reinforced blocks, Figure 19A, B and C, respectively) which can be found in the supplementary materials section.

As previously mentioned, Gholizadeh et al. [9] proposed a correlation between Na/Si, Ca/Si and the swelling potential of synthetic ASR gel while the potassium content of ASR gel has not been fully considered in that study. Thus, this study tried to correlate the aforementioned ratio with K/Si obtained from ASR gels of real concrete elements (restrained and unrestrained). Considering the abovementioned discussion, the higher the Na/Si, Ca/Si and K/Si ratios, the higher the swelling potential of ASR gel. Thus, the authors believe that the ASR gel with the highest swelling potential (i.e., represented by the red and orange color) in each direction of concrete blocks can be easily detected with the aid of these contour plots. For instance, it can be seen that an ASR gel retrieved from the aggregate particles of unrestrained directions of reinforced concrete blocks with $0.29 < Ca/Si < 0.35$, $0.074 < Na/Si < 0.082$, $0.25 < K/Si < 0.29$ would have the highest swelling potential in that direction and is likely to be deleterious in concrete. Another benefit of the contour plots displayed in Figure 15 (and Figures 17, 18 and 19 in the supplementary materials section) is that they help engineers and researchers while studying the microstructure of ASR-damaged concrete structure to predict the ASR gel's composition obtained from various locations of those inaccessible/ unavailable directions by comparing the results gathered from the available cored specimens.

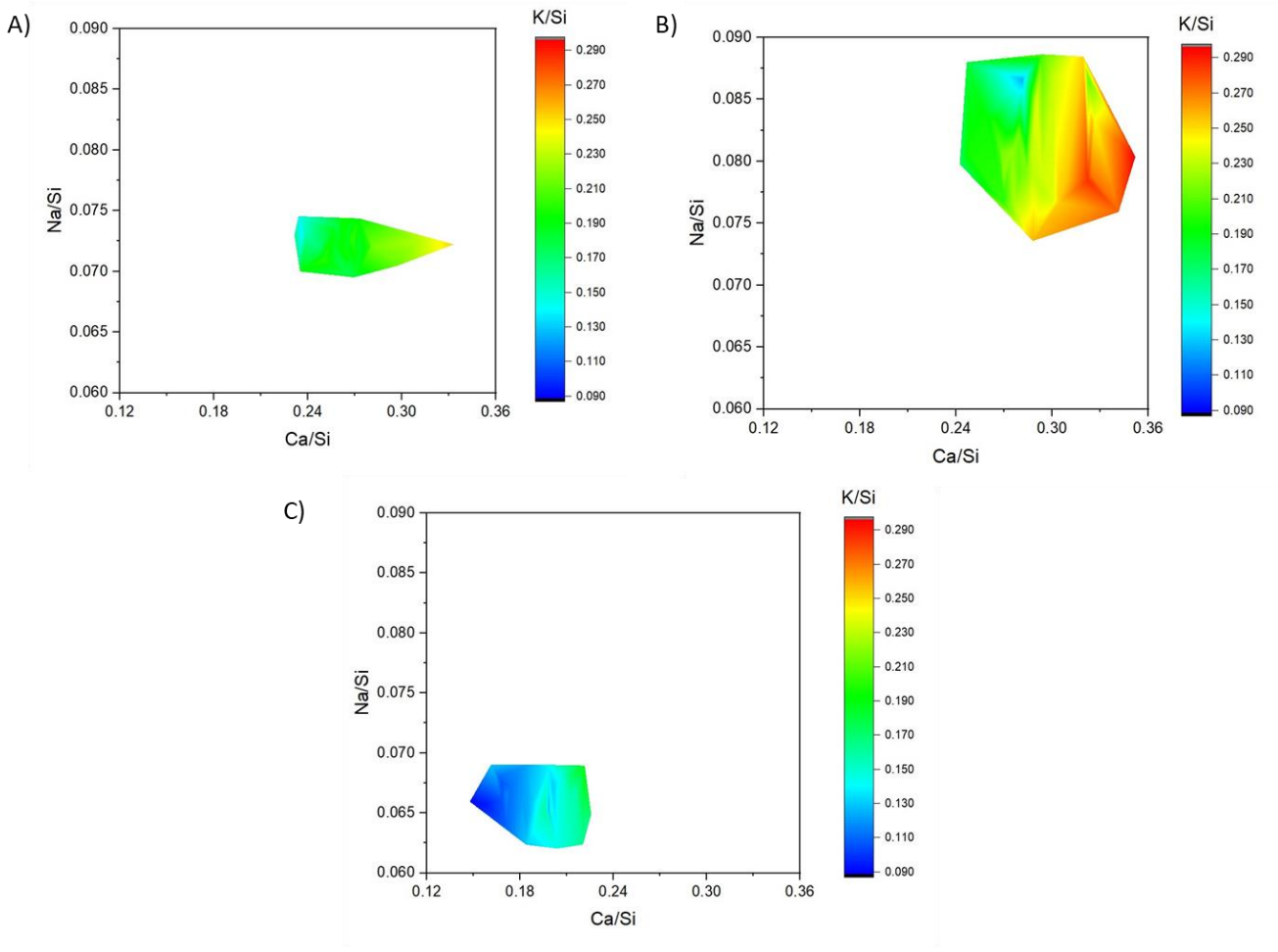

Figure 15: The contour plots of K/Si as a function of Na/Si and Ca/Si obtained from aggregate particles of A) unrestrained blocks, B) unrestrained directions of reinforced blocks and C) restrained direction (of reinforced blocks).

10.6.2 Effect of restraint on the mechanical properties of ASR gel

A number of computer models have previously been developed to predict the service-life of ASR affected structures [3]. Although their outcomes are very interesting, most of them have never considered the mechanical properties of ASR gels as a function of the gel composition. In this section, the compressive strength and hardness of ASR product will be discussed as follows:

10.6.2.1Compressive strength of ASR gel

Previously Gholizadeh et al. [15] proposed the following equation to calculate the compressive strength of ASR gel with the aid of its chemical composition. Looking at the equation, one clearly sees that the chemical composition of ASR gel could play a significant role in the compressive strength of ASR gel.

$$\sigma_c(MPa) = 7.14 + 47.7\left(\frac{Ca}{Si}\right) - 5.91\left(\frac{Na}{Si}\right) - 28.1\left(\frac{K}{Si}\right) - 70.1\left(\frac{Ca}{Si}\right)^2 - 23.3\left(\frac{Ca}{Si}\right)\left(\frac{Na}{Si}\right) + 54.1\left(\frac{Ca}{Si}\right)\left(\frac{K}{Si}\right)$$

Therefore, this study calculated the compressive strength (CS) of ASR reaction product obtained from distinct locations of various concrete blocks as per the abovementioned equation. Tables 5A, B and C display the CS of ASR gel obtained from aggregate particles, ITZ and cement paste of various concrete blocks, respectively. Comparing the calculated CS of ASR gel obtained from aggregate particles, one notices the anisotropic effect of confinement in reinforced concrete; the CS of ASR gel obtained from aggregate particles of unrestrained directions of reinforced blocks demonstrated higher values compared to those gathered from the restrained direction. For instance, the CS of ASR gel found in vertical core of 2D blocks (i.e., unrestrained direction) was 11.50 MPa while the CS of those obtained from transverse and longitudinal cores (i.e., restrained directions) of 2D blocks was 10.6 MPa. Otherwise, not a considerable difference has been observed on the CS of ASR gel obtained from ITZ and cement paste of various locations of reinforced blocks. It is worth noting that despite the CS values gathered through the use of the aforementioned analytical equation, experimental results can provide better information on the effect of distinct restraint configurations on the mechanical properties of ASR gel. Therefore, the results of the microhardness (and viscosity) test will be discussed in the next section.

10.6.2.2Hardness of ASR gel

As per figure 10, although not much difference was observed on the "overall" Vickers hardness of various concrete blocks of this study, as discussed in previous sections, a thorough study on the effect of ASR anisotropy on the hardness of ASR gel in various locations of concrete blocks is required to fully understand the effect of restraint on the micro-characteristics of ASR gel. Therefore, Figures 16A and B illustrate the result of Vickers hardness test (i.e., loading rate of 50mN) conducted on the ASR gel found in aggregate particles and cement paste of distinct directions of various concrete blocks of this study, respectively. It is worth mentioning that Figures 20, 21, and 22, in the supplementary materials section, display the results of Vickers hardness test performed with various loading rates of this study (12mN, 25mN and 50mN) on ASR gel found in aggregate particles of unrestrained, 1D, and 2D concrete blocks, respectively.

Comparing the hardness results obtained from the aggregate particles of various concrete blocks (Figure 16A), only a slight difference has been observed on the ASR gels (i.e., at the center of the crack- around 350 µm from the initial point) of various directions of each concrete block. As such, the Vickers hardness of 30, 29, and 28 were gathered for the ASR gel found in the aggregate particles of vertical, transverse, and longitudinal cores of unrestrained blocks, respectively. On the other hand, the Vickers hardness of 22, 23, and 30 by 1D blocks, as well as 18, 28, and 29 by 2D blocks have been achieved on the ASR gel obtained from aggregate particles of vertical, transverse, and longitudinal cores, respectively. Such inconsiderable differences amongst the hardness of ASR gel obtained from aggregate particles of various reinforced concrete blocks of this study could probably be due to the fact that all ASR gel formed in aggregate particles

propagated to the cement paste; thus, it is expected to observe anisotropic hardness of ASR gel in cement paste of restrained concrete. As such, evaluating those results gathered from the cement paste (Figure 16B) of various directions of distinct concrete blocks, one sees the quite different behavior as per the restraint condition. Similar to the other properties of ASR gel in unrestrained blocks, not a considerable difference has been observed on the hardness of ASR gel gathered from cement paste of distinct directions; the Vickers hardness of 216, 215, and 216 were found on the ASR gel obtained from the cement paste (at the center of the crack- around 175 μm from the initial point) of vertical, transverse and longitudinal cores of unrestrained blocks, respectively. Conversely, the ASR gel found in cement paste of vertical, transverse, and longitudinal cores showed to have the Vickers hardness of 253, 245, and 190 in 1D blocks and 285, 184, and 181 in 2D concrete blocks, respectively. The above results once again attest the anisotropic behavior of ASR gel in reinforced concrete blocks where the ASR gel in cement paste of unrestrained directions of restrained blocks demonstrates significantly higher Vickers hardness value when compared to the restrained directions of the same concrete element.

Moreover, according to Broitman [51] and Shuman et al. [58], the higher the hardness of a material, the harder that material is; for instance, comparing the hardness values obtained on ASR gel found in cement paste of various concrete elements, one sees that those obtained from the unrestrained directions of restrained concrete (i.e., vertical and transverse in case of 1D and vertical in case of 2D concrete blocks) are harder material than the ones found on the restrained directions. Otherwise, as per Gholizadeh et al. [9], the softer the ASR gel, the higher the potential to flow and thus the lower the viscosity. This therefore clearly suggests that unlike the ASR gel obtained from the cement paste of unrestrained directions, those gathered from restrained directions have lower viscosity compared to the latter. On the other hand, as previously mentioned, the higher the viscosity of the ASR gel, the higher the deleterious potential they have [5,9,16]. Consequently, the above discussions demonstrate that the ASR gels obtained from the cement paste of unrestrained directions of restrained concrete elements are significantly more deleterious than unrestrained blocks and restrained directions of reinforced blocks. The above finding is in accordance with the other results gathered previously in this study; restraint causes anisotropy on ASR-induced development and mechanical degradation.

A)

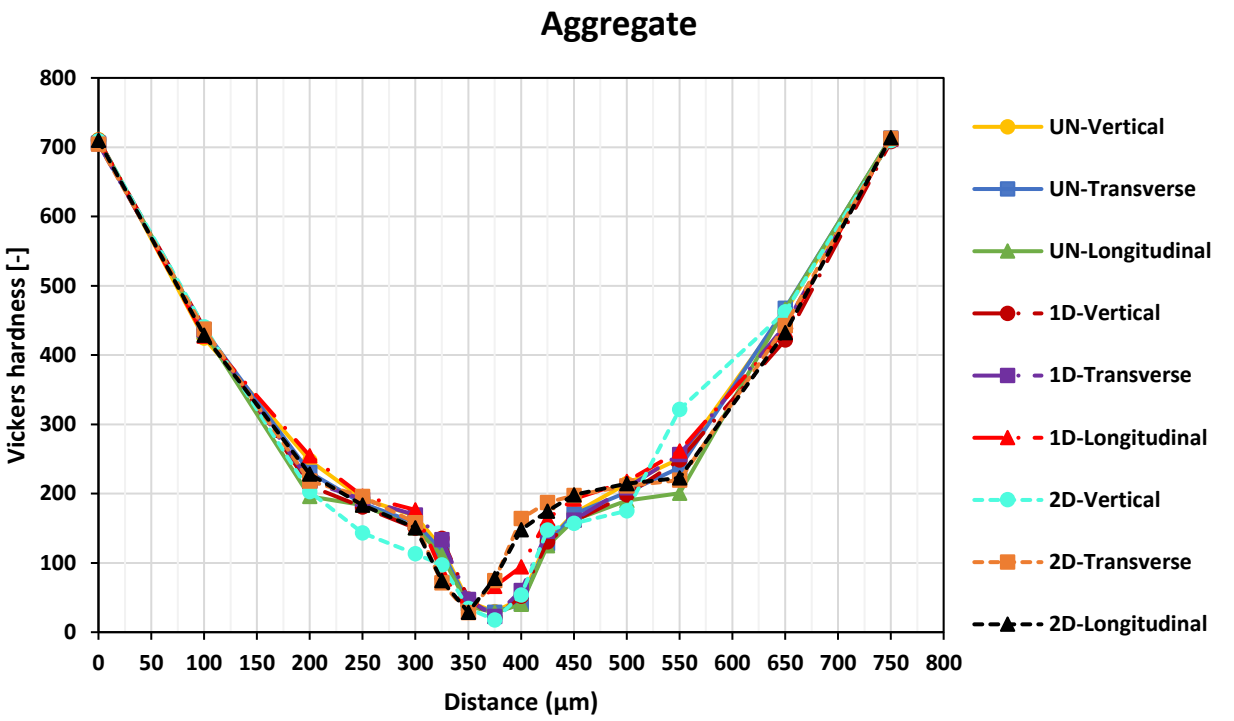

B)

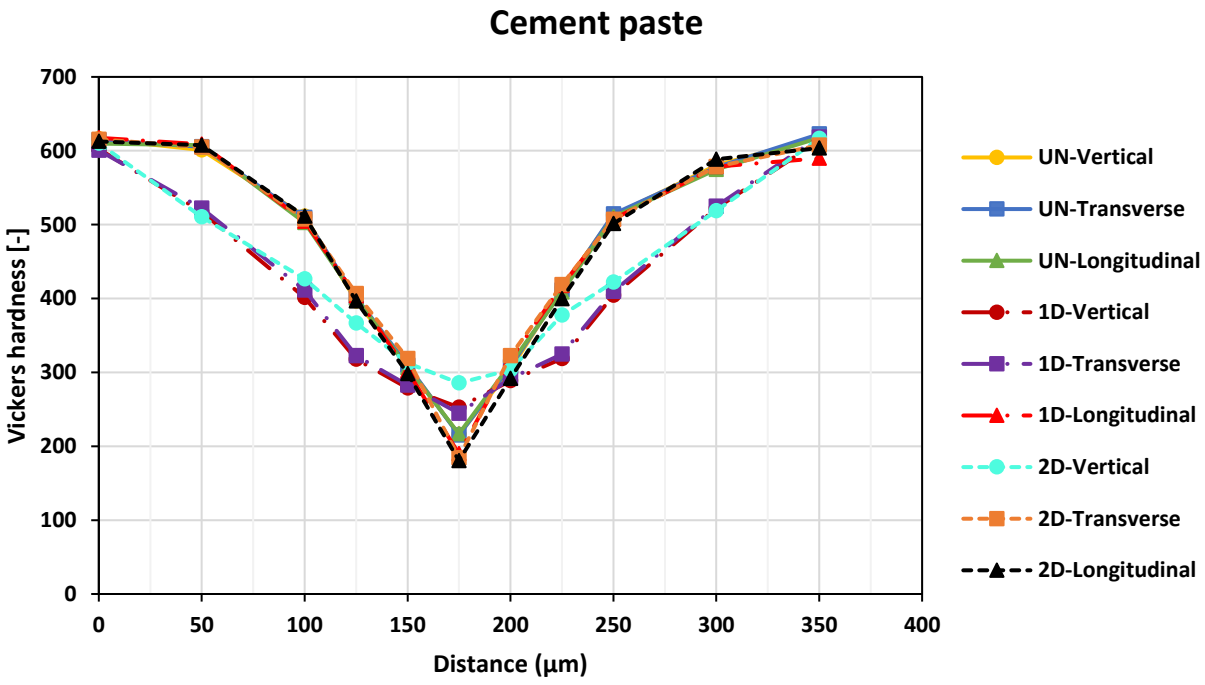

Figure 16: Vickers hardness of obtained from A) aggregate particles and B) cement paste of distinct directions of various concrete blocks of this study.

10.7 Conclusions

This study has been conducted with the aim to microscopically and mechanically characterize ASR gel formed in various locations (i.e., aggregate particles, ITZ and cement paste) of concrete blocks having different restraint configurations (i.e., none, 1D and 2D). Accordingly, the results of this study exhibit that restraint could affect the chemical composition and mechanical properties of ASR gel. The major conclusions are summarized as follows:

- The overall characterization (i.e., average of three distinct directions) of ASR gels obtained from various blocks of this study showed to have an identical value. In other words, the "Overall" chemical compositions and mechanical properties of ASR gel do not seem to considerably change as a function of the restraint condition.

- Similar to the induced expansion where it has been significantly affected by the restraint configuration (ASR-induced expansion transferred from restrained to unrestrained/less restrained directions of restrained blocks), an important anisotropic behaviour in terms of the chemical composition of ASR gels gathered from distinct locations (aggregate particles, ITZ and cement paste) of restrained blocks has also been detected. As such, the ASR gel obtained from the unrestrained directions of restrained concrete has significantly higher (Na+K)/Si and Ca/Si when compared to the unrestrained directions of those blocks.

- Investigating the effects of restraint on distinct chemical compositions of ASR gel, one notices that the gels originating from the restrained directions of reinforced concrete have higher sodium and silicate and lower calcium and potassium content. Such observation could probably be due to the fact that those ASR gels are restrained and cannot easily leave the reaction site; thus the dissolution of the reactive aggregate of those directions is retarded, which could reduce the reactivity of the aggregate, and, hence, the gel formation. The above could be the reason that the induced expansion of restrained directions is lower than unrestrained areas.

- At the end of this study, a number of easy to use distinct chemical compositions of ASR gel (i.e., K/Si, Na/Si and Ca/Si) contour plots have been developed. The use of such plots could be a very useful tool for researchers and engineers in order to either detect the highest swelling potential of various directions of each concrete block or predicting the ASR gel's composition of inaccessible/ unavailable directions of affected concrete members.

- Although not a significant difference has been observed on the results of hardness test obtained from ASR gel originated from aggregate particles (which probably could be due to the fact that all

ASR gel formed in aggregate particles propagated to the cement paste), those gathered from the cement paste was found to be different. As such, the ASR gel obtained from the cement paste of unrestrained directions of restrained blocks showed to have significantly higher hardness and thus deleterious potential than unrestrained blocks and restrained directions of reinforced blocks.

Acknowledgments

The authors would like to thank Drs. Gamal Elnabelsya and Muslim Majeed, technical officers of Materials and Structures Laboratory in the Department of Civil Engineering at the University of Ottawa, as well as Ms. Cassandra Trottier and Nusrat Zubaida who helped with the casting and testing of the test specimens used in this work. Likewise, the authors would like to thank Mr. Matthew McDonald and his colleagues from Advance Cutting & Coring Ltd. for facilitating the critical process of drilling and retrieving core samples from the studied concrete blocks. Lastly, the first author of this study benefits from the prestigious University of Ottawa admission scholarship for international Ph.D. students.

References

[1] A. Zahedi, C. Trottier, L. Sanchez, M. Noël, Microscopic Assessment of ASR-Affected Concrete Under Confinement Conditions, Cem Concr Res. (2021) 106456. https://doi.org/https://doi.org/10.1016/j.cemconres.2021.106456.
[2] Y. Zhu, A. Zahedi, L.F.M. Sanchez, B. Fournier, S. Beauchemin, Overall assessment of alkali-silica reaction affected recycled concrete aggregate mixtures derived from construction and demolition waste, Cem. Concr. Res. 142 (2021) 106350. https://doi.org/10.1016/j.cemconres.2020.106350.
[3] F. Rajabipour, E. Giannini, C. Dunant, J.H. Ideker, M.D.A. Thomas, Alkali-silica reaction: Current understanding of the reaction mechanisms and the knowledge gaps, Cem. Concr. Res. 76 (2015) 130–146. https://doi.org/10.1016/j.cemconres.2015.05.024.
[4] A. Leemann, B. Münch, The addition of caesium to concrete with alkali-silica reaction: Implications on product identification and recognition of the reaction sequence, Cem. Concr. Res. 120 (2019) 27–35. https://doi.org/10.1016/j.cemconres.2019.03.016.
[5] A. Gholizadeh-Vayghan, F. Rajabipour, The influence of alkali–silica reaction (ASR) gel composition on its hydrophilic properties and free swelling in contact with water vapor, Cem. Concr. Res. 94 (2017) 49–58. https://doi.org/10.1016/j.cemconres.2017.01.006.
[6] X. Hou, R.J. Kirkpatrick, L.J. Struble, P.J.M. Monteiro, Structural investigations of alkali silicate gels, J. Am. Ceram. Soc. 88 (2005) 943–949. https://doi.org/10.1111/j.1551-2916.2005.00145.x.
[7] A. Leemann, T. Katayama, I. Fernandes, M. Broekmans, Types of alkali-aggregate reactions and the products formed, Proc. Inst. Civ. Eng. 169 (2016) 128–135. https://doi.org/10.1680/jcoma.15.00059.
[8] Z. Shi, B. Lothenbach, The combined effect of potassium, sodium and calcium on the formation of alkali-silica reaction products, Cem. Concr. Res. 127 (2020) 105914. https://doi.org/10.1016/j.cemconres.2019.105914.
[9] A. Gholizadeh-Vayghan, F. Rajabipour, Quantifying the swelling properties of alkali-silica reaction (ASR) gels as a function of their composition, J. Am. Ceram. Soc. 100 (2017) 3801–3818. https://doi.org/10.1111/jace.14893.
[10] A. Leemann, Z. Shi, J. Lindgård, Characterization of amorphous and crystalline ASR products formed in concrete aggregates, Cem. Concr. Res. 137 (2020) 106190. https://doi.org/10.1016/j.cemconres.2020.106190.
[11] A. Leemann, Z. Shi, M. Wyrzykowski, F. Winnefeld, Moisture stability of crystalline alkali-silica

reaction products formed in concrete exposed to natural environment, Mater. Des. 195 (2020) 109066. https://doi.org/10.1016/j.matdes.2020.109066.
[12] H. Wu, J. Pan, J. Wang, Nano-scale structure and mechanical properties of ASR products under saturated and dry conditions, Sci. Rep. 10 (2020) 1–9. https://doi.org/10.1038/s41598-020-66262-9.
[13] A. Leemann, P. Lura, E -modulus of the alkali – silica-reaction product determined by micro-indentation, Constr. Build. Mater. 44 (2013) 221–227. https://doi.org/10.1016/j.conbuildmat.2013.03.018.
[14] C. Hu, B.P. Gautam, D.K. Panesar, Nano-mechanical properties of alkali-silica reaction (ASR) products in concrete measured by nano-indentation, Constr. Build. Mater. 158 (2018) 75–83. https://doi.org/10.1016/j.conbuildmat.2017.10.006.
[15] A. Gholizadeh-Vayghan, F. Rajabipour, M. Khaghani, M. Hillman, Characterization of viscoelastic behavior of synthetic alkali–silica reaction gels, Cem. Concr. Compos. 104 (2019) 103359. https://doi.org/10.1016/j.cemconcomp.2019.103359.
[16] A. Gholizadeh Vayghan, F. Rajabipour, J.L. Rosenberger, Composition-rheology relationships in alkali-silica reaction gels and the impact on the Gel's deleterious behavior, Cem. Concr. Res. 83 (2016) 45–56. https://doi.org/10.1016/j.cemconres.2016.01.011.
[17] C.P. Ostertag, C.K. Yi, P.J.M. Monteiro, Effect of confinement on properties and characteristics of alkali-silica reaction gel, ACI Mater. J. 104 (2007) 276–282. https://doi.org/10.14359/18673.
[18] H. Song, K. Cheng, C.P. Ostertag, Influence of matrix properties on alkali silica reaction rates, Mater. Struct. Constr. 41 (2008) 47–57. https://doi.org/10.1617/s11527-006-9217-6.
[19] M. Kawamura, K. Iwahori, ASR gel composition and expansive pressure in mortars under restraint, Cem. Concr. Compos. 26 (2004) 47–56. https://doi.org/10.1016/S0958-9465(02)00135-X.
[20] S. Diamond, A REVIEW OF ALKALI-SILICA REACTION AND EXPANSION MECHANISMS, Cem. Concr. Res. 6 (1976) 549–560.
[21] S. Chatterji, Chemistry of alkali-silica reaction and testing of aggregates, Cem. Concr. Compos. 27 (2005) 788–795. https://doi.org/10.1016/j.cemconcomp.2005.03.005.
[22] L.S.D. Glasser, N. Kataoka, The chemistry of "alkali-aggregate" reaction, Cem. Concr. Res. 11 (1981) 1–9.
[23] A.K. Varsheneya, J.C. Mauro, Fundamentals of Inorganic Glasses, Elsevier, 2019. https://doi.org/10.1016/b978-0-12-816225-5.09992-2.
[24] E. Boehm-Courjault, S. Barbotin, A. Leemann, K. Scrivener, Microstructure, crystallinity and composition of alkali-silica reaction products in concrete determined by transmission electron microscopy, Cem. Concr. Res. 130 (2020) 105988. https://doi.org/10.1016/j.cemconres.2020.105988.
[25] A. Gholizadeh Vayghan, Characterization of the Rheological and Swelling Properties of Synthetic Alkali Silicate Gels in Order To Predict Their Behavior in Asr Damaged Concrete, [PhD Thesis] Department of Civil and Environmental Engineering, The Pennsylvania State University, (2017) 245.
[26] H. Maraghechi, F. Rajabipour, C.G. Pantano, W.D. Burgos, Effect of calcium on dissolution and precipitation reactions of amorphous silica at high alkalinity, Cem. Concr. Res. 87 (2016) 1–13. https://doi.org/10.1016/j.cemconres.2016.05.004.
[27] M.D.A. Thomas, The role of calcium hydroxide in alkali recycling in concrete, in: J. Skalny, J. Gebauer, I. Odler (Eds.), Materials Science of Concrete Special Volume on Calcium Hydroxide in Concrete, American Ceramic Society, Westerville, OH, 2001.
[28] S. Diamond, A review of alkali-silica reaction and expansion mechanisms 1. Alkalies in cements and in concrete pore solutions, Cem. Concr. Res. 5 (1975) 329–345. https://doi.org/10.1016/0008-8846(75)90089-7.
[29] S.M.H. Shafaatian, A. Akhavan, H. Maraghechi, F. Rajabipour, How does fly ash mitigate alkali-silica reaction (ASR) in accelerated mortar bar test (ASTM C1567)?, Cem. Concr. Compos. 37 (2013) 143–153. https://doi.org/10.1016/j.cemconcomp.2012.11.004.
[30] R.F. Bleszynski, M.D.A. Thomas, Microstructural studies of alkali-silica reaction in fly ash concrete immersed in alkaline solutions, Adv. Cem. Based Mater. 7 (1998) 66–78. https://doi.org/10.1016/S1065-7355(97)00030-8.
[31] T.C. Powers, H.H. Steinour, An Interpretation of Some Published Researches on the Alkali-

Aggregate Reaction Part 1-The Chemical Reactions and Mechanism of Expansion., J. Am. Concr. Inst. 26 (1955) 497–516.
[32] P.J.M. Monteiro, K. Wang, G. Sposito, M.C. Dos Santos, W.P. De Andrade, Influence of mineral admixtures on the alkali-aggregate reaction, Cem. Concr. Res. 27 (1997) 1899–1909. https://doi.org/10.1016/S0008-8846(97)00206-8.
[33] A. Leemann, T. Katayama, I. Fernandes, M.A. Broekmans, Types of alkali-aggregate reactions and the products formed,", Institut. Civ. Eng. - Constr. Mat. 169 (2016) 128.
[34] Š. Šachlová, R. Přikryl, Z. Pertold, Alkali-silica reaction products: Comparison between samples from concrete structures and laboratory test specimens, Mater. Charact. 61 (2010) 1379–1393. https://doi.org/10.1016/j.matchar.2010.09.010.
[35] C. Hu, B.P. Gautam, D. Shang, F. Wang, D.K. Panesar, Atomic force microscopy characterisation of alkali-silica reaction products to reveal their nanostructure and formation mechanism, Ceram. Int. 44 (2018) 7310–7314. https://doi.org/10.1016/j.ceramint.2018.01.069.
[36] I. Fernandes, F. Noronha, M. Teles, Examination of the concrete from an old Portuguese dam: Texture and composition of alkali-silica gel, Mater. Charact. 58 (2007) 1160–1170. https://doi.org/10.1016/j.matchar.2007.04.007.
[37] K. Peterson, D. Gress, T. Van Dam, L. Sutter, Crystallized alkali-silica gel in concrete from the late 1890s, Cem. Concr. Res. 336 (2006) 1523–1532.
[38] Niels Thaulow, U.H. Jakobsen, B. Clark, Composition of alkali-silica gel and ettringite in concrete railroad ties: SEM-EDX AND X-ray diffraction analysis, Cem. Concr. Res. 26 (1996) 309–318.
[39] Z. Shi, A. Leemann, D. Rentsch, B. Lothenbach, Synthesis of alkali-silica reaction product structurally identical to that formed in field concrete, Mater. Des. 190 (2020) 108562. https://doi.org/10.1016/j.matdes.2020.108562.
[40] C. Zhang, L. Sorelli, B. Fournier, J. Duchesne, J. Bastien, Z. Chen, Stress-relaxation of crystalline alkali-silica reaction products : Characterization by micro- and nanoindentation and simplified modeling, 148 (2017) 455–464.
[41] M. Prezzi, P.J.M. Monteiro, G. Sposito, The alkali-silica reaction, part I: Use of the double-layer theory to explain the behavior of reaction-product gels, ACI Mater. J. 94 (1997) 10–17. https://doi.org/10.14359/280.
[42] N. Roussel, Understanding the Rheology of Concrete, A volume in Woodhead Publishing Series in Civil and Structural Engineering, 2012.
[43] L. Sun, X. Zhu, X. Zhuang, G. Zi, Chemo-mechanical model for the expansion of concrete due to alkali silica reaction, Appl. Sci. 10 (2020). https://doi.org/10.3390/app10113807.
[44] A.B. Giorla, K.L. Scrivener, C.F. Dunant, Influence of visco-elasticity on the stress development induced by alkali-silica reaction, Cem. Concr. Res. 70 (2015) 1–8. https://doi.org/10.1016/j.cemconres.2014.09.006.
[45] S. Multon, A. Sellier, M. Cyr, Chemo-mechanical modeling for prediction of alkali silica reaction (ASR) expansion, Cem. Concr. Res. 39 (2009) 490–500. https://doi.org/10.1016/j.cemconres.2009.03.007.
[46] Y. Zhuang, C. Qian, W. Xu, Calculation of alkali silica reaction (ASR) induced expansion before cracking of concrete, J. Wuhan Univ. Technol. Mater. Sci. Ed. 28 (2013) 110–116. https://doi.org/10.1007/s11595-013-0650-4.
[47] J. Moon, S. Speziale, C. Meral, B. Kalkan, S.M. Clark, P.J.M. Monteiro, Determination of the elastic properties of amorphous materials: Case study of alkali-silica reaction gel, Cem. Concr. Res. 54 (2013) 55–60. https://doi.org/10.1016/j.cemconres.2013.08.012.
[48] C.F. Dunant, K.L. Scrivener, Effects of uniaxial stress on alkali-silica reaction induced expansion of concrete, Cem. Concr. Res. 42 (2012) 567–576.
[49] ASTM C1293, Standard test method for determination of length change of concrete due to alkali-silica reaction, Annu. B. ASTM Stand. (2015) 1–7. https://doi.org/10.1520/C1293-08B.2.
[50] L.F.M. Sanchez, B. Fournier, M. Jolin, D. Mitchell, J. Bastien, Overall assessment of Alkali-Aggregate Reaction (AAR) in concretes presenting different strengths and incorporating a wide range of reactive aggregate types and natures, Cem. Concr. Res. 93 (2017) 17–31.

https://doi.org/http://dx.doi.org/10.1016/j.cemconres.2016.12.001.
[51] E. Broitman, Indentation Hardness Measurements at Macro-, Micro-, and Nanoscale: A Critical Overview, Tribol. Lett. 65 (2017) 1–18. https://doi.org/10.1007/s11249-016-0805-5.
[52] B.P. Gautam, D.K. Panesar, S.A. Sheikh, F.J. Vecchio, Multiaxial expansion-stress relationship for alkali silica reaction-affected concrete, ACI Mater. J. 114 (2017) 171–184. https://doi.org/10.14359/51689490.
[53] P. Morenon, S. Multon, A. Sellier, E. Grimal, F. Hamon, E. Bourdarot, Impact of stresses and restraints on ASR expansion, Constr. Build. Mater. 140 (2017) 58–74. https://doi.org/10.1016/j.conbuildmat.2017.02.067.
[54] P.M. Dove, The dissolution kinetics of quartz in aqueous mixed cation solutions, Geochim. Cosmochim. Acta. 63 (1999) 3715–3727. https://doi.org/10.1016/S0016-7037(99)00218-5.
[55] R. Lal, M. Shukla, Principles of Soil Physics, CRC, Amsterdam, 2004.
[56] J.H.M. Visser, Fundamentals of alkali-silica gel formation and swelling: Condensation under influence of dissolved salts, Cem. Concr. Res. 105 (2018) 18–30. https://doi.org/10.1016/j.cemconres.2017.11.006.
[57] A. Leemann, B. Lothenbach, The influence of potassium-sodium ratio in cement on concrete expansion due to alkali-aggregate reaction, Cem. Concr. Res. 38 (2008) 1162–1168. https://doi.org/10.1016/j.cemconres.2008.05.004.
[58] D.J. Shuman, A.L.M. Costa, M.S. Andrade, Calculating the elastic modulus from nanoindentation and microindentation reload curves, Mater. Charact. 58 (2007) 380–389. https://doi.org/10.1016/j.matchar.2006.06.005.
[59] B. Hilloulin, M. Robira, A. Loukili, Coupling statistical indentation and microscopy to evaluate micromechanical properties of materials: Application to viscoelastic behavior of irradiated mortars, Cem. Concr. Compos. 94 (2018) 153–165. https://doi.org/10.1016/j.cemconcomp.2018.09.008.

SUPPLEMENTARY MATERIALS

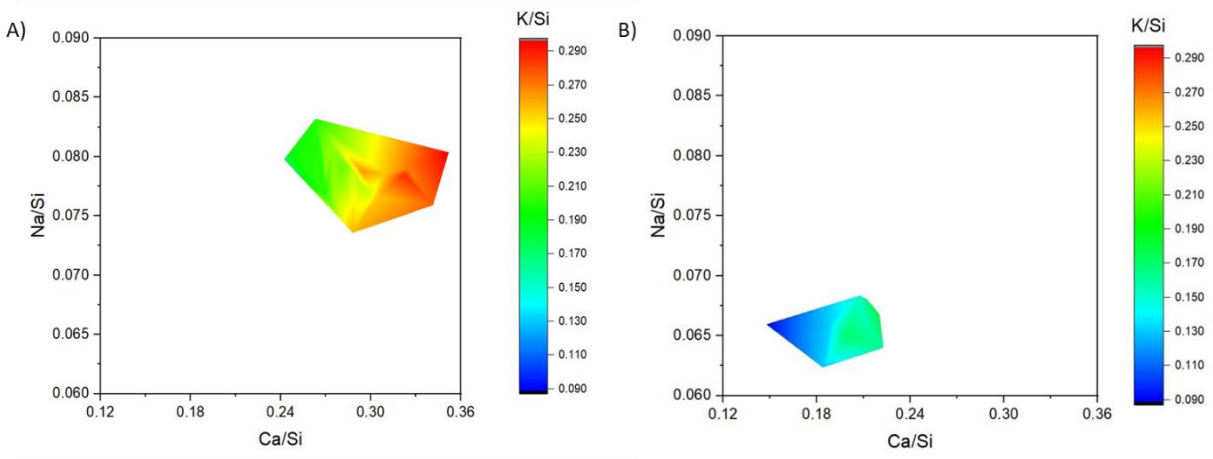

Figure 17: The contour plots of K/Si as a function of Na/Si and Ca/Si obtained from aggregate particles of A) unrestrained directions (vertical and transverse) and B) restrained direction (longitudinal) of 1D concrete blocks.

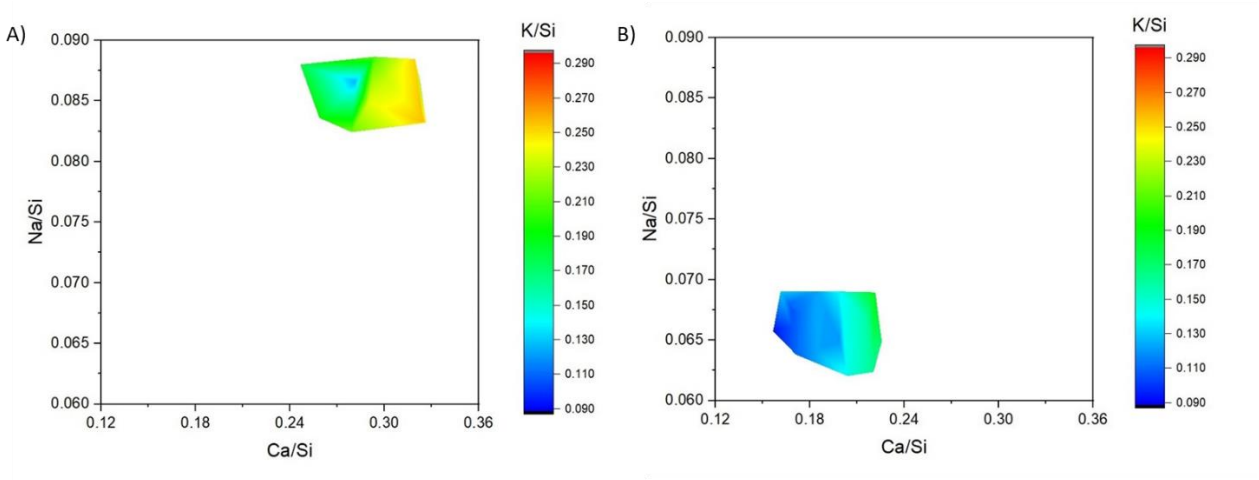

Figure 18: The contour plots of K/Si as a function of Na/Si and Ca/Si obtained from aggregate particles of A) unrestrained direction (vertical) and B) restrained directions (longitudinal and transverse) of 2D concrete blocks.

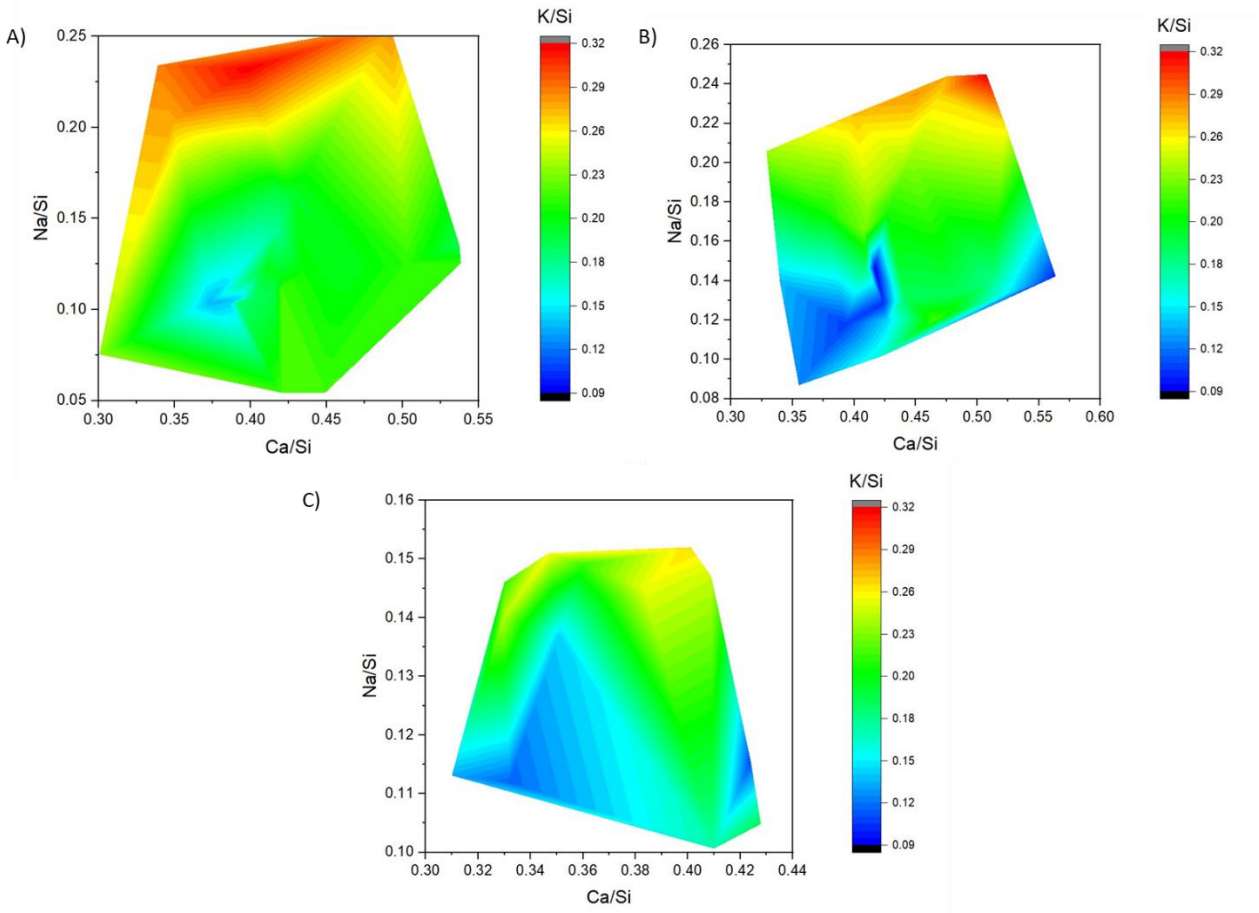

Figure 19: The contour plots of K/Si as a function of Na/Si and Ca/Si obtained from cement paste of A) unrestrained blocks, B) unrestrained directions of reinforced blocks and C) restrained direction (of reinforced blocks).

A)

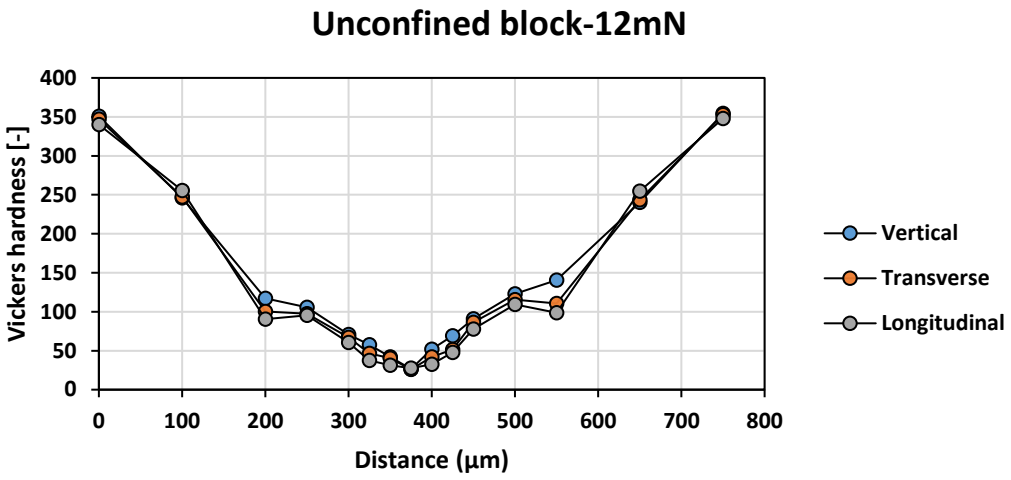
Unconfined block-12mN
Vickers hardness [-]
Distance (µm)
Vertical
Transverse
Longitudinal

B)

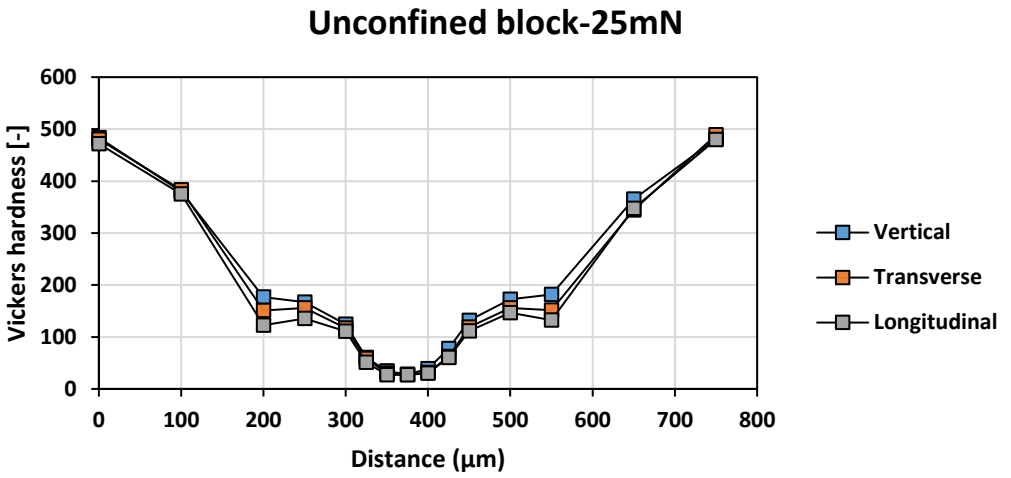
Unconfined block-25mN
Vickers hardness [-]
Distance (µm)
Vertical
Transverse
Longitudinal

C)

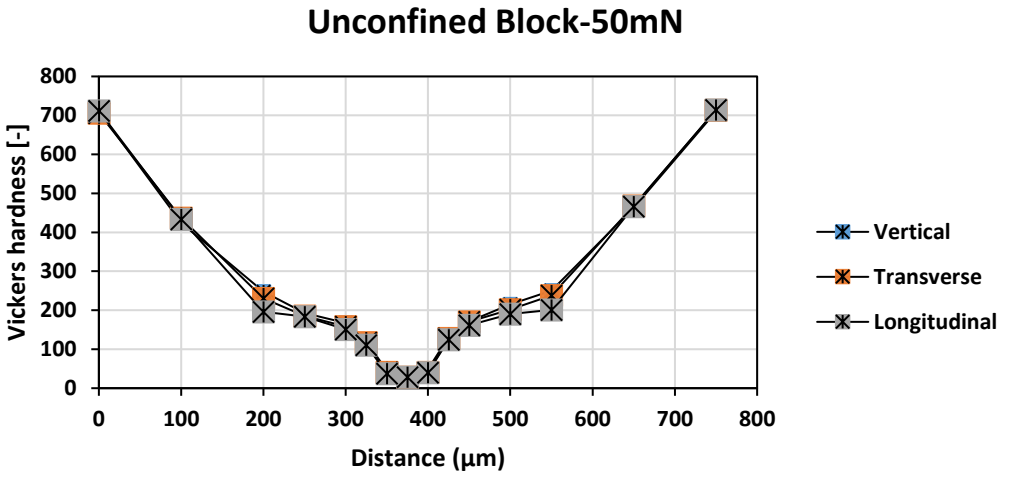
Unconfined Block-50mN
Vickers hardness [-]
Distance (µm)
Vertical
Transverse
Longitudinal

Figure 20: Vickers hardness profile across a crack of distinct directions of unrestrained concrete blocks, derived from indentation with the loading of A)12mN, B) 25mN and C) 50mN.

A)

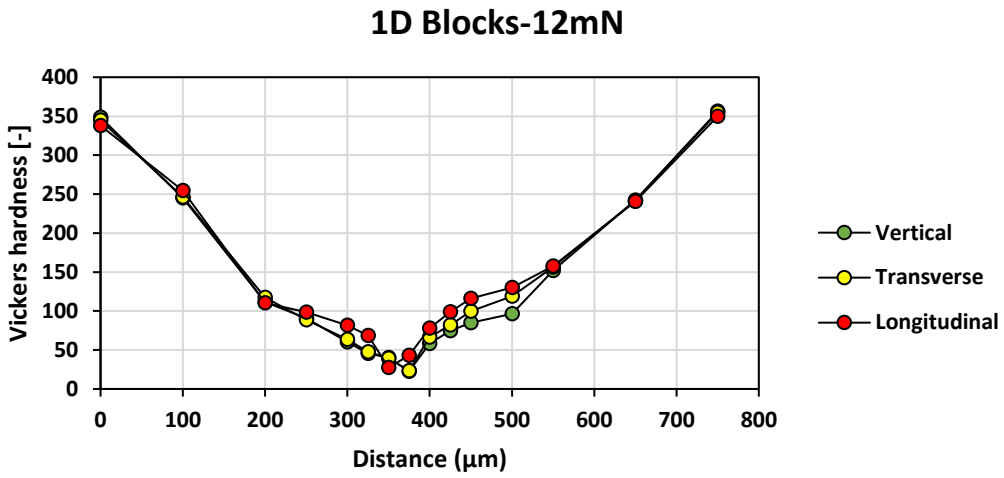

B)

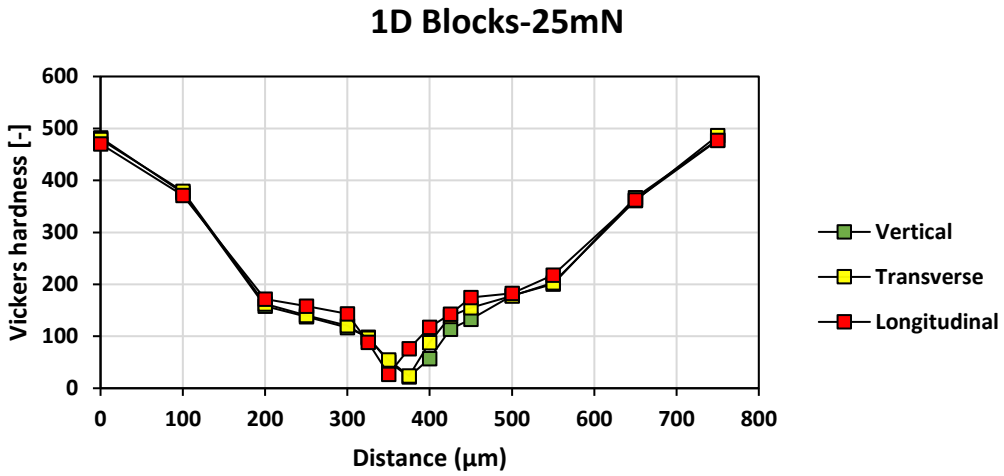

C)

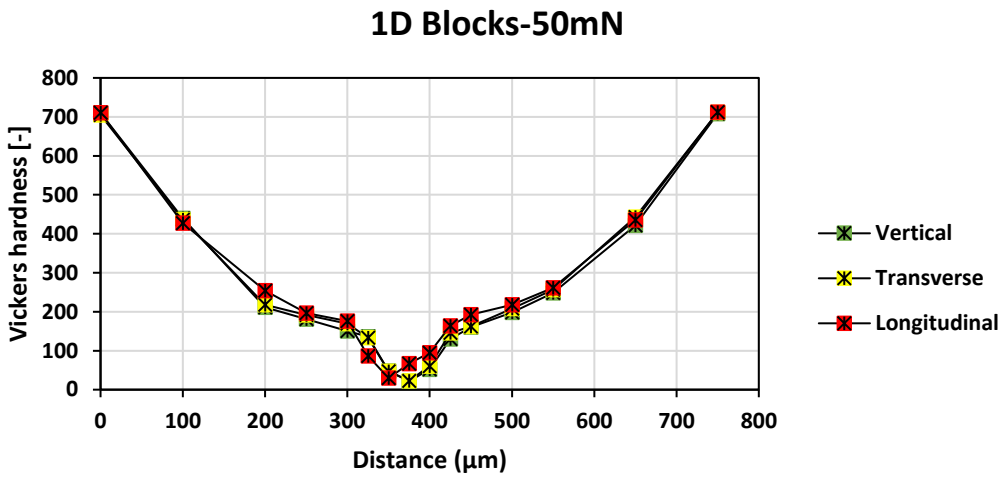

Figure 21: Vickers hardness profile across a crack of distinct directions of 1D-concrete blocks, derived from indentation with the loading of A)12mN, B) 25mN and C) 50mN.

A)

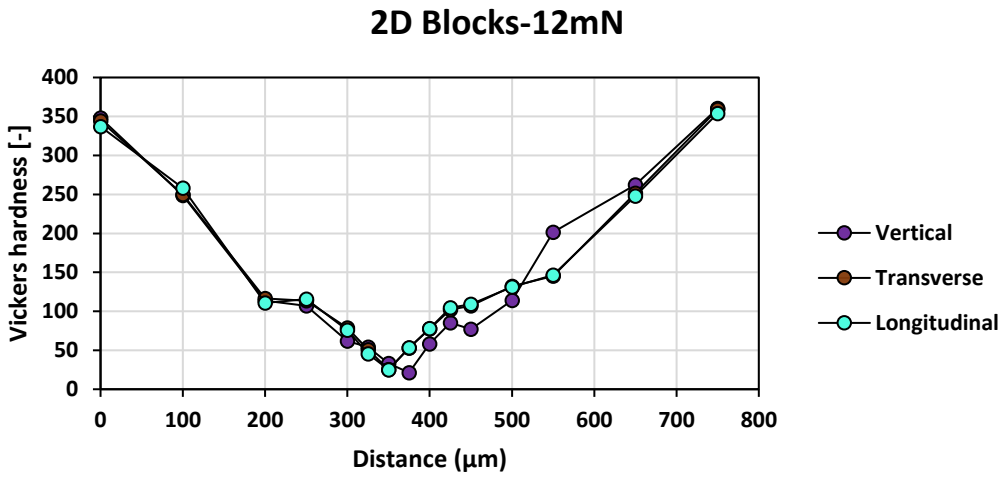

B)

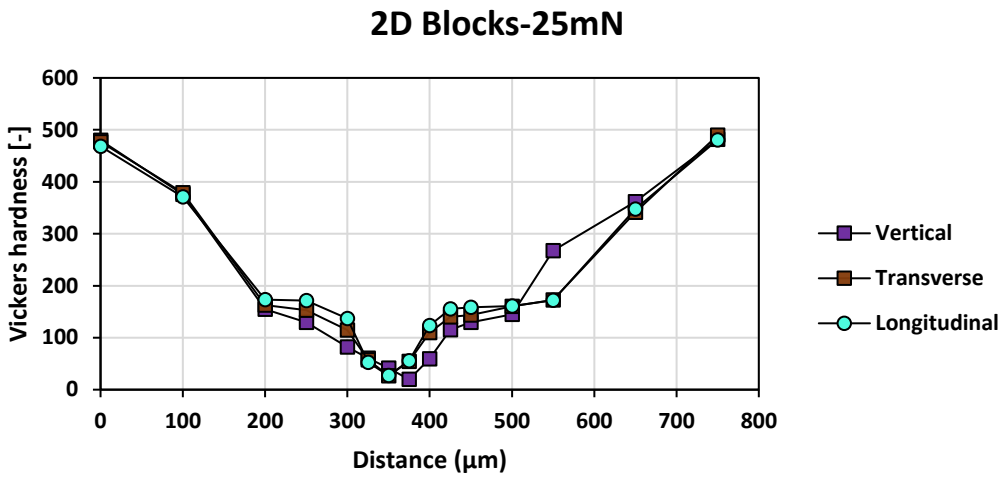

C)

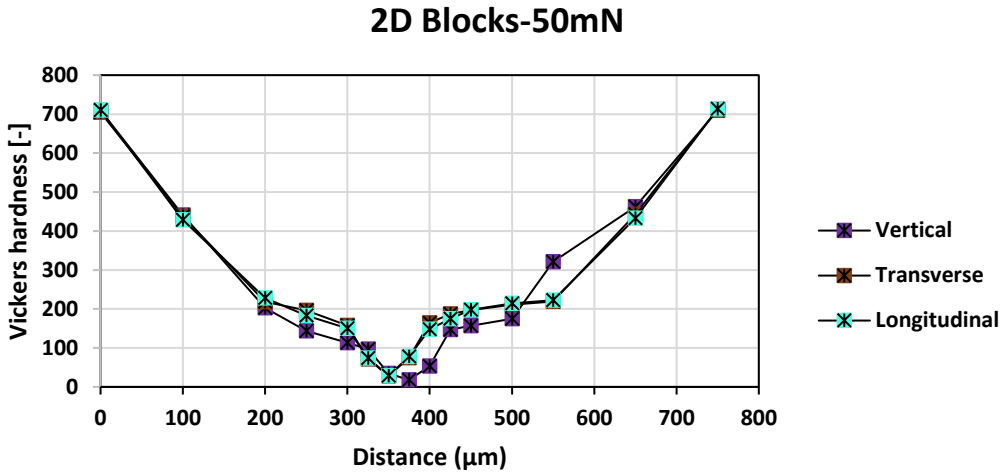

Figure 22: Vickers hardness profile across a crack of distinct directions of 2D- concrete blocks, derived from indentation with the loading of A)12mN, B) 25mN and C) 50mN.

11. FUTURE WORKS

As previously mentioned in the objective's section, this work has been conducted not only to investigate the impact of restraint on ASR-induced physicochemical development, but also to propose novel and efficient approaches to evaluate the potential for further expansion of ASR-affected concrete specimens in the laboratory. Second, this study also aims to improve the comprehensive management protocol previously proposed by Berube et al. [1] and Fournier et al. [2] with the aid of the results obtained from the diagnosis and prognosis parts of this study. It is worth noting that, due to the time limitation for the submission of this PhD thesis, although the experimental campaign has already been started, the final results will be analyzed during the one-year postdoctoral work of the author. Therefore, the following methodology is proposed for this part of this PhD work, as displayed in Figure 17.

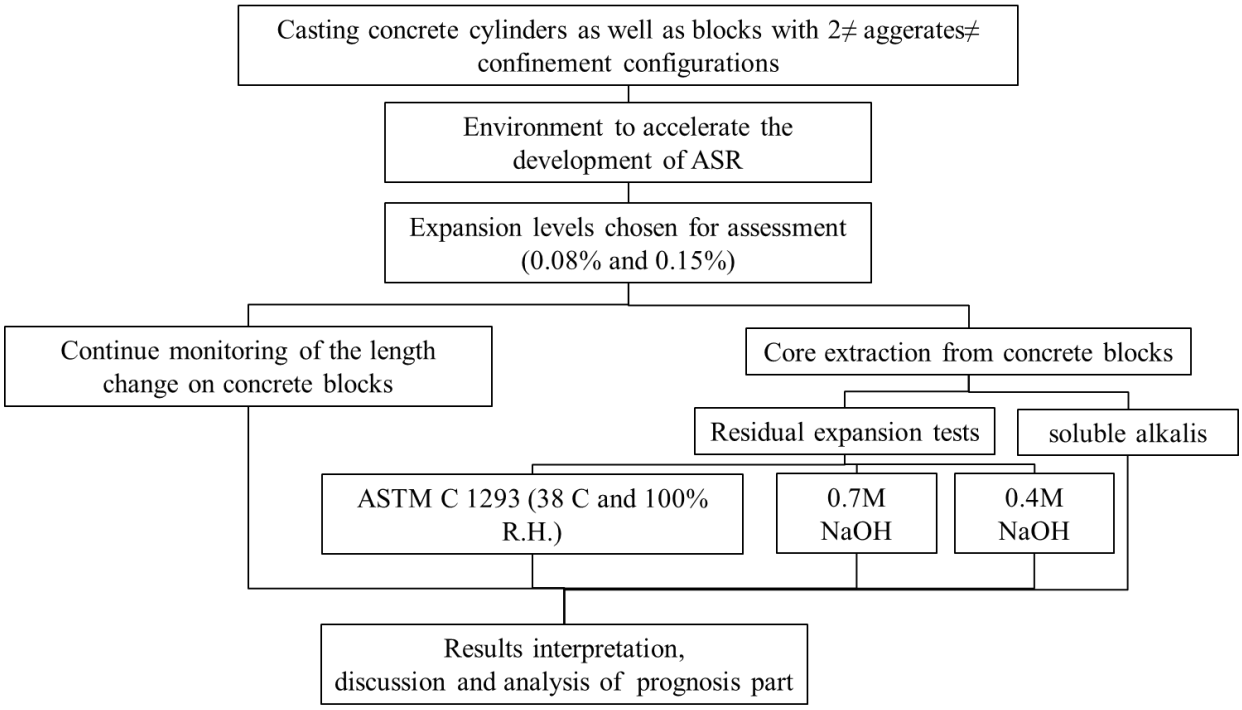

Figure 18: Structure of the future works of this PhD project.

11.1 Experimental procedures

For this section, eight additional concrete blocks to those investigated in the 1st part were manufactured in the laboratory with the same aggregate type, mix design and restraint configurations and stored in environmental conditions enabling ASR-induced development. Table 4 presents the number of concrete blocks for each aggregate type and restraint configuration.

Table 4: Number of concrete blocks per expansion and restraint configuration for the future work.

Mix design	Number of concrete blocks per expansion and restraint configuration					
	unrestrained Block		1D block		2D block	
	0.08%	0.15%	0.08%	0.15%	0.08%	0.15%
OT+SP	4	4	4	4	4	4
Tx+LS	-	-	-	-	4	4
					Total Samples: 32	

Similar to the first part of this PhD work, upon reaching the targeted expansion levels (i.e., 0.08% and 0.15%) concrete core specimens were extracted from distinct directions of each concrete blocks. Later, all cored specimens in addition to those eight additional concrete blocks which have been manufactured for this part of this PhD research (Table 5), were kept in the environmental chamber enabling ASR development (38ºC and 100% RH). All concrete blocks and cored specimens were regularly monitored over time. The testing program was carried out on various concrete specimens of this study at different expansion levels included residual expansion and Soluble Alkalis. Table 6 illustrates the typical testing program carried out on each set of extracted cored specimens and distinct restrained concrete blocks of this study. Comparing the results obtained from the expansion measurements conducted on the distinct surfaces of each concrete blocks with the ones gathered from those displayed in Table 6, this part of this PhD study is aimed to determine:

- The most reliable test method to predict the potential of further damage to ASR-affected concrete (restrained and non-restrained);
- The discrepancies between the RE of cores retrieved from affected non-restrained and restrained concrete blocks and tested in the laboratory, and the behaviour of the blocks themselves;
- Whether the use of different types of aggregates (i.e., fine vs. coarse reactive aggregates) may impact on the results of RE tests in affected concrete, and;
- Whether the use of distinct restraint configurations influences the RE outcomes.

Table 5: Number of concrete blocks per restraint condition kept in the environmental chamber for the future work.

Mix design	Number of concrete blocks per restraint ratio kept in the environmental chamber (ASTM C 1293)		
	unrestrained Block	1D block	2D block
OT+SP	2	2	2
TX+TM	-	-	2
			Total Blocks: 8

Table 6: Testing matrix for cores extracted from each set of distinct restrained concrete blocks for future work.

Test carried out	Coring direction	Number of specimens per direction for a given expansion level	
		0.08%	0.15%
Residual expansion	Vertical	6	6
	Transversal	6	6
	Longitudinal	6	6
Soluble Alkalis	Vertical	1	1
	Transversal	1	1
	Longitudinal	1	1
			Total Samples: 42

11.1.1 Residual Expansion test (RE)

A total of 144 extracted concrete specimens (i.e., 36 per set of distinct concrete blocks) were analyzed in this part of this study. Small holes of 8.5 mm in diameter by 19 mm long, were drilled in both ends of each cored specimen and stainless-steel gauge studs were glued in place, with fast setting cement slurry for longitudinal expansion measurements. Based on the available data in the literature, the authors proposed the following three test procedures for "classical" RE methods as described below, aiming to overcome some of the issues reported in the literature with the current methods:

- Sealed plastic containers (22 liters) lined with a damp cloth (4 cylinders per bucket). All buckets were stored at 100% RH and 38°C (Figure 19A);
- Sealed plastic containers (22 liters) containing a 0.7M NaOH solution (4 cylinders per bucket). All cylinders were soaked in the solution at 38°C (Figure 19A); and,
- Plastic mold displaying a slightly bigger diameter than the concrete specimens, containing a low amount (i.e., 50 ml) of 0.4M NaOH solution. Later, containers were placed horizontally in an environmental chamber at 100% RH and 38°C (Figure 19A).

For comparison purposes, 8 concrete blocks (i.e., 2 blocks per sets of distinct restrained concrete blocks as Table 5 displays) maintain in an environmental chamber enabling ASR development (38°C and 100% RH). Moreover, due to variability of the extent of damage for ASR-affected concrete members, a minimum of two specimens with 100 mm in diameter and 200 mm in length for all three proposed test procedures are required for each set of testing procedures. All of the concrete specimens were regularly monitored over time. Also, all concrete specimens were cooled down to 23°C for 16 ± 4 h prior to periodic expansion measurements.

A.  B.  C. 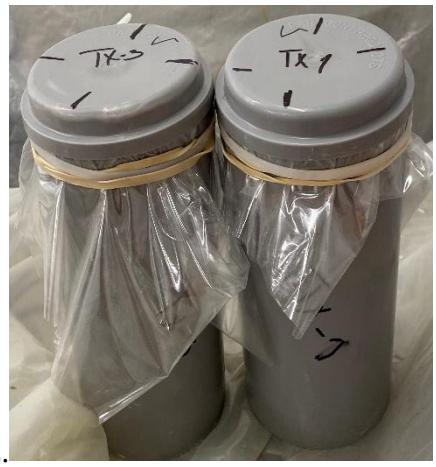

Figure 19 :Different storage conditions for ASR RE testing: (a) 38ºC and 100% R.H; (b) 0.7M NaOH solution at 38ºC and; (c) concrete mold containing a 0.4M NaOH solution and 38ºC.

11.1.2 Soluble Alkalis (SA)

To study the soluble alkali content of concrete specimens, a total of 24 extracted concrete cores (i.e., 6 per set of distinct restrained concrete blocks) are being investigated in this part of the project. Later, two 10g subsamples of ground concrete (>160 µm) are boiled in water for 10 minutes and the solution is left at room temperature to stand overnight. The volume of the filtered solution is adjusted to 100 ml by adding distilled water. Later, the Na and K concentration of the solution will be measured using atomic absorption, where the results are expressed on a kg/m^3 Na_2O_e basis.

11.2 Anticipated results and outcomes impact

It is anticipated that at the end of this part, the authors could evaluate the different expansion levels and deterioration of distinct concrete specimens as a function of time through the use of previously used techniques (i.e., expansion measurements, DRI and SDT). Thus, this could help the authors to find the most efficient methods to predict the potential for further expansion of concrete blocks displaying various restraint configurations by comparing the expansion obtained through the cored specimens and those gathered from the surface of concrete blocks. The above finding could also help practitioners/ engineers and researchers to find the most reliable test method for predicting the potential for further expansion of concrete infrastructure displaying various reinforcement configurations.

11.3 References

[1] M. Berube, J. Frenette, A. Pedneault, Rivest, Laboratory Assessment of the Potential Rate of ASR expansion of Field Concrete, Cem. Concr. Aggregates. 24 (2002) 13–19. https://doi.org/10.1520/CCA10486J.

[2] B. Fournier, A. Bérubé, J. Folliard, M. Thomas, Report on the Diagnosis, Prognosis, and Mitigation of Alkali-Silica Reaction (ASR) in Transportation Structures, Report No. FHWA-HIF-09-004, Federal Highway Administration, U. S. Department of Transportation, Washington, DC, 2010.

12. SCIENTIFIC AND ENGINEERING CONTRIBUTIONS OF THE PHD THESIS

As previously stated, this PhD study aims to have a better understanding of the effect of restraint on ASR-induced physicochemical development (i.e., kinetics and induced expansion, damage generation and propagation, crack pattern and orientation as well mechanical degradation). Furthermore, proposing a more reliable testing method to predict the potential for further expansion of ASR affected concrete under various restraint configurations could be count as another goal of this study. The specific findings of this research can be cited as being either scientific or engineering contributions, as presented hereafter:

Scientific contributions

- Understanding of the ASR-induced expansion in restrained and unrestrained concrete blocks used in this study;
- Understanding of the development of ASR microscopic features of deterioration in concrete elements under various restraint configurations;
- Understanding on how the microscopic distress features of ASR impact the mechanical behaviour of restrained concrete specimens;
- Understanding on how various aggregate types (fine and coarse) could change the mechanism of deterioration of ASR affected restrained blocks;
- Understanding on how ASR affect the visual integrity (i.e., surface damage) of affected concrete under distinct restraint conditions;
- Understanding on how restraint could impact the characterization of ASR gel in various directions of reinforced blocks; and,
- Proposal of a global quantitative damage chart based on ASR micro-mechanical coupling of distinct directions of restrained concrete.

Engineering contributions

- Demonstrating the diagnostic potential of the *Stiffness Damage Test (SDT) and Damage Rating Index (DRI)* for quantifying damage in ASR affected concrete under various restraint configurations;

- Proposal of the use of the proposed global chart as “reference” values for either selecting data from a similar restraint configuration and coring direction or comparing the results gathered from the available cored specimens to predict the behavior of those inaccessible/ unavailable directions;
- Proposal of the use of the new correlation suggested in this study in order to correlate the visual integrity (i.e., surface damage) with the actual expansion level of affected elements; and,
- Proposal of ASR-induced damage model on various surfaces of concrete elements displaying distinct restraint configurations.

13. CONCLUSIONS AND RECOMMENDATIONS

13.1 Conclusions

The main goals of this PhD work, which detailed results were presented and analyzed in the five scientific papers, are presented hereafter, as a function of the main objectives of the research identified in Section 3 (objective):

- Evaluating ASR-induced development of the distinct concrete blocks appraised in this work, one confirms that the restraint mitigates the ASR-induced expansion; the higher the restraint degree, the lower the expansion attained over time. Also, restraint would cause an anisotropic behavior in the reinforced concrete blocks where the induced expansion transfers from restrained to less/non-restrained directions. The latter clearly displays the impact of the restraint configuration on the achieved expansion levels (i.e., transverse > longitudinal top > longitudinal side).

- At the end of exposure time, all restrained concrete blocks with a rectangular cross section deformed into trapezoidal sections after a high (i.e., 0.25%) ASR-induced expansion.

- The expansion results gathered through the use of strain gauges affixed to the steel bars displayed considerable differences compared to those gathered from the DEMEC points. Such observation could be due to localized strain variations, lack of an adequate bond between the concrete and steel bars, and development of creep in the strain gauge adhesive system.

- Comparing the ASR-induced expansion level attained by distinct concrete blocks (regardless of restraint configuration) and concrete cylinders (100 by 200 mm- expansion measurements conducted longitudinally), one sees that the latter demonstrate a much faster ASR development. Such observation could be attributed to the impact of the specimen's size on ASR-induced expansion and deterioration. This phenomenon is likely due to the faster moisture transfer taking place in small scale specimens.

- Analysis of the pictures captured through the use of image-based detection techniques helps to better understand the procedure of ASR-induced damage development on the surfaces of concrete blocks where the latter follow the minimum energy law. As such, a significant number of new cracks will generate on the surface of concrete elements at the beginning of the chemical reaction, later it is easier for the expanding system to propagate (widening and lengthening) those initially formed cracks rather than creating new ones. Thus, the rate of crack generation on the surface of concrete elements will start to slow down. A correlation between visual inspection and the measured expansion level of concrete blocks has been proposed which could help engineers to

estimate the damage degree of ASR affected concrete infrastructure based only on a visual inspection of the concrete surface.

- Models for the development of ASR damage on the surface of affected elements as a function of expansion in concrete displaying distinct restraint configurations were proposed. While the distinct surfaces of unrestrained concrete blocks tend to propagate ASR-induced cracks with a random nature following a polygonal pattern, known as "map-cracking", most of the damages observed on the top and longitudinal surface of 1D were propagated along the longitudinal rebars. Conversely, the vast majority of the ASR-induced cracks on the transverse surfaces were randomly oriented which could be attributed to the lack of restraint across those surfaces. Moreover, while the ASR cracks on the top surface of 2D blocks were aligned along the transverse rebars, most of the damage on the longitudinal surface was developed parallel to the longitudinal steel bars. Also, the transverse surfaces of 2D blocks follow the same trend as the 1D blocks where more randomly oriented cracks were propagated. Moreover, comparing the various damage models proposed in this work, one sees that the higher the restraint, the higher the number of cracks generated on the surface of affected concrete; Such observation can be due to the mitigation nature of steel bars where the latter intended to decrease/mitigate the damage on the case but rather transfer those damage to the concrete cover and surface of affected elements.

- The Stiffness Damage Test (SDT) and the Damage Rating Index (DRI) are reliable and effective tools for the condition assessment of unrestrained/restrained concrete affected by ASR. As such, Statistical analysis (two-way analysis of variance - ANOVA) confirmed the significance of the SDT as a diagnostic tool for assessing the condition (i.e., physical integrity and stiffness reductions) of ASR-affected concrete under distinct confinement/restrainment configurations.

- The "overall" degree of damage (i.e., averaging the results obtained from the main coring directions at each damage degree) of the various concrete blocks obtained by using the aforementioned tools are in accordance with the ranges corresponding to the classification of damage degrees proposed in 2017 by Sanchez et al. for unrestrained concrete samples.

- Similar to the induced expansion, an important anisotropic behaviour in terms of crack development and mechanical degradation has also been observed for both 1D and 2D restrained concrete blocks, where greater damage features, DRI numbers and mechanical degradation were observed in the non-restrained directions than in the directions with confinement restrictions. Moreover, the higher the restraint degree, the higher the induced damage in the unrestrained

directions, while less deterioration is observed in the restrained direction(s), especially for the 2D configuration

- A quantitative four-quadrant chart and a damage classification table were developed for the various directions of the distinct ASR-affected restrained concrete blocks; the above was based on the correlation of the following multi-level parameters: a) SDI or PDI b) DRI and c) damage variable "δ" (i.e., stiffness reduction in this work). Such chart an table could contribute engineers to use the latter as a "reference" point for either selecting data from a similar reinforcement condition and coring direction or forecasting the behavior of inaccessible/ unavailable directions of affected concrete members.

- A thorough analysis of the samples extracted from the different directions of the ASR-affected restrained concrete blocks through mechanical (i.e., SDT-NLI) and microscopic (i.e., DRI- image analysis protocol) tools clearly attested a preferential orientation for ASR-induced crack propagation. The vast majority of cracks in restrained/confined blocks were developed parallel to the longitudinal steel bars. This finding is a very important point to be considered to assess and understand the structural performance of ASR-affected restrained concrete members in the field.

- Microscopic and mechanical investigations performed on the reinforced and non-reinforced concrete blocks incorporating reactive fine and coarse aggregates clearly displayed the different deterioration mechanisms taking place; those specimens manufactured by reactive fine aggregate particles not only display faster ASR kinetics and higher potential for ultimate expansion than those produced with reactive coarse aggregates, but they also exhibit a quite different deterioration pattern. For instance, ASR-affected concrete incorporating reactive fine aggregates presents more sparsely distributed cracks while a much more localized and the sharp cracking pattern is observed in concrete specimens cast with reactive coarse aggregates.

- Similar to the induced damage development of restrained concrete, an important anisotropic behaviour in terms of the chemical composition of ASR gels gathered from distinct locations (aggregate particles, ITZ and cement paste) of restrained blocks have also been detected. As such, those gels gathered from the unrestrained directions of reinforced concrete has significantly higher (Na+K)/Si and Ca/Si when compared to the unrestrained directions of those blocks. Accordingly, the ASR products obtained from the restrained directions of reinforced concrete have higher sodium and silicate and lower calcium and potassium content. This can be attributed to the restrainemnt caused by the reinforcement which does not let the ASR gels easily leave the reaction site; thus the

dissolution of the reactive aggregate of those directions is retarded, which could reduce the reactivity of the aggregate, and, hence, the gel formation.

- After investigating the impact of restraint configuration on the chemical composition of ASR gel, some easy-to-use contour plots of various chemical compositions of ASR gel (i.e., K/Si, Na/Si and Ca/Si) have been developed. Such plots can act as a very useful tool for researchers and engineers in order to either detect the highest swelling potential of various directions of each concrete block or forecasting the ASR gel's composition of inaccessible/ unavailable directions of affected concrete members.

- Evaluating the effect of restraint on the hardness of ASR gels gathered from distinct locations of each concrete block, one sees that not a considerable variation has been observed on results of hardness test obtained from ASR gel originated from aggregate particles (which probably could be due to the fact that all ASR gel formed in aggregate particles propagated to the cement paste). Conversely, those obtained from the cement paste of restrained concrete demonstrate anisotropic behavior where the hardness of ASR gel obtained from the cement paste of unrestrained directions of restrained blocks showed to have significantly higher hardness and thus deleterious potential than unrestrained blocks and restrained directions of reinforced blocks.

13.2 Recommendations for future works

After conducting extensive experimental research on the effect of restraint on ASR affected concrete, and taking into account the study conclusions stated above, some recommendations and suggestions for future research can be proposed, as follows:

- Since the SDT and DRI have proven their efficiency for the assessment of the mechanical and microscopic damage deterioration of ASR affected concrete under distinct restraint configurations, engineers can use those tools for the condition assessment of concrete elements or structures in service;

- Based on the data obtained in this study and previous studies on the efficiency and reliability of SDT and DRI on the condition assessment of concrete elements under distinct restraint configurations, efforts should be made to standardize those tests with the objective of reducing variations related to the use of different procedures from one lab/person to another;

- Since the proposed equation, which correlates the visual integrity (i.e., damage obtained through visual inspection) and the internal damage of concrete under various restraint elements, has proven its efficiency to assess the internal damage of concrete blocks manufactured in the laboratory

displaying distinct restraint configurations, it is now recommended to validate (and improve whether required) its efficiency while the assessment of concrete structures and structural components in the field.

- Generally, all restrained concrete blocks of this study were found to present the same trend through the different mechanical and microscopic analyses performed, which enabled the generation of a data envelop for restrained concrete. However, to better understand the effects of restraint on various concrete elements, further investigation is still required in reinforced concrete presenting distinct geometries and restraint configurations. This would allow a better understanding of the effect of restraint on ASR-induced distress development and how it impacts damage generation and propagation in affected concrete;

- This work only dealt with two extremely reactive aggregate particles (SP-coars aggregate and TX-fine aggregate) and tested two damage levels; however in order to generate a large database for the coupling of microscopic features of deterioration and the corresponding mechanical behaviour of ASR affected concrete, more data on various aggregates presenting distinct potential reactivity and affected concrete displaying different damage degrees are required in order to confirm the above coupling in the case of ASR concrete members in service;

- Similarly, the extremely reactive aggregates generally generate a thin and low-viscosity ASR gel, however, slower reactivity aggregates could generate higher viscosity ASR gels and deterioration, therefore, a comprehensive experimental investigation to characterize the ASR gel through the use of various aggregate types and natures with different reactivity level could be a topic of interest for future works;

- This works only used the aggregate generating alkali silica reaction (ASR) damage. However, in order to have a broader picture of the effect of restraint on the concrete elements affected by *alkali-aggregate reaction* (AAR), it is suggested to perform similar testing campaign on the aggregate particles triggering the so-called *alkali-carbonate reaction* (ACR);

- Ultimately, when the questions about how and how much ASR developed “damage” as a function of progressive expansion in restrained/unrestrained concrete elements are at least partially answered, which was the main objective of this PhD work, the development of practices that could predict the future expansion of ASR affected concrete could be topic of interest for future works. Moreover, with the aid of the aforementioned data, development of a comprehensive management protocol for ASR-affected concrete which always was one of the biggest challenges of engineers

in charge, could help them for making decision in order to select efficient rehabilitation methods and optimum application periods for distressed concrete infrastructures.